ProQuest LLC.
789 East Eisenhower Parkway
P.O. Box 1346
Ann Arbor, MI 48106 – 1346

UNIVERSITY OF SURREY

Carbon Nanotubes (CNT): Feasibility as nano-bio agents to target cancer

Vera Neves© 2010

Doctor of philosophy thesis

Faculty of Health and Medical Sciences, University of Surrey

Author declaration

I certify that this is my original work; except where sources are acknowledged, and that this thesis has not been submitted in part or in whole to fulfill the requirements of any other subject or course.

Vera Neves

Signature: Date: 25/10/2010

Abstract

With the advent of molecularly targeted agents in place of the traditionally employed chemotherapeutic cytotoxic compounds, cancer treatment has recently entered a new and exciting phase. Thus, the aim of this thesis was to explore the use of nanotechnology to deliver new-targeted cancer therapies using a carbon nanotube based interfering RNA (RNAi) gene delivery system.

To consider carbon nanotubes (CNTs) as nano-bio agents for gene therapy, it is important first to understand how they behave at a cellular level. CNTs, in the form of double-walled CNTs, were oxidised and wrapped with biomolecules prior to incubation with cells. Evidence of CNT uptake and release was demonstrated through Raman spectroscopy, of single cells and cell lysates, from PC3 and HeLa cancer cell lines. Results show a maximum uptake at 3 hours with 20 % of CNTs being internalised by PC3 cells (5.85 μg/mL) and a consequent release within a 24-hour time frame (< 0.31 μg/mL). An increase of I_D/I_G ratio and loss of the outer diameter of the DWNT during incubation period suggests that CNTs are being degraded in the intracellular environment. However, the internalisation of complexes led to no significant changes in cell components, such as DNA/RNA, proteins and lipids. In addition, no significant stress, evaluated by activation of phosphorylated MAPK, was induced when cells were exposed to carbon nanotubes.

Intracellular localisation and trafficking of carbon nanotubes was studied by means of antibody staining to specific cellular compartments and revealed that an endocytic pathway is involved in the internalisation of carbon nanotubes. In this endocytic pathway, carbon nanotubes were found to co-localise specifically with clathrin coated vesicles, early endosomes, lysosomes, and slow recycling endosomes.

To study the feasibility of applying CNTs to deliver nucleic acids, green fluorescent protein (GFP) was employed as a reporter gene for both gene delivery and gene silencing in an *in vitro* model. Firstly, gene delivery protocols were optimised by transfecting GFP-encoding plasmid DNA (pDNA) to mammalian cells via CNTs. Secondly, CNTs were used to deliver siRNA to the target GFP gene integrated into the host cell genome (through Lipofectamine transfection of pDNA). Gene targeting was achieved by silencing the GFP gene through small interfering RNA-CNT

complexes (siRNA-CNT) delivered to GFP expressing cells. However, results indicate that CNTs-nucleic acids (pDNA and siRNA) complexes do not reach their target sites, resulting in poor GFP expression or silencing. Data analysed by fluorescent microscopy and flow cytometry revealed that less than 1 % of cells were expressing the GFP gene (plasmid DNA delivery) or 2 % of cells presented knockdown of GFP gene (siRNA delivery). The expression and silencing using CNTs was very low compared to delivery of constructs with transfection reagent (Lipofectamine), which led to 43 % of cells expressing GFP and around 40 % of cells where the GFP gene was silenced.

Nevertheless, the experience of other researchers has been that the GFP gene is very difficult to silence to a significant degree because of its high level of endogenous expression. We therefore used CNTs to deliver siRNA targeting *survivin*, an anti-apoptotic protein, which is known to be overexpressed in several cancer cells lines and is thought to contribute to their oncogenic character. Reduced *survivin* silencing effect by immunoblotting was observed when siRNA-CNTs were employed, in comparison with DharmaFECT transfection reagent. However, after extended incubation periods the silencing induced via *survivin*-siRNA delivered through CNT cause cells to undergo apoptosis.

Acknowledgements

First and foremost I would like to thank my supervisors Professor Jonhjoe McFadden, Professor Ravi Silva and Doctor Helen Coley for their support and encouragement throughout my PhD; your advice and expertise has been invaluable. Additional thanks for the CARBIO members and supervisors for the collaborative work, interesting scientific discussions and the good moments during our biannual meetings. Individual thanks for Sara Costa for teaching me Raman and all the help analysing the data.

I would like to thank the bionanotechnology lab members, especially Elena Heister for helpful discussions and for helping me in so many ways both in and out of the lab.

Thanks also to Dr. Andreas Gerondopoulos for his advice and guidance through my work at the confocal microscope and Dr. Alexandra Bermudez-Fajardo for her assistance with sample preparation and analysis by flow cytometry.

I would like to thank all my friends from Surrey, thanks for making my PhD so much fun. Especially people that got together for lunch at the "pink room" and the ones that joined for a drink at "channies" every Friday. You've all helped make this PhD such a memorable experience.

Out of the lab, I would like to thank all my friends for their unwavering support and encouragement. To my parents and sister, I am grateful for your never-ending love and support. Thanks must also go to Miguel Nogueira for his constant support, faith and words of encouragement.

Publications

Neves, V., Heister, E., Tîlmaciu, C., Flahaut, E., Silva, S. R. P., McFadden, J., Coley H. M.. **Design of carbon nanotubes for biomedical applications.** (in preparation).

Neves, V., Gerondopoulos, A., Heister, E., Tîlmaciu, C., Flahaut, E., Silva, S. R. P., McFadden, J., Coley H. M.. **Cellular localisation, accumulation and trafficking of carbon nanotubes.** (submitted to ACS nano).

V. Neves, H. M. Coley, J. McFadden and S. R. P. Silva. **Uptake, intracellular localization and biodistribution of carbon nanotubes.** Book chapter, in "Carbon nanotubes for biomedical applications", R. Klingeler, R. B. Sim (eds.), Spinger 2010 (in press).

Heister, E., Neves, V., Lamprecht, C., Silva, S.R.P., Coley, H. M. and McFadden, J. **Targeted drug delivery with carbon nanotubes: optimization of drug loading, dispersion stability, and therapeutic efficacy.** (submitted)

Neves, V., Heister, E., Costa, S., Borowiak-Palen, E., Tîlmaciu, C., Flahaut, E., Coley H. M., Silva, S. R. P., McFadden, J.. **Uptake and Release of Double-Walled Carbon Nanotubes by Mammalian Cells.** Adv. Funct Mat., 2010, 20 (19) 3272-3279.

Heister E., Lamprecht C., Neves V., Tîlmaciu C., Datas L., Flahaut E., Soula B, Hinterdorfer P., Coley H.M., Silva SPR, McFadden J.. **Higher dispersion efficacy of functionalized carbon nanotubes in chemical and biological environments.** ACS Nano, 2010, 4 (5), pp 2615–2626

Lamprecht, C., I. Liashkovich, V. Neves, J. Danzberger, E. Heister, M. Rangl, H.M. Coley, J. McFadden, E. Flahaut, H.J. Gruber, P. Hinterdorfer, F. Kienberger, A. Ebner, AFM **Imaging of Functionalized Carbon Nanotubes on Biological Membranes**. Nanotechnology, 2009, 20(43), 434001

Heister E., V. Neves, C. Tilmaciu, K. Lipert, V. Sanz Beltrán, H.M Coley, S. R. P. Silva, and J. McFadden. **Triple functionalisation of single-walled carbon nanotubes with doxorubicin, a monoclonal antibody, and a fluorescent marker for targeted cancer therapy**, Carbon, 2009, 47, 2152-216.

Conferences

Neves, V. Contributed talk. "Carbon nanotubes: Interaction with cells for gene targeting". NT09: Tenth International Conference on the Science and Application of Nanotubes, Beijing, China, 21-26 June, 2009

Neves, V. Contributed talk. "Carbon nanotubes: Interaction with cells for gene targeting". 2nd ESF Summer School Nanomedicine, Lisbon, Portugal 12-16 June 2009

Neves, V. Poster. "Carbon nanotubes: Delivery to cancer cells for gene targeting and therapy", CNTBM08 Satellite Symposium, Montpellier, France, 28 July 2008.

Neves, V. Contributed talk. "Carbon nanotubes: Delivery to cancer cells for gene targeting and therapy", - INNANO conference, Innsbruck, Austria, 9-11 April 200

Bi-annual Marie Curie framework project meetings - CARBIO: Multifunctional Carbon Nanotubes for Biomedical applications: 22-26 March 2010, University of Szczecin, Poland; 28 October – 2 November 2009 University of Oxford, UK; 3-6 February 2009 University of Linz, Austria; 6-9 October, University of Twente, Enschede, The Netherlands; 26-29 June, 2008, University Paul Sabatier, Toulouse, France; 11-14 December 2007, University Hospital Dresden, Germany; 3-5 June 2007, University of Surrey, Guilford Surrey, UK.

Table of contents

List of Figures

Chapter 4

Chapter 5

Chapter 6

List of Tables

List of abbreviations

AFM	Atomic force microscopy
ANNOVA	Analysis of variance
ATP	Adenosine triphosphate
Bcl2	B-cell lymphoma 2
BIR	Baculovirus IAP repeat
BIRC	Baculovirus IAP repeat contain
BSA	Bovine serum albumine
CCVD	Catalytic chemical vapour deposition
CMV	Cytomegalovirus promoter
CNT	Carbon nanotubes
CPPs	Cell penetrating peptides
CV	Constitutive secretory vesicles
DC	Detergent compatible
DMSO	Dimethylsulfoxide
DNA	Deoxyribonucleic acid
DTPA	Diethylenetriaminepentaacetic
DWNT	Double-walled carbon nanotubes
EDC	1-Ethyl-3-[3—dimethylaminoplropyl]carbodiimide hydrochloride
EE	Early endosome
EEA	Early endosome antigen
EGF	Epidermal growth factor
EPR	Enhanced permeation and retention
ER	Endoplasmatic reticulum
Erk	Extracellular signal-related kinase
FACS	Fluorescence-activated cell sorter
FBS	Fetal bovine serum
FDA	Food and drug administration
FITC	Fluorescein isothiocyanate
GAPDH	Glyceraldehyde 3-phosphate dehydrogenase
GFP	Green fluorescent protein
GTPases	Hydrolyse guanosine triphosphate
HER1	Human endothelial receptor
HPLC	High-performance liquid chromatography
IAP	Inhibitor of apoptosis proteins

I_D	Intensity of D band
I_G	Intensity of G band
IGF1R	Insulin-like growth factor 1 receptor
IL	Interleukine
i.p.	Intraperitoneal
i.v.	Intravenous
Lamp	Lysosome associated membrane protein
LE	Late endosome
MAPK	Mitogen-activated protein kinase
MCS	Multiple cloning site
MEM	Minimum Essential Medium
MPS	Mononuclear phagocyte
mRNA	Messenger ribonucleic acid
MTD	Maximum tolerated dose
MWNT	Multi-walled carbon nanotube
NBS	Non-specific binding
NHS	N-hydroxy-succinimidyl
NIR	Near-infrared
ODNs	Oligodeoxynucleotides acids
ox	Oxidised
p53	Tumour suppressor protein
PBS	Phosphate buffer saline
PC3	Prostate cancer cells
pDNA	Plasmid DNA
PEG	Polyethylene glycol
PEI	Polyethylenimine
PI	Propidium iodide
PI-3	Phosphatidylinositol 3-kinases
PMSF	Phenylmethanesulfonyl fluoride
PS	Phosphotidylserine
Rab	Ras related superfamily
RBM	Radial breathing mode
RE	Recycling endosome

RES	Reticuloendothelial system
RGD	Arginine-glycine-aspartic acid
RISC	RNA-induced silencing complex
RNA	Ribonucleic acid
RNAi	RNA interference
RNase	Ribonuclease
RPMI	Roswell Park Memorial Institute medium
RV	Regulated secretory vesicles
SEM	Scanning electron microscope
STM	Scanning tunnelling microscope
siRNA	Silencing RNA
shRNA	Short-hairpin RNA
SWNT	Single-walled carbon nanotube
SPT	Single particle tracking
SDS	Sodium dodecyl sulfate
TEM	Transmission electron microscopy
TERT	Telomerase reverse transcriptase
UV-VIS-NIR	Ultra violet– visible-near infrared

Glossary

DWNT-PL-PEG-NH_2-pDNA or DWNT-PL-PEG-NH_2-siRNA	Pristine DWNT wrapped with PL-PEG-NH_2 followed by binging of pDNA or siRNA
DWNT-Poly(Lys:Phe)-pDNA or DWNT-Poly(Lys:Phe)-siRNA	Pristine DWNT wrapped with Poly(Lys:Phe) followed by binging of pDNA or siRNA
PL-PEG-NH_2	phospholipid molecules with PEG
PL-PEG-NH_2-pDNA-oxDWNT or PL-PEG-NH_2-siRNA-oxDWNT	pDNA or siRNA bound to PL-PEG-NH_2 followed by wrapping of oxidised DWNT
Poly(Lys:Phe)	Polyaminoacid (Lysine:Phenylalanine) 1:1 hydrobromide
Poly(Lys:Phe)-pDNA-oxDWNT or Poly(Lys:Phe)-siRNA-oxDWNT	pDNA or siRNA bound to Poly(Lys:Phe) followed by wrapping of oxidised DWNT
oxDWNT	Oxidised DWNT
oxDWNT-PL-PEG-NH_2-pDNA or oxDWNT-PL-PEG-NH_2-siRNA	Oxidised DWNT wrapped with PL-PEG-NH_2 followed by binging of pDNA or siRNA
oxDWNT-Poly-FS	Oxidised DWNT wrapped with Poly(Lys:Phe) attaching Fluorescein
oxDWNT-Poly(Lys:Phe)-pDNA or oxDWNT-Poly(Lys:Phe)-siRNA	Oxidised DWNT wrapped with Poly(Lys:Phe) followed by binging of pDNA or siRNA
oxDWNT-Poly-siRNA	Oxidised DWNT wrapped with Poly(Lys:Phe) followed by binging of siRNA
oxDWNT-Poly-ThiolsiRNA	Oxidised DWNT wrapped with Poly(Lys:Phe) followed by conjugation with siRNA containing a thiol group
oxDWNT-RNA	Oxidised DWNT coated with RNA
oxDWNT-RNA-FS	Oxidised DWNT wrapped with RNA tagged with fluorescein
oxSWNT-PL-PEG-NH_2-pDNA or oxSWNT-PL-PEG-NH_2-siRNA	Oxidised SWNT wrapped with PL-PEG-NH_2 followed by binging of pDNA or siRNA
oxSWNT-Poly(Lys:Phe)-pDNA or oxSWNT-Poly(Lys:Phe)-siRNA	Oxidised SWNT wrapped with Poly(Lys:Phe) followed by binging of pDNA or siRNA

Chapter 1: Introduction

Nanotechnology concerns the knowledge and control of components generally in the 1-1000 nm dimensional range [1]. The application of nanotechnology to medicine, referred to as nanomedicine, concerns the use of precisely engineered materials in this size range in the development of novel therapeutic and diagnostic modalities [2, 3]. The nanoscale materials involved – such as liposomes, polymeric carriers, dendrimers, micelles, nanotubes, nanoshels and others (Figure 1.2) have been developed for the treatment of cancer, diabetes, pain, asthma, allergy, infections and many more [4, 5]. In addition, these agents may provide more effective and/or more convenient routes of administration, lower therapeutic toxicity, extend the product life cycle, and ultimately reduce health care costs. Figure 1.1 displays the applications and research targets of nanomedicine [6]. For diagnostic applications, nanoparticles allow detection on the molecular level, by identifying abnormalities such as fragments from viruses, pre-cancerous cells and disease markers that cannot be detected by traditional established diagnostics [7]. As therapeutic delivery systems, nanoparticles permit targeted delivery and controlled release. Nanoparticles are recognized for their many advantages, such as delivery of drugs in a targeted manner to minimize side effects, precise delivery to only the affected area, release of drugs at a sustained rate, prolonging the half-life of drug systemic circulation by reducing immunogenicity and improvement of dispersibility of poorly water-soluble drugs. In addition, the use of nanoparticle systems allow the possibility for delivering two or more drugs simultaneously for combination therapy in order to generate a synergistic effect [7].

There are many examples of nanoparticles being used in current clinical practice, which are at various stages of clinical development [8-10] (Figure 1.2); these complex agents show improved pharmacological and toxicological properties in comparison to the parent non-complexed counterparts. Amongst these products, liposomal drugs and polymer-drug conjugates are the two dominant classes, accounting for more than 80 % of the total amount [7].

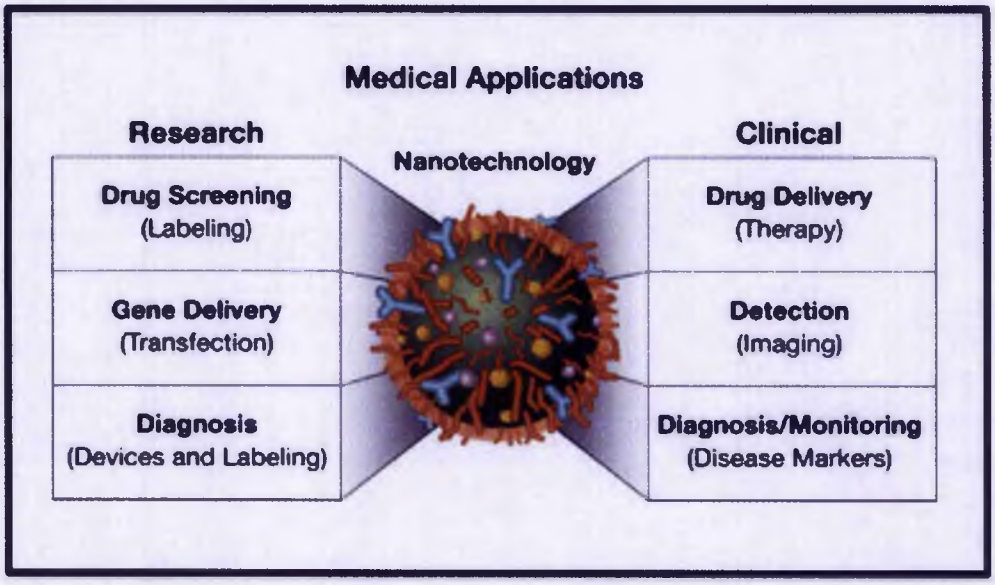

Figure 1.1: Medical applications of nanotechnology. Nanoparticles have been designed with chemically modified surfaces onto which various ligands attach, which can turn the nanomaterials into biosensors, molecular-scale fluorescent tags, imaging agents, target molecular delivery vehicles and other useful biological tools (adapted from reference [6]).

Liposomes are spherical lipid vesicles with bilayered membrane structure composed of natural or synthetic amphiphilic lipid molecules [11, 12]. Liposome-encapsulated formulations of doxorubicin were approved 10 years ago for the treatment of Kaposi's sarcoma, and are now used for the treatment of breast cancer and refractory ovarian cancer.

Magnetic resonance imaging (MRI) contrast enhancement has been obtained by protocols using several types of nanoparticles. These comprise gadolinium-based [13], iron-oxide-based nanoparticles [14-19] and multiple-mode imaging contrast nano-agents that combine magnetic resonance with biological targeting [20] and optical detection [12, 20]. Low-density lipid nanoparticles have been used to enhance ultrasound imaging [21, 22], and show promise in the clinical setting.

Furthermore, many polymer-based nanoparticles have been investigated [23, 24]. For example, dendrimers are self-assembling synthetic polymers with elegantly adjustable nanoscale dimensions [24].

Silicon [25] and silica [26] are emerging as attractive candidate materials for nanoparticles for medical applications. Porosified silicon is biodegradable [27], with

kinetics that are much more rapid (minutes to hours) than those of biodegradable polymers (weeks to months). Another type of studied nanoparticles are the nanoshells [28], which include a gold layer over a silica core. The thickness of the gold layer can be precisely tuned, so that the nanoshell can be selectively activated through tissue irradiation with near-infrared light to perform localized therapeutic thermal ablation.

Following the discovery of fullerenes by Kroto, Curl and Smalley and the identification of carbon nanotubes (CNTs) by Iijima [29], carbon nanotechnology has also been intensively studied in terms of their potential for biomedical applications.

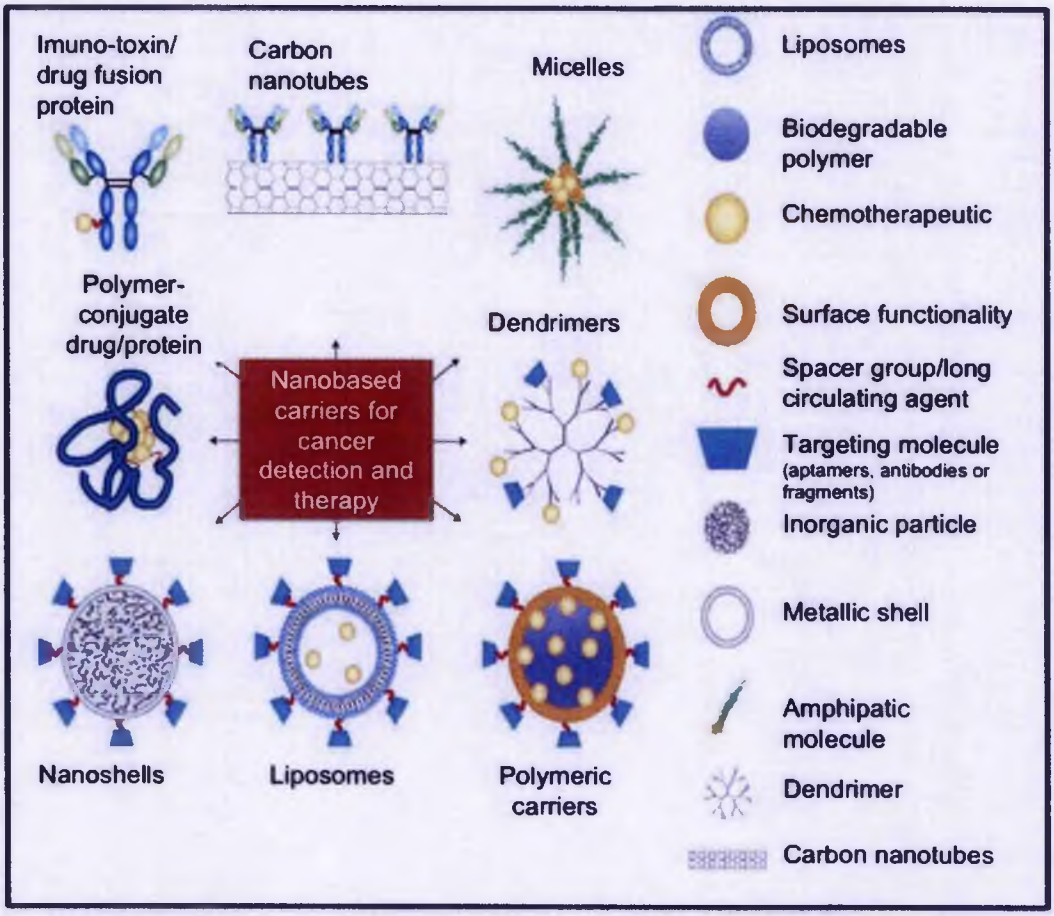

Figure 1.2: Example of different nanoparticles currently studied. Nanoparticles can be designed with a whole range of delivery agents, but the main components typically include the nanoparticle, a targeting moiety conjugated to the nanoparticle, and a cargo (such as chemotherapeutic drugs) (adapted from Peer *et al.* 2007 [30]).

1.1 Nanotechnology for cancer therapy

Cancer is a fundamental aberration in cellular behaviour and may be described at the molecular biology level. Most cell types of the body can give rise to malignant tumour (cancer) cells. Cancer cells can multiply in absence of growth-promoting factors required for proliferation and are resistant to signals that normally program cell death (apoptosis) [31].

Current cancer therapy typically involves intrusive processes that include the application of catheters for chemotherapy, initial chemotherapy to shrink the cancer (adjuvant therapy), and surgery to then remove the tumour(s), followed by more chemotherapy and radiation. Cancer drugs are used to destroy malignant cells, generally via their DNA damaging effects and the induction of cell death processes such as apoptosis (programmed cell death). However, due to their untargeted mode of action (i.e. in that they damage DNA whether in tumour cells or normal healthy body cells) cancer chemotherapeutic drugs frequently kill healthy cells/tissue giving rise to toxic side-effects.

As mortality due to cancer remains a worldwide problem, two approaches are bringing hope to improved therapies. Firstly, genomic and proteomics research is/will be capable of identifying new tumour-specific molecular targets [32], and secondly, innovative drug delivery systems [33, 34] are being developed to guide drugs more precisely to tumour cells and away from non-specific sites thus reducing toxicity. Further, new drug delivery systems can introduce favourable and improved pharmacokinetic modifications, which can for example prolong drug half-life so effective dosing is maintained over long periods of time. Several therapeutic nanoparticles have been recently approved for clinical use, as shown in Table 1.1.

Table 1.1: Examples of nanoparticle-based drug currently available on the market (adapted from Peer *et al.* 2007 [30]).

Compound	Commercial name	Nano-agent	Indications
Styrene maleic anhydride-neocarzinostatin (SAMNCS)	Zinostantin/Stimalmer	Polymer-protein conjugate	Hepatocellular carcinoma
PEG-L asparaginase	Oncaspar	Polymer-protein conjugate	Acute lymphoblastic leukemia
PEG-granulocyte colony-simulating factor (G-CSF)	Neulasta/PEGfilgrastim	Polymer-protein conjugate	Prevention of chemotherapy associated neutropenia
IL2 fused to diphtheria toxin	Ontack (Denilelukin diftitox	Immunotoxin (fusion protein)	Cutaneous T-cell lymphoma
Anti-CD33 antibody conjugated to calicheamicin	Mylotarg	Chemo-immunoconjugate	Acute myelogenous leukemia
Anti-CD20 conjugated to yttrium-90 or indium-111	Zevalin	Radio-immunoconjugate	Relapsed or refractory, low-grade, follicular, or transformed non-Hodgkin's lymphoma
Anti-CD20 conjugated to iodine-131	Bexxar	Liposomes	Kaposi's sarcoma
Daunorubicin	DaunoXome	Liposomes	Combinational therapy of recurrent breast cancer, ovarian, Kaposi's sarcoma
Doxorubicin	Doxil/Caelyx	PEG-Liposomes	Refractory Kaposi's sarcoma, recurrent breast cancer, ovarian cancer
Vincristine	Onco TCS	Liposomes	Relapsed aggressive non-Hodgkin's lymphoma
Paclitaxel	Abraxane	Albumin-bound paclitaxel nanoparticles	Metastatic breast cancer

1.1.1 Targeted delivery to tumours

A single cancerous cell surrounded by healthy tissue will replicate at a higher rate than other cells, placing a strain on the nutrient supply and elimination of metabolic waste products [4]. Thus, in order to survive a tumour must successfully recruit a blood supply to meet its nutritional requirements. The vascularity of tumours is highly heterogeneous, with areas of vascular necrosis and areas densely vascularised,

which promote the adequate supply of oxygen and nutrients to the growing tumour. Tumour blood vessels have several abnormalities compared to normal blood vessels, including a high proportion of proliferating endothelial cells with aberrant underlying basement membrane, increased tortuosity of blood vessels, and deficiency in pericytes [35]. Tumour microvessels demonstrate enhanced permeability, which is regulated in part by abnormal secretion of vascular endothelial growth factor (VEGF), bradykinin, nitric oxide, prostaglandins, and matrix metalloproteinases [35]. The transport of macromolecules across tumour microvasculature may occur through open interendothelial junctions or transendothelial channels. *In vivo* experiments (in tumour xenographs) using liposomes of different mean sizes, suggested that the threshold vesicle size for extravasation into tumours is approximately 400 nm [36]. However, other studies have shown that particles with diameters below 200 nm are more effective [36-39].

The tumour lymphatic system is also abnormal, resulting in fluid retention in tumours and high interstitial pressure with an outward convective interstitial fluid flow [40]. This property is thought to promote tumour cell extravasation, resulting in tumour metastasis and blockage of nanoparticle extravasation from microvasculature into the tumour interstitium. However, the lack of an intact lymphatic system also results in retention of the nanoparticles in the tumour interstitium since these particles are not readily cleared from this compartment. When taken together, the leaky microvasculature and the lack of intact lymphatic system results in the enhanced permeation and retention (EPR) effect and "passive" cancer targeting through the preferential accumulation of nanoparticles in the tumour compared with the plasma and in other tissues [41]. The release of drugs from nanoparticles in this case results in a relatively higher intratumoural drug concentration translating into enhanced tumour cytotoxicity. These nanoparticles may be further modified for "active" cancer targeting by functionalising the surface of nanoparticles with ligands such as antibodies, aptamers, peptides, or small molecules that recognise tumour-specific or tumour associated antigens in the tumour microenvironment. When nanoparticles are prepared to target tumour antigen at the extracellular portion of transmembrane, they may be specifically taken up by cancer cells through receptor-mediated endocytosis [42-48]. The specific targeting, enhanced intracellular uptake and regulated therapeutic delivery of a payload are parameters that can potentially be controlled via rational design of nanoparticles. Figure 1.3 presents the different mechanisms by which nanoparticles can deliver drugs to cancer cells, either by "passive" or "active" targeting.

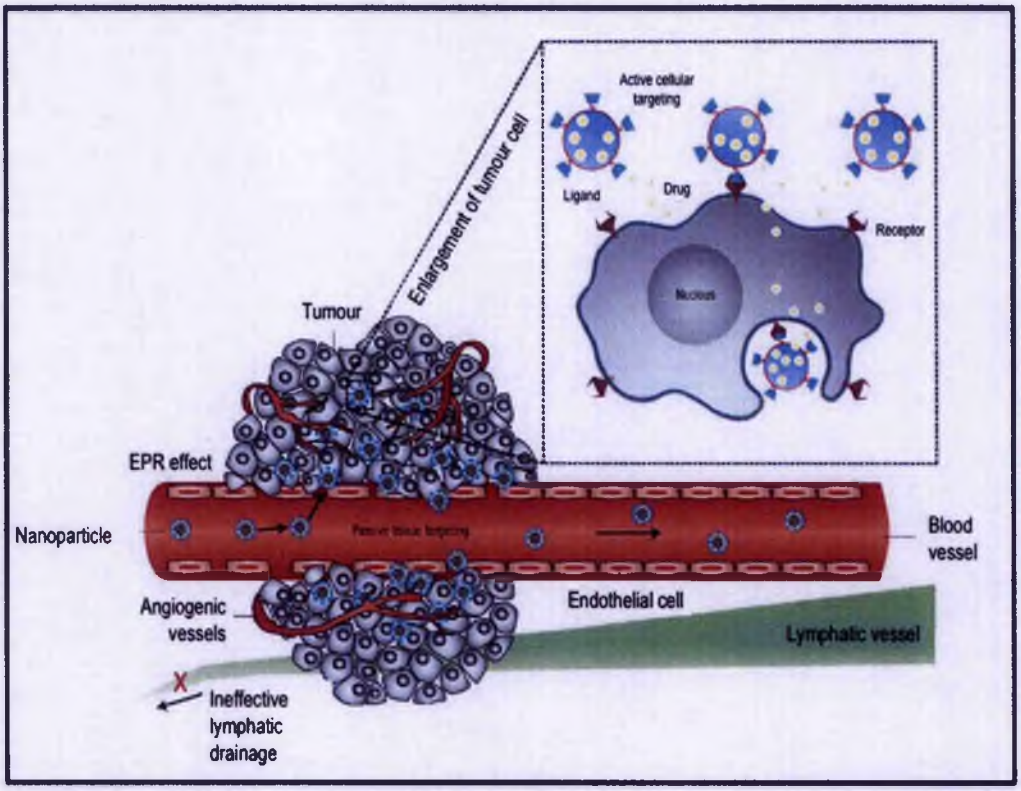

Figure 1.3: Schematic representation of different mechanisms by which nanoparticles can deliver drugs to tumours. Passive tissue targeting is achieved by extravasation of nanoparticles through increased permeability of the tumour vasculature and ineffective lymphatic drainage (EPR effect). Active cellular targeting (inset) can be achieved by functionalisation the surface of nanoparticles with ligands that promote cell-specific recognition and binding (adapted from Peer *et al.* 2007 [30]).

1.1.2 Nucleic acid-based nanoparticles (DNA, RNAi, anti-sense)

Following the sequencing of the human genome and many key model organisms, nucleic acid-based approaches that act to silence a specific gene expression in a sequence-specific manner have emerged as powerful tools to investigate gene functions. Furthermore, these nucleic acid molecules are also being developed as therapeutic agents that target disease-causing genes.

The greatest impact of these technologies is expected to be in cancer therapy where there is a differentially abnormal pattern of gene and protein expression between normal and tumour cells.

Different types of molecules capable of knocking-down gene expression by sequence-specific targeting of mRNAs have been developed in the hope of creating therapeutic agents. The three major nucleic-acid-based gene-silencing molecules are chemical modified antisense oligodeoxyribonucleic acids (ODNs), ribozymes and siRNAs. ODNs are generally ~20 nucleotides in length and act by hybridizing to pre-mRNA and mRNA to produce a substrate for ribonuclease H (RNase H), which specifically degrades the RNA strand of the formed RNA-DNA duplexes [49]. Ribozymes bind to RNA through Watson-Crick base pairing and act to degrade target RNA by catalysing the hydrolysis of the phosphodiester backbone [50]. siRNAs are 21-23 nucleotide duplexes, which are components of the RNAi machinery leading to the cleavage of mRNA containing perfectly complementary sequences (see below).

Comparison between the different approaches for gene silencing suggests that siRNA is far more potent and longer lasting than ODNs. Additionally, inhibition levels of siRNA are some 100- to 1000-fold higher that the optimal obtain for ODNs directed against the same target [51-53].

Recently, the mechanism and strategies for effective delivery of antisense and siRNA oligonucleotides were summarised and surveyed by Juliano *et al.* [54]. There are several obstacles, which have to be overcome in order to achieve the sufficient delivery of siRNA molecules into targeted cancer cells [55]. The first problem is significant degradation by serum and tissue nucleases. Unlike DNA, the RNA backbone contains ribose that has a hydroxyl group in the 2' position of the pentose ring instead of a hydrogen atom [54]. It is this feature that makes the RNA backbone more susceptible to hydrolysis by serum nucleases in the extracellular environment via cleavage along the phosphodiester backbone of nucleic acids. The second problem is the rapid renal excretion due to the size of siRNAs; these molecules are relatively small and consequently are rapidly excreted through urine when administrated into the blood stream [56]. The third challenge is the inefficient endocytosis by targeted tumour cell coupled with inefficient release from the endosomes.

1.1.2.1 Mechanism of RNAi

RNA interference (RNAi) therapeutics represent a fundamental new route to treat human disease as there are a huge number of targets that are otherwise "untreatable" with existing medicines [57]. In 1998, RNAi gained international attention, when Fire, Mello and colleagues discovered the ability of double-stranded RNA to silence gene expression in the nematode worm *Caenorhabditis elegans* [58]. Three years later, Tuschl and co-workers published the experiment that was regarded as the proof-of-principle, and revealed that synthetic small interfering RNA (siRNA) could achieve sequence-specific gene knockdown in a mammalian cell line [59].

RNAi is a fundamental pathway in eukaryotic cells by which sequence-specific siRNA is able to target and cleave complementary mRNA [59]. RNAi is triggered by the presence of long pieces of double-stranded RNA, which are cleaved into fragments known as siRNA (21-23 nucleotides long) by the enzyme Dicer (Step 1, Figure 1.4) [60]. In practice, siRNA can be synthetically produced and then directly introduced into the cell, thus circumventing Dicer mechanics. This shortcut reduces the potential for an innate immune response and the shutdown of cellular protein expression that can occur following the interaction of long pieces (>30 nucleotides) of double-stranded RNA (dsRNA) with intracellular RNA receptors [61]. Initial applications using long dsRNA, showed that dsRNA was not effective in most mammalian cells because it induced the antiviral interferon (IFN) response [62], which leads to cell death.

Figure 1.4 shows a schematic representation of the RNAi mechanism, once siRNA is present in the cytoplasm of the cell (step 2), it is incorporated into a protein complex called the RNA-induced silencing complex (RISC) [63]. Argonaute 2 (AGO2), a multifunctional protein contained within the RISC, unwinds the siRNA, after which the sense strand of the siRNA is cleaved [64]. The activated RISC, which contains the antisense strand (or guide strand) of the siRNA, selectively seeks out and degrades mRNA that is complementary to the antisense strand (Figure 1.4) [65]. The cleavage of mRNA occurs at a position between nucleotides 10 and 11 on the complementary antisense strand, relative to the 5'-end [66]. The activated RISC complex can then move on to destroy additional mRNA targets, which further propagates gene silencing [67]. This extra potency ensures a therapeutic effect for 3-7 days in rapidly dividing cells, and for several weeks in non-dividing cells [68]. Eventually, siRNA is diluted below a certain therapeutic threshold or degraded within the cell, and so repeated administration is necessary to achieve a persistent effect [57]. Theoretically, when

using suitable designed siRNA, the RNAi machinery can be exploited to silence particular genes in the body, giving it a broader therapeutic potential than typical small-molecule drugs [57].

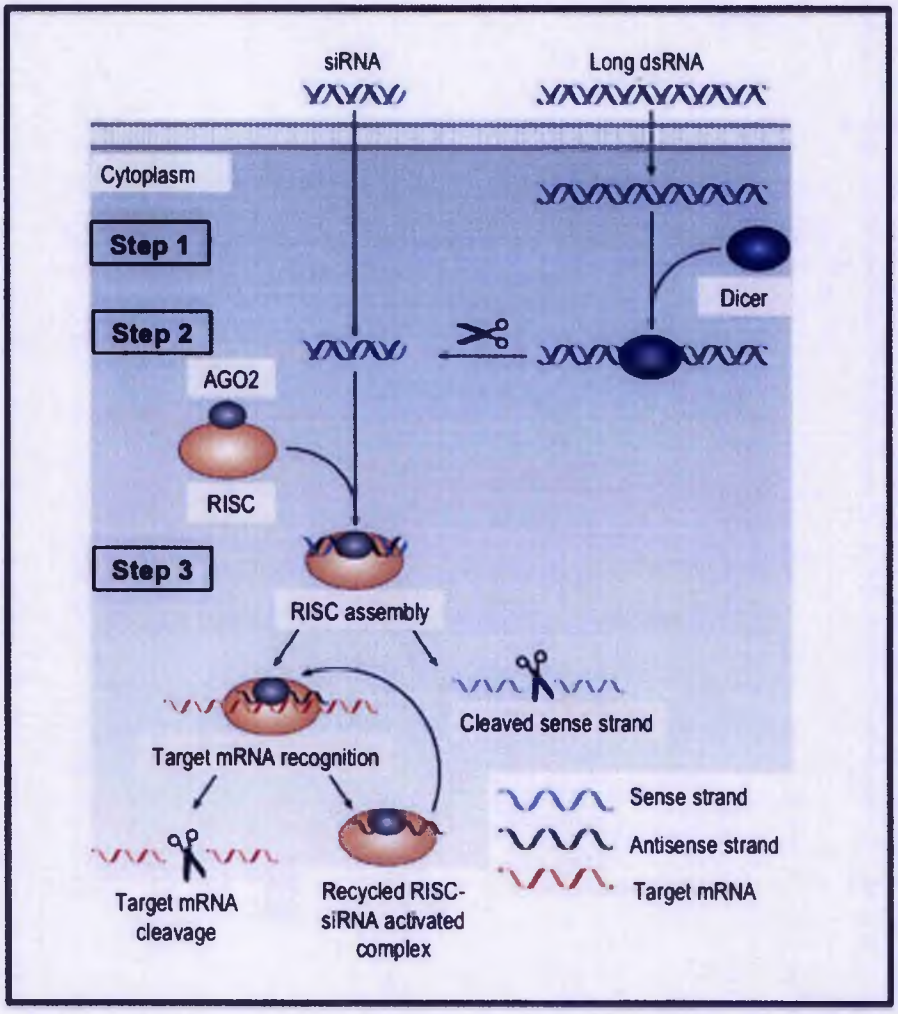

Figure 1.4: Mechanism of RNA interference. Long double-stranded RNA (dsRNA) is introduced into the cytoplasm, where it is cleaved into small interfering RNA (siRNA) by the enzyme Dicer (step 1). Alternatively, siRNA can be introduced directly into the cell (step 2). The siRNA is then incorporated into the RNA-induced silencing complex (RISC), resulting in the cleavage of the sense strand of RNA by argonaute 2 (AGO2). The activated RISC-siRNA complex selectively seeks, binds to and degrades complementary mRNA, which leads to the silencing of the target gene. The activated RISC-siRNA complex can then be recycled for the destruction of identical mRNA targets (adapted from Whitehead *et al.* 2009 [69]).

1.1.2.2 Targeting individual genes by RNA interference

To date, various individual genes in different tumour cell models have been targeted using RNAi and their knockdown led to profound biological consequences. These genes include oncogenes/anti-apoptotic molecules, telomerase, growth factor receptor genes, and signalling molecules. A representative sample of these studies is given below (Table 1.2) [70].

The anti-apoptotic protein Bcl-2, for example, is an oncogene that is over-expressed in many human tumours. Treatment of human cancer cells *in vitro* by siRNA targeting bcl-2 induced apoptosis in 50 % of cells. Moreover, expression of short-hairpin RNAs (shRNAs) against bcl-2 in mice with xenograft tumour suppressed tumour growth by more than 60 % [71].

Survivin is a member of the mammalian IAP family and a biofunctional regulator of spindle microtubule function during mitosis. Survivin is significantly up-regulated in many human cancers [72] but practically undetectable in normal human tissues. It has been shown that expression of shRNA against *survivin* diminished expression *in vitro* and induced apoptosis in transfected cells [73]. Downregulation of survivin by RNAi in esophageal squamous cell carcinoma resulted in significant inhibition of tumour growth *in vitro* and *in vivo,* via induction of apoptosis [74]. In contrast, downregulation of *survivin* by RNAi in sarcomas did not lead to apoptosis, but to G2 arrest and a reduction in clonogenic survival independently of p53 status [75]. Transient transfection of survivin siRNA led to downregulation of survivin in apoptosis-resistant lung cancer cells and sensitized these cells to cell death [76].

Table 1.2: Potential targets for anti-cancer therapy, suppressed by RNA interference (adapted from Gartel *et al.* 2006 [70]).

Target	Cancer type	*In vitro/In vivo*	Result
Bcl-2	Cervical Gastric Prostate	*In vitro* *In vivo*	Apoptosis Tumour growth inhibition
X-IAP	Breast	*In vitro*	Apoptosis
Survivin	Esophageal	*In vitro*	Apoptosis Tumour growth inhibition G2 arrest
Skp-2	Lung Squamous cell Carcinoma	*In vitro* *In vivo*	Apoptosis Inhibition of cell growth (*in vitro*) Tumour growth inhibition (*in vivo*)
Stat3	Breast Prostate Laryngeal	*In vitro* *In vivo*	Apoptosis Inhibition of cell growth Tumour growth inhibition
MDR1	Uterine sarcoma Colon	*In vitro* *In vivo*	Enhanced the cytotoxicity of vincristine, paclitaxel, and doxorubicin
HPV E6, E7	Cervical	*In vitro*	Increased sensitivity to cisplatin
Telomerase	Colon Melanoma Bladder	*In vitro* *In vivo*	Inhibition of cell growth Tumour growth inhibition
Integrin-linked Kinase	Pancreatic adenocarcinoma	*In vitro*	Inhibition of cell growth
EWS-FL11 VEGF	Ewing's sarcoma	*In vivo*	Tumour growth inhibition
ERK1/2	Ovarian	*In vitro*	Apoptosis Necrosis Inhibition of cell growth
Polo-kinase 1	Prostate Glioblastoma Cervical	*In vitro*	Apoptosis Cell cycle arrest
HER2/neu	Breast	*In vitro*	Apoptosis Inhibition of cell growth
C-Myc	Breast	*In vitro*	Apoptosis Inhibition of cell growth
RhoA	Breast	*In vitro* *In vivo*	Stimulates breast cancer cell invasion Inhibited the growth and angiogenesis
RhoC	Breast	*In vitro*	Impedes breast cancer cell invasion
Met	Prostate Sarcoma Glioblastoma Gastric	*In vitro* *In vivo*	Inhibition of invasion *in vitro* Apoptosis Tumour growth inhibition
IGFBP-5	Neuroblastoma	*In vitro*	Apoptosis Inhibition of cell growth Sensitization to X-ray irradiation
EGFR	Lung	*In vitro* *In vivo*	Inhibition of cell growth Tumour growth inhibition Sensitization to cisplatin

Table1 (*continued*)

Target	Cancer type	*In vitro/In vivo*	Result
BRAF NRAS	Melanoma	*In vitro* *In vivo*	Apoptosis Inhibition of cell growth Inhibition of invasion *in vitro*
uPA uPAR	Prostate Glioma	*In vitro* *In vivo*	Apoptosis Inhibition of cell growth Inhibition of invasion and angiogenesis
Paxillin	Osteosarcoma	*In vitro*	Inhibition of motility
Androgen receptor	Prostate	*In vivo*	Apoptosis
Cyclophilin A	Lung	*In vitro* *In vivo*	Apoptosis Inhibition of cell growth Tumour growth inhibition
Pin1	Prostate	*In vitro* *In vivo*	Apoptosis Inhibition of cell growth Tumour growth inhibition Inhibition of invasion and angiogenesis
Fatty acid synthase	Prostate	*In vitro*	Apoptosis Inhibition of cell growth
Acetyl-CoA-carboxylase	Prostate	*In vitro*	Apoptosis Inhibition of cell growth

1.1.2.3 Different delivery strategies for siRNA

The simplicity of siRNA delivery is partially dependent on the accessibility of the target organ or tissue within the body. Localised siRNA delivery, directly to the target tissue, offers several benefits, such as higher bioavailability given the proximity to the target tissue, and reduced adverse effects typically associated with systemic administration [69]. There are several tissues that are susceptible to topical or localised therapy, including the eye, skin, mucous membranes, and local tumours [77-80]. Contrasting, systemic delivery, i.e., the intravenous injection of delivery particles that travel throughout the body to the target organ or tissue, requires that particles have the ability to avoid the uptake and clearance by non-targeted tissues [69]. Therefore, cell-specific delivery of siRNAs *in vivo* is an important consideration in developing an effective, RNAi-based therapeutic agent. Duplex siRNAs are negatively charged and so cannot easily penetrate hydrophobic cellular membranes without assisting carriers such as liposomes or nanoparticles [81].

Another strategy for siRNA delivery is the viral transport of RNAi-inducing agents. Treatment of chronic diseases require long-term RNAi, which must be mediated by viral expression vectors; this involves a gene therapy approach to incorporate small

hairpin RNA (shRNA) transgenes into cells for genomic integration. Gene therapy vectors have been under development; however there have been ongoing issues of safety, mainly immune responses, which also apply to the RNAi-based therapies. Thus, progress is needed for targeting viral vectors to specific cell types and to minimise their toxicity.

1.2 Design of nanoparticles

In 2008, Sanhai *et al.* [82] commented on the seven challenges for nanomedicine. Establishing priorities based on regulations formalised at a workshop that visioned the creation of a more efficient and transparent "critical" path for nano-product development, by the FDA and Alliance for NanoHealth. The seven areas of concern are presented below:

1. The determination of the distribution of nanoparticle carriers in the body following the systemic administration through any route. With special focus on imaging modalities for visualising the biodistribution over time.
2. The ability of the nanoparticle to carry and deliver multiple therapeutic and imaging payloads [83], and individual tracking.
3. Understanding the transport across the compartmental boundaries in the body and achieving targeted delivery.
4. Mathematical models that will contribute to a "periodic table" of nanoparticles [84] to predict risk and benefit parameters.
5. Computer models that will contribute to a "periodic table" of nanoparticles to predict risk and benefit parameters.
6. Establish standards, reference materials and testing protocols that can provide benchmarks for the development of novel classes of materials
7. Present an analytical toolkit for nano-pharmaceutical manufacturing, accompanied by a specification sheet of toxicological, safety and biodistribution properties obtained through standardized, validated methods.

1.2.1 Size matters

An obvious advantage of nanotechnology for biomedical applications is the ability to control the size of the resulting particles and devices. Nanoparticles are in the same size range as biomolecular entities, as shown in Figure 1.5. Nanoscale constructs are smaller than human cells (10000 – 20000 nm in diameter) and organelles; however, they are similar in size to large biological macromolecules such as enzymes and receptors [6]. Nanoparticles smaller than 20 nm can transit through blood vessel walls and have the ability to penetrate the blood-brain barrier and the stomach epithelium [85-89].

To be suitable as a drug-delivery platform, the size of nanoparticles must be small enough to avoid rapid filtration by the spleen, with junctions spaced at roughly 200 nm [90]. Similarly, to transverse the liver, the particles must be small enough to pass through the organ's 150-200 nm-sized fenestrae and avoid the Kupffer cell-lined sieve plates [91]. The size of nanoscale devices also allows them to interact readily with biomolecules on the cell surface and within the cell, often in ways that do not alter the behaviour and biochemical properties of those molecules [92].

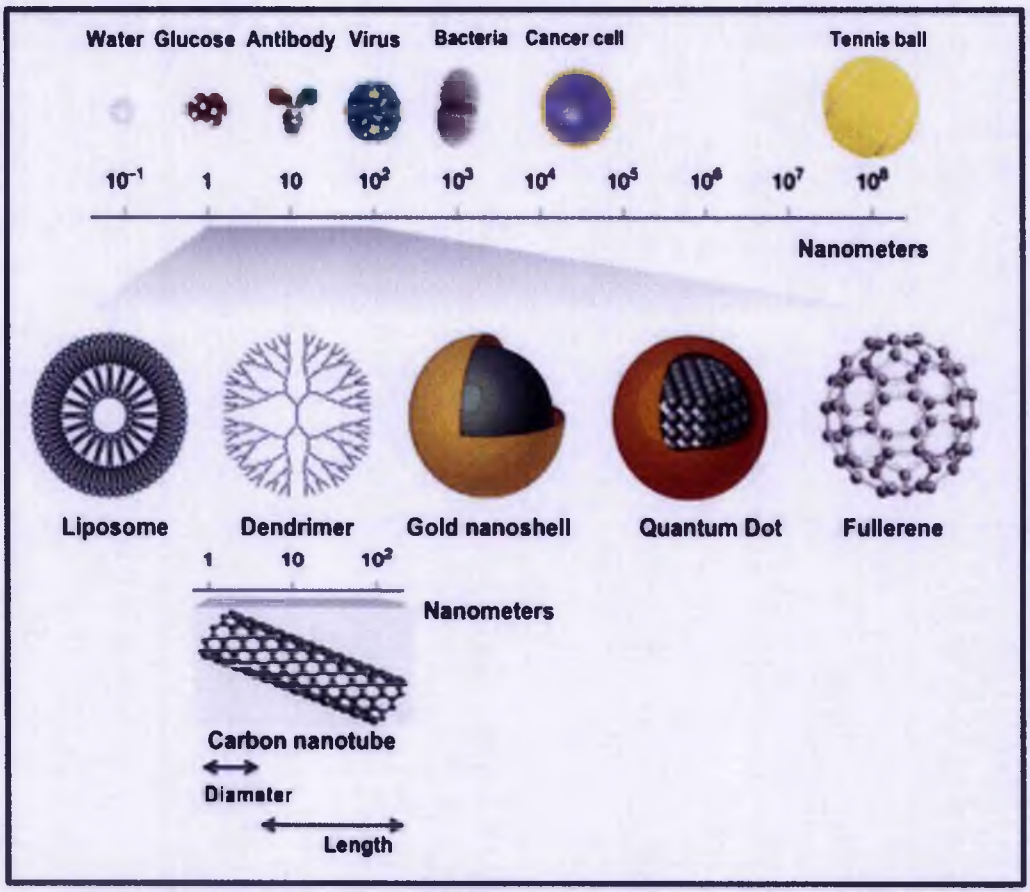

Figure 1.5: Relative sizes of nanoparticles. Relative size of nanoparticles compared with familiar items (adapted from McNeil *et al.* 2005 [6]).

1.2.2 Dispersibility matters

Modification of the nanoparticle surface allows that a variety of chemical, molecular, and biological entities to be covalently or otherwise bound. These types of manipulations provides advantageous properties to the particle, such as increased dispersibility and biocompatibility [6]. For example the attachment of hydrophilic polymers to the surface, such as PEG, greatly increases the hydration, and consequent dispersibility of the nanoparticles and can protect the payloads from enzymatic degradation when used for *in vivo* applications [93]. These hydrophilic polymers can also act as a platform for lipophilic molecules and overcome the dispersibility barrier. Insoluble compounds can be attached, adsorbed, or encapsulated in the hydrated nanoparticle [94, 95]. Therefore, dispersibility of the

composite entity becomes a function of the nanoparticle rather then being strictly dependent on the drug itself [6].

The surface addition of PEG ("PEGylation") and other hydrophilic polymers increases the *in vivo* compatibility of nanoparticles [6]. When injected intravascularly, uncoated nanoparticles are cleared rapidly from the bloodstream by the reticuloendothelial system (RES) [96]. Nanoparticles coated with hydrophilic polymers have prolonged circulating half-life, believed to result from decreased opsonization and subsequent clearance by macrophages [97].

1.2.3 Biodistribution and transport across the compartmental boundaries

The circulating half-life of a drug complex, maximal tolerated dose (MTD), and target selectivity are the most important factors culminating in a high therapeutic index (ratio between the amount of therapeutic effect and the amount of drug toxicity). The therapeutic load is typically conjugated to the surface of nanoparticles, or encapsulated and protected inside the core. The nanoparticle can also be designed to provide either controlled or triggered release of the therapeutic molecule [98]. The particle surface can then be functionalised by various methods with the objective of increasing the circulating half-life, and by reducing nonspecific distribution in some cases by targeting tissue with specific cell surface antigens with a targeting ligand (peptide, aptamer, antibody, small molecule). Surface functionalisation can address the major limiting factor of long-circulating nanoparticles, notably protein absorption. Proteins adsorbed on the surface of the nanoparticle promote opsonization, leading to aggregation with subsequent rapid clearance from the bloodstream [99-101]. The resultant rapid clearance is due to phagocytosis by the mononuclear phagocyte system (MPS) in conjunction with the liver and spleen filtration network. Typically, the majority of opsonized particles are cleared by a receptor-mediated mechanism within minutes due to a high concentration of phagocytic cells in the liver and spleen or alternatively they may be excreted [100].

Numerous biological barriers exist to protect the human body from invasion by foreign particles. The biodistribution of any nanoparticle is primarily ruled by their ability to transverse biological barriers [1]. These barriers include: the RES,

endothelial/epithelial membranes, complex networks of blood vessels, abnormal flow of blood and interstitial gradients. Endothelia composing the blood vessels have been classified as continuous, fenestrated, or discontinuous, depending on the morphological features and organ location. Continuous endothelium morphology appears in arteries, vessels [102], and the lungs [103]. In contrast, fenestrated endothelium appears in glands [104], digestive mucosa, and kidney (wherein fenestrae form pores of approximately 60 nm). Discontinuous endothelium is a characteristic of the liver (fenestrae of 50-100 nm) [105]. Endothelial cells from the blood vessels are able to respond to the physiological environment, resulting in angiogenic activity. Angiogenesis pertaining to tumour biology has been well characterised in many studies. During tumour growth, angiogenesis results in defective hypervasculature and a deficient lymphatic drainage system, which explains the concept of passive targeting of nanoparticles to tumours through the EPR effect [106, 107]. The EPR effect is a unique tumour-related feature, which allows macromolecules or nanoparticles (cutoff size of >400 nm) to preferentially accumulate and diffuse within tumour tissues [39].

Additionally, boundaries exist at a cellular level, for example, the cell membrane and the different organelles inside the cell, in particular the nuclear envelope and endosomes [82]. For example, if internalisation of nanoparticles is via receptor-mediated endocytosis, it is usually through the endosome/lysosome pathway and can lead to the therapeutic agent to being trapped in the organelle or be degraded.

More recently, CNTs have been considered for biomedical applications and a number of research groups are currently involved in elucidating their uptake and biodistribution.

1.3 CNTs in nanotechnology

Carbon is the most versatile element of the periodic table, owing to the type, strength, and number of bonds it can form with many different elements. Carbon in the solid phase can exist in four main allotropic forms: diamond, graphite, buckminsterfullerene, and amorphous carbon (Figure 1.6) [108]. Diamond (Figure 1.6 A) is one of the best-known allotropes of carbon; its crystalline network gives diamond its hardness (it is the hardest known natural mineral) and excellent heat conduction

properties (about five times better than copper). The sp^3 hybridized bonds account for its electrically insulating property and optical transparency. Graphite (Figure 1.6 B) is made by layered planar sheets of sp^2 hybridized carbon atoms bonded together in a hexagonal network. The different geometry of the chemical bonds makes graphite soft, slippery, opaque, and electrically conductive [108].

Buckminsterfullerenes (Figure 1.6 C), or fullerenes, are part of a family of spherical or cylindrical molecules with all the carbon atoms sp^2 hybridized. The tubular form of fullerenes gives rise to CNTs (Figure 1.6 D).

In the mid 1980's, Smalley and co-workers developed the chemistry of fullerenes [109]. After their discovery, fullerenes led to the synthesis of CNTs. CNTs are long, thin fullerenes where the walls of the tubes are hexagonal carbon (graphite structure) and often capped at each end.

These forms of carbon, which are essentially segments of a graphene sheet that have been rolled up as a cylinder, have extreme exceptional properties that are a consequence of their symmetric structure. For the past nineteen years, CNTs have gained increasing interest due to their remarkable mechanical and electrical properties. CNTs are among the stiffest and strongest tube known due to the strength of the sp^2 carbon-carbon bonds. In reality, the stiffness of CNTs measured in terms of its Young's modulus (ratio of stress over strain) can be as high as 1 TPa, which makes them 5-times stiffer than steel. In addition, their tensile strength or breaking strain can reach values of up to 63 GPa, which is around 50-times higher than steel [110]. Despite the strength, CNTs also exhibit extraordinary electronic properties; they can be metallic or semiconducting, depending on their structure (chirality) [111]. Consequently, some nanotubes have conductivities higher than copper, while others behave like silicon. Lastly, CNTs display the highest known thermal conductivity at moderate temperatures alongside with two other carbon-based materials; diamond and in-plane graphite [108].

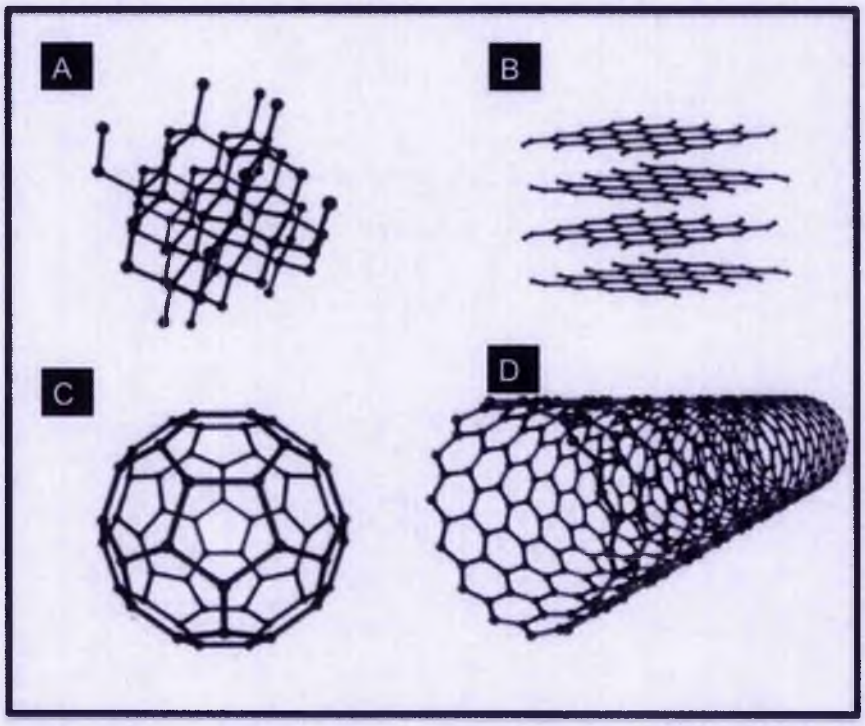

Figure 1.6: The allotropes of carbon. (A) Diamond; (B) C_{60} Buckminsterfullerenegraphite; (C) graphite; and (h) single-walled carbon nanotube (SWNT) (adapted from O'Connell *et al.* [108]).

These all-carbon hollow graphitic tubes with high aspect and nanoscale diameter [112] can be classified by their structure into two main types: single-walled nanotubes (SWNTs), which consist of a single layer of graphene sheet seamlessly rolled into a cylindrical tube, and multi-walled nanotubes (MWNTs), which comprise multiple layers of concentric cylinders with a space of about 0.34 nm between the adjacent layers [113].

In recent years, efforts have been dedicated to explore the potential biological applications of CNTs, motivated by their interesting size, shape and structures, as well as their unique physical properties [114-117]. These cylindrically shaped entities can have diameters of 0.4 to 10 nm for SWNTs and 2 to 100 nm for MWNTs; and lengths ranging from as short as 10 nm up to 1 cm. Their dimensions along with their one-dimensional structure, contribute to their distinct behaviour in the form of spherical nanoparticles in biological environments, offering new opportunities in biomedical research [118]. The flexible one-dimensional nanotube can bend to facilitate multiple

binding sites of a functionalised nanotube in one cell, leading to a multi-valence effect, and improved binding affinity of nanotubes conjugated with targeting ligands [118]. With all atoms exposed on the surface, CNTs have an ultrahigh surface area that permits efficient loading of multiple molecules along the length of the nanotube sidewall. In addition, supramolecular binding of aromatic molecules can be easily achieved by π-π stacking of those molecules onto the polyaromatic surface of nanotubes [119].

The intrinsic optical and electrical properties of CNTs can be employed for multimodal imaging and therapy. Owing to the quantum effect, CNTs behave as quasi 1-D quantum wires with sharp densities of electronic states (electronic DOS) at the van Hove singularities, which can correlate with their distinctive optical properties [120]. For example, SWNTs are highly absorbing materials with strong optical absorption in the near-infrared (NIR) range (800-1600 nm). These wavelengths include the tissue transparent region of the electromagnetic spectrum (800-1400 nm), in which radiation passes through without significant scattering, absorption, heating or damage to tissues [121]. Moreover, semiconducting SWNTs with small band gaps exhibit photoluminescence in the NIR range. The emission range of SWNT is 800-2000 nm [117, 122, 123], which covers the biological tissue transparency window, and is therefore suitable for biological imaging. CNTs also have distinctive resonance-enhanced Raman signatures for Raman detection and imaging, with large scattering cross-sections for single tubes [124, 125]. Therefore, CNTs have various attractive properties that have led to research into their potential biomedical applications.

1.3.1 Uptake and intracellular localisation of carbon nanotubes

Pantarotto and colleagues published the first evidence that CNTs translocate across cell membranes [126]. In that particular study, water-disperse, amino-functionalised SWNTs were conjugated to a fluorescent dye via either a short organic linker or a peptide. When incubated with fibroblasts (Human 3T6 and murine 3T3) both conjugates were internalised but the peptide-SWNTs were found to accumulate in the nucleus, whereas the directly labelled SWNTs were solely confined to the cytoplasm. The uptake mechanism described was shown to be endocytosis-independent given

that internalisation was unaffected by temperature or presence of endocytosis inhibitors. Thus, it was proposed that CNTs behave like cell penetrating peptides (CPPs) and related synthetic oligomers [126]. Following this study, uptake of CNTs was also demonstrated by changes in gene expression [127] when CNTs were used for gene delivery. The interaction of SWNTs with HeLa cells (human cervical cancer) was reported using transmission electron microscopy (TEM) with evidence of nanotubes crossing the plasma membrane. A mechanism whereby CNTs pass through the cell membrane as "nanoneedles" without loss of cell viability, was proposed [127]. In this study they have suggested that the cationic functional groups facilitate a spontaneous insertion mechanism allowing them to pass through the biomembrane. Additionally, it was demonstrated that various types of functionalised CNTs can be taken up by a wide range of cells, some of which were deficient in phagocytotic function (i.e. fibroblasts) or lacked the capacity to undergo endocytosis (e.g. fungi, yeast and bacteria) [128]. Hence the term "nanosyringe" was adopted to describe these properties and this was further explored by Lopez *et al.*. They proposed a model whereby nanotubes interact with lipid bilayers via a diffusion process directly through the biomembrane, as illustrated in Figure 1.7. The mechanism involves a two-step process in which the nanotubes are first associated onto the membrane surface and then reoriented to adopt a transmembrane configuration [129].

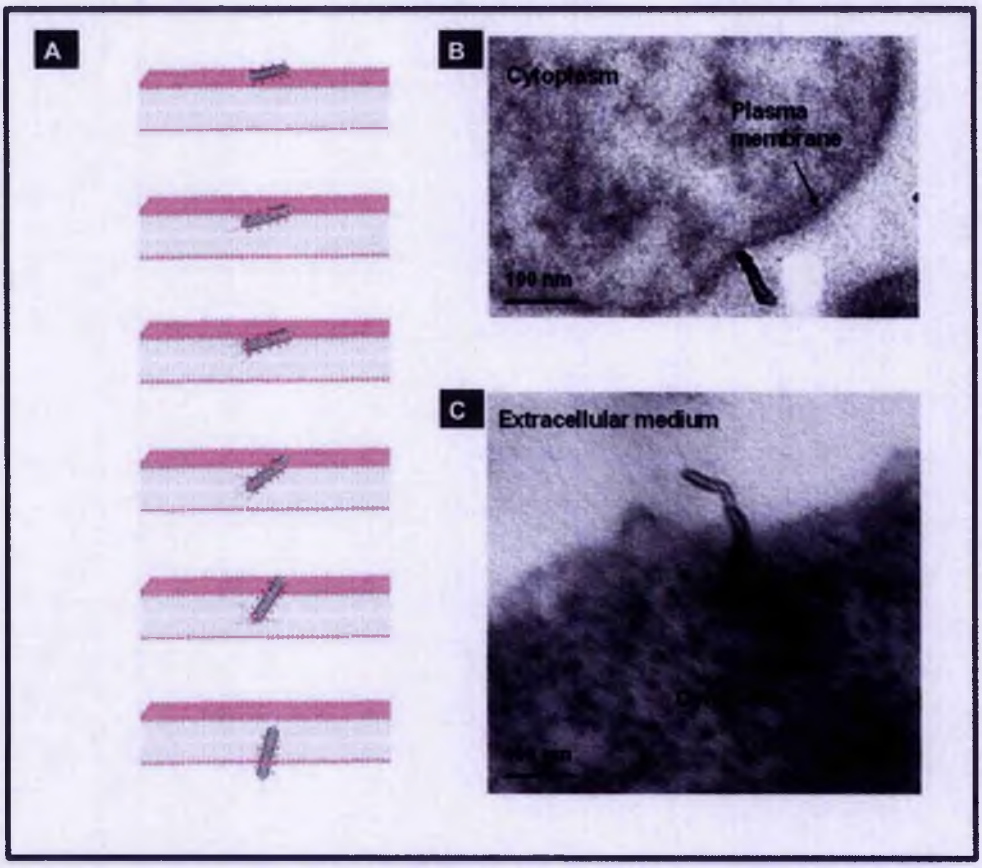

Figure 1.7: CNTs acting as nanoneedles. (A) Schematic of a carbon nanotube crossing the plasma membrane; (B) TEM image of MWNT-NH_3^+ interacting with the plasma membrane of A549 cells; and (C) TEM image of MWNT-NH_3^+ crossing the plasma membrane of HeLa cells (adapted from Lacerda *et al.* 2007 [130]).

As an alternative to the "nanoneedle" mechanism, Kam *et al.*, subsequently reported uptake of SWNT and SWNT-streptavidin by human promyelocytic leukemia and human T cells (HL60 and Jurkat cell lines, respectively) via an endocytic pathway. In that study, not only it is shown that CNTs are taken up by cells but they can also carry large cargos such as streptavidin (MW ≈ 60kD) [115]. To elucidate the mechanism of entry of CNTs into the cells, a membrane/ endosome marker FM 4-64, and reduced temperature were used. By adding both endosome marker and nanotube conjugates co-localisation was observed which provided direct evidence for the endocytotic uptake. A later study from the same group further demonstrated uptake of CNTs conjugated with different labelled proteins: streptavidin, protein A, bovine serum albumin and cytochrome c in various adherent and suspension cell line cultures. Data obtained were in support of an endocytic pathway, showing co-localisation of

nanotubes with an endosomal marker but absence of nuclear localisation (Figure 1.8) [131]. To investigate the release of nanotubes by the endosomes they added chloroquine to the cell medium during incubation of cells with protein-SWNT conjugates. Chloroquine is a membrane permeable basic drug capable of localizing inside endosomes, increasing the pH and giving rise to endosomal rupture. With chloroquine addition it was shown that the intracellular fluorescence signal was more diffuse and uniform as opposed to a more punctuate staining pattern. To assess the role of clathrin coated vesicles, further experiments were carried out in the presence of sucrose and potassium-depleted medium, which revealed a significantly reduced level of CNT uptake [132]. The study also demonstrated that the nanotubes were not internalised via the caveolae or lipid-raft pathway. Moreover, using filipin and nystatin treatment, known to perturb the cholesterol distribution on the cell membrane had no influence on uptake of CNTs. In conclusion, SWNTs, complexed with proteins and nucleic acids, penetrate cell membranes following a clathrin-dependent endocytotic process.

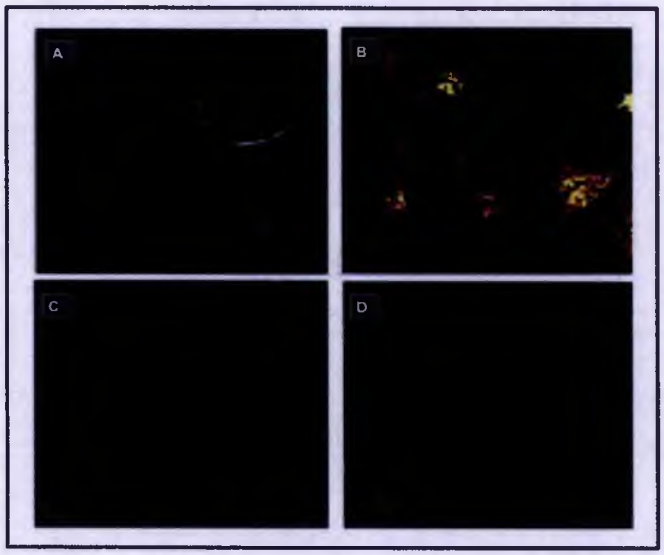

Figure 1.8: Confocal microscopy of cells after incubation with protein-SWNT (proteins labeled to fluoresce green). (A) HL60 cells after incubation with BSA-SWNTs. (B) HeLa cells after incubation with cytochrome c-SWNTs in the presence of the FM 4-64, a red membrane and endocytic vesicle marker. Co-localisation of proteins and lysosomes is demonstrated by the yellow colour in the image. Endosomal rupture, was revealed by the release of SWNT-protein conjugate (D), where overall green is visualised across the cell due to incubation with chloroquine, contrasting with the green individualised spots localised inside cells (C) (adapted from Kam *et al.* 2005 [131]).

In the approaches described above carbon nanotube uptake was studied by visualising internalisation by covalent linkage of a visible-wavelength fluorophore. Caution should be exercised when considering this approach with respect to parameters such as: chemical linkage that must resist enzymatic cleavage, also the emission from the visible-wavelength fluorophore, which must be detected above background endogenous fluorescence and the chemical processing of nanoparticles may dramatically change their ultimate biological fate. Cherkuti *et al.* presented a technique that permits the observation of pristine, hydrophobic SWNTs in biological media by near-infrared (NIR) fluorescence [117]. CNTs present a unique NIR intrinsic fluorescence making them advantageous for use in biological systems, as there is minimal background autofluorescence from cells, tissues, and other biological molecules in this spectral range. Furthermore, biological tissues facilitate high transmission penetration of NIR light (near ~ 1 μm) for detection within an organism or under the surface of tissues [133]. Using this technique, mouse macrophage-like cells have been seen to actively engulf significant quantities of SWNTs, with an average ingestion rate of approximately 1 nanotube per second per cell. It was further shown that incubating cells at a reduced temperature of 27 °C caused a reduction of uptake of nanotubes compared with incubation at 37 °C, suggesting an active ingestion of the nanotubes [117]. Another uptake study involving spectroscopic measurement of DNA-wrapped CNTs indicated a length-selective uptake of nanotubes. The assay determined an approximate uptake threshold of approximately 189(±17) nm. After 16-hours incubation 32 % of nanotubes remained in solution, suggesting that only a proportion of nanotubes available may be ingested [134]. Heller *et al.*, used a combined approach of NIR and Raman spectroscopy for assessment of cellular uptake [124]. Raman spectroscopy is a general, rapid (~1 min per spectrum) non-destructive technique that operates at standard room temperature (~300 K) and pressure conditions, and uses readily available Raman characterisation instrumentation [135]. Due to electronic structure and diameter of CNTs strong resonance-enhanced Raman bands are produced at 150-300 cm^{-1}, ~1350 cm^{-1}, 1590-1600 cm^{-1}, and ~2600 cm^{-1} away from the excitation wavelength [136]. The first, termed the radial breathing modes (RBMs), are caused by uniaxial vibrations and depend linearly on the nanotube diameter; then the tangential mode (or G band), which is caused by stretching along the C-C bonds of graphene [136-138]; the ~1350 cm^{-1} for the disorder-induced D band, and at ~2900 cm^{-1} for its second-order harmonic, the 2D band [136]. After incubation, of murine myoblast stem cell and 3T3

fibroblast cells, with DNA-wrapped SWNT, persistent Raman scattering and a parallel marked decrease in intensity in fluorescence (relative to Raman) was observed due to internalisation of nanotubes. The deposition of the nanotubes could be determined up to three months in culture. Raman signal of cells incubated with DNA-SWNT left in culture for 48-hours and 8 days showed that the nanotubes concentrated near, but outside, the nuclei of cells. The perinuclear accumulation of nanotubes was confirmed by TEM where it was shown that CNTs formed uniaxial, ordered bundles inside vesicles located near the nucleus, but not within the nuclear envelope. In view of these observations it was suggested that there was an endocytic transport mechanism for DNA-SWNT aggregates. Interestingly, it was also reported that aggregates remained in cells during repeated cell divisions [124]. By use of Raman spectroscopic measurement carbon nanotube uptake was analysed in SWNTs dispersed in media containing fetal bovine serum or a peptide (nano-1), indicating this to be a time- and temperature-dependent process [139]. Measurements of the G band in different regions within the cell were performed showing that it was detected in both the cytoplasm and nucleus. However, it was suggested that the localisation was more realistically associated with CNTs at the perinuclear region and/or in the cytoplasm immediately above or below the nucleus. It was proposed that the intensity of the G band produced was due to an active uptake of CNTs, as incubation at 4 °C resulted in a 98% decrease in intensity [139]. Yehia *et al.* conducted a similar study with time-dependent uptake studied using Raman spectroscopy in conjunction with TEM to examine intracellular distribution. They reported that CNTs were not associated with mitochondria, Golgi bodies or the nucleus, but they accumulated in cytoplasmatic vacuoles [140].

Another label-free approach for visualising CNT uptake is by AFM. Lamprecht *et al.*. demonstrated that AFM could be used to visualise non-covalently functionalised SWNT and double walled CNTs (DWNT) immobilised on different biological membranes, such as plasma membranes and nuclear envelopes, as well as on a monolayer of avidin molecules [141].

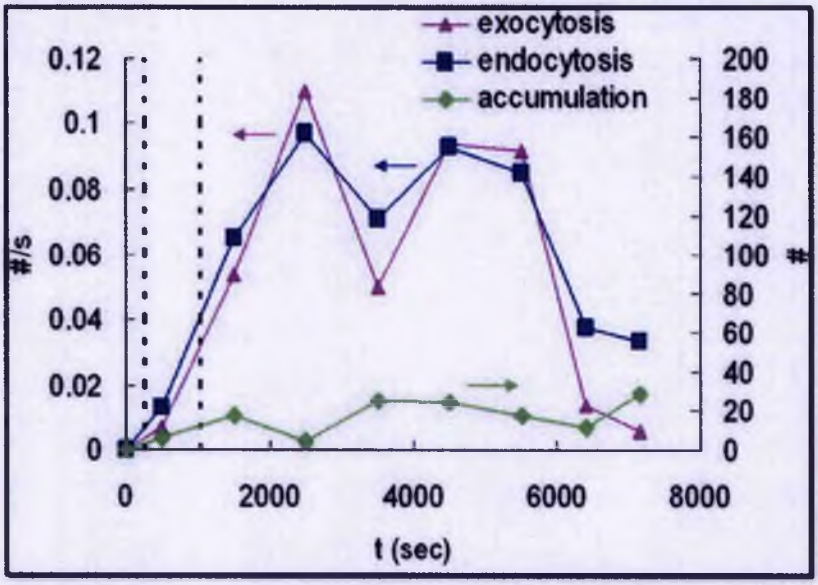

Figure 1.9: A comparison of net internalization (endocytosis) and exocytosis rates (#/s) and net accumulation (#/cell) over time by single particle tracking. This results in NIH3T3 fibroblast cells, shows that the data imply that endocytosis and exocytosis rates for DNA-SWNT are closely regulated (adapted from Jin *et al.* 2008 [142]).

Jin and colleagues were the first to report evidence of exocytosis by cells containing CNTs; by single particle tracking (SPT); they demonstrated that the rate of exocytosis closely matches that for endocytosis [142]. NIH-3T3 fibroblast cells were exposed to DNA- SWNTs for approximately 16 min, followed by media perfusion for a period of approximately 2 hours. Endocytosis took place throughout the duration of the experiment at a slow rate, with an uptake of CNT aggregates occurring as a later event. It has been suggested that the DNA-SWNT could be recycled back to the membrane together with its receptors. The endocytotic rate was higher initially, and the exocytosis rate closely matched with a negligible temporal offset (Figure 1.9). Given that Au nanoparticles of diameters from 14 to 100 nm undergo exocytosis – according to a size associated linear relationship, with the larger particles being less likely to be exocytosed [143]. Those data were in agreement with the previously reported agglomeration observed within cell (as above). However it should be noted that the accumulation observed represented a small fraction of SWNTs processed by the cell, as illustrated in Figure 1.9. The fundamentals for the endocytotic mechanism is explained by adsorption of proteins from the media to the surface of functionalised SWNTs, confirmed by electrophoretic mobility and zeta potentials of DNA-SWNT in

water and in media [142]. Additionally, the same group has recently published a study on size-dependent uptake and expulsion of SWNTs using the same methodology (SPT) [144]. This study comprises a mathematical model for size dependent uptake and shows that for SWNTs an optimal endocytotic rate occurs around 25 nm [144].

Intracellular trafficking of CNTs was firstly described by Lacerda *et al.* [145]. The previously described "nano-needle" CNTs (SWNT-NH_3^+), which contains a luminescence signal due to the functionalisation method, were incubated with human lung carcinoma cells (A549 cell line) without staining. The results demonstrated that uptake of nanotubes led to perinuclear accumulation with no effect on cell viability. As this set of experiments was not performed under standard tissue culture conditions (i.e. absence of serum), which differed from the experimental conditions used in the exocytosis experiments, this could explain the effects seen on intracellular accumulation [145].

In summary, progress has been made towards our understanding of how nanotubes interact with the cell. However, it is important to note, that besides different mechanisms of uptake described, there are many variations on experimental design and methodologies used, - such as functionaiisation of the material, concentration and others.

1.3.2 Biodistribution of CNTs

Elucidating the pharmacological profiles of *in vivo* administered CNTs, is very important when considering their potential for medical use. Potential harmful effects associated with nanotubes, due to their nanoscale dimensions and carbon backbone may arise from their ability to readily enter the respiratory tract, deposit in the lung tissue, redistribute from their site of deposition, escape from the normal phagocytic defences, and modify the structure of proteins. Therefore, nanotubes might potentially activate inflammatory and immunological responses, affecting normal organ function and could give rise to a harmful pathological response [146].

Initial studies of biodistribution of CNTs focused on their toxicological profile *in vivo* [147-153]. Studies focused on the effects of CNTs in terms of pulmonary toxicity following inhalation, intratracheal instillation [149, 150], and pharyngeal aspiration [151], in addition to their effects on skin toxicity after topical application [147], and

subcutaneous administration [152, 153]. These reports cited acute pulmonary toxicity effects, induction of granulomas, and inflammatory reactions to CNT. However, all of those particular studies used pristine, non-functionalised CNTs, usually dispersed in an aqueous buffer with the aid of a surfactant such as Tween 80 [150]. In contrast, toxicity of acid-treated CNTs of two different lengths (200 and 825 nm) subcutaneously administered to rats showed, no severe inflammatory response such as necrosis, tissue degeneration, or neutrophil infiltration [153]. Thus, functionalisation and aqueous dispersibility contribute significantly to biocompatibility of these materials, improving dramatically their *in vitro* toxicity profile [154, 155].

The first *in vivo* study on functionalised CNTs biodistribution was reported by Wang *et al.*, using mice treated with intraperitoneai (i.p.) administered short hydroxylated single walled CNTs. SWNTs were shown to accumulate mainly in the liver and kidney, lesser so in the spleen and lung, and excreted mainly by the kidney within 18 days [156]. In another study, using intravenous administration (*i.v.*) it was demonstrated that functionalised SWNTs with a chelating molecule diethylenetriaminepentaacetic (DTPA) and labelled with indium (^{111}In) – [^{111}In]DTPA-SWNT, followed by radioactivity tracing using gamma scintigraphy, resulted in no retention in any RES organs (liver or spleen) and were rapidly cleared from the systemic blood circulation again via renal excretion [146]. In addition this study allowed a comparison of the biodistribution of two types of functionaiisation: the first with no free amino groups and a second one with 40% free amino groups resulting in surface charge. Both functionalised SWNTs were found in kidney, muscle, skin, and blood after 30 minutes. However the surface-charged SWNTs led to a higher affinity for kidney, muscle, skin, and lung, leading to their rapid clearance from all tissues. As rapidly as 3-hours the nanotubes were cleared from all organs down to levels of 1-2 % (relative to the 30 minute time point). TEM analysis of urine samples indicated high levels of intact functionalised CNTs showing that they are rapidly cleared from the systemic circulation via the kidney [146]. Subsequently, Lacerda *et al.* presented an elimination mechanism for CNT complexes using [^{111}In]DTPA-MWNT. The CNT complexes were tail vein injected and showed very rapid entry into the systemic blood circulation followed by rapid urinary clearance (Figure 1.10) [157]. The reason for rapid elimination observed here, when compared to CNTs functionalised with surfactants is that once in the blood these surfactants desorbed from the CNTs, which leads to bundles circulating and consequent accumulation in the liver tissue. The mechanism of [^{111}In]DTPA-MWNT elimnations has been shown to be via the kidney glomerular filtration system. It is important to note that [^{111}In]DTPA-MWNT complexes

used in this study were considerably larger than the dimensions of the glomerular capillary wall. Hence, the length does not appear to be a critical parameter in their renal clearance. The mechanism by which CNTs pass through the glomerular filtration system is believed to involve the acquisition of a conformation in which the longitudinal dimension of the nanotube is perpendicular to the glomerular fenestrations, (cross section is between 20-30 nm) and small enough to allow permeation through the glomerular pores [157]. This hypothesis was later confirmed by TEM imaging, where individualised, well-dispersed MWNTs were observed in the renal capillary lumen. During their translocation through the glomerular filtration barrier their longitudinal axis was shown to be vertically oriented to the endothelial fenestrations [158]. Moreover, histological examination of the different tissues confirmed that those MWNT complexes did not induce any physiological abnormality after 24-hours post-injection [159].

Systemic clearance of SWNTs was also demonstrated by NIR. SWNTs were dispersed in a solution of Pluronic-F108 surfactant and injected in rabbits showing that the concentration of nanotubes in the blood serum decreased exponentially with a half-life of 1 hour. Moreover, near-IR fluorescence microscopy on tissue revealed that only SWNTs in the liver were detected at significant levels at 24 hours [160]. Considering the safety and efficacy of CNT-complexes for medical applications issues other than their clearance have to be addressed. They need to achieve good biodistribution and show good target specificity in order to have therapeutic efficacy. The targeted accumulation of CNTs *in vivo* was first demonstrated by Lui *et al.*, using PEGylated SWNTs linked to an arginine-glycine-aspartic acid (RGD) peptide. This modified RGD peptide is a potent integrin $\nu\beta3$ antagonist, aiming the *in vivo* targeting of integrin a vb3-positive tumours in mice via specific RGD – integrin a binding [161]. *In vivo* models of U87MG human glioblastoma and HT-29 human colorectal tumour were used (with an implantation protocol of injection of $5x10^6$ cells in phosphate buffer saline (PBS) into front legs of mice and allowed to reach a tumour volume of 200-300 mm^3). Furthermore, with the purpose of increasing the circulating half-life, two different lengths of PEG chains were used (molecular weight of PEG chains of 2000 and 5400, respectively). The lengths of the PEG molecule influenced biological behaviour, with the longer PEG chain leading to increased blood levels and reduced RES uptake when compared with the shorter chain complex. The explanation for this was suggested to be due to the fact that PEG_{5400} renders SWNTs more hydrophilic and resistant to protein non-specific binding (NSB). These properties were not seen with the CNT complex involving functionalisation with PEG_{2000}, which was unable to

prevent protein NSB to SWNT. In addition, the CNT bound to the RGD peptide, which is a ligand for cell-surface integrins, led to an increased in uptake into the tumour, with PEG_{5400} achieving higher tumour accumulation due to its increased plasma half-life. Moreover, the study used Raman spectroscopy to directly detect SWNT in the various murine tissues. The analysis revealed the existence of SWNT in the liver and tumour samples with high G band Raman intensities, proving the tumour uptake of the complex [161]. Subsequently, Raman spectroscopy was also used to image the localisation of SWNT in live rodents [162]. Similar to the previous study, increased accumulation of RGD-SWNT in tumour was demonstrated, compared to control non-targetted SWNT. These findings demonstrated the ability of Raman spectroscopy to non-invasively localise targeted SWNT *in vivo* [162]. The biodistribution and long-term fate of CNTs injected intravenously *in vivo*, was later studied, using the same technique, of Raman spectroscopy [163]. Besides the enhancement in blood half-life of CNTs (up to 15-hours), SWNT have also been detected in various organs and tissues of mice *ex vivo* over a period of up to 3 months. To study in depth the excretory pathway CNTs were injected at high dose in mice and urine and faeces collected at different time points. There was evidence for CNTs in faeces and intestine revealing excretion via the hepato-biliary pathway. The Raman signal was measured in the kidney and bladder after 24-hours, suggesting SWNTs were also renal excreted, as demonstrated in other studies. Since the average of lengths used in that study exceeded the renal excretion threshold and the majority of CNTs accumulated in the liver, it was suggested the urinary excretion occurs for a small percentage of CNTs of very short length (<50 nm in length, diameter 1-2 nm). The overall conclusion from these studies is that in fact CNTs are excreted chiefly via the biliary pathway, with faecal elimination [163]. In addition, necropsy, histology and blood chemistry reveal no toxicity in mice injected with SWNT with no impact on body weight or mortality [163].

The findings described above have revealed that CNTs can be designed in many ways to form pharmaceutical complexes, which allow them to enter blood circulation, target cells, deliver payloads, be exocytosed and finally eliminated from the body. A variety of approaches have been described above, for example, chemical modification via functionalisation, which increased circulatory half-life and led to enhance tumour accumulation. As a nanoparticle for medical applications, the carbon nanotube shows promise in offering lower toxicity with enhanced efficacy.

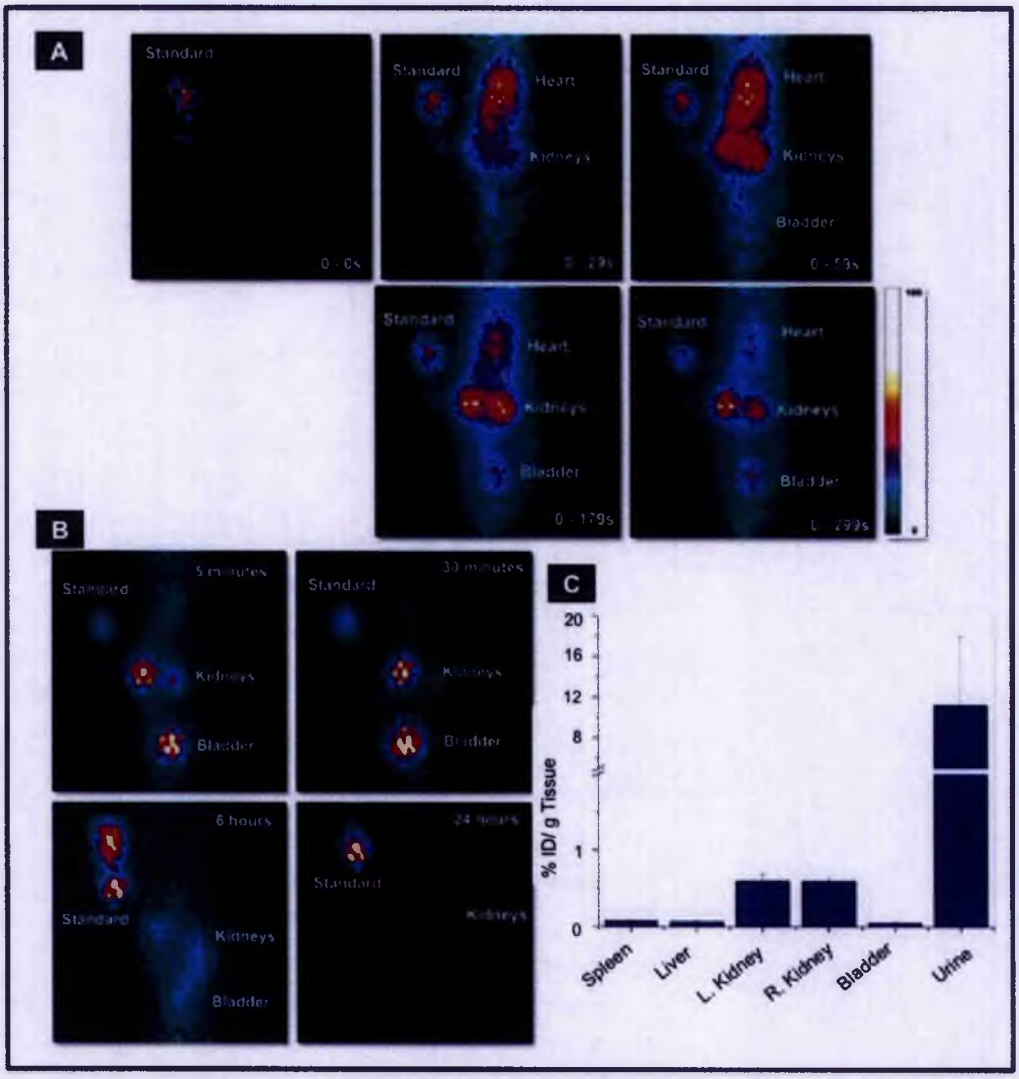

Figure 1.10: Rat distribution of radioactive labelled multi-walled CNTs ([111In]DTPA-MWNT). (A) Dynamic anterior planar images of whole body distribution of [^{111}In]DTPA-MWNT within 5 min after intravenous administration in rats. (B) Static anterior planar images of whole body distribution of [^{111}In]DTPA-MWNT within 5 and 30-minutes, 6 and 24-hours post-injection. (C) % ID radioactivity per gram tissue at 24-hours after intravenous administration of [^{111}In]DTPA-MWNT quantified by gamma counting (n=3 and error bars for standard deviation) (adapted from Lacerda *et al.* 2008 [157]).

1.3.3 Nucleic acid-base delivery using CNTs

Along with the first evidence that CNTs translocate across cell membranes, Pantarotto *et al.* [127] reported the first study using CNTs as a gene delivery system. In their work CNTs were covalently modified using the a method based on the 1,3-dipolar cycloaddition of azomethine ylides [164]. Both SWNTs and MWNTs were functionalised with pyrrolidine ring holding a free amine-terminal oligoethylene glycol moiety attached to the nitrogen atom. The presence of this functional group increases the aqueous dispersibility of CNTs. The delivery of plasmid DNA and the expression of β-galactosidase in Chinese hamster ovary cells (CHO cell line) were evaluated. Like other nonviral gene delivery systems, the amine-functionalised nanotube was able to condensate pDNA to form supramolecular complexes with globular conformations through electrostatic interactions [165]. In addition, they found that the charge ratio between the amino groups at the CNT surface and the phosphate groups of DNA backbone are important factors that determine the level of gene expression. The expression obtained was only 10 times higher than the naked DNA, which is still much less effective than liposomes. On the other hand, they found that DNA-CNT complexes do not wield any mitogenic or toxic effect on the activated lymphocyte, which is in contrast with other nonviral gene delivery vectors, such as dendrimers and liposomes. These traditional non-viral gene deliver systems generally cause destabilisation of the cell membrane and lead to pronounced cytotoxicity whilst achieving effective gene delivery [127]. In the work from Pantarotto *et al.* the lower cytotoxicity was attributed to the ability of the DNA-CNT complexes to penetrate the cell membrane. As described previously (section 1.3.2) the mechanism of internalisation of the amino functionalised CNTs was found to pierce the cell membrane as "nano-needles" [129].

To increase the efficiency of DNA condensation, Liu and colleagues reported a non-covalent association of plasmid DNA onto the surface of CNT functionalised with polyethylenimine (PEI) – a polymer with high density of terminal amine groups [166]. The complexes were tested at different charge ratios in different cell lines (293, COS7 and HepG2 cells) and the level of gene (pCMV-Luc) expression was found to be much higher than those of DNA alone. This study suggested that the uptake mechanism of the CNT–PEI–pDNA conjugates took place by endocytosis. The high transfection efficiency of PEI-MWNTs was attributed to several factors. The first was the secure

immobilisation of DNA onto the surface of MWNTs, which leads to the formation of stable complexes that protect the DNA from degradation. The second factor is that the proton-sponge effect of the grafted PEI would allow the DNA-PEI-MWNT complexes to escape easily from endosomes or other vesicles in the cells [167]. In addition, the large complexes of DNA-PEI-MWNTs would improve the proton-sponge effects of the PEI and facilitate a more effective sedimentation onto the cells [168].

In support of the above, Wang *et al.* employed ammonium-functionalised SWNTs to deliver siRNA targeted to cyclin A_2 in chronic myelogenous leukemia K562 cells, resulting in suppression of cyclin A_2 expression [169]. The depletion of cyclin A_2 causes cell proliferation arrest and promotes apoptosis of chronic myelogenous leukemia K562 cells. Furthermore, the described ammonium-functionalized SWNTs were applied to mediate the delivery of telomerase reverse transcriptase (TERT) siRNA into tumour cells [170]. TERT is an essential gene for development and growth of tumours, therefore the treatment with SWNT-TERT siRNA complexes led to suppression of cancer cell growth. Through injection of these complexes to mice bearing Lewis lung carcinoma tumour or HeLa cell xenografts, tumour growth was inhibited and the average tumour weight was significantly reduced when compared with untreated animals. A second report on SWNT mediated nucleic acid delivery *in vivo* was carried out by Podesta *et al.* [171]. SiRNA was employed for the treatment of a human lung carcinoma model, by delivery of ammonium-functionalized MWNTs. The results demonstrate that MWNT-NH_3^+:siRNA complexes were active by triggering an apoptotic cascade, leading to extensive necrosis of the human tumour mass and increased survival of tumour-bearing animals. This work provided the first comparative *in vivo* study comparing "benchmark" nanoparticles, such as liposomes with CNTs. In this work they found that MWNT-NH_3^+:siRNA complexes were more effective in prolonging the survival of tumour-bearing animals, presumably due to their facile translocation into the tumour cell cytoplasm (Figure 1.11) [171]. Although, the complexes were administered by intra-tumourai local injection the work seems promising for the development of new therapeutic formulations to battle various diseases.

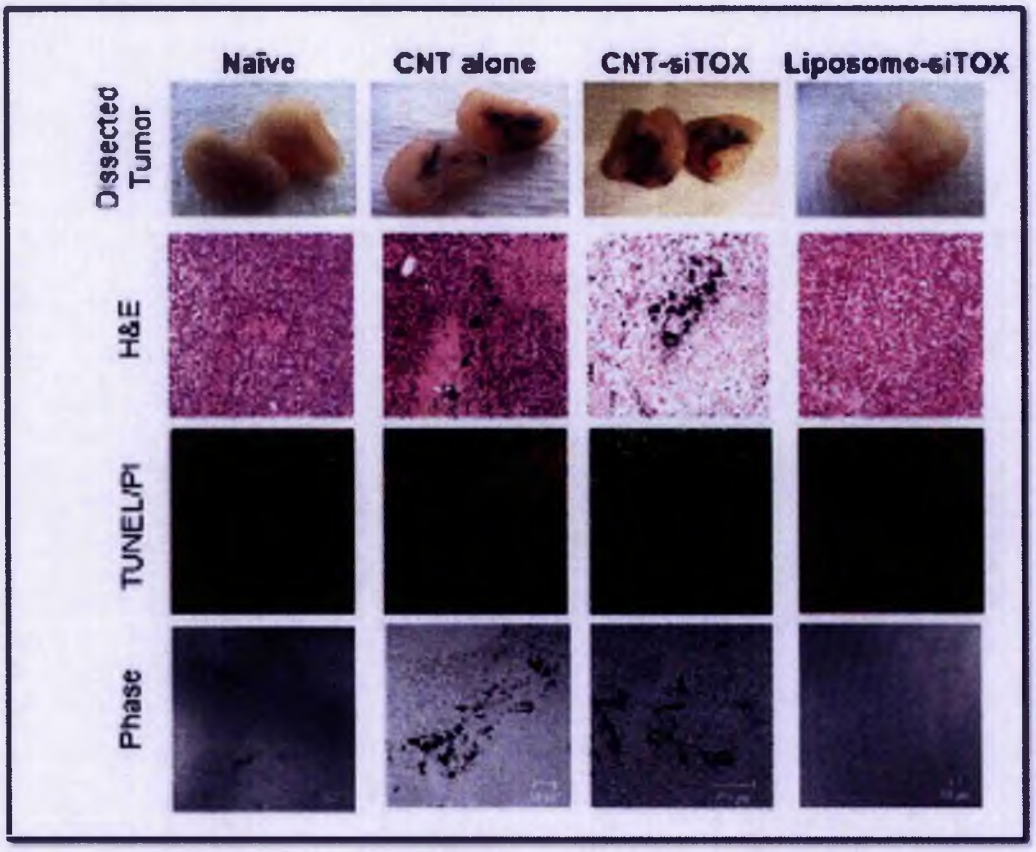

Figure 1.11: A proprietary toxic siRNA sequence (siTOX) was complexed with either one of the most widely used cationic liposome delivery systems (DOTAP:cholesterol) or with functionalized multi-walled CNTs (f-MWNTs). MWNT-NH3+:siTOX complexes induced tumour collapse and apoptosis of human Calu 6 lung xenograft tumours. Whole tumours were excised upon reaching 800–1000 mm^3 and photographed. Top-row images (left to right) are representative tumours from naïve, MWNT-NH3+ alone, MWNT-NH_3^+:siTOX, and liposome:siTOX groups. Tumours were then fixed in 10% buffered formalin, paraffin embedded, and sectioned. Haematoxylin/eosin (H&E) staining was performed (second row) or sections were deparaffinised and rehydrated through graded ethanol; then TUNEL and propidium iodide (PI) nuclear counterstain were used to identify apoptotic (green) cells from the total cell population (red, third row). Phase images of corresponding fields of view for TUNEL/PI are shown in the last row to indicate MWNT-NH_3^+ localisation (adapted from Podesta *et al.* 2009 [171]).

Another SWNT mediated *in vivo* delivery of siRNA for tumour therapy was published in 2006 by Yang *et al.* [172]. In this study they believed that phagocytosis was the mechanism by which functionalised SWNTs entered cells. Based on the mechanism they hypothesised that *i.v.* delivered SWNTs might be preferential engulfed *in vivo* by antigen-presenting cells that possess phagocytic potential, such as dendritic cells and macrophages. The experimental results demonstrated that *i.v.* injection of siRNA-SWNT complexes significantly reduced tumour growth after 15 days while siRNA alone or the mock SWNTs complex had no significant effect. This group was also involved in the development of an approach for target delivery of DNA mediated by SWNTs [173]. First, double stranded DNA (20 bp) was complexed with ammonium-functionalised SWNTs, and then the obtained complex was mixed with phospholipid-PEG containing a tumour targeting moiety (folic acid), followed by sonication in an ice bath for 30 min and agitation in the dark for 24 hours. Although the authors did not test the therapeutic effect of this targeting DNA-complex they found that the complex had good cell targeting properties.

Dai and colleagues have developed "smart" DNA/siRNA delivery systems based on SWNTs [121, 174, 175]. In contrast to the approaches described above, DNA and siRNA cargos can be controllably released from the carbon nanotube surface upon cellular uptake for efficient targeting and deliver [55]. Firstly, their work started with conjugation of antisense ONs or siRNAs onto functionalised CNTs by incorporation of biologically triggered cleavable bonds [174]. The first step involves making a stable aqueous suspension of short SWNTs by non-covalent adsorption of phospholipid molecules with poly(ethylene glycol) (PL-PEG) chains and terminal amine or maleimide groups. The PL-PEG strongly binds to the SWNTs via Van der Waals and hydrophobic interaction, via two PL alkyl chains and the SWNT sidewall, with the PEG chain extending into the aqueous phase to impart the dispersibility in water. The suspension is very stable in PBS buffer even if heated at 70 °C for weeks. Thiol-modified DNA or siRNA cargo molecules can be linked to the amine or maleimide groups on the sidewalls of SWNTs through cleavable disulfide bonds, which can be cleaved by thiol reducing enzymes thus releasing the cargos from the SWNTs once the conjugates are internalised into the endosomal or lysosomal compartments through endocytosis. The released cargos can freely reach their intended biological destination.

This system was employed to deliver siRNA into human T cells and primary cells that are difficult to transfect by traditional nonviral agents, like liposomes [175]. They found

that the delivery ability and RNAi efficiency of these CNTs far exceed those of several existing nonviral transfection agents including four formulations of liposomes. The high efficiency observed for CNTs was attributed to the large surface area of SWNT for siRNA loading, high intracellular transporting ability of SWNTs and high degree of endosome/lysosome escape due to intracellular cleavage of the disulfide bond.

CNTs were also studied for innovative methods for nucleic acid delivery into cells. Rojas-Chapana *et al.* [176] reported that CNTs can be used as nanoscale "electroporation vectors" to deliver plasmid DNA into bacteria, taking advantage of the unique shape (large aspect ratio) and electronic properties of CNTs. Under microwave radiation, MWNTs created temporary transmembrane "nanochannels" to facilitate plasmid DNA delivery into cells. When placed in an electric field, charges are induced on the tip of CNTs and the electric field at the tips drastically enhanced by a factor if 10-100 depending on their length to diameter aspect ratios.

Along a similar line, Cai *et al.* [177] proposed a spearing technique for cellular internalisation of CNTs and plasmid DNA. CNTs containing ferromagnetic nickel catalyst particles enclosed on their tips can respond to a magnetic agitation. The spearing technique involves a two-step procedure. First the cells and CNTs are exposed to a magnetic field. This allows the CNTs to spear the cell membrane. Next the cells are transfected to fresh medium and a static field is applied that enhances the spearing procedure and pulls the CNTs into the cell. The expression of the enhanced green fluorescent protein (EGFP) gene was evaluated by fluorescence microscopy and flow cytometry. Gene delivery through CNT-Ni produced 80–100% fluorescent cells, while CNT deprived of Ni particles did not produce any fluorescence signal. In this way, another illustration of the possible use of CNT to transport and express a gene was demonstrated. However, such techniques are only appropriate for *in vitro* or *ex vivo* gene transfer.

1.3.4 CNTs-mediated delivery of drugs

CNTs have been, in the recent years, intensively investigated as a new type of drug delivery system, as they can be can be loaded with therapeutic molecules on their surface and the inner cavity. Furthermore, due to their high surface area other therapeutic and diagnostic molecules can be conjugated, such as targeting or imaging agents.

One of the first studies on the use of CNTs for drug delivery was carried out by Wu and co-workers in 2005, who conjugated the antibiotic amphotericin B to MWNTs [178]; a drug considered problematic due to its narrow therapeutic index and poor aqueous dispersibility. Both issues could be improved by conjugating amphotericin B to MWNTs, which reduced the toxicity of the drug and mantained its antifungal activity. As stated previously, nanoparticles hold great promise in the area of new cancer therapeutics and both *in vitro* [119, 179-185] and *in vivo* [186-189] systems have been the subject of extensive study. So far, SWNTs have been the preferred type of nanotubes, perhaps owing to their smaller dimensions. In terms of functionalisation, several covalent and non-covalent methods have been developed, according to the therapeutic requirements. Non-covalent binding, for example, is susceptible to environmental factors, such as pH and salt concentration, and it is in general less stable than a covalent bond. This may be a disadvantage for efficient attachment of the drug, but advantageous for its release at the target location. In contrast to this, covalent attachment of drug molecules to CNTs provides a strong and stable chemical bond, but needs to include a part that is cleavable within intracellular conditions to allow for release of the drug. In almost all cases, this is facilitated by the reductive environment in the cytoplasm. For example, Chen and co-workers conjugated a taxane to SWNTs via a cleavable disulfide bond [179], based on former work of Kam *et al.* [174]. Similar to this, two other studies on the delivery of cisplatin as a platinum(IV)-prodrug accomplish drug release by intracellular reduction of platinum(IV) to its active form platinum(II) under concomitant loss of the axial ligands, by which the drug is tethered to the nanotube surface [182, 190]. Regarding to non-covalent approaches, the release of drugs inside the target cells is often pH-dependent. A typical example is the non-covalent binding of the anticancer drug doxorubicin to CNTs via π-π interactions. At a high pH, the amino group in the sugar moiety of doxorubicin is deprotonated, promoting strong hydrophobic interactions with the nanotubes' sidewalls and a low dispersibility in water. However, at a lower pH the

amino group becomes protonated and thus charged, which increases the molecule's hydrophilicity and dispersibility in water. This property can be used in relation to cellular uptake pathways based on endocytosis, as first demonstrated by Liu *et al.*, who showed that the lower pH environment inside endosomes triggered the release of doxorubicin from SWNTs due to increased hydrophilicity [191]. Work in our lab has further investigated the fate of doxorubicin-loaded CNTs by labelling the nanotubes with a fluorescent dye and visualising the separate localisation of the drug and of the nanotubes upon cellular uptake by confocal microscopy. It could be demonstrated that doxorubicin is indeed released inside the cells and translocates to the nuclei, whereas the nanotubes remain in the cytoplasm [185]. An entirely different strategy in terms of drug loading has been applied by Hempel *et al.*, who filled MWNTs with the anticancer drug carboplatin by a wet chemical approach [183]. *In vitro* studies revealed a concentration-dependent cytotoxic effect of carboplatin-filled nanotubes on human bladder cancer cells in contrast to unfilled, opened nanotubes - however, the study did not provide quantitative data on the release of carboplatin from their nanotube container.

The already described aspect of active targeting (section 1.1.1), by which agents are attached on the surface of the carrier, may involve antibodies, aptamers or ligand binding to cell surface receptors. A widely-employed example in this category is the attachment of cyclic arginine-glycine-aspartic acid (RGD) peptides to CNTs, as shown by Liu *et al.* and Villa *et al.* [187, 188]. RGD peptides impart a recognition moiety for integrin $\alpha_v\beta_3$ receptors; a class of transmembrane cell adhesion receptors that are up-regulated in a variety of solid tumours. A similar strategy exploits the interaction of folate and its receptor, which is a common, though relatively non-specific tumour marker expressed at high levels by a broad spectrum of human cancers [186]. Binding of folate to its receptor facilitates cellular internalization of folate-conjugated SWNTs by receptor-mediated endocytosis, as shown by Dhar *et al.* [184]. Antigen-antibody interactions have also been employed as a targeting strategy for carbon nanotube-mediated drug delivery, though not very frequently. For example, McDevitt *et al.* designed a SWNT-antibody construct to target the CD20 epitope on human Burkitt lymphoma cells (U-937 cell line) and deliver a radionuclide to these cells, whilst quantifying tumour uptake *in vivo* [186]. Their study showed that covalent attachment of antibodies to the nanotube conjugates altered their pharmacokinetics and biodistribution dramatically when comparing tumour bearing and non-tumour bearing mice. In the same year, Shao and co-workers reported that SWNTs functionalised with HER2- and IGFR1-specific antibodies showed selective

attachment to breast cancer cells compared to SWNTs functionalised with non-specific antibodies [192].

Successful targeting and sufficient therapeutic efficacy *in vitro* are the prerequisites for testing drug delivery systems in an *in vivo* setup, which has so far been achieved by three published studies. In 2007, McDevitt *et al.* reported the design a SWNT-CD 20 antibody construct to deliver a radionucleotide to mice bearing lymphoma xenografts [186]. Apart from the targeting aspect and quantification of tumour uptake, this study was one of the first to yield information regarding blood clearance and the distribution of the nanotube complexes to key organs. In 2008, Liu *et al.* conjugated paclitaxel, a widely used anticancer drug, to branched PEG chains on SWNTs and tested these carbon nanotube-based drug delivery vehicles to achieve efficient *in vivo* tumour treatment in mice [187]. The conjugate afforded similar efficacy in *in vitro* experiments and a higher efficacy in suppressing tumour growth than paclitaxel in a murine 4T1 breast cancer model, owing to prolonged blood circulation and 10-fold higher tumour uptake of paclitaxel by nanotube delivery; likely mediated by the EPR effect (Figure 1.12). In a very recent study by Bhirde and co-workers, SWNTs were functionalised with the anticancer drug cisplatin, epidermal growth factor (EGF) as a targeting agent, and quantum dots as imaging agents [189]. These conjugates were injected into mice bearing a head and neck squamous carcinoma tumour xenograft and tumour growth was monitored for two weeks. Mice treated with the targeted conjugates showed a rapid decrease of tumour size, whereas mice treated with a non-targeted nanotube-cisplatin conjugated did not show tumour regression.

Drug delivery is clearly one of the most promising bioapplications of CNTs and the coming years will reveal their true potential in comparison with more established drug delivery systems.

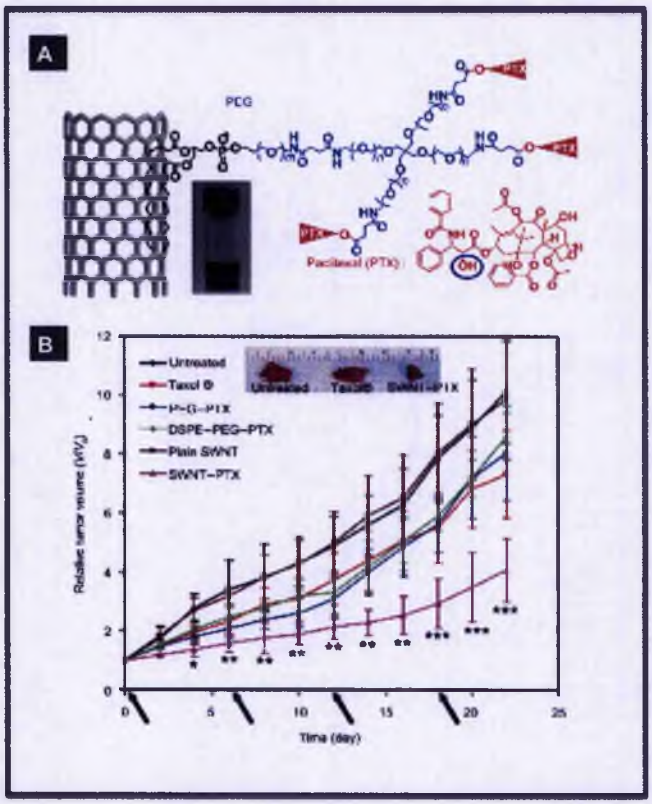

Figure 1.12: *In vivo* drug delivery with CNTs for cancer treatment. (A) Illustration of paclitaxel conjugation to SWNT functionalised by phospholipids with branched PEG chain. (B) Tumour growth curves of tumour-bearing mice receiving the different treatments indicated. The same PTX dose (5 mg/kg) was injected on days 0, 6, 12 and 18. Inset: A photo of representative tumours taken out of an untreated mouse, a taxol treated mouse and an SWNT-PTX treated mouse and the end of the treatments (adapted from Liu *et al.* 2008 [187]).

1.3.5 CNTs as selective cell destruction agents

Apart from destroying diseased or dysfunctional cells by delivering drugs and therapeutic nucleic acids, CNTs can also be applied for selective cancer cell destruction by acting as NIR heating devices. This technology is based on the fact that biological systems are highly transparent to NIR light, whereas CNTs exhibit a strong optical absorbance in this spectral window. Thus, treating tissue or cell layers after internalisation of CNTs with continuous NIR radiation can cause cell death due

to excessive local heating. The first study to demonstrate this effect was published by Kam *et al.* in 2004 [121]. In their work, SWNTs functionalised with phospholipid-PEG and folate as a targeting moiety were incubated for 12-18 hours with HeLa cervical carcinoma cells over-expressing the folate receptor. After abundant washing, the cells were irradiated continuously with an 808 nm laser (1.4 W/cm^2) for 2-minutes, causing drastic morphology changes and extensive cell death. HeLa cells that did not overexpress the folate receptor, however, did not internalise the nanotubes and were thus not affected by the laser treatment. A similar study by Shao *et al.* in 2007 used the same method, but a different targeting strategy [192]. In their approach, SWNTs were functionalised with antibodies targeting the insulin-like growth factor 1 receptor (IGF1R) and the human epidermal growth factor receptor 2 (HER2), both over-expressed by certain breast cancer cell lines. Unoccupied surface spaces on the nanotube surface were coated by PEG_{8000}, which supposedly formed a self-assembled monolayer to prevent undesirable binding with other molecules. Following incubation of MCF7 breast cancer cells (over-expressing IGF1R) and BT474 breast cancer cells (over-expressing HER2) with the SWNT-antibody conjugates, laser light of 808 nm (0.8 W/cm^2) was dosed for 3-minutes to all samples. The localized photo-thermal effect produced heat that lead to complete destruction of the cells when targeted with the specific nanotube-antibody conjugate. Targeting with non-specific antibody conjugates only caused minor collateral damage. In a more recent study, Chakravarty *et al.* have designed and prepared anti-CD22 and antiCD25-targeted SWNT constructs to thermally ablate human Burkitt's lymphoma cells (U-937 cell line) ($CD22^+CD25^-$) and peripheral blood mononuclear cells (PBMCs) ($CD22^-CD25^+$) *in vitro* [193]. Once more, it could be demonstrated that the binding of the antibody-nanotube constructs to their respective antigen-positive target cells leads to their specific ablation after exposure to NIR light. Compared to the earlier studies, a higher laser power (5 W/cm^2) and a longer radiation time (7-minutes) was applied in these experiments. A novel approach using carbon nanotube-mediated hyperthermia based on heat release in a radio frequency field was pursued by Gannon *et al.* to produce thermal cytotoxicity in malignant cells *in vitro* and *in vivo* [194]. Exposure to a 13.56 MHz radio frequency field induced efficient heating of aqueous suspensions of SWNTs. This effect was used to induce non-invasive, selective, and SWNT concentration-dependent thermal destruction of human cancer cells having internalised SWNTs. Furthermore, direct intratumoural injection of SWNTs in rabbits bearing hepatic tumour xenografts was shown to lead to complete necrosis of all SWNT-treated tumours after 48 hours, whereas control tumours without SWNTs

remained completely viable. Another study recently published by Kang *et al.* used the photoacoustic effect of SWNTs for targeting and selective destruction of cancer cells via a "firecracker-like explosion" at the nanoscale triggered by irradiation of a 1064-nm Q-switched millisecond pulsed laser [195]. The treatment was targeted by functionalising SWNTs with folic acid, causing 85 % cell death compared to 10 % cell death for the non-targeted SWNT sample. It should be noted that during the treatment no temperature changes exceeding ± 3 °C were observed, suggesting that the destructive effect of nanotubes on cancer cells is mainly due to mechanical damage induced by the strong shockwave generated during the photoacoustic explosion, rather than a thermal damage caused by high temperatures as in studies mentioned previously. This approach might, therefore, provide a new mechanism for using the photoacoustic properties of SWNTs in therapeutic and biological imaging applications.

As for other biomedical applications, the use of CNTs for selective cancer cell destruction is still in an early developmental state. Only three *in vitro* studies have been published in five years of research on CNTs as NIR heating agents, which indicates the difficulties encountered with this approach. The next few years will most likely show whether this area of application deserves to be further investigated. Even less reported is the approach of magnetic hyperthermia based on the incorporation of magnetic materials into CNTs, which provides more efficient heat transfer to deep tissues than the NIR approach and allows for positioning and induction of local heating effects by a combination of static and alternating external magnetic fields at the same time [196]. Although much has been achieved regarding the filling of CNTs with magnetic materials, there are still no studies investigating magnetic heating effects of filled CNTs in cells, tissue or living systems to date. Hence, CNTs as heating agents are currently inferior in comparison to magnetic nanoparticle-based systems, which are already being used successfully in the clinic [197]. However, the NIR heating effect of CNTs is a unique property of this material and requires further investigation, although its application in cancer therapy will always be restricted to surface tissues, since NIR light is only capable of passing through several centimetres of tissue and its interaction with biological matter is by far larger than that of magnetic fields [196].

1.3.6 CNTs toxicity

Undeniably, CNTs are emerging as one of the key innovative materials for biomedical applications, which may bring revolutionary strategies to solve some current untreatable diseases and help solving fundamental biological issues. However, their potential toxic effects have become an issue of considerable concern for the environment and human health. Therefore, the successful application of CNTs in medicine is dependent on proper assessment of the potential hazards to humans and other biological systems [55].

In the literature titles such as "Pulmonary toxicity of single-wall carbon nanotube in mice 7 and 90 days after intratracheal instillation" [149]; "Unusual inflammatory and fibrogenic pulmonary responses to single-walled CNTs in mice" [151]; "CNTs introduced into the abdominal cavity of mice show asbestos-like pathogenicity in a pilot study" [198]; "DNA damage induced by multi-walled CNTs in mouse embryonic stem cells" [199]; "Direct and indirect effects of single-walled CNTs on RAW 264 7 Macrophages: Role of iron" [200] are frequent. On the other hand many other published work, present consistent results showing internalization, imaging, targeting, biodistribution and therapy with no toxic effects [117, 121, 126, 127, 131, 139, 146, 177, 200-210]. In Table 1.3 is presented a compilation of some *in vitro* and *in vivo* studies of CNT toxicity. The discrepancies and large diversity in conclusions reported for a number of studies in the literature are an outcome of the application of CNTs with a wide range of distribution of tube diameters, lengths, and chiralities produced by the current synthesis methods. In addition to the different functionalisations, varied degrees of functionalisation, and plethora of functionalisations have been employed. Therefore, explicit discrimination of toxicity of CNTs and implementation of precise measurements, complete characterisations, and the use of well-defined high precision materials is mandatory. In addition, the use of different protocols, cell lines, and animal models in evaluating the toxicity and long term fate of CNTs may be very important reasons for the inconsistency. Standard experimental protocols (including but not limited to animal models, cell assays, quantification, and characterisation methodologies) should be established so that studies may be compared across laboratories [55].

Table 1.3: Compilation of CNTs toxicity studies *in vitro* and *in vivo*. (adapted from Ji *et al* 2010 [210])

***In vitro* studies**

Reference	Cells	CNTs	Length (μm)	Purity (wt%)	Solubilizer	Concentration (μg/mL)	Duration of exposure	Toxicity
Bottini *et al* [211]	Human T Lymphocytes	Pristine and oxidised MWNTs	1-5	> 95	Water	40	5 days	Loss of >80% of cells
Sayes *et al* [212]	Human dermal fibroblasts (HDF)	Different degrees of functionalised SWNTs	< 1	> 95	1% Plutonic F108	3-30000	48 hours	The more functionalised SWNT becomes, the less cytotoxic it is
Wick *et al* [213]	Mesothelioma cell line MSTO-I 1H	CNT agglomerates CNT bundles	Unknown	97.1 94.2	PS 80	30	3 days	~ 25 % viable cells ~ 50 % viable cells
Pryluska *et al* [214]	Rat erythrocytes and thymocytes	MWNT	1-4	> 95	Water	5-25	24 h	No effect on cell viability
Cheng *et al* [215]	Mature human monocyte-derived macrophage (HMM) cells	Unpurified MWNT Purified MWNT	26±22.7 12±9.9	93.8 99.9	BSA and PBS	20	4 days	57 % viable cells 65 % viable cells
Simon-Deckers *et al* [216]	A549 human pneumocytes	Long MWNT Short MWNT	0.1-3.5 0.1-1.2	> 95	Water	50	48 h	10% cell death

***In vivo* studies**

Reference	Animals	CNTs	Purity (wt%)	Dosage	Duration of exposure	Route of administration	Toxicity
Muller *et al* [217]	SD rats female 200-250 g	MWNTs	> 95	0.5, 2 or 5 mg/animal	2 months	Intratracheally	Formation of granulomas in the bronchial lumen; alveolitis in the surrounding tissues
Yang *et al* [218]	CD-ICR mice male, ~25 g	SWNTs	> 95.4	40-1000 μg per mouse	3 months	Intravenously	Only serum biochemical changes; no obvious cell apoptosis
Miyawaki *et al* [219]	Wistar rats SPF, male, ~130 g	SWNTs	> 90	17.3 mg/kg	2 months	Intratracheally	No mortality; rare for all animals group, black lung spots and anthracosis
Schipper *et al* [220]	Nude mice	SWNTs	Unknown	151 mg totally	4 months	Intratracheally	Without apparent toxicity
Poland *et al* [197]	C57B1/6 mice female	MWNTs	Unknown	50 μg/animal	7 days	Intraperitoneally	Inflammation and formation of granulomas on the peritoneal side of the diaphragm
Yang *et al* [221]	BALB/C nu/nu male	Magnetic MWNTs	> 95	0.94 mg/animal	15 days	Subcutaneously	No clinical signs of abnormalities; no particle agglomerates in major organs

1.4 Thesis hypothesis and aim

RNA-wrapped CNTs have several potential advantages for biomedical applications in comparison with DNA. DNA has been shown to efficiently functionalise CNTs and has been used for several studies [132, 223-225], as discussed above. Firstly, unlike DNA, RNA cannot integrate directly into the host chromosome and is therefore less likely to be mutagenic [226]. Secondly, modification of RNA has been shown to suppress recognition by the mammalian immune system [227]. Modified RNA-wrapped CNT may therefore be able to bypass the host immune system and more efficiently deliver their payload to the host cells. Thirdly, unlike DNA (which has to be transcribed), RNA is directly functional in cells. RNA released from CNT may be translated to yield a protein, may act as antisense RNA to inhibit protein synthesis, or may act as interfering RNA (RNAi) to silence a target gene.

More recently, RNAi approach is being intensively investigated as a therapeutic strategy for gene targeting and holds great promise for targeted cancer therapy.

The hypothesis of this thesis is that CNT are able to be internalised and deliver their cargo into particular cellular compartments. Therefore, research will be carried out to explore the uptake of CNT and their intracellular localisation and trafficking through cells. Studies regarding the efficiency of CNT construct were also assessed in particular cell lines in order to demonstrate *in vitro* feasibility to target cancer genes. Therefore, the individual objectives of this thesis are as follow:

1. Study the cellular uptake of RNA-wrapped CNTs in mammalian cells, with full characterisation of complexes and measurement of cytotoxic effects.
2. Study the uptake mechanism by which CNTs are internalised by mammalian cells and determine the intracellular localisation of the complexes by compartmental staining
3. Determine the ability of CNTs to deliver nucleic acids, and evaluate its capability for gene expression and gene silencing.
4. Investigate the feasibility of CNT-siRNA complexes to target specific cancer genes (e.g. the anti-apoptotic factor *survivin*).

Chapter 2: General methods

This chapter includes the description of the methods applied, as well as a description of the primary material of study: the CNTs. Owing to the multi-disciplinary nature of this project, a variety of techniques were employed, including: microscopy, spectroscopy and other chemical analysis; and also techniques used routinely in molecular biology.

2.1 Introduction to CNTs

CNTs were discovered by Sumio Iijima in 1991. CNTs are molecular-scale tubes of graphitic carbon, and they are members of the fullerene structural family. Their name is derived from their size, since the diameter of a nanotube is in the order of a few nanometers (approximately 1/50,000th of the width of a human hair) and, up to several millimetres in length. CNTs possess a unique and fascinating one-dimensional nanostructure, which impart a formidable range of properties to the nanomaterial, such as tremendous strength [228], high thermal conductivity [136] and amazing electronic properties, ranging from metallic to semiconducting [229-232]. They can exist in three forms: SWNT, MWNT (figure 2.1) [29] and double-walled nanotubes (DWNT). DWNTs are intermediary in structure between SWNT and MWNT. The main interest in this material is the possibility of functionalisation of the outer wall, which will ensure the contact with the external environment, while retaining the remarkable mechanic and electronic properties of the inner wall. For these reasons we have employed DWNT in all our studies.

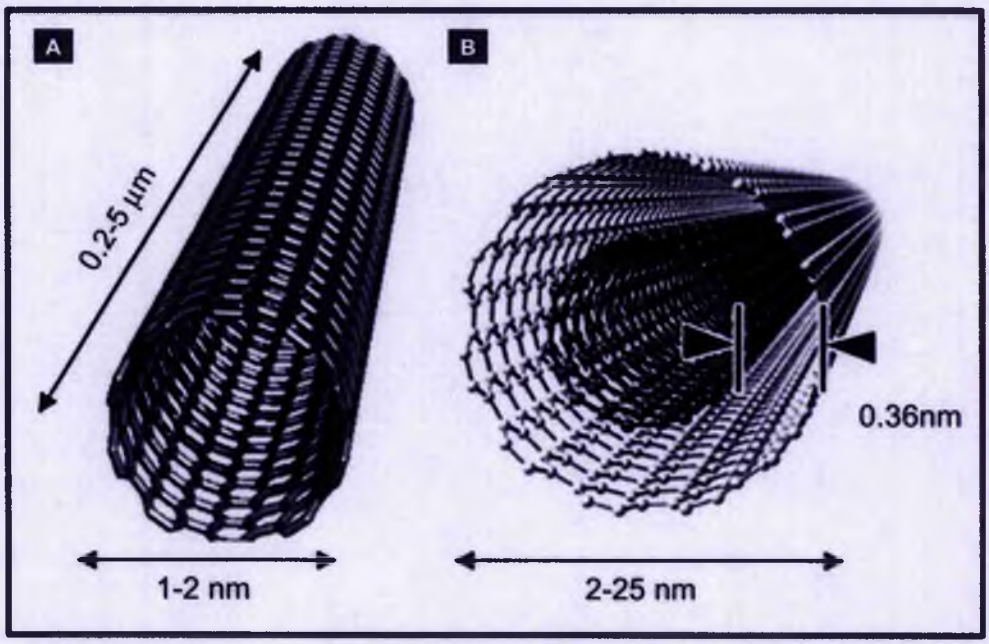

Figure 2.1: Carbon nanotube structure. Molecular structures of defect free SWNT (A) and MWNT (B) with open ends, showing typical dimensions of length, width, and separation distance between graphene layers in MWNTs (adapted from Reilly *et al.* [233]).

2.2 Synthesis of CNTs

CNTs can be synthesised mainly by three procedures: laser evaporation, carbon arc discharge and catalytic chemical vapour deposition (CCVD). All these synthesis techniques use metallic catalysts for the decomposition of the carbon source. Depending on the technique the metals can be mixed with: (a) carbonaceous solid electrodes – arc discharge - or target – laser ablation method, or included in a substrate (substitution, impregnation) in the case of CCVD.

DWNTs applied in the present work were produced by the CCVD technique. The mechanism of nanotube "growth" during production is not fully understood. Since the metal catalyst is necessary for the growth of SWNTs, it must involve a role for the Co or Ni atoms. One proposal, referred to as the "scooter mechanism", suggests that atoms of the metal catalyst attach to the dangling bonds at the open end of the tubes,

and that these atoms scoot around the rim of the tube, absorbing carbon atoms as they arrive [234].

Generally, when nanotubes are synthesised, the result is a mix of different kinds of CNTs, some being metallic and some semiconducting, depending on their geometrical characteristics, namely their diameter and the orientation of the hexagons with respect to the nanotube axis (chiral angle) [230, 231, 235]. CNTs of different structures can be produced considering the way the graphite sheet is rolled up. They can be of an "armchair" structure, when the C–C bonds of the carbon hexagons are parallel. And when the tubes have different orientations in the graphite plan, they can have a zigzag or chiral structure. The raw material that is produced, contains up to 70 % CNTs by weight. The contaminants are mainly amorphous carbon and catalyst particles, which can be removed by treatment with oxidizing acids [113, 236-241], microfiltration [242], or chromatographic procedures [243, 244].

2.2.1 Synthesis of DWNT by catalytic chemical vapour deposition (CCVD)

In this work, DWNT were prepared by CCVD synthesis prepared by Flahaut *et al.* (our collaborators from CARBIO network in Toulouse). DWNTs were produced by CCVD decomposition of CH_4 over $Mg_{1-x}Co_xO$ solid solution containing small addition of molybdenum in a CCVD reactor (Figure 2.2). After the CCVD the catalyst and by-products were removed by treatment of the sample with a concentrated aqueous HCl solution. High-resolution transmission electron microscopy showed that a typical sample consists of *ca.* 80% DWNTs, 20% SWNT, and a few triple-walled CNTs. The diameter distribution of the DWNTs ranged from 0.5 to 2.5 nm for inner tubes and from 1.2 to 3.2 nm for outer tubes. The length of individual DWNTs usually ranges between 1 and 10 micrometers, although bundles may be much longer (up to 100 micrometers at least). Due to the synthesis and catalyst-elimination process, the walls of the DWNTs are not expected to have been functionalised (and in particular not by oxygen-containing functional groups) [245].

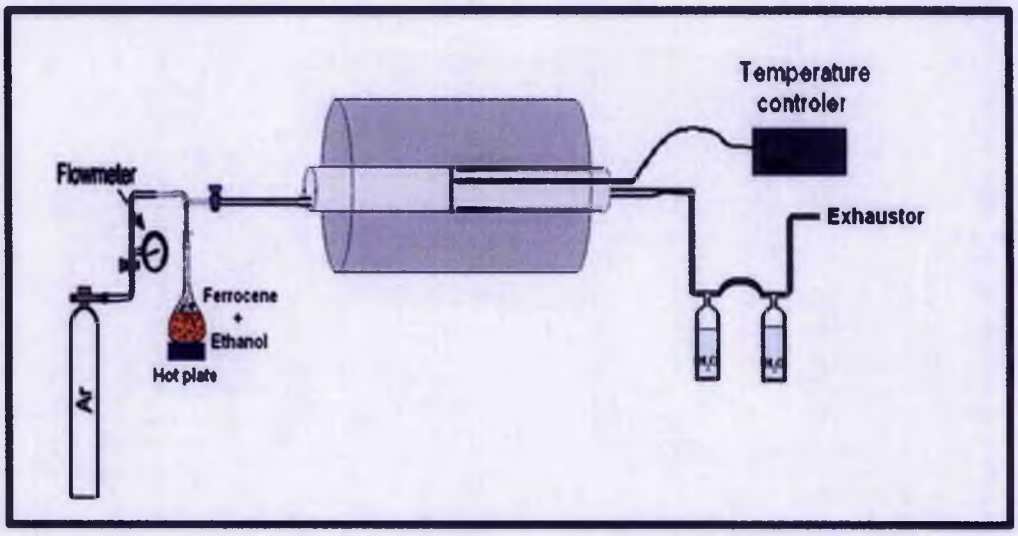

Figure 2.2: CCVD reactor. Consisting of a horizontal quartz tube housed in a cylindrical furnace, in which a constant nitrogen gas flow rate is maintained at pressures slightly above the atmospheric, in order to provide the condition of a laminar gas flow. A Pyrex flask containing the reagent mixture (composed by a carbon precursor and a catalyst source) is connected, via T joint, to the tube close to the nitrogen inlet. A heater plate is located below the flask [246].

The final product obtained typically has an 97.7 mol% carbon content and the HRTEM observation did not reveal any significant amorphous deposit on the CNTs. The CNTs were mainly isolated, or gathered into small bundles, mainly composed of DWNTs (Figure 2.3A). Analysis of HRTEM of 96 isolated CNTs images revealed the diameter distribution of CNTs (Figure 2.3 B, C and D). The distribution of CNTs *vs.* number of walls (Figure 2.3B) shows that final product contains mainly DWNTs (77 %) and only 18 % of SWNTs or 5 % triple-walled CNTs. The distributions *vs.* diameter for all 96 CNTs and for the DWNTs alone are shown in Figure 2.3 C and D respectively. The inner and outer diameters range from 0.53 to 2.53 nm and from 1.23 to 3.23, respectively [247].

In addition, Raman analysis revealed that the ratio between the intensity of the D and G band is close to 8.9 % and that the analysis of the radial breathing mode (RBM) indicates the presence of CNTs with diameters ranging from 0.7 to 2.13 nm, with many pairs of peaks (with a difference of about 0.7 nm between the corresponding diameters), which could correspond to the inner and outer diameters of DWNTs [247, 248].

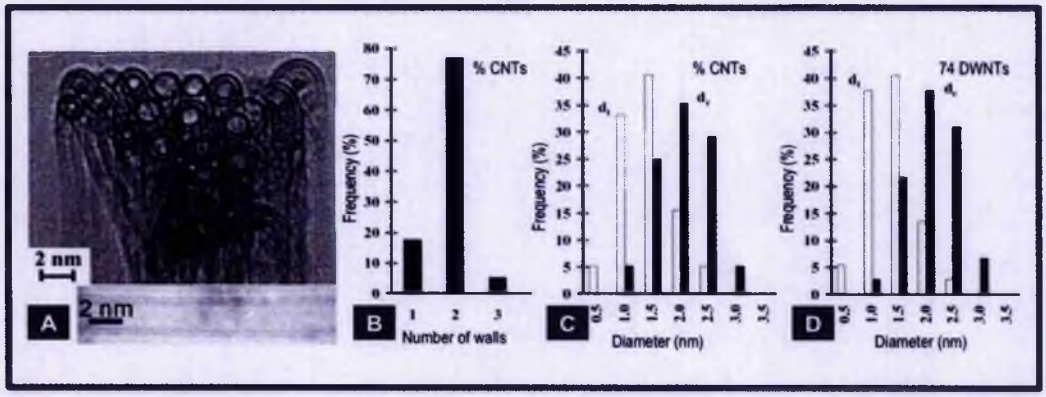

Figure 2.3: HRTEM characterisation of DWNT synthesised by CCVD. (a) HRTEM images of DWNTs and (b) distribution of the numbers of walls for the whole population (established from 96 individual CNTs). Distribution of inner (*di*) and outer (*do*) diameter for the whole population of CNTs (c) and for DWNTs only (d) (adapted from Flauhaut *et al.* [247]).

2.3 Purification of CNTs

As-prepared CNTs (pristine nanotubes) usually contain impurities, which can be divided into carbonaceous impurities and metal catalyst particles. These impurities can interfere with the desired properties of the nanotubes. Therefore, many purification techniques have been developed to improve the quality of the raw carbon nanotube material.

Acid oxidation of CNTs can gasify amorphous carbon and oxidise metallic catalyst particles, which then become disperse in the acid. However, it also opens up the tubes' ends and introduces carboxylic groups to the ends and results in further defect sites [249]. This can be useful if the nanotubes are to be further functionalised by covalent coupling chemistry. In summary, acid oxidation is considered to be a very efficient process, resulting in the formation of very short tubes (pipes) 100 - 300 nm in length [113]. However, with under these harsh conditions, there can be a loss of up to 90% of the initial material [250].

2.3.1 DWNT acid oxidation

Herein, as-prepared CNTs were purified by a two-step procedure based on acid oxidation. In the first step, 100 mg CNTs were dispersed in 20 mL concentrated nitric acid, sonicated with a tip sonicator (MSE Soniprep 150, amplitude 8 µm) for 6-times for 10s, and incubated in a water bath (Grant ultrasonic bath XB2, Farnell, UK) at 95 °C for 2-hours. After oxidation, the acid was diluted with water and the mixture centrifuged (10 min, at 50000g, 4 °C) (Beckman Avanti J25, Buckinghamshire, UK), followed by through washing with water (distilled water). These pre-treated CNTs were then re-dispersed in a 3:1 mixture of concentrated nitric and sulphuric acid and the above described process was repeated. Afterwards, the oxidised CNTs were vacuum filtered using a 0.2 µm polycarbonate filter (Whatman Ltd., UK) until the eluate was clear and of neutral pH. The filtrate was then sonicated with a tip sonicator for 6-times for 10s and centrifuged three times at 75000 g to remove big agglomerates and CNT bundles. The concentration of these dispersions was determined gravimetrically and adjusted to 100 µg/mL for storage in the fridge at 4 °C.

2.4 Functionalisation of CNTs

One important feature of CNTs is that this material is practically insoluble in both aqueous and polar/nonpolar organic solvents. They can be dispersed in some solvents by sonication, but precipitation immediately occurs when this process is interrupted. On the other hand, it has been demonstrated that CNTs can interact with different classes of compounds [238, 239, 251-257]. CNTs can undergo chemical reactions that make them more disperse for their integration into inorganic, organic, and biological systems [258].

The main approaches for modification of CNTs can be grouped into three categories: (a) covalent attachment of chemical groups through reaction onto the π-conjugate skeleton of the CNT; (b) noncovalent adsorption or wrapping of various functional molecules; and (c) endohedral filling of their inner empty cavity.

A number of routes to covalent functionalisation of CNTs have been developed. According to the location of the functional groups, the strategies to covalently functionalise CNTs can be classified into two main types: (a) defect functionalisation

and (b) sidewall functionalisation. The covalent functionalisation of nanotubes is more robust and better controllable compared to functionalisation based on noncovalent methods.

Covalent functionalisation of CNTs takes advantage of carboxylic acid moieties of acid-treated CNTs or via derivatisation. The acid treatment is basically carried out in the same way as for acid purification techniques, only sometimes, stronger acids are used in order to increase the amount of functional groups. The treatment has to be adjusted for every nanotube sample with respect to acid concentration, time and temperature, as some samples are more sensitive to oxidation than others, which might destroy them more easily. Once oxidised, CNTs can be coupled covalently to a variety of different biomolecules bearing amino groups. However, the carboxylic groups of oxidised nanotubes are not reactive enough to undergo spontaneous reactions. A common solution to this problem is to convert the carboxylic groups into amine-reactive esters using Sulfo- NHS (Nhydroxysulfosuccinimide) and EDC (1-Ethyl-3-[3-dimethylaminopropyl] carbodiimide hydrochloride), the latter serving as a dehydrating agent [259]. One of the main advantages of this procedure is that both EDC and Sulfo-NHS are soluble in water and thus allow for coupling reactions in physiological environments.

In the search for non-destructive purification methods, CNTs are wrapped or covered with molecules which act as surfactants, in non-covalent approaches. These can be common anionic, cationic or non-ionic surfactants, but also complexing agents, organic biopolymers, proteins, oligomers, or bile salts [260]. The lipophilic part of these molecules generally attaches to the sidewalls of the nanotubes via hydrophobic interactions or π-stacking, in contrast the hydrophilic part sticks out into the solution and provides aqueous dispersibility. A particularly interesting method is the wrapping of CNTs with single-stranded DNA or RNA, as this increases the biocompatibility of the nanotubes and enables them to interact with living tissue [261]. The advantage of the non-covalent approach is that the sp^2 orbital structure of the nanotubes is preserved and hence so are their electronic characteristics. However, non-covalent binding is dependent on environmental factors, such as pH and salt concentration, and it is in general less stable than covalent binding.

The wrapping with a phospholipid, as PL-PEG-NH_2 and a polypeptide, such as Poly(Lys:Phe) (applied in this study) rely on the interaction between the hydrophobic regions of the polypeptide that binds to the hydrophobic surface of the CNTs through

π-π interactions leaving the hydrophilic groups exposed to the solvent and allowing for the dispersion of the CNTs in aqueous media.

2.5 Characterisation of CNTs

CNTs can be classified according to their number of walls, but they can also vary in diameter distribution, length distribution, chirality, purity, catalyst material, impurity species and defects; factors mostly dependent on the production method. Therefore, it is important to distinguish between these materials and determine the quantity, quality, and properties of nanotubes in a sample.

Characterisation techniques can be divided into microscopic techniques, spectroscopic techniques, and thermogravimetric techniques. The first group comprises scanning electron microscopy (SEM), transmission electron microscopy (TEM), atomic force microscopy (AFM), and confocal microscopy, in contrast spectroscopic techniques include Raman spectroscopy and Ultra Violet–Visible-Near Infrared (UV/Vis/NIR) absorption spectroscopy.

2.5.1 Transmission electron microscopy (TEM)[1]

Electron beams can be used to produce images of nanoparticles and provide crystallographic information about these structures. Under TEM the electrons from a source such as an electron gun enter the sample, and scatter as they pass through it. Electrons are subsequently focused by an objective lens, are amplified by a magnifying (projector) lens, and finally produce the desired image [234].

There are a number of drawbacks to using the TEM technique. Many materials require extensive sample preparation to produce a sample thin enough to be electron transparent, which makes TEM analysis a relatively time consuming process with a low throughput of samples [234].

[1] TEM was performed by Ewa Borowiak-Palen at West Pomeranian University of Technology in Szczecin

2.5.2 Atomic force microscopy (AFM)[2]

AFM has become an important technique in biology and chemistry due to its unique ability to image and characterise structures in liquid, ambient and vacuum environments [262-265]. When the tip is brought into proximity of a sample surface, forces between the tip and the sample lead to deflection of the cantilever. Typically, the deflection is measured using a laser spot reflected from the top of the cantilever into an array of photodiodes. Compared to other microscopic techniques, AFM can produce a true, three-dimensional surface profile of a sample, rather than a two-dimensional projection. Concerning CNT characterisation, AFM can be used to obtain size and length distributions and provides information about surface coatings.

2.5.3 Confocal microscopy

Confocal microscopy is a widely used tool for fluorescent imaging of biological objects. Confocal microscopy can constitute the bridge connecting high-resolution analysis and observation of spatially extended areas. Fluorescence provides the possibility to analyse location and expression of many target molecules at the same time. Furthermore, confocal microscopy has the unique ability to optical section a sample into thin slices almost in real time, thereby providing a full three-dimensional view of the sample.

Therefore, we have used confocal laser scanning microscopy (CLSM) (Zeiss Axiovert LSM510) using 63x oil immersion objective lens (Carl Zeiss Inc., Thornwood, NY) to view fluorescently tagged CNTs in a method similar to that of viewing biological materials such as antibodies, in order to accurately analyse and quantify the interaction between them.

[2] AFM imaging was performed by Cristina E. Glusca at University of Surrey.

2.5.4 UV-VIS-NIR spectroscopy

UV-VIS-NIR involves the spectroscopy of photons in the UV-visible region. It uses light in the visible and adjacent near ultraviolet (UV) and near infrared (NIR) ranges. In this region of the electromagnetic spectrum, molecules undergo electronic transitions. The optical spectrum of CNT was found to be very structured. Moreover, it was found that nanotubes fluoresce in the near-IR, with clearly identifiable and similar spectra [266].

In UV/vis/NIR absorption spectroscopy, the intensity of a beam of light is compared before and after interaction with a sample. This provides information about concentration, as according to Lambert-Beer's Law, the absorbance is proportional to the concentration. Furthermore, the vis/NIR part of a CNT spectrum (600 to 2500 nm) exhibits characteristic absorption features called "van-Hove singularities", which are due to the one-dimensional nature of the conducting electron states in CNTs and originate from the inter-band transitions in semiconducting and metallic SWNTs [267]. According to Itkis *et al.,* the strength of these characteristic features in comparison with the featureless baseline provides a measure of the purity of the SWNT material [268]. However, van-Hove singularities can only be observed for good dispersions and non-oxidised CNTs, since strong acid treatment destroys the electronic properties of CNTs [269].

The first peak centred at 1700 nm is due to the first van Hove singularity in semiconducting nanotubes while the second one is seen centred at 900 nm. A third set of peaks centred near 650 nm is assigned to the first transition of metallic SWNT [270]. The van Hove peaks are overlapped on a background that decreases smoothly from the UV to the NIR.

2.5.5 Raman spectroscopy

Raman spectroscopy is a powerful technique with a wide-range of applications for the study of CNTs. As a vibrational spectroscopy it has been shown to be an invaluable tool for characterisation of CNT diameter distributions and monitoring production methods [271-273]. Experimentally, the technique is relatively simple, in particular for bulk samples and the instrumentation is widely available. Spectra can be recorded at room temperature, and the technique is quick, non-destructive and sensitive. Raman

can also be applied to individual nanotubes, however it is experimentally more demanding. Easy evaluation of nanotube diameters is made possible by the presence of the radial breathing mode (RBM), which appears at low frequency (100-400 cm^{-1}) region of the nanotube. The Raman spectrum and has an inverse dependence on nanotube diameter (Figure 2.5 B, left) [274]. The Raman is also capable of identifying the nanotube electronic nature through analysis of the nanotube G-band, found near 1600 cm^{-1} (Figure 2.5 B, right). A typical spectrum of a SWNT sample is presented in Figure 2.5 A. The main features can be identified as: a) the low-frequency mode (< 200 cm^{-1}), RBM; b) strong feature at around 1340 cm^{-1}, so called D line, assigned to disorder graphitic material; c) G band in the approximate range 1550-1600 cm^{-1}. In graphite the G band exhibits a single peak at 1582 cm^{-1} related to the tangential mode vibrations of the C atoms. d) A line at around 2600 cm^{-1}, the second order harmonic of the D mode, it is labelled as 2D (or G').

The frequency of the radial breathing mode, ω_{RBM}, varies inversely with diameter, d, at least for small tubes [273]

$$\omega_{RBM} = \alpha / d$$

Equation 1.

where α is a factor that depends on the nature of the sample. This has been confirmed in a number of experimental studies [125]. For CNTs with diameters larger than 2 nm, the character of the electronic states becomes essentially independent of the tube diameter, and therefore approximates to that of the graphene sheet. It has also been established that ω_{RBM} is dependent on the (n, m) chiral indices of a tube [275].

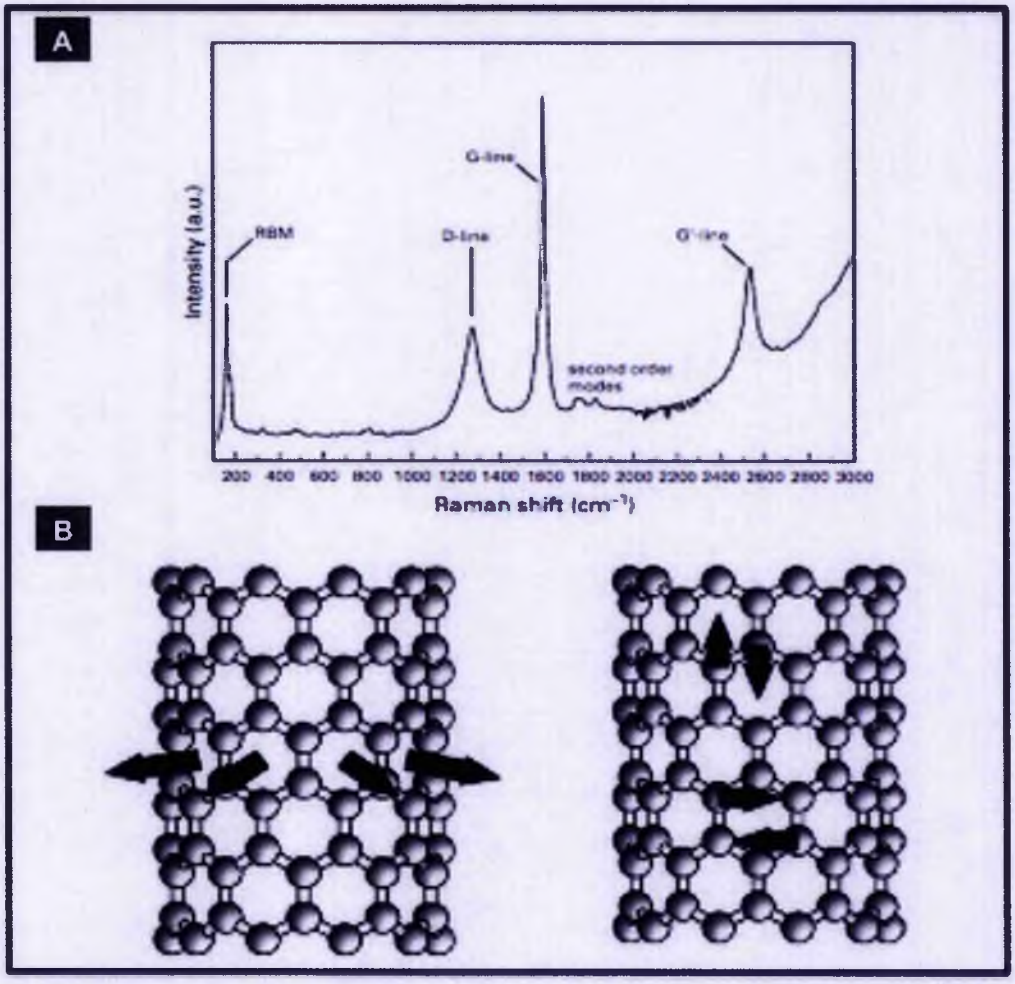

Figure 2.5: Raman characterisation of CNTs. Raman spectrum of SWNT (A) and atomic displacements associated with the RBM and G-band normal mode vibrations (B) (adapted from *et al.* [276]).

In addition to the RBM line, the G band can also be used to determine the nanotube diameter. However, this is only true for SWNT, where the G band is composed of two features, one at 1590 cm^{-1} labelled G^+ and the other at about 1570 cm^{-1} named G^-. Dresselhaus *et al.* demonstrated that on individual SWNTs the frequency of the G^+ band is essential independent of diameter, but the G- band depends on the diameter [277-279]. It has also been shown that this band can be used to distinguish between metallic and semiconducting SWNTs, through differences in their Raman line-shapes. Furthermore, information about the structure and electronic properties can be obtained by analysing the second order bands in the spectrum, D and 2D (G') bands, although these are usually much weaker that the first order features [280].

2.6 Tissue cell culture

Tissue cell culture refers to maintenance of viable single cells (cell culture) or functional unit of cells (organ culture) outside their normal multicellular organism of origin. The cells may be removed from the tissue directly and disaggregated by enzymatic or mechanical means before culture, or they may be derived from a cell line or cell strain that has already been established.

There are three main types of cultures: a primary culture, which refers to the stage of the culture after the cells are isolated from the tissue and proliferated under the appropriate conditions until they occupy all of the available substrate (i.e., reach 70 to 80 % confluence). At this stage, the cells have to be subcultured (i.e., passage) by transferring them to a new vessel with fresh growth medium to provide more room for continued growth. After the first subculture, the primary culture becomes known as a cell line or subclone. A large component of cell lines derived from primary cultures have a limited life span (i.e., they are finite; see below), and as they are passaged, cells with the highest growth capacity predominate, resulting in a degree of genotypic and phenotypic uniformity in the population. If a subpopulation of a cell line is positively selected from the culture by cloning or some other method, this cell line becomes a cell strain. A cell strain often acquires additional genetic changes subsequent to the initiation of the parent line. In the work presented different cell lines were utilized but also work involved derivations of a cell strain expressing green fluorescent proteins (GFP) (see chapter 6). For the present work mainly two cell lines were used as cellular model system: human prostate adenocarcinoma cells (PC3) (ECACC, Porton Down, Salisbury, UK) and human cervical carcinoma cells (HeLa) (ATCC, supplied by Promechem, Teddington, UK). However, human colon adenocarcinoma (SW948 and WiDr) and human prostate cancer (DU145) (from ATCC, supplied by Promechem, Teddington, UK), were also used for controls and comparison (Chapter 6). SW948 and WiDr are adherent cells from human colon with colorectal adenocarcinoma. The SW948 are from a stage Dukes' type C, grade 3 (81-year-old, female, Caucasian), while WiDR is derivative of HT-29 cell line. PC3 and DU145 are also adherent cells from a prostate carcinoma. PC3 was established from a grade 4, prostatic adenocarcinoma from a 62-year-old male Caucasian, while DU145 derives from a metastatic brain (69-year-old male Caucasian).

Cell culture is one of the major tools used in cellular and molecular biology, providing excellent model systems for studying the normal physiology and biochemistry of cells (e.g., metabolic studies, aging), the effects of drugs and toxic compounds on the cells, and mutagenesis and carcinogenesis. It is also used in drug screening and development, and large scale manufacturing of biological compounds (e.g., vaccines, therapeutic proteins). The major advantage of using cell culture for any of these applications is the consistency and reproducibility of results that can be obtained from using a batch of clonal cells.

Regardless the ultimate goal of the work, the cell type or the cells to be cultured, the methodology in tissue culture is the same: to maintain viable functional cells outside of their normal, *in vivo* environment. In the environment of origin the cell was protected from external pathogens. It had a regular supply of nutrients and oxygen, its metabolic by-products, potentially toxic at high concentrations, were removed at regular intervals. If it were part of a mammal, its environment also included a constant temperature.

The most elegant cell culture systems and experiments will not be worth much if the cells are contaminated with microorganisms. Culture work requires that all reagents and equipment in contact with the cells to be sterile. To maintain sterility, aseptic techniques are used at all times (i.e., autoclave, radiation and filtration).

2.6.1 Maintaining cell cultures

Adherent, such as HeLa and PC3, cultures should be passaged when they are in the log phase, before they reach confluence reach 70 to 80 % confluence). Normal cells stop growing when they reach high confluence (contact inhibition), and it takes them longer to recover when reseeded. Therefore, passaging cells according to a strict schedule ensures reproducible behaviour and allows monitoring their health status.

Many continuous mammalian cell lines can be maintained on a relatively simple medium such as minimum essential medium (MEM) supplemented with serum, as described for HeLa cells. However, when a specialized function is expressed, a more complex medium may be required. Information for selecting the appropriate medium for a given cell type is usually available in published literature, and may also be obtained from the source of the cells or cell banks. For example, PC3 cells it is

recommended to use (RPMI) medium supplemented with serum and glutamine.

2.6.2 Freezing and thawing cells

Cell lines in continuous culture are prone to genetic drift, finite cell lines are fated for senescence, all cell cultures are susceptible to microbial contamination, and even the best-run laboratories can experience equipment failure. Because an established cell line is a valuable resource and its replacement is expensive and time consuming, it is vitally important that they are frozen down and preserved for long-term storage. As soon as extra cells becomes available from subculturing, they should be frozen as a seed stock, protected, and not be made available for general laboratory use. Working stocks can be prepared and replenished from frozen seed stocks. If the seed stocks become depleted, cryopreserved working stocks can then serve as a source for preparing a fresh seed stock with a minimum increase in generation number from the initial freezing.

The best method for cryopreserving cultured cells is storing them in liquid nitrogen in complete medium in the presence of a cryoprotective agent such as dimethylsulfoxide (DMSO). Cryoprotective agents reduce the freezing point of the medium and also allow a slower cooling rate, greatly reducing the risk of ice crystal formation, which can damage cells and cause cell death.

The thawing procedure is stressful to frozen cells, and using good technique and working quickly ensures that a high proportion of the cells survive the procedure. As with other cell culture procedures, therefore it is recommend thawing frozen cells rapidly (less than 1 minute) at 37 °C water bath.

2.6.3 Counting cells in an haemocytometer

A haemocytometer is a graduated counting chamber that can be viewed under a microscope to determine the concentration of cells in a suspension. There are a number of manufactures of these types of chambers and some have a slight variation

in style. Herein, the "Neubauer" type chamber was used. The chamber is made of ground glass with a central area that is defined by a set of grooves that form an "H" shape. In order to determine the concentration of cells in a suspension, count the cells in the large, central gridded square, corresponding to 1 mm^2 (multiplying by 10^4 gives an estimation of the number of cells per mL). The haemocytometer can be used for determining cell viability using trypan blue. Cell viability is calculated as the number of viable cells divided by the total number of cells within the grids on the haemocytometer. If cells take up trypan blue, they are considered as non-viable.

2.6.4 Transfection of mammalian cells

The reason, for introducing DNA into mammalian cells is to analyse gene expression. There are several techniques to introduce DNA into mammalian cells, such as: calcium phosphate transfection, Diethylaminoethyl-dextran (DEAE-dextran) transfection, electroporation, liposome-mediated transfection and nanoparticles. The first two procedures produce a chemical environment that results in DNA attaching to the cell surface; the DNA is then endocytosed.

Electroporation uses an electric field to open up pores in the cell. The DNA presumably diffuses into the cell through the pores. This technique therefore is not dependent upon special characteristics of the cell and can be used with virtually any cell type. The optimal amplitude and length of pulse will vary for each cell type.

In liposome-mediated transfection, negatively charged phosphate groups on DNA bind the positively charged surface of the liposome, and the residual positive charge then presumably mediates binding to negatively charged sialic acid residues on the cell surfaces, with consequent internalisation by endocytosis [281].

Nanoparticles have been recently introduced as new transfection methodologies. Herein CNTs are used to study their feasibility as delivery agents for genetic material, such as plasmid DNA and small interfering RNA (siRNA) (Chapter 5 and 6).

2.6.5 Plasmid DNA transformation, screening and selection

Plasmids are circular, double-stranded DNA (dsDNA) molecules that are separated from a cell's chromosomal DNA. These extrachromosomal DNAs, which occur naturally in bacteria, yeast, and some higher eukaryotic cells, exist in a parasitic or symbiotic relationship with their host cell. Many naturally occurring plasmids contain genes that provide some benefit to the host cell, for example, some bacterial plasmids encode enzymes that inactivate antibiotics.

Plasmids can be engineered to be used as cloning vectors, basically they need to contain: a replication origin, a drug-resistance gene, and a region in which exogenous DNA fragments can be inserted. In the particular case of the study presented here the plasmid DNA (pAcGFP-N1) is already engineered, containing an early promoter (CMV) and a SV40 origin of replication in mammalian cells; a multi-cloning site (MCS); a selection marker for bacteria – the kanamycin gene and a selection marker for mammalian cells – geneticin (G148). Furthermore the plasmid holds a gene of interest – the GFP gene.

Plasmid DNA is generally transformed into *E.coli* that results in an alteration of a cell caused by the uptake and expression of foreign DNA. The uptake of plasmids by *E.coli* is stimulated by a high concentration of calcium chloride ($CaCl_2$). Even in the presence of $CaCl_2$, transformation occurs with quite low frequency, and only a few cells are transformed by incorporation of a single plasmid molecule. Cells that are not transformed die on selective media, containing antibiotics. Once incorporated into a host cell, a plasmid DNA can replicate independently of the host-cell chromosome. As a transformed cell multiplies into a colony, at least one plasmid segregates to each daughter cell.

Further investigation of the resulting colonies must be required to confirm that cloning was successful. This may be accomplished by means of PCR, restriction fragment analysis and/or DNA sequencing.

Restriction enzymes are bacterial enzymes that recognise specific 4- to 8-bp sequences, called restriction sites, and then cleave both DNA strands at this site. After digestion with restriction enzymes the isolated DNA fragments can be separated and analysed by gel electrophoresis. Before transfection into mammalian cells plasmid DNA should be purified for ultra-pure, transfection grade plasmid DNA. This can be achieved using commercial kits, such as Qiagen purification kits (See chapter 5).

2.7 Western blotting

A particular protein can be detected in a complex mixture by combining a resolving gel electrophoresis, specific antibodies and sensitive enzymatic assays. The technique is named Western blotting or immunoblotting, and consists of this three-step procedure that is commonly used to separate proteins and then identify a specific protein of interest. As shown in figure 2.6, two different antibodies are used in this method, one specific for the desired protein and the other linked to a reporter enzyme for amplification of the signal for final visual detection of protein expression.

2.8 Flow cytometry

A flow cytometer can identify different populations of cells by measuring the light they scatter, or the fluorescence they emit, as they flow through a laser beam; thus it can sort out cells of a particular type from a mixture. In fact, a fluorescence-activated cell sorter (FACS), is an instrument based on flow cytometry and can select one cell from thousands of other cells (Figure 2.7). For example, as it will be demonstrated in chapter 6 GFP expressing cells will be separated from other cells when they fluoresce in the FACS. Once sorted from the other cells, the selected cell can be grown in culture.

Another use of flow cytometry includes the measurement of a cell's DNA and RNA content and the determination of its general shape and size. The FACS can make simultaneous measurements of the size of a cell (from the amount of scattered light) and the amount of DNA it contains (from the amount of fluorescence from a DNA-binding dye). As an example, apoptosis can be evaluated using a flow cytometer, which is possible by applying a Annexin V-FITC apoptosis detection kit as described in chapter 7.

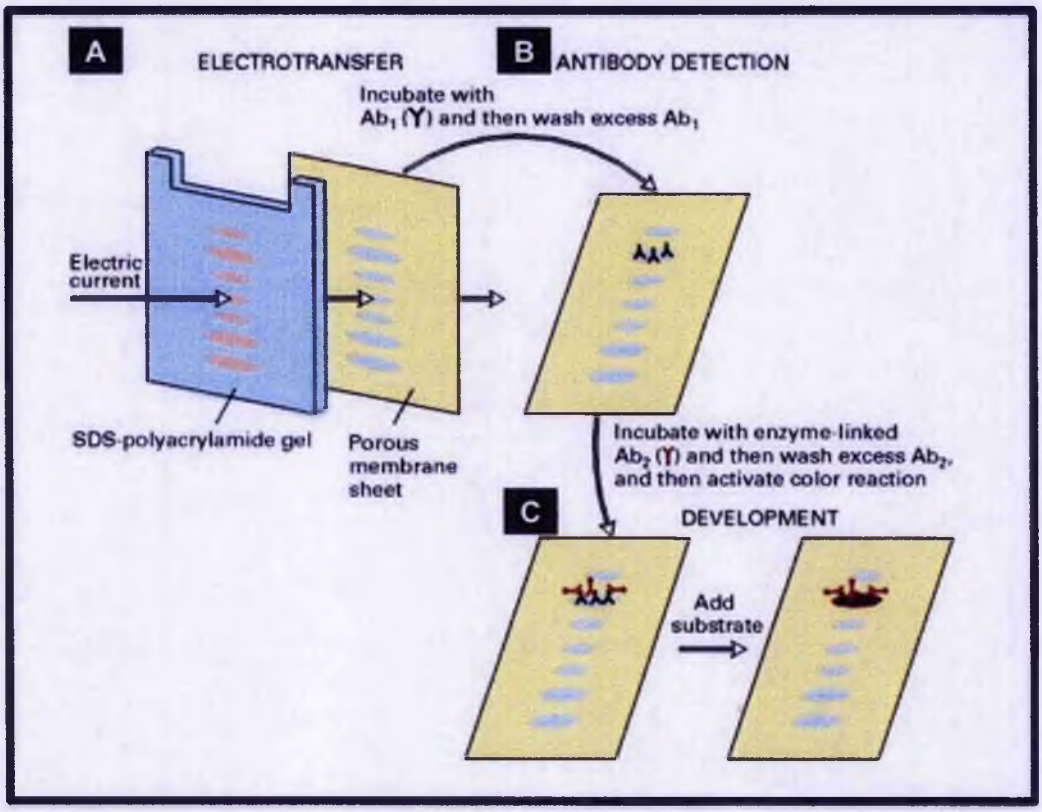

Figure 2.6: Western blotting or immunoblotting. (A) A protein mixture is electrophoresed through an SDS gel, and then transferred from the gel onto a membrane. (B) The membrane is flooded with a solution of antibody (Ab1) specific for the desired protein. Only the band containing this protein binds the antibody, forming a layer of antibody molecules (although their position can't be seen at this point). After sufficient time for binding, the membrane is washed to remove unbound Ab1. (C) In the development step, the membrane first is incubated with a second antibody (Ab2) that binds to the bound Ab1. This second antibody is covalently linked to alkaline phosphatase. In the final step, the substrate is added and will luminesce when exposed to the reporter on the secondary antibody. The light is then detected by a photographic film (adapted from Lodish *et al.* [31]).

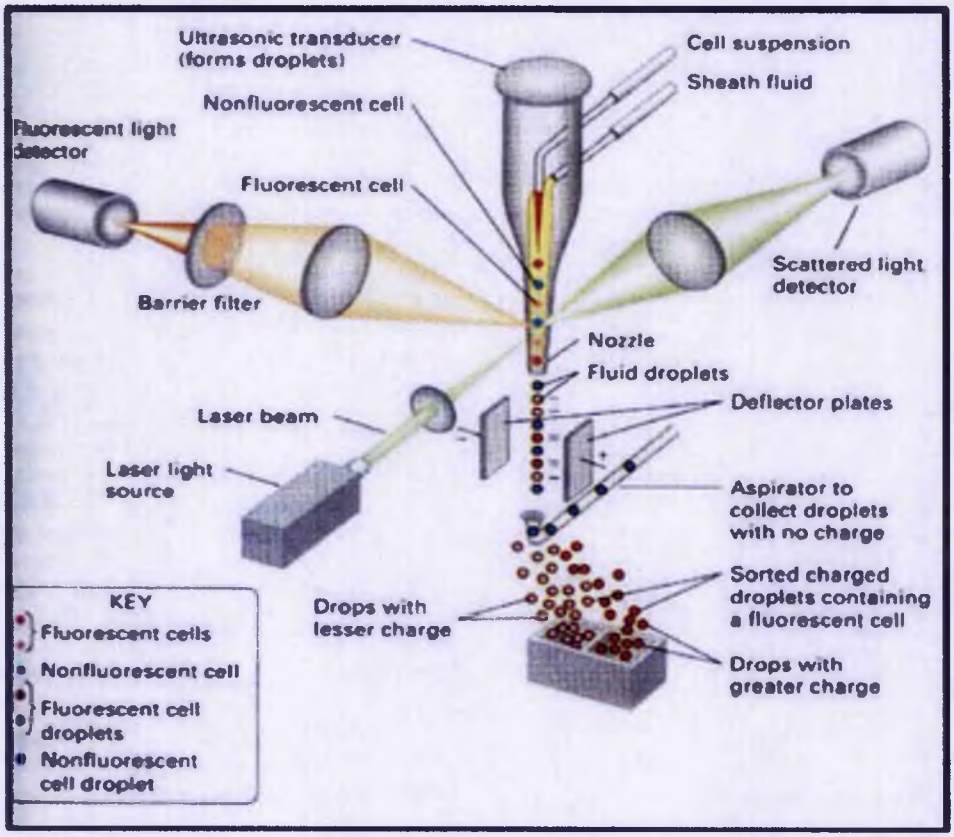

Figure 2.7: Fluorescence-activated cell sorter (FACS). A concentrated suspension of cells is allowed to react with a fluorescent antibody or a dye that binds to a particle or a molecule such as DNA. The suspension is then mixed with a buffer, the cells are passed single-file through a laser light beam, and the fluorescent light emitted by each cell is measured. The light scattered by each cell can be measured at the same time as the fluorescence; from measurements of the scattered light, the size and shape of the cell can be determined. The suspension is then forced through a nozzle, which forms tiny droplets containing at most a single cell. At the time of formation, each droplet is given an electric charge proportional to the amount of fluorescence of its cell. Droplets with no charge and with no different electric charges (due to different amounts of bound dye) are each separated by electric field and collected. It takes only milliseconds to sort each droplet, so up to 10 million cells per hour can pass through the machine. By this means, cells that have desired properties can be separated and then grown (adapted from Lodish *et al.* [31]).

Chapter 3: Uptake and release of DWNTs in mammalian cells

3.1 Introduction

An important characteristic of CNTs is their ability to cross cell membranes [115, 126]. The uptake of CNTs has been previously described to occur via two major pathways. One method describes nanotubes as "nanoneedles" that have the capability to penetrate cell membranes [126], in contrast the second method refers to an active uptake via clathrin mediated endocytosis [115]. As controversy the mechanism of uptake of CNTs persists, the final fate of nanotubes has been largely open to speculation. The previously described "nanoneedle" CNTs internalisation, has been proposed to lead to perinuclear accumulation with no effect on cell viability [145]. Conversely, CNTs wrapped with biomolecules, such as DNA, have been shown to be subjected to exocytosis by NIH-3T3 fibroblast cells in a study carried out by Jin *et al.* [142].

Previously, the most commonly used technique to visualise the uptake of CNTs focused on visualising internalisation facilitated via the covalent linking of a visible-wavelength fluorophores [115, 126, 128, 131, 145, 282]. However, as discussed above it is important to consider certain particular parameters (section 1.3.1) such as the chemical linkages must resisting enzymatic cleavage (due to activity in cytosolic compartments), and also the chemical processing of nanoparticles may dramatically changing their ultimate biological fate. As an alternative to the linking of fluorophores, it is possible to use the unique NIR intrinsic fluorescence associated with CNTs. The latter property is considered as being advantageous for use in biological systems since there are minimal background signals associated with autofluorescence from cells, tissues, and other biological molecules in this spectral range, as this property has largely been shown to be confined to the visible spectral range [117]. Raman spectroscopy is a multi-purpose, rapid (~1 min per spectrum) non-destructive technique that operates at normal ambient (room temperature) (~300 K) and pressure conditions, and uses readily available Raman characterisation instrumentation. [135] Due to the electronic structure and diameter of CNTs, strong resonance-enhanced Raman bands are produced at 150-300 cm^{-1}, 1590-1600 cm^{-1}, and ~2600 cm^{-1} away

from the excitation wavelength [136]. The first of these, referred to as the radial breathing mode (RBMs), is caused by uniaxial vibrations and depend linearly on the nanotube diameter. The RBM is then followed by the disorder-induced D-band, the tangential mode (or G band), which is caused by stretching along the C-C bonds of graphene [136-138]; and finally the 2D or G' band, a two-phonon mode [136].

Besides the fate of CNTs, the major challenge of using them in biological systems is assessing whether CNTs are inherently cytotoxic [200, 283-288]. At the present, there are roughly as many publications reporting no apparent cytotoxicity [117, 121, 126, 127, 131, 139, 146, 177, 200-210], as there are reporting varying degrees of significant loss of cellular viability associated with CNTs [150, 213, 285, 289-297]. Two major considerations in this area are how the CNTs are presented and another is their purity and concentration. For example, pulmonary toxicity of SWNTs has been established when large doses of dry, unpurified SWNTs have been blown into lungs of rats [149, 150, 298]. This method of presentation is not relevant to the small measured doses of CNTs that would be used as chemotherapy and drug delivery systems. In fact, the biodistribution of chemically modified SWNTs injected into mice or rabbits, was studied recently, and the CNTs were reported to be rapidly excreted with no evidence of toxicity [146, 160, 161]. The purity of CNT preparation is a crucial consideration their use as bio-nano agents. Many methods of CNT synthesis use metal catalysts that are known to be toxic. Such impurities, and other carbonaceous impurities, must be removed from the samples in order to reach safe conclusions regarding the inherent toxicity of CNTs. At the present the data is unclear in relation to which factors contribute to the various reported toxicological profiles of CNTs.

As stated, in our experiments we use DWNT, which were oxidised and therefore shorter, rendering them less toxic. Our CNT system possesses carboxylic groups at their sidewalls, which allows further fuctionalisation suitable for biomedical applications. This could be in the form of a triple functionalisation of SWNTs with an anti-cancer agents and fluorescent markers [185]. The benefit of using DWNT is that apart from creating defects at the outer wall that allow better funtionalisation, the physical and mechanical properties of CNTs are maintained by the inner wall.

Herein, we propose to study cellular uptake and release of DWNTs by Raman spectroscopy using single cell mapping and spectroscopy analysis of whole cell lysates incubated with RNA-wrapped oxidised DWNTs (oxDWNT-RNA), and evaluate their toxicity by examining cells for any sign of cellular stress response to CNTs uptake.

3.2 Experimental section

In this section, a detailed description of the methodology employed is presented. First CNTs were prepared in order to be biocompatible and to allow further attachment of different molecules such as RNA. Secondly, Raman was used to evaluate uptake and release of the complexes, changes in the cellular biochemistry and concentration of internalised CNTs. Finally cellular stress response was assessed for cells exposed and not exposed to CNTs.

3.2.1 Preparation of biofunctional CNTs

DWNTs synthesised by the CCVD technique [247] were purified in concentrated nitric acid and oxidised in a mixture of nitric and sulphuric acid (detailed information in general methods) [185]. After oxidation, nanotubes were sterilised by autoclaving at 121 °C for 1-hour and were maintained under sterile conditions for the duration of the experiment. In a second step, the oxidised DWNTs were coated with RNA in a proportion of 1:1 (w/w) [261]. Complexes were formed by sonication in a water bath for 60-minutes. To remove excess of RNA, the suspension of oxDWNT-RNA was filtered using a 100 kDa filter devices (Amicon Ultra-4 centrifugal filter devices from Millipore, UK) and then resuspended in deionised water. The concentration of the complexes was determined by the total weight after oxidation. The final supernatant was analysed by AFM and TEM.

3.2.2 Raman mapping of single cells

PC-3 and HeLa in culture were used as cellular model systems for the present study. PC-3 cells were cultured in RPMI-1640 medium, supplemented with 10 % (v/v) fetal bovine serum (FBS), 2mM Glutamax™ and 1 % (v/v) penicillin-streptomycin (all obtained from Invitrogen, Paisley, UK). HeLa cells were cultured in MEM medium, supplemented with 10 % (v/v) FBS, 1 % (v/v) non-essential amino acids and 1 % (v/v) penicillin-streptomycin (all obtained from Invitrogen, Paisley, UK). Cells were cultured in 35 mm sterile petri dishes (Nunc, Thermo scientific) containing glass coverslips.

Assessment of the uptake of CNTs, was performed at different time points ranging from 0.5 to 24-hours. 3-hours after the incubation with oxDWNT-RNA (concentration of 30 μg/mL) diluted in Opti-MEM serum-free culture medium, the cells were washed twice with ice cold, sterile PBS and fresh medium containing serum and antibiotics was added. At the end of each time point (0, 0.5, 3, 6, 9, 12, 18 and 24-hours) the medium was removed and the cells washed several times with PBS, as before. Cells were subsequently fixed with 4% paraformaldehyde solution (Sigma Aldrich, Poole, UK) to prevent morphological and chemical changes during acquisition. Finally, the samples were again washed with PBS and slides mounted and hermetically sealed using nail lacquer. Raman mapping was performed using a Renishaw InVia Raman microscope, E_{laser}=1.59 eV (785 nm wavelength). RBMs were used to map the intensity of oxDWNT-RNA in cells, where the RBMs peaks acquired were at 156, 205, 230 and 266 cm^{-1}. Applying the equation $\omega_{RBM} = 248/d_t$, where ω_{RBM} is the RBM frequency in cm^{-1} and d_t the diameter in nm [275], it was possible to extrapolate the diameters present in the mixture. The diameters in the sample ranged from: 0.9 nm to 1.1 nm, 1.2 nm and 1.58 nm, with 0.9 nm and 1.58 nm being the most abundant. Thus, the diameter of 0.9 nm was used for all data analysis.

3.2.3 Raman spectroscopy of whole cell lysates

PC-3 and HeLa cells were grown in medium as described above and cultured in 25 cm^2 tissue culture flasks until 80 % confluence was reached. At this point, they were incubated for various times ranging from 0.5 to 24-hours with oxDWNT-RNA at a concentration of ~30 μg/mL diluted in serum-free Opti-MEM medium. After 3-hours incubation, the remaining samples were washed twice with PBS and then with fresh medium containing serum and antibiotics. At each time point, the medium was removed from the cells, followed by several washes with PBS. The cells were subsequently trypsinized, washed with ice cold PBS and ruptured via hypotonic shock using a lysis buffer (Tris buffer containing 50 mM Tris HCl and 150 mM NaCl at pH 7.5 and additionally 1 % NP-40, 0.2 % SDS, 1 mM phenylmethanesulfonyl fluoride (PMSF), 10 μg/mL aprotinin, 10 μg/mL leupeptin, 1 mM sodium orthovanadate (Na_3VO_4) as cellular protease inhibitors). After lysing, suspensions were spun down (10 min, at 500 g, 4 °C) (Eppendorf 5415R, Hamburg, Germany) to remove nuclei and unbroken cells and supernatants were used to evaluate CNT content. For Raman

measurements, a droplet of cell lysate (4 μL) was allowed to dry on a glass slide. Spectra of samples were recorded using the E_{laser}=2.64 eV (473 nm wavelength) of an NT-MDT NTEGRA Spectra Probe NanoLaboratory inverted configuration microscope.

3.2.4 Protein quantification and SDS polyacrylamide gel electrophoresis

Protein quantification was performed according to instructions in the manual of the DC (detergent compatible) protein assay (Bio-Rad Laboratories, UK). A standard curve was prepared with BSA concentrations from 0.2-1.5 mg/mL (detailed information in the general methods). Protein/sample from cell lysates were electrophoresed on SDS-polyacrylamide gel (Novex, Invitrogen, Paisley, UK), with subsequent coomassie staining for 2-hours.

3.2.5 Concentration of DWNTs per cell

G band intensity (section 3.2.3) was use to detect the concentration of CNTs inside cells. A calibration curve was determined by measuring the G band intensity for different concentrations of RNA-wrapped oxidised DWNTs (93.50; 46.75; 23.37; 11.69; 5.84 and 2.92 μg/mL). The concentration of the previously prepared RNA-wrapped oxidised DWNTs dispersion was determined by weighing the mass of filtrate in pre-weighted polycarbonate filters (Millipore, UK), followed by serial dilutions. A logarithmic fit was used to determine the equation that permits one to calculate the concentration in the whole cell lysates. Finally, an estimation of cell volume of 5.75×10^{-9} μL [299] was used to determine the concentration of DWNTs per cell.

3.2.6 Western blotting

Whole-cell lysates were obtained by trypsinizing the monolayer of adherent cells and washing with PBS at 4°C. Cell pellets were then subjected to osmotic rupture in hypotonic detergent-based buffer (1 mM PMSF, 1 mM $NaVO_4$, 2 μg/mL aprotinin, and 2 μg/mL leupeptin as protease inhibitors, 150 mM NaCl in 50 mM Tris buffer, 0.2% SDS, 1% Nonidet P-40, pH 7.5) and 50 μg of protein/sample were then

electrophoresed on SDS-polyacrylamide gel electrophoresis (Novex, Invitrogen, Paisley, UK) with subsequent transfer blotting. Membranes were incubated overnight at 4°C with primary antibodies to MAPK, or phospho-MAPK (Cell signalling technology®, UK). After washing, membranes were incubated with a secondary horseradish peroxidase-linked appropriate species antibody preparation at room temperature (± 21) for 1-hour with chemiluminescence used for visualisation. After the probing of each membrane with the primary antibody of choice, the membrane was stripped and re-probed using a *GAPDH* antibody (Sigma Aldrich, Poole, UK) to act as a loading control.

3.3 Results and discussion

Efforts to develop CNTs as nano-vehicles for precise and controlled drug and gene delivery, as well as markers for *in vivo* biomedical imaging, are currently hampered by uncertainties with regard to their uptake, their fate in the body and their safety [115, 128, 142, 145, 160, 198, 205]. All those processes are likely to be affected by the purity of CNT preparation, as well as size and concentration of CNT used, parameters often poorly controlled in biological experiments [134, 198]. For instance, a concentration limit of 30 μg/ml was employed in our studies, since in a study by Becker et al [134] concentrations above 25 μg/ml cause a decrease in cell viability. Herein, we demonstrate that under standard transfection methodologies DWNT are taken up by cultured cells but are then release after 24-hours with no discernable stress response.

3.3.1 Characterisation of DWNT

The successful preparation of RNA-purified CNTs has been already demonstrated in our group [261] and permits suitable dispersions of CNTs for potential medical applications. Similarly to what has been described for DNA [124, 132, 134, 144], RNA coating gives rise to high dispersion rates [300]. For these studies not only were the CNTs non-covalently wrapped using RNA, but they were also oxidised. Oxidation processes generate shorter CNTs, an aspect which is specially important when considering their potential biomedical applications since it has recently been

described that longer CNTs are asbestos-like in their toxicology profile in contrast the shorter length CNTs are significantly less toxic [198].

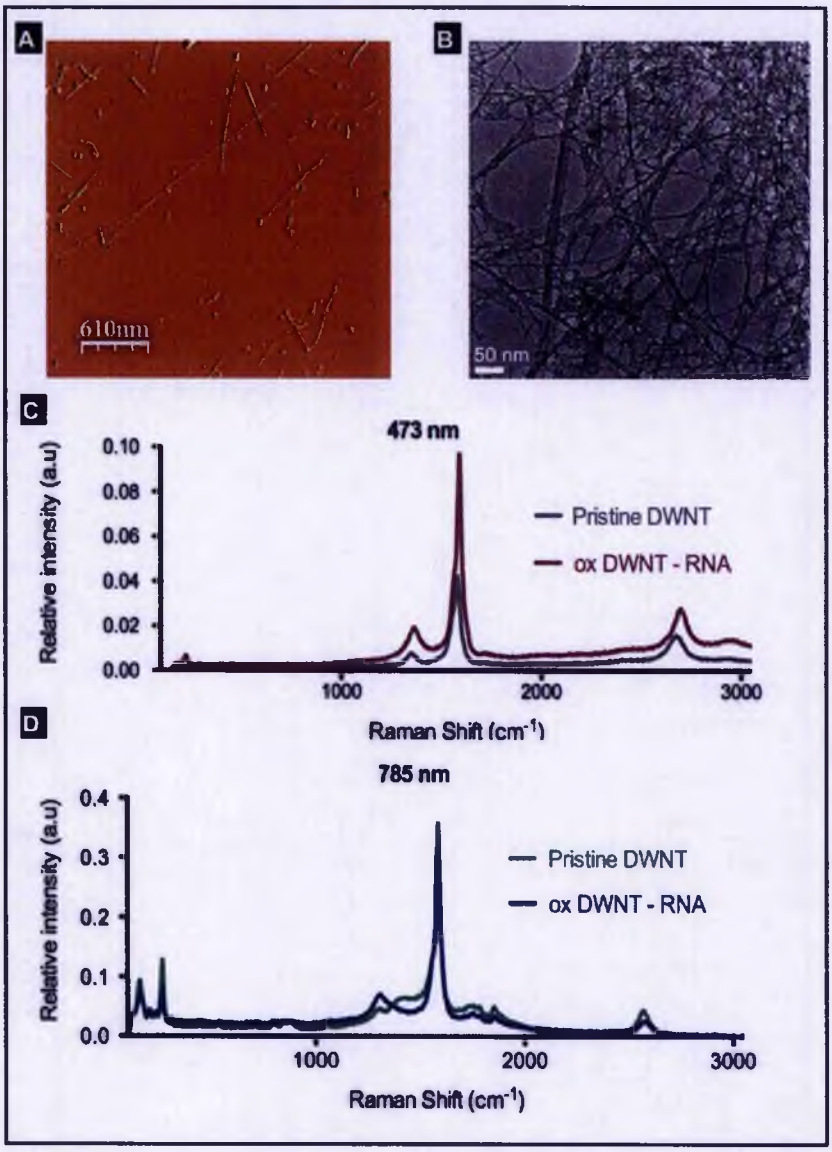

Figure 3.1: Structural characterisation of double walled CNTs (DWNT) by AFM (A), TEM (B) and Raman spectroscopy (C and D). (A) and (B) Surface analysis of RNA-wrapped oxidised DWNTs (oxDWNT-RNA) by AFM and TEM, respectively. Image shows that wrapping of CNTs is not complete, by AFM it is possible to visualise parts of the CNT not covered by the RNA. In addition, oxDWNTs-RNA were found to range between 200 nm and 2 μm in length. (C) and (D) Raman spectrum of pristine and oxDWNT-RNA at different laser energies: 473 and 785 nm. Intense bands can be seen at 120-350 cm^{-1} for the radial breathing modes (RBM); at ~1590 cm^{-1} for the tangential G-band; at ~1350 cm^{-1} for the

disorder-induced D band, and at ~2900 cm^{-1} for its second-order harmonic, the G' band [136].

Recently, direct and label-free mapping of CNTs inside living cells has been demonstrated using the intrinsic NIR [117, 124, 301] and Raman scattering [124]. Figure 3.1C and 3.1D represents the Raman spectra of pristine and oxidised-wrapped with RNA double walled CNTs (DWNT and oxDWNT-RNA, respectively) in two different laser energies: 473 and 785 nm, respectively. As displayed, Raman spectroscopy of CNTs present intense bands at 120-350 cm^{-1} for the RBM; at ~1590 cm^{-1} for the tangential G-band; at ~1350 cm^{-1} for the disorder-induced D band, and at ~2900 cm^{-1} for its second-order harmonic, the 2D or G' band. The different laser energies present the same structure for oxDWNT-RNA and the pristine sample, indicating that the resulting Raman spectrum is originated from the same nanotubes. Additionally, TEM and AFM demonstrate that oxidised samples wrapped with RNA (Figure 3.1A and 3.1B) were more de-bundled and individualised, with length ranging from 200 nm to 2 μm.

3.3.2 Cellular uptake and release of DWNT by Raman spectroscopy

Detection of CNTs inside cells is not trivial as (in their pure form) they consist of only carbon atoms linked by covalent C=C double bonds and thus are not easily discernable from biological materials by standard spectroscopic methods. Their small size and low contrast also makes them difficult to distinguish from cellular structures by microscopy techniques. Direct and label-free mapping of CNTs inside living cells has recently been demonstrated using the characteristic intrinsic NIR fluorescence [117, 124, 301] and Raman scattering [124] of CNTs. However, a marked decrease in intensity of CNT intrinsic fluorescence has been observed [124] following protracted periods (8 days) in culture; in contrast the Raman signal is stable over the same time period. The aim of this study was to further investigate cellular uptake and fate of DWNTs.

3.3.2.1 RBM mapping of single cells

The RBM is a unique phonon mode, appearing only in CNTs and its observation in the Raman spectrum provides direct evidence that a sample contains single or double walled CNTs. It depends linearly on the nanotube diameter and each nanotube wall in a sample will have different RBM spectra. The same distribution of RBMs with peaks at 156, 205, 230 and 266 cm^{-1} were detected in pristine DWNTs, DWNTs inside PC3 cells (human prostate adenocarcinoma cells) and extracellular DWNTs, indicating that there was no selectivity of DWNTs by the cellular system (Figure 3.2A). Applying the equation $\omega_{RBM} = 248/d_t$, where ω_{RBM} is the RBM frequency in cm^{-1} and d_t the diameter in nm [275], it is possible to extrapolate the diameters present in the mixture. The diameters in the sample ranged from: 0.9 nm to 1.1 nm, 1.2 nm and 1.58 nm, where the diameters 0.9 nm and 1.58 nm dominate. This unique property allows the identification of structural features of DWNTs and for that reason can be used to accurately identify their distribution inside cells.

PC-3 cells, were used to evaluate the temporal uptake of CNTs by means of Raman mapping of RBMs. Cells were exposed to nanotubes for a period of 3-hour and further incubated for 24-hour. Before data acquisition, a grid was defined on a single cell, and then mapping obtained by collecting spectra with 1-minutes exposure time and moving the sample with increments of 1 μm (spectral resolution of 4 cm^{-1}). To analyse the data an intensity of ~260 cm^{-1} was used, corresponding to the 0.9 nm diameter, as that was the most recurrent peak in the sample collection.

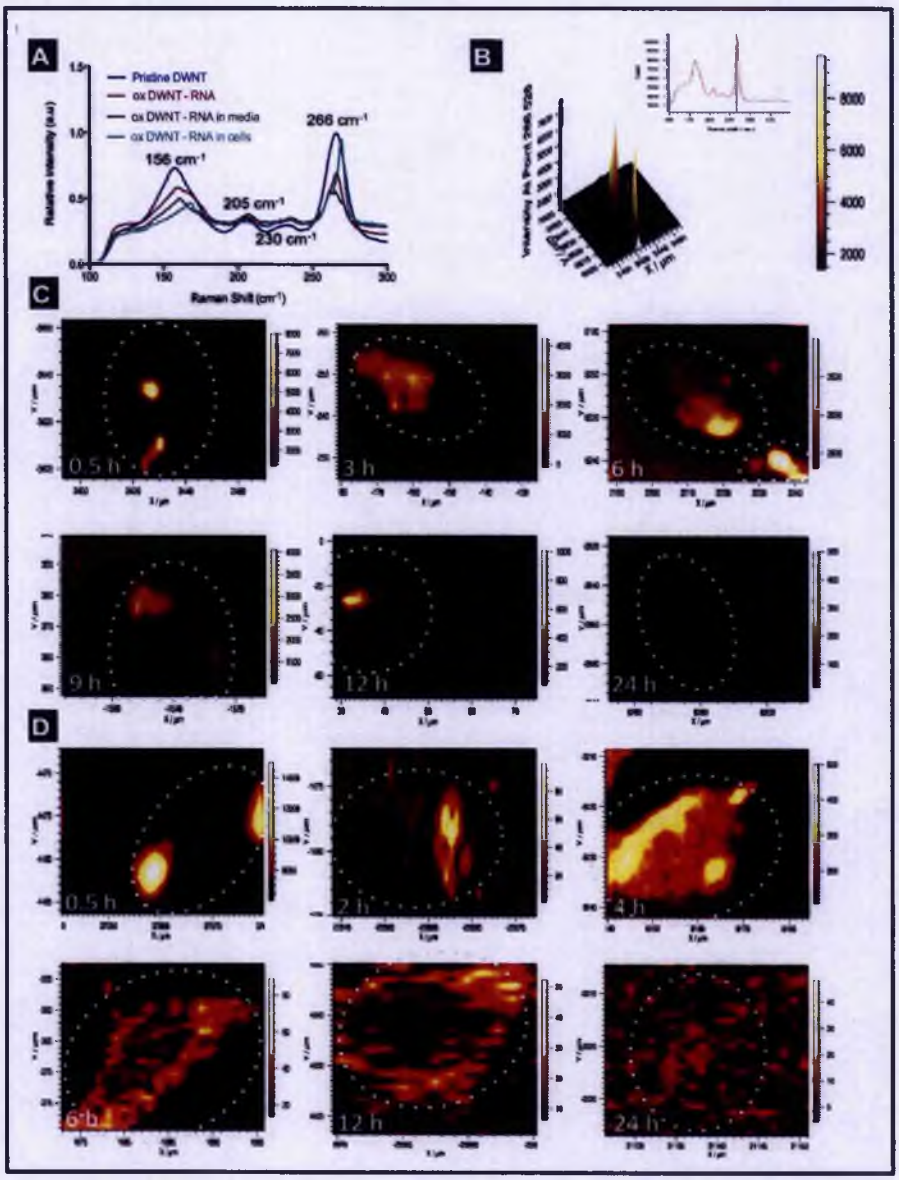

Figure 3.2: Single cell mapping of PC3 and HeLa cells exposed to DWNTs. RBMs were used to track DWNTs in cells. As displayed, a uniform distribution of diameters is obtained in all different conditions: pristine nanotubes, oxidised DWNT wrapped with RNA, and the same oxDWNT-RNA in cell medium and inside cells (A). A grid was defined on a single cell, and a map obtained by collecting spectra with 1 min exposure time and moving the sample with increments of 1 μm (spectral resolution of 4 cm^{-1}). Data analysis was performed at ~260 cm^{-1} as illustrated by RBM spectra and the 3D map (B). (C and D) 2D mapping at various time points from 0.5 to 24-hours in PC3 (C) and HeLa (D). The broken line in the different figures from 0.5 to 24-hours crudely represents the boundaries of the cell and demonstrates that a high intensity is confined to the cell, an effect not observed for media alone. Different scales are exhibited at different time points demonstranting a reduction in the signal with time.

Figures 3.2C and 3.2D illustrates the distribution of those nanotubes inside PC3 and HeLa cells at different time points, from 0.5 to 24-hours. It exhibits different levels of intensity at the different time points, starting with high intensity after 0.5-hours, which gradually loses intensity after 9-hours of incubation. The broken line in the different figures from 0.5 to 24-hours crudely represents the boundaries of the cell and demonstrates that high intensity is confined to the cell an effect not observed for media alone. Additionally at 0.5-hours, an interesting feature was detected whereby the intensity associated with CNTs was well confined as dots. This is suggestive of nanotubes residing inside subcellular structures, possibly endosomes. Between 3 and 9-hours the intensity is lower but more spread throughout the cell indicating that CNTs have been released from their initial site of sequestration. After 12-hours the intensity drops, until finally at 24-hours no intensity for RBM mode at 260 cm^{-1} could be measured (merely a residual signal which can be related with an increase in the signal/ noise ratio).

3.3.2.2 Cell viability and percentage of carbon nanotube intake in mammalian cells

An estimation of the percentage of cells containing CNTs is presented in Table 3.1, which indicates the number of cells with CNT specific Raman peaks. The maximum percentage of cells with nanotubes was obtained at 3-hours, with 50 % of the cells giving rise to a Raman signal. The proportion of cells containing CNTs decreased roughly 3-fold at 12-hours and 5-fold at 24-hours. Finally, viable cells were counted over time, demonstrating that no significant cell death occurred during incubation with CNTs complexes described herein (Table 3.1).

Table 3.1: Cell viability after exposure to CNTs. Cell count and percentage of cells containing to CNTs over 24-hour.

Time points (hours)	Cell count (cell/mL)	Proportion of cells containing CNTs (%)
0	8.25×10^4	0.00
0.5	7.25×10^4	20.00
3	8.58×10^4	50.00
6	8.50×10^4	37.50
9	7.42×10^4	22.00
12	8.25×10^4	16.67
24	11.58×10^4	11.00

3.3.2.3 G band intensity on whole cell lysates

In another approach PC3 and HeLa cells exposed to CNTs were disrupted and the cellular content was used to evaluate the time dependent uptake. By disrupting the cells only the cytoplasm is considered, excluding CNTs associated with the plasma membrane and nucleus. Our findings therefore possible eliminate the possibility that CNTs might merely be associated with the cell surface and not represent an experiment artifact. Furthermore, one could consider that reduction of the Raman signal observed over the 24-hour time-course in individual cells (Figure 3.2) could be due to diffusion of discrete concentrations of DWNTs (for instance, from endosomes) throughout the entire volume of the cell; or by loss of DWNTs by the cell. Though, by lysing the cells, CNTs were measured in the same volume for all samples throughout the time-course. Our results focus essentially on the 700cm^{-1} to 3000 cm^{-1} region of the spectra, giving a full picture of the behaviour of the different Raman bands observed. Figure 3.3 displays the Raman spectra for PC3 cells exposed to DWNTs at the various time points. The CNT-characteristic G, D and 2D (G') Raman bands were detected. Additionally, four other peaks were visualised at ~1090, ~1450, ~1660 and ~2900 cm^{-1}, which previous studies [302-304] have associated with cellular constituents.

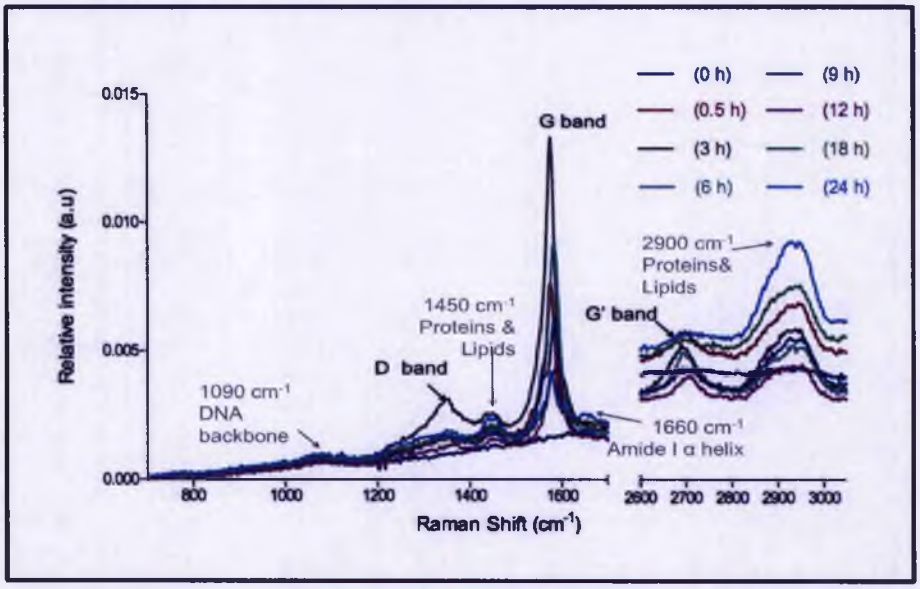

Figure 3.3: Temporal evaluation of CNT uptake by PC3 prostate cancer whole cell lysates. Raman spectrum at different time points obtained after exposure to oxidised, oxDWNT-RNA. CNT features are visualised at 1350, 1590 and 2700 cm^{-1} with D, G and G' bands and cellular constituents at 1090, 1450, 1660 and 2900 cm^{-1}. Spectra are normalized such that in each data set 100% represents the sum of all values in the data set.

The CNT-specific G band at 1590 cm^{-1}, is derived from the symmetry breaking of the tangential vibration when the graphene sheet is rolled to make a cylindrically shaped tube. For SWNTs the G band produces a multi-peak, which permits differentiation between metallic and semiconducting nanotubes. This multi-peak feature is not observable for DWNTs and MWNTs due to the large tube diameters. The G band corresponds to the LO phonon breathing modes of CNTs that is characteristic of all sp^2 carbon materials [305] and is therefore a useful tool to quantify DWNTs.

Figure 3.4 illustrates the variation of the area of G peak over time, in both PC3 and HeLa cells. Revealing a maximal intensity at 3-hours (statistically significant $p<0.0001$, one-way *ANOVA*) and a minimum at 24-hours ($p > 0.05$, one-way *ANOVA*), which corresponds to the times for maximum uptake and release measured in individual cells (Figure 3.2 and Table 3.1). The observed reduction of Raman signal in cell lysates indicates that the DWNTs are being lost from the cell, rather than merely diffusing through the cells. In addition, to investigate the effect of proteins and biomolecules on the G band intensity over time, cell lysates were incubated with known concentrations of DWNTs. In Figure 3.5 no significant alterations for the G

band are visualised suggesting that proteins and biomolecules do not alter the peak intensity.

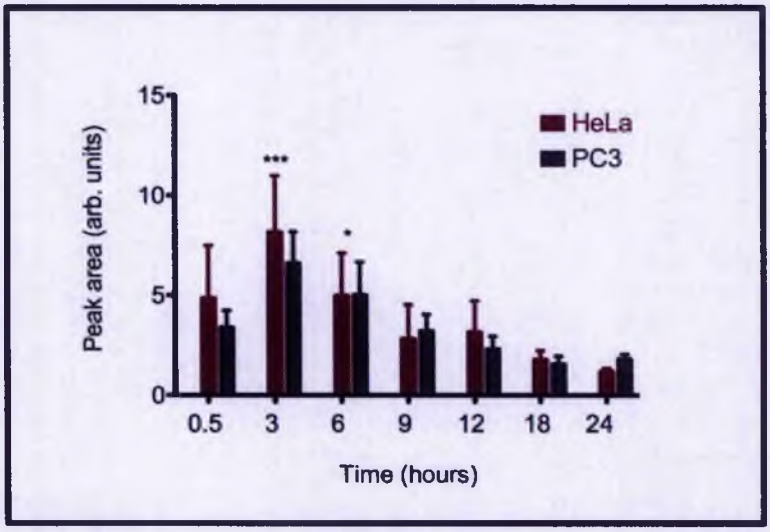

Figure 3.4: G band intensity in PC3 and HeLa cells exposed to CNTs. (A) Area under the curve (AUC) of G band intensity at the various time points. (*** indicates $p < 0.0001$ and * $p < 0.05$ relative to point 0-hours, one-way *ANOVA*). Demonstrating uptake with maximum at 3-hour and subsequent release. Results presented as Mean±SEM (n=6).

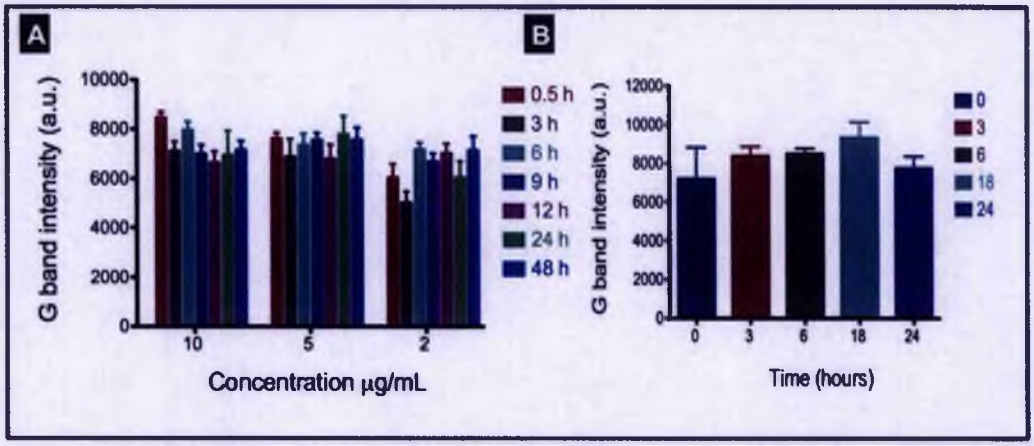

Figure 3.5: Effects of proteins and biomolecules on the G band intensity over time. (A) G band intensity of cell lysates incubated with different concentrations of DWNTs (p value non significant for data set ($p > 0.4$ relative to point 0-hours, one-way *ANOVA*). (B) G band intensity of different time point lysates, incubated with 5 µg/mL of DWNTs ($p > 0.2$ relative to point 0-hours, one-way *ANNOVA*). Results presented as Mean±SEM (n=6).

3.3.2.4 Concentration of CNTs per cell

The G band intensity was calibrated by reference to quantify samples of pure RNA-wrapped oxidised DWNTs and used to provide an estimate of CNT concentration within the cell lysates, Figure 3.6.

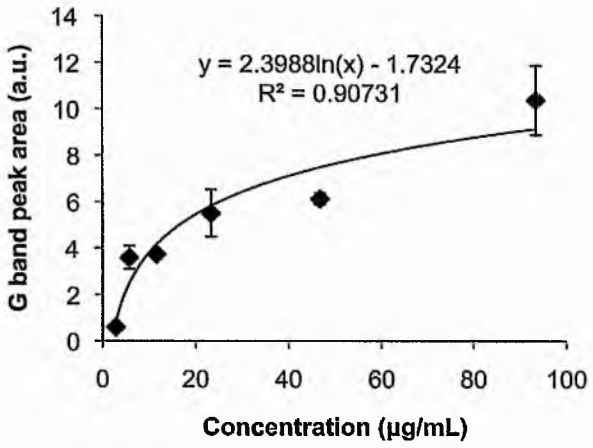

Figure 3.6: G band Calibration curve. Correlation between G band intensity and CNT concentrations (µg/mL).

To determine the concentration of CNTs in whole cell lysates and also on a per cell basis, the relation between G band and concentration was used. Using the G band intensity at each time point and an approximate cell volume of 5.75×10^{-9} µL, the concentration of DWNTs inside cells was estimated in pg per cell, Table 3.2. Taking the maximum intensity, 3-hours, and given that the initial concentration of CNTs in the media was 30 µg/mL, approximately 20 % of the initial dose was internalised by cells (5.85 µg/mL). This maximum with 33.63×10^{-6} pg per cell was then gradually released over a period of 24-hour (due to a decrease in the noise to aspect ratio the 24-hour time point was excluded from the data set).

Table 3.2: Concentration of CNTs in cells. Correlation between G band intensity and concentration of CNTs was used to determine the concentration of internalised CNTs per cell (Cell volume = 5.75×10^{-9} µL [299]).

Time points (h)	G band area peak (a.u.)	Concentration per lysate (µg/mL)	Concentration per cell (pg/cell)
0.5	1.11	0.55	3.1×10^{-6}
3	9.324	5.85	33.6×10^{-6}
6	6.255	4.23	24.3×10^{-6}
9	1.891	1.25	7.2×10^{-6}
12	1.414	0.83	4.8×10^{-6}
18	0.8723	0.31	1.8×10^{-6}

3.3.2.5 Defects/degradation of DWNT walls.

An additional finding was obtained from the ratio of the intensity of the D band intensity by the intensity of G band (I_D/I_G). The D band has been related with the defects intensity in a sample, for example during the process of oxidation (see Figure 3.1, after oxidation peak is more intense). While G band has been related to vibration along the C-C bonds. Therefore, the ratio of I_D/I_G can be used to monitor the integrity of DWNTs [305]. This ratio is plotted in Figure 3.7A, where it was apparent that the intensity of the D band increases roughly linearly relative to the G band with increasing incubation periods suggesting that more defects were added to the nanotubes. As shown only I_D/I_G ratio after 3-hour was considered, as this was the point where cells were washed to remove extracellular DWNTs. Due to a increase in the signal/ noise ratio at 24-hour time point was excluded from the data set. These results suggest that the nanotubes are being modified or degraded during their incubation inside cells. However, the D peak is relatively weak and therefore difficult to quantify. So, to investigate this phenomenon further the RBM obtained from single cell mapping was analysed. First, only diameters of 0.9 and 1.58 nm were considered, as those were acquired in larger numbers. Besides, the diameters of 1.1 and 1.2 nm are believed to be part of a population of single walled or even inner walls of larger nanotubes. DWNT used in these experiments have been fully characterised [247] and

it was shown that 20 % of the nanotubes are single walled. In addition, as shown by TEM (section 2.2), the pristine DWNT contain nanotubes with larger diameters. However, Raman cannot acquire the diameter of these nanotubes as they are away from Raman spectral resolution. Secondly, we propose that the 1.58 nm diameter consists on the outer wall of a 0.9 nm inner wall (Figure 3.7B). This assumption accurately matches the interlayer spacing of CNTs, which is 0.344 nm [306]. For the different diameters, a sample collection of 10 spectra were taken into account. The percentage of distribution of the diameters over time is displayed in Figure 3.7C and 3.7D. For the diameter of 1.58 nm the distribution linearly decreases, suggesting that fewer nanotubes with 1.58 nm diameter were found in cells after 6-hours when compared with the initial time point. Contrasting with this, the 0.9 diameter distribution shows uniformity until 12-hours and only decreases after this point, which could be associated with possible disintegration of the outer wall after the 6-hour time point but the preservation of the inner wall up to 12-hours. The subsequent sharp decrease in the inner wall signal at 24-hours could be due to loss of nanotubes from the cell or defects accumulating in the inner tube. However, even at this time-point the peak corresponding to the outer wall is still apparent in 30 % of samples so we consider it is more likely that the tubes are being lost from the cell at this time-point. Additionally, *in vitro* studies by Allen *et al.* 2008 [307] found significant degradation of SWNTs but only after 12-weeks incubation at 4 °C with low concentrations of H_2O_2 and peroxidase. Also, Liu *et al.* 2010 [308] incubated SWNTs with a chemical mixture simulating the phagolysosomal compartment and found that only oxidised but not pristine SWNT were significantly degraded after 90-days. Together, these results suggest that besides the defects on the DWNTs during 24-hour incubation, the DWNT are probably being lost from the cells, rather than being entirely degraded.

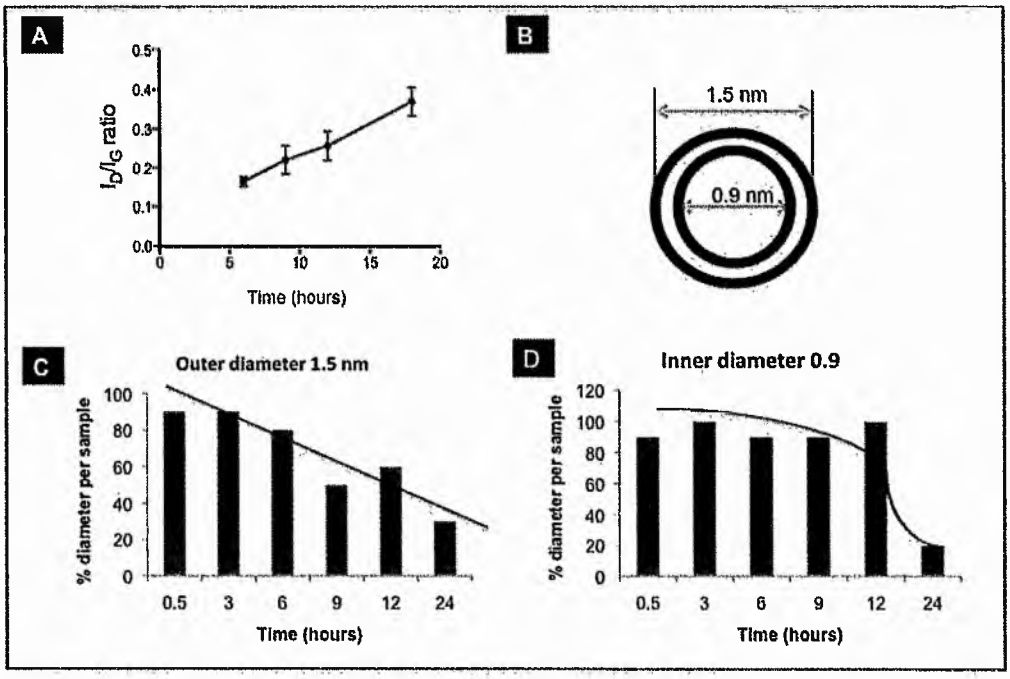

Figure 3.7: Increase in defects on DWNT walls. A) Raman D/G intensity ratio for CNTs in PC3 cells at different time points from 6 to 18-hours (3-hour was the point where absorption finished and from then on *only* excretion occurred. Due to the increase in the signal-to-noise ratio at 24-hours, this time point was excluded from the data set). Error bars were calculated using the standard mean error (n=6). B) Conformation of a DWNT (matching interlayer spacing of CNTs of 0.344 nm). C) 1.58 nm diameter distribution over time inside cells. D) 0.9 nm diameter distribution over time inside cells (lines in C and D represent the trend visualised for diameter distribution of the different nanotube walls).

3.3.3 Cell biochemistry analysis by Raman over a 24-hour time frame on cells exposed to DWNTs and controls

Raman spectroscopy has been previously used as a biological tool to assay and study cells and present several advantages when compared with conventional methods. It is fast; non-invasive and no labels are required, and no damage is induced to the cell if suitable laser wavelength and intensities are used [303, 309]. During the analysis of Raman spectra of cell lysates other peaks could be perceived which were not related to CNTs (Figure 3.3). Bands were essentially detected at: ~1090 cm^{-1}; 1450 cm^{-1}; 1660 cm^{-1}; and 2900 cm^{-1}. In the literature, these bands are related to cellular constituents such as DNA/RNA, proteins and lipids [302-304]. For instance, the band

at 1090 is the most closely related to the process of cell death; this peak corresponds to DNA O–P–O backbone stretching. If a decrease of the intensity of the peak occurs then this indicates that breaks of phophodiester bonds are taking place leading to disintegration of the nucleic acids [310].

Figure 3.8 shows a spectrum that illustrates the behaviour of the different cellular component bands on PC3 cells exposed to CNTs and the PC3 controls overtime. As demonstrated, no significant variation is visualised for the DNA O–P–O backbone stretching (at 1090 cm^{-1}). Moreover, similarly behaviour was perceived at ~1660 cm-1; this peak corresponds to amide I vibrations in proteins and C=C in lipids according to the work of Puppies *et al.* [309]. In addition protein and lipid concentrations are indirectly revealed by spectra profiles of C-H stretch vibration bands in the interval from 2800 to 3100 cm^{-1}. Symmetric and antisymmetric CH_3 stretch vibrations are located near 2930 and 2950 cm^{-1}, respectively. Similar CH deformation bands have been shown to occur in lipids near 1440 cm^{-1} and proteins near 1450 cm^{-1} [304]. Once more, no significant changes were detected with the exception of a slight increase for ~2900 cm^{-1}. This increase was observed for both cells exposed to CNTs and in controls and as demonstrated by both cell count and protein quantification can be correlated with normal cell proliferation. Additionally, overall protein levels were monitored by gel electrophoresis, which confirmed that no significant changes in protein levels occurred during the incubation (Figure 3.9). Together, these results indicate that the uptake of DWNTs did not induce any detectable biochemical alterations in the cell.

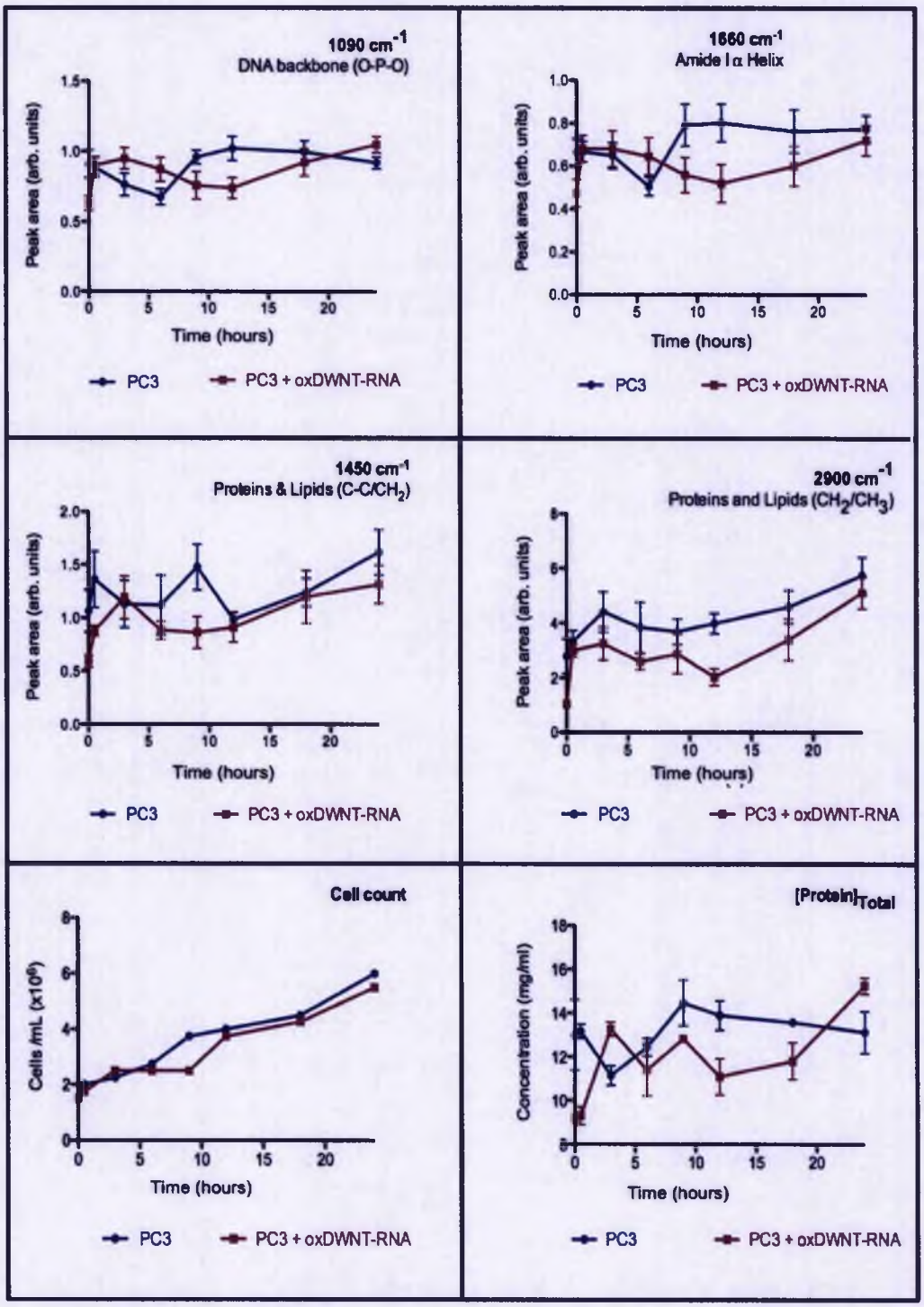

Figure 3.8: Temporal evaluation of cellular constituents on PC3 prostate cancer whole cell lysates. Intensity of Raman bands associated cellular components, such as DNA/RNA, proteins and lipids, cell count and total protein over time on cells exposed to CNTs and controls. Spectra are normalized such that in each data set 100% represents the sum of all values in the data set. Results presented as Mean±SEM (n=6).

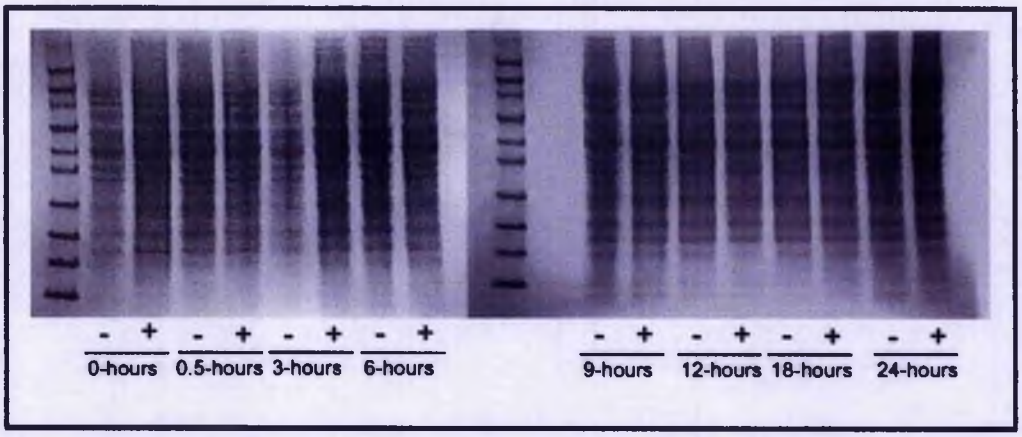

Figure 3.9: Protein electrophoresis gel of PC3 cell lysates treated (+) and untreated (-) with CNTs. No gross changes in the protein pattern were observed throughout experiment, from 0 to 24-hour.

3.3.4 Evaluation of stress response over 24-hour time frame on cells exposed to DWNT and controls

As previously stated, cell viability was unchanged during the course of the experiment, indicating no direct effect of DWNTs on cell mortality. However, we also examined cells for any sign of cellular stress response to DWNT uptake. Initially two markers, commonly employed to measure levels of cellular stress, were considered, p53 and mitogen-activated protein kinase (MAP kinase). p53 is a tumour suppressor gene and its protein is hardly detectable [311]. However, on cellular stress, particularly induced by DNA damage, p53 can arrest cell cycle progression, thus allowing DNA to be repaired [312], which can lead to apoptosis [313]. In cancer cell lines that possess a mutant p53 allele, the protein is no longer able to control cell proliferation, which results in inefficient DNA repair and the emergence of genetically unstable cells [314-317]. PC3 prostate cancer cell line possess mutated p53 [318], as suggested by western blot data (Figure 3.10) whereby a lack of induction (i.e. increase) is apparent from the flat response in p53 protein levels, for both CNT-exposed cells and untreated controls.

Cells recognise and respond to extracellular stimuli by engaging specific intracellular pathways, such as the signaling cascade that leads to activation of mitogen-activated protein kinases (MAPKs) [319]. Part of the MAPK family, are the extracellular-signal-related kinase 1 (Erk 1, 44 kDa protein - p44) and 2 (Erk 2, 42 kDa protein - p42) and their activation requires phosphorylation by upstream kinases. In Figure 6 both phosphorylated (Erk1/2) and non-phosphorylated (Erk 2) forms were detected. No change in the expression levels of native protein for Erk p44/p42 was perceived. In contrast the phosphorylated activated form was only observable in the positive control sample and with negligible amounts seen for PC3 cells exposed to CNTs over a 24h period.

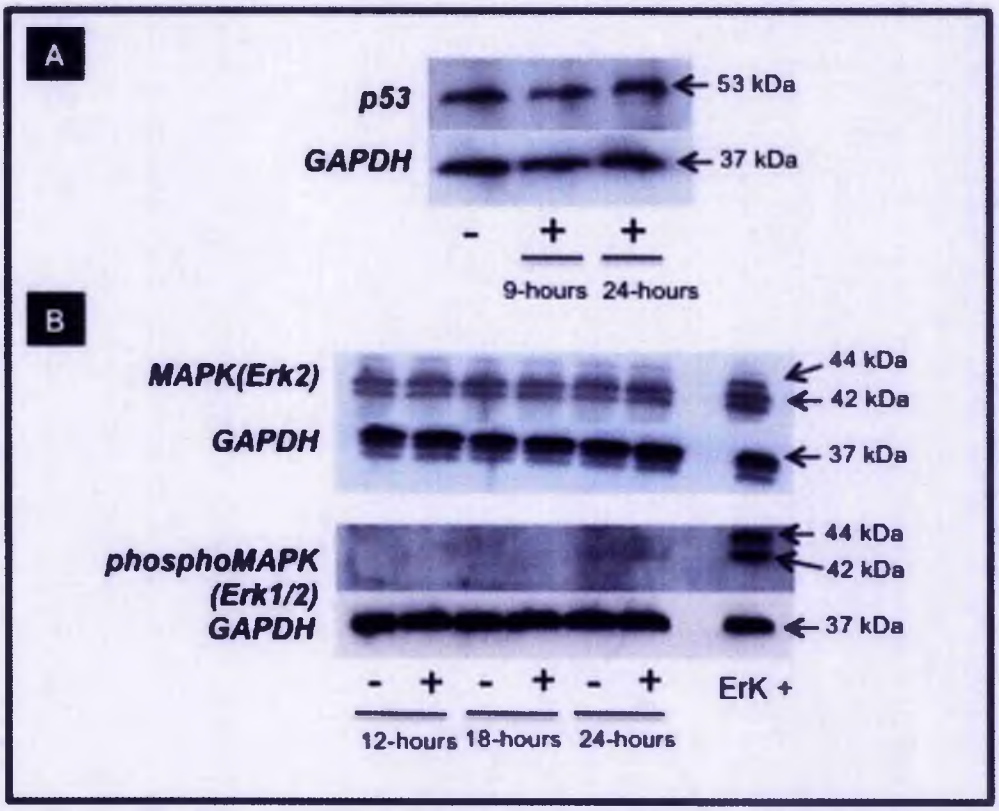

Figure 3.10: Stress response of PC3 cells exposed to DWNTs (+). p53 (A), MAPK (Erk 2) and phosphorylated MAPK (Erk 1/2) (B) expression on cells exposed to CNTs. Negative control without CNTs (-) was also considered.

3.4 Conclusions

The application of CNTs for biomedical purposes, including drug and gene delivery has been intensively study in the recent years. The key aspect, however, is to understand their interaction with cells. Controversy has arisen as to how CNTs are taken up by cells, their final fate and especially their safety. For any study, it is extremely important to consider the purity of CNT preparation, their size and concentration. The results presented in this chapter show evidence that the prepared biofunctional DWNT (by oxidation and RNA-wrapping) can be taken up *in vitro* and subsequently released by cells over a 24-hour time period. The fate of CNT visualised in our studies is certainly dependent on the modification of CNTs and methodology, RNA-wrapping and incubation conditions, 3-hour exposure to DWNT and consequent release over a 24-hour time course. Jin *et al.* 2008 reported the first evidence for exocytosis of CNTs by using single particle tracking (SPT). In their report it was demonstrated that the rate of exocytosis closely matches the rate for endocytosis [142]. The time frame of this study was shorter then the one presented here, cells where exposed to DNA wrapped single-walled CNTs for approximately 16-minutes after which media was perfused for a period of approximately 2-hours. In addition, that particularly study reported aggregation of SWNT that remained internalised through the duration of the experiment [142].

Although these results can be correlated with previous studies, in the work presented here it was demonstrated that nearly all CNTs were eventually released from the cells. This was shown with both studies of individual cells, but also with lysates from cell populations. Furthermore, strong evidence was presented of non-toxicity at a cellular level from both Raman analysis of DNA/RNA; proteins; and lipids; and activation of stress responses by immunobloting. There was no evidence of any detectable effect following the DWNT uptake and release.

A novel feature of these studies was that changes in I_D/I_G ratios and RBM modes were observed during the course of incubation of cells with DWNTs. The source of these changes is currently uncertain, but suggests that the outer walls of DWNTs are being modified during their passage through the cells.

In conclusion, our results demonstrate that DWNTs prepared appropriately and administered in reasonable quantities are non-toxic for human cells and potentially suitable for medical applications.

Chapter 4: Intracellular localisation of CNTs

4.1 Introduction

The mechanisms that control the cellular uptake of CNTs are currently poorly understood. So far, besides the demonstration of the ability of CNTs to enter and penetrate cell membranes [126, 128, 131], the uptake mechanism is still debated and may concern more than one process. Hence, Kam *et al.* and Jin *et al.* reported that protein or single-stranded oligonucleotide-modified CNTs could enter cells by means of endocytosis [115]. In contrast, Kostarelos *et al.* suggested an energy-independent non-endocytic mechanism involving the insertion and diffusion of CNTs through different cellular barriers [128].

Endocytosis is a frequent cellular event that transfers extracellular or membrane-bound cargoes, such as nutrients, from the plasma membrane into the cell interior via vesicular transport. In this process, endocytic vesicles form invaginations of the plasma membrane that subsequently pinch off, move internally, and fuse with other endocytic vesicles to form an early endosomal compartment (Figure 4.1). The endocytic process may involve so-called clathrin coated pits (I.e. be clathrin-dependent). Clathrin forms a complex network in the form of a lattice that is built up to form a coat. Alternatively, there may be clathrin-independent endocytic processes involved in cellular trafficking. The early endosome is the major sorting station in the endocytic pathway. From this organelle, material can be directed toward the pathway of recycling to the plasma membrane, to subsequent endocytic compartments and to regulated secretory vesicles [320]. The example of transferrin, a monomeric iron transporting serum glycoprotein is processed in the late-endosome, after which the transferrin receptors are recycled by a recycling endosome [318]. The recycling endosome is typically less acidic (pH 6.4-6.5) than the sorting endosome (pH 6.0) and exhibits a pericentriolar localisation [321]. Late endosomes contain active degradative enzymes. However, these are more concentrated in the lysosomes. The transfer of material between late endosomes and lysosomes appears to be a direct fusion event that results in a transient hybrid organelle [320].

As illustrated in Figure 4.1 each of these steps is independently regulated by the interaction of multiple proteins. Among the proteins present are several small GTP-binding proteins of the Rab family. These proteins have been particularly examined because of their effectiveness as molecular markers for various types of endosomes. Rab5, an example of such GTPase, regulates the rate of Clathrin-dependent endocytosis at the plasma membrane [322] and can be used as a marker for early sorting endosomes in addition or in conjunction with the transferrin receptor. Rab11 localises to a pericentriolar subpopulation of recycling endosomes [323]. It is pertinent to point out that the process of endocytosis is a complex process that has yet to be completely defined despite the significant progress in understanding its various components.

Figure 4.1: Mechanism of endocytosis. After internalisation by endocytosis, the cargo can undertake different routes post-sorting in the early endosome (EE). It can be recycled back to the plasma membrane either directly or via a perinuclear recycling endosome (RE) compartment, or transported to late endosomes (LE) and lysosomes. The biosynthetic and endocytic circuits (arrows) exchange material at the level of the Golgi apparatus and the endosomal elements. The localisation of selected mammalian Rab proteins in the membrane compartments participating in these transport are indicated. (ER, endoplasmic reticulum; TGN, trans-golgi network; CV, constitutive secretory vesicles; RV, regulated secretory vesicles) (adapted from Stanmark *et al.* [324].

Identification of the mode by which CNTs move between cellular compartments after their internalisation, and the sites in which they localise has been thus far mainly accomplished by simple staining of lysosomes by pH-dependent markers (e.g. Lysotracker red) [132, 142] by TEM [127, 142, 324], or by pharmacological inhibition of the endocytic pathway [128, 132]. For example, Kam *et al.* first described an energy dependent mechanism. In their studies clathrin mediated endocytosis was proven by experiments carried out at inhibitory conditions (Chapter 1, section 1.3.1). Using TEM, Yehia *et al.* 2007 observed that SWNTs dispersed in media were endocytised and localised in the plasma membrane, cytoplasm, endosome, lysosome and golgi bodies [140]. Similar methodology was used by Mu *et al.* 2009, who proposed a working model for cell uptake of MWNTs modified by carboxilation or amidation, using TEM imaging [325]. In their model CNTs were not only internalised via endocytic pathways but also through membrane penetration, depending on the CNT bundles or highly dispersed single CNTs, respectively. After internalisation, through endocytosis or membrane penetration, CNTs were both found in lysosomes followed by excretion. However, no data was presented on the mechanism of exocytosis [325]. Jin *et al.* 2009 presented the first evidence of exocytosis of CNTs, which was found to closely match the endocytic rate [142].

In contrast to the endocytic pathway, Lacerda *et al.* reported for the first time that membrane penetrating CNTs (SWNTs modified via cycloaddition) can lead to their accumulation in the perinuclear region of mammalian cells. Besides, another study performed by Zhou *et al.* in 2010, also showed an endocytosis-independent mechanism for non-covalently modified SWNTs [326]. In their studies, incubations at 4 °C and with NaN_3 were carried out, which did not prevent CNTs from being internalised. In addition, HeLa cells were transfected with plasmids encoding fusion proteins, such as DsRed-golgi (to label golgi apparatus), DsRed-ER (to label ER), and CFP-lamp (to label lysosome). MitoTracker marker was also employed for staining of mitochondria. Their results show that functionalised SWNTs co-localise exclusively in mitochondria of both tumour and normal cells, but CNTs were also found in lysosomes of macrophages due to phagocytosis [326].

Besides the great effort to elucidate the uptake mechanism of CNTs and their intracellular localisation, an appreciation of global intracellular trafficking is yet missing. Herein, we attempt to complete this study using organelle specific markers to describe and to identify the mechanisms through which CNTs transport itself as they enter and eventually effluxes from cultured human prostate cancer cells.

4.2 Experimental section

In the experimental section a description of the methodology is presented. Firstly, the labelling of CNTs with a fluorophore is introduced that permits the visualisation of these complexes inside cells. Secondly, different immunofluorescent methods were applied to identify cellular structures involved in endocytic pathways. Consequently, the co-localisation or overlapping of these colours, observed by confocal microscopy, of both stainings (CNT-fluorophore and stained cellular compartment) determines the intracellular localisation of CNTs.

4.2.1 Preparation of fluorescently labelled oxidised DWNTs

DWNTs synthesised by the CCVD technique [247] were purified in concentrated nitric acid and oxidised in a mixture of nitric and sulphuric acid (detailed information is given Methods – Chapter 2) [185]. After oxidation, nanotubes were sterilized by autoclaving at 121 °C for 1-hour and were maintained under sterile conditions for the duration of the experiment. In a second step, the oxidised DWNTs (oxDWNT) were coated with fluorescently labelled molecules: RNA and Poly(Lys:Phe) as described bellow.

4.2.1.1 RNA-fluorescein wrapped oxidised DWNT

Coating of oxDWNT with RNA was achieved using ready-made fluorescently labelled RNA (Eurofins – MWG Operon), with the oligonucleotide sequence (5') CAUUCCGAGUGUCCACAUUCCGAGUGUCCA-FLU (3') (RNA-FS). Synthesis reports oligonucleotide with molecular weight of 10052 g/mol, Tm of 69.5 C, GC-content of 53.3 % and purification by High-Performance Liquid Chromatography (HPLC). A solution of 1.0 mg/mL (prepared in sterile water) was diluted 1 to 5 in a solution of oxDWNT at a concentration of 200 µg/mL (Ratio CNT/RNA 1:1). After that, the complexes were allowed to form by stirring for 2-hours at room temperature (± 21

°C), in the dark. To remove the unbound RNA-FS, the solution was filtered and washed several times using 100 kDa centrifugal filters (Millipore). Finally the RNA-Fluorescein wrapped oxidised DWNT (oxDWNT-RNA-FS) were resuspended in sterile water to a final concentration of 200 μg/mL.

4.2.1.2 Poly(Lys:Phe)-Fluorescein wrapped oxidised DWNT

To prepare fluorescently labelled Poly(Lys:Phe), a solution of NHS-Fluorescein (0.2 mg/mL) was diluted 1:4 in a solution of Poly(LysPhe) (0.2 mg/mL), prepared in carbonate buffer 20 mM, pH 8.5 (all sterilised by filtration). Followed by incubation for 2-hours in the dark, at room temperature, while stirring. Next, the complexes were conjugated with oxidised DWNT (final concentration 500 μg/mL) and once more incubated for 2-hours in darkness at room temperature (± 21 °C), while stirring. The unreacted fluorescein and Poly(Lys:Phe) was filtered and washed several times using 100 kDa centrifugal filters (Millipore). Finally the Poly(Lys:Phe)-Fluorescein wrapped oxidised DWNT (oxDWNT-RNA-FS) were resuspended in sterile water to a final concentration of 200 μg/mL.

4.2.2 Cellular incubation with CNTs-complexes

PC3 cells were cultured in RPMI-1640 medium supplemented with 10 % FBS, 2mM Glutamax™ and 1 % penicillin-streptomycin (all obtained from Invitrogen, Paisley, UK). Cells were cultured in 24-well (13 mm-well) sterile plates (Nunc, Thermo Scientific) containing glass coverslips (VWR) for 24-hours so they were 50 % confluent at the time of exposure to CNT-complexes.

4.2.2.1 Incubation with inhibitory drugs

For adenosine triphosphate (ATP) depletion studies, a PBS buffer solution, supplemented with 10 mM sodium azide (NaN_3) and 50 mM D-glucose was diluted 1 to 2 in complete RPMI media and incubated with cells for 2-hours at 37 °C, followed by incubation in a solution of CNT-complexes. For inhibitory conditions with Ly294002 (phosphoinositide 3-kinase inhibitor) and 3-methyladenine (inhibitor of autophagic sequestration), cells were incubated overnight with 10 μM of drug before adding the CNT-complexes.

4.2.2.2 Incubation with CNT-complexes

PC3 cells growing in 24-well plates were incubated with 30 μg/mL CNT-complexes diluted in complete RPMI media. After incubation for 2-hours, cells were washed twice with sterile PBS (Invitrogen, Paisley, UK) and fresh media containing FBS was added for 5- and 20-minutes. Cells were again washed with sterile PBS and treated for 10-minutes with cellscrub (Genlantis, San Diego, USA) washing buffer, to remove all extracellular CNT-complexes. Finally, cells were washed twice more with sterile PBS.

4.2.3 Cell fixation

To prevent morphological changes, cells were fixed with 4 % (w/v) paraformaldehyde (Sigma Aldrich, Poole, UK) solution in PBS, for 1-hour at room temperature. Then cells were washed once more with sterile PBS and treated with 0.1 % Triton X100 (Sigma Aldrich, Poole, UK) in PBS, to allow permeabilisation of cell membranes.

4.2.4 Compartment staining (using phalloidin, ToPro3, lysotracker red & transferrin)

Cell membranes associated actin filaments were stained using phallotoxins (Alexa fluor 555 phalloidin – emission 565 nm) with a final concentration of 0.044 μM. Transferrin conjugates (Alexa Fluor® 546 - emission 573 nm) at a concentration of 20 μg/mL were applied to stain endosomes from clathrin-dependent endocytosis, and acidic cell compartments (lysosomes) were stained using LysoTracker® Red DND-99 (emission 590 nm) at a final concentration of 1 μM. All agents were diluted from freshly made stock solutions in 0.5 % bovine serum albumin (BSA) in sterile PBS and given to cells after fixation, for a period of 15-minutes. Then cells were washed 3-times with PBS and finally, To-Pro®-3 (emission 661 nm), monomeric cyanine nucleic acid stain was applied in order to visualise the cell nucleus in all samples. It was employed at a final step with a concentration of 0.1 μM in PBS (all reagents from Invitrogen- Molecular Probes Corp).

4.2.5 Immunostaining

Subsequent to cell fixation and permeabilisation, cells were incubated for 90-minutes with primary antibodies (Santa Cruz Biotechnology, Inc; supplied by insight biotechnology; Harrow, UK) diluted in PBS containing 0.5 % BSA, as described in Table 4.1. Cells were then washed three times with PBS and incubated for 1-hour with fluorescent secondary antibody (Alexa fluor® 546 from Invitrogen) diluted 1:100 in 0.5 % BSA in PBS, followed by three, 5-minutes washes in PBS. After immunostaining cells were also stained with To-Pro®-3 as described (above), followed by mounting on glass slides.

Table 4.1: Immunostaining. Primary antibodies employed and respective secondary antibodies

Primary antibody	Dilution factor for primary antibody	Secondary antibody
Clathrin HC (H-300): sc-9069	1:100	Anti-Rabbit
Caveolin-1 (N20): sc-894	1:200	Anti-Rabbit
Early endosome antigen (EEA1) (C15): sc-6414	1:500	Anti-Goat
Lysosome-associated membrane proteins (Lamp 2) (H4B4): sc-18822	1:2000	Anti-Mouse
Ras-related superfamily - Rab 4/14 (FL-213): sc28569	1:200	Anti-Rabbit
Ras-related superfamily - Rab 11 (H87): sc-9020	1:80	Anti-Rabbit

4.2.6 Mounting glass-slides and microscopy

Following the final step for all samples, in which nucleic acids are stained with To-Pro®-3, coverslips were removed from the 24-well plate using fine forceps and were then held vertically against tissue to remove excess liquid. A small drop of Vectashield fluid (Vector Laboratories, UK) was placed in a glass slide and the coverslip, cells facing down and was positioned on top of the Vectashield drop. After removing the excess liquid, coverslips were sealed using a standard commercial nail lacquer and allowed to dry.

Images were captured using 63 x lenses of using a Zeiss LSM 510 inverted confocal microscope and analysed using LSM 510 META software (Zeiss).

4.3 Results and Discussion

In the previous chapter, cellular uptake and release of CNTs was demonstrated by Raman microscopy. In addition, to the importance of the fate of CNTs, it is also imperative to understand their intracellular route via trafficking and subcellular localisation during their transit through cells. Hence, in this chapter we present a detailed study using confocal microscopy in combination with organelle-specific markers to examine the intracellular distribution of CNTs. In addition, pathway inhibitory drugs were employed to identify major processes through which CNTs traffic as they enter and eventually efflux from cells. For this purpose, two coating approaches were considered. For both approaches, DWNTs were previously oxidised, however in the first method RNA was used to wrap DWNT, whereas in the second approach oxidised DWNT were wrapped with a polypeptide – Poly(Lys:Phe). As demonstrated in chapter 3, RNA-coated CNTs is a successful method to visualise CNT inside cells. However, the method does not permit further attachment of functional molecules, i.e. fluorescent moeties. On the other hand, Poly(Lys:Phe) is a polypeptide that contains several free amino groups, which by wrapping around CNTs, Poly(Lys:Phe) gives not only a positive charge but also the possibility of covalent attachment of active molecules.

4.3.1 Characterisation of CNT-complexes

CNT-complexes were characterised using microscopic techniques in particular AFM and TEM. Coating of oxDWNT with RNA was already demonstrated in chapter 3 and it is resumed here in Figure 4.2 A. In addition, wrapping with Poly(Lys:Phe) was also applied to allow the binding of molecules, such as fluorescein. In this case, fluorescein was used as a cargo however that could be substituted with a different molecule (i.e. DNA or siRNA). Figure 4.2 B exhibits the AFM scan over a surface of a single carbon nanotube, in which it is possible to see the wrapping with Poly(Lys:Phe) throughout the nanotube. Furthermore, the TEM imaging exhibits an individualised CNT with noticeable two wall characteristic of DWNT and once more the wrapping with Poly(Lys:Phe).

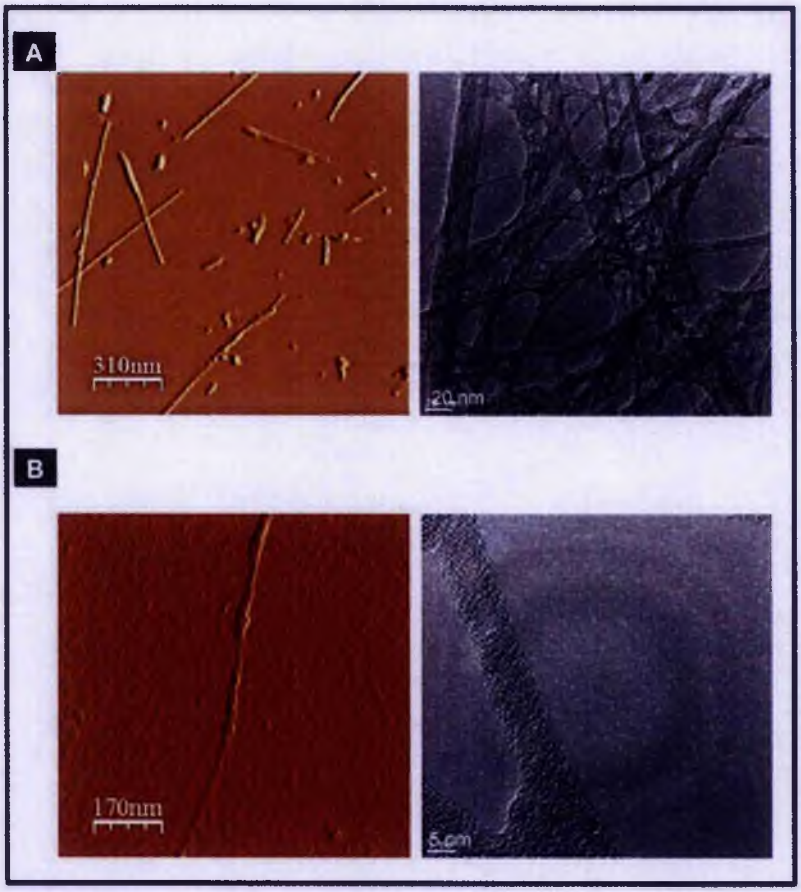

Figure 4.2: Characterisation by AFM and TEM of different CNT preparations. RNA-wrapped oxidised DWNT (A) and Poly(Lys:Phe)-FS wrapped oxidised DWNT (B) surface analysis by AFM and TEM, respectively. Image shows that wrapping of CNTs is not complete, by AFM it is possible to visualise parts of the CNT not covered by the RNA or polypeptide.

4.3.2 Cellular uptake by Raman

Raman spectroscopy was further used to demonstrate that-PC3 human prostate cancer cells internalised the fluorescein-CNT complexes. Figure 4.3 exhibits the G-band intensity of a single cell after exposure to RNA-Fluorescein wrapped oxidised DWNT (oxDWNT-RNA-FS) Figure 4.4 shows the temporal relationship of uptake of Poly(Lys:Phe)-fluorescein wrapped oxidised DWNT (oxDWNT-Poly(Lys:Phe)) in whole cell lysates. This data correlates with data presented for RNA-wrapped oxidised DWNT (oxDWNT-RNA, Chapter 3) suggesting that the pattern of uptake and

release is preserved for both wrapping methods. The Raman experiments (to demonstrate CNT physical properties) in combination with positive fluorescence by microscopy (involving CNT labelling with a fluorophore) demonstrate that CNTs localise inside cells, and accompany transport of a cargo, in this particular instance - fluorescein.

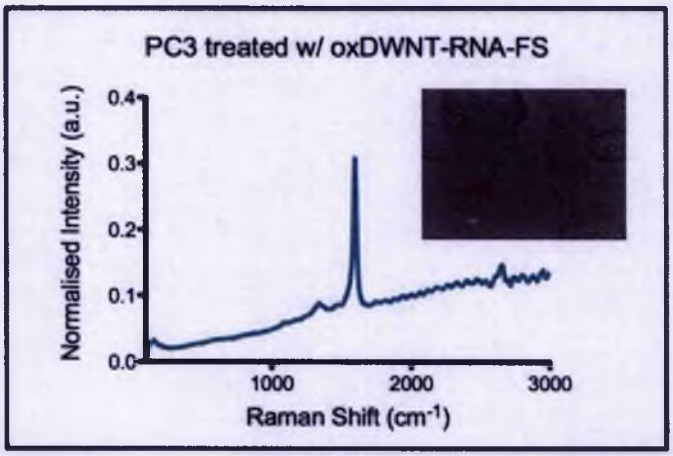

Figure 4.3: Raman spectra of PC3 cells exposed to oxDWNT-RNA-FS. G-band intensity of a single cell after incubation with 30 μg/mL of oxDWNT-RNA-FS for 2-hours. Inset shows selected cell and approximate site of Raman acquisition. Data acquired using Renishaw InVia Raman microscope, Elaser=1.59 eV (785 nm wavelength).

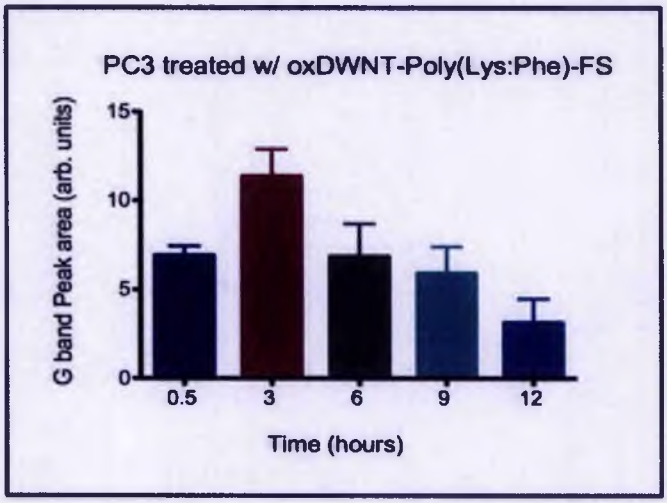

Figure 4.4: Temporal evaluation of oxDWNT-Poly(Lys:Phe)-FS uptake in PC3 cells. Area under the curve (AUC) of G band intensity at various time points, demonstrating uptake with maximum at 3-hour and consequent release. Results presented as Mean±SEM (n=6).

4.3.3 Cellular internalisation of CNT-complexes

As previously described internalisation of CNT-complexes was proven by Raman spectroscopy. Confocal microscopy was used to demonstrate the internalisation of fluorescently labelled CNTs Figure 4.5 reveals that cellular incubation with 30 μg/mL of RNA-wrapped oxidised DWNT labelled with fluorescein (oxDWNT-RNA-FS) produced readily detectable fluorescence in the cytoplasm (in green), which is absent from the nucleus (nuclear stain only (blue)). After 2-hours exposure to CNT-complexes, cells were washed and fresh media was added. One set of cells that were incubated for further 5-minutes (Figure 4.5A), while another set was incubated for 20-minutes (Figure 4.5B). This different time-incubation gave rise to a substantial variability in the intensity of oxDWNT-RNA-FS inside cells. After incubation in parallel for 2-hours cells were washed and fresh media was added. Followed by incubation for 5 and 20-minutes. Figure 4.5 A, shows that fluorescence after 5-minutes is restricted to intracellular compartments (possible endosomes). In contrast after 20-minutes the fluorescence is spread throughout the cytoplasm (Figure 4.5 A). This evidence was a result of several time point incubations and testing of several conditions. In addition, when cells were incubated continuously with CNTs (i.e. media containing CNTs was not removed) then fluorescence at cell surface was observed (Appendix 3). However, if CNT exposure was halted by supplementation with fresh media, then CNTs were more equally spread in the cytoplasm and less attached to the membrane (See appendix 3 for more information on experimental optimisation). Therefore, 5 and 20-minutes incubations with fresh media, post-exposure to CNTs was selected to follow the intracellular localisation of oxDWNT.

To facilitate the visualisation and confirm the internalisation of CNTs in cells, actin filaments were stained with Alexa 546 phalloidin (red) and the nucleus with ToPro3 (blue). As displayed in Figure 4.5, CNT-complexes (green) were in the same plane as the nucleus of the cells (blue). In addition, CNTs could be visualised within actin filaments of cell membranes. Besides multiple staining, internalisation was also evident on z-scan of cells incubated with CNT-complexes and revealed different levels of fluorescence intensity observed for different cell slices (Figure 4.6A). As mentioned previously, oxidised DWNTs were wrapped with both RNA-FS or Poly(Lys:Phe)-FS (Figure 4.6B). In our study, it was found that both coating methods reveal the same trend, leading to the same pattern of internalisation and co-localisation. We therefore, presented our results as CNT-complexes modified via both methods: oxidised DWNTs wrapped with RNA-FS and Poly(Lys:Phe)-FS.

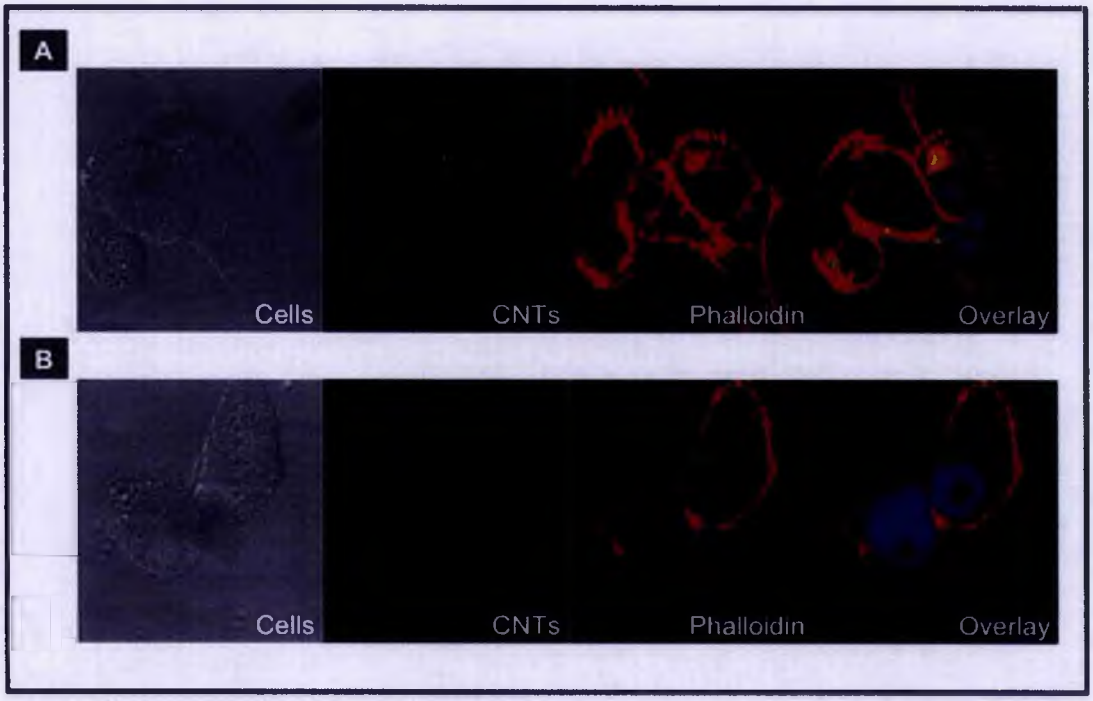

Figure 4.5: Distribution of CNT-complexes in PC3 cells. Cells were incubated with 30 μg/mL of oxDWNT-RNA-FS for 2-hours. After incubation first panel (A) was washed and incubated for 5-minutes with fresh media, in contrast bottom panel (B) was incubated for 20-minutes. Both panels were fixed and stained for presence of actin filaments (red) with Alexa 546 phalloidin and with ToPro3 for nuclei (blue) prior to being imaged for CNT-complexes accumulation (green). (A) Fluorescence restricted to intracellular compartments (dots); (B) Fluorescence spread in the cytoplasm.

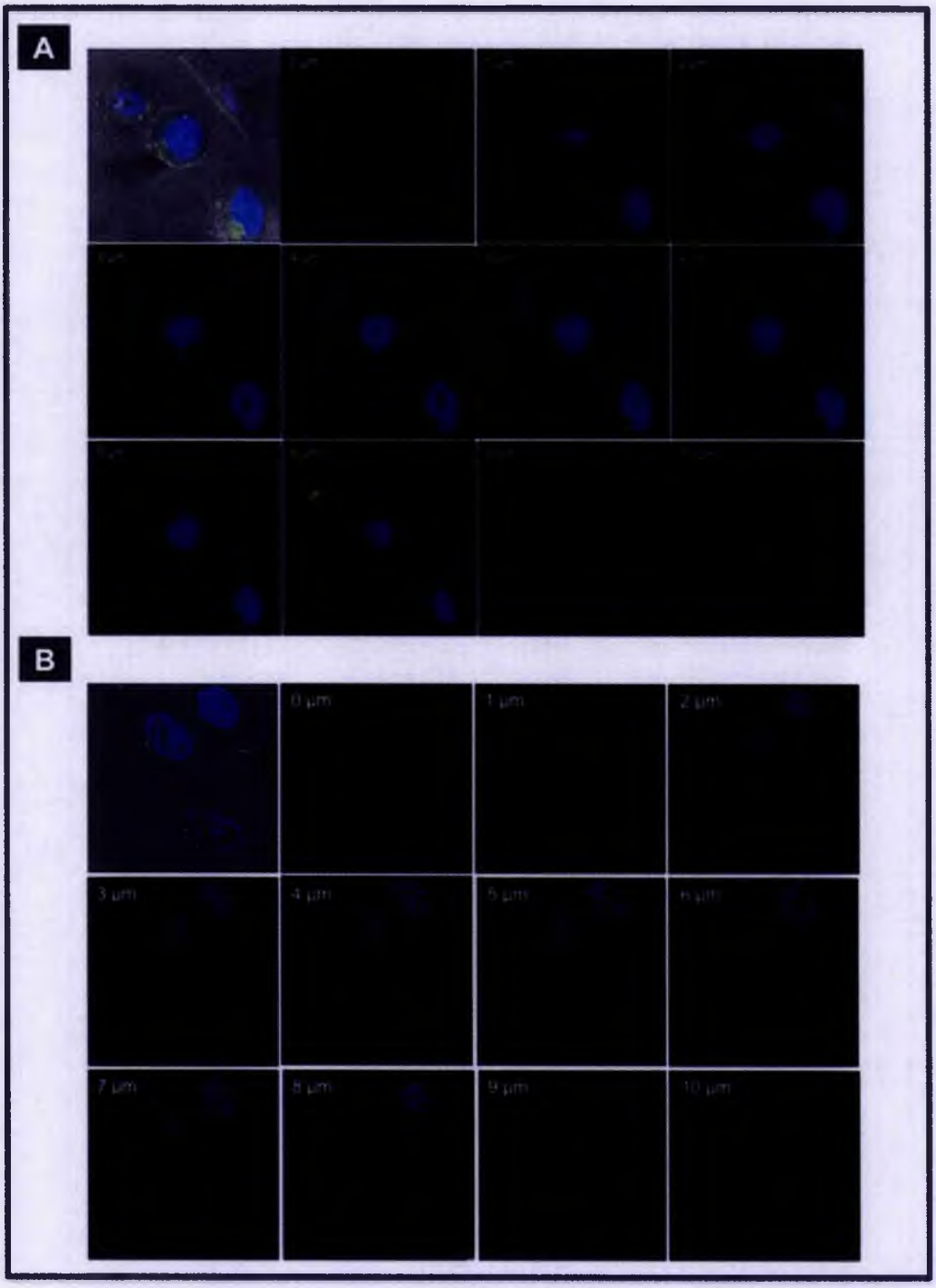

Figure 4.6: Variation in distribution of CNT-complexes as a function of the Z-stack. Cells were exposed to 30 µg/mL of CNT-complexes. (A) oxDWNT-RNA-FS and (B) oxDWNT-Poly(Lys:Phe)-FS.

4.3.3.1 Subcellular distribution of CNT-complexes

To determine the cellular compartments in which CNT-complexes localise and traffic, organelle-specific antibodies were employed. For these studies, cells were exposed to CNT-complexes and then fixed. After fixation to prevent morphological changes, cells were incubated with a primary antibody specific to a protein (e.g. clathrin) and then a fluorescently labelled secondary antibody was employed specific to the source of the primary antibody (e.g. rabbit).

As shown in Figure 4.1, the internalisation via the endocytic route involves a cascade of intracellular events, with different vesicles and regulators. The observation of CNT-complexes in intracellular endosome-like structures (Figure 4.5) led us to believe that an endocytic pathway was involved in the internalisation of the complexes. Therefore, it was decided to use markers such as clathrin and caveolin involved in the first step of endocytosis, invagination of the cell membrane. Clathrin mediated endocytosis is characterised by membrane-bounded vesicles inside a coat composed primarily of the fibrous protein – clathrin. In contrast, caveolae, are plasma membrane invaginations that are enriched in cholesterol and sphingolipids. In addition, these invaginations also accumulate special cholesterol-binding proteins, termed caveolins, on the cytosolic face of vesicles [327-330]. Certain ligands, which are internalised via caveolae, are likely to be delivered to a special endosomal compartment referred to as a "caveosome" [331]. Caveosomes containing caveolins do not localise transferrin, lack EEA1 and other early endosomal markers, have normal pH, and can act as sorting stations [327]. Figure 4.7B shows co-localisation of CNT-complexes (green) with clathrin (red); whereas CNTs did not co-localise with caveolin (Figure 4.7A). These results are in agreement with the work reported by Kam *et al.* [132] who proposed a clathrin mediated endocytosis. In their work they demonstrated a clathrin-dependent mechanism which was inhibited by low temperature (4 °C); NaN_3 (ATP depletion); and in sucrose and potassium depleted environments (which lead to disruption of formation of clathrin-coated vesicles) [132]. Furthermore, the SWNT-complexes they described (which had been acid functionalised and wrapped with BSA and streptavidin or; DNA) were not internalised via caveolae or lipid-rafts pathways [132]. As caveolae-dependent cell entry relies on the presence of cholesterol domains, they pre-treated cells with the drugs filipin and nystatin, which are known to disrupt the cholesterol distribution within the cell membrane [132].

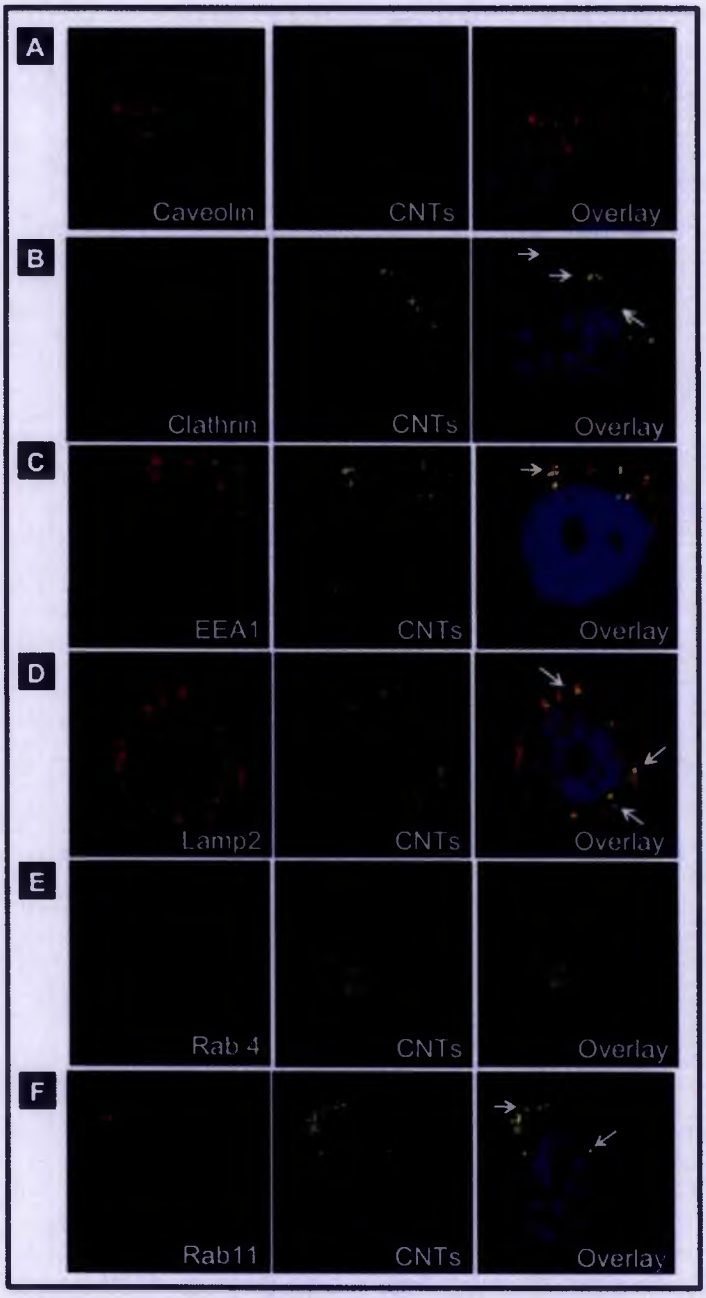

Figure 4.7: Co-localisation of CNT-complexes (green) with antibody-specific compartmental markers (red) in PC3 cells. Cells exposed to 30 μg/mL of CNT-complexes for 2 h. (A) conterstaining of CNTs with caveolin, showing no co-localisation; (B), specific co-localisation with clathrin-positive vesicles; (C), co-localisation with EEA1-positive early endosomal vesicles; (D), co-localisation of CNT-complexes with Lamp2-positive lysosomes, (E) conterstaining of CNTs with Rab4, showing no co-localisation; (F), co-localisation of CNT-complexes with Rab11-positive recycling endosomes. In yellow (arrows), cell compartment positive for both CNT-complexes and organelle markers. Nuclei are stained with ToPro3 (blue).

Generally, newly formed plasma membrane derived endocytic vesicles lose their clathrin coat, and fuse with each other or with pre-existing compartments known as sorting endosomes [332, 333]. The first endosomal compartment, the sorting or early endosome, has a role in sorting the cargo for further transport. The early endosome can be identified using an early endosome antigen (EEA1) in combination with a fluorescence secondary antibody. Our data show that CNT-complexes are closely associated with this location, as seen via co-localisation studies of CNT-complexes (green) with EEA1 (red) (Figure 4.7C).

The drop in the pH (for more acidic environment) within the sorting endosome dissociates many ligands from their receptor, allowing the receptors to be recycled back to the plasma membrane. As described in section 4.1, small GTPases have emerged as central regulators of vesicle budding, motility and fusion (Figure 4.1, highlighted in green). One of these proteins is Rab 4, involved in the recycling back to the plasma membrane from the early endosome. However, from our results Rab 4 does not seem to have a function in CNT-complexes traffic through the cell, as it was not visualised via overlapping of staining (Figure 4.7E).

Maturation of sorting endosomes into late endosomes or multivesicular bodies is coincident with a fall in the pH. The endosome becomes incapable in committing to further fusion with vesicles from the cell surfaces, or other sorting endosomes [328], thus preventing new cargo and receptors from being inadvertently degraded by 'joining' a late endosome as it matures into/fuses with a lysosome [329]. The lysosome can be identified using antibodies for lysosome membrane proteins (LMP). LMPs reside mainly in the lysosomal limiting membrane and have diverse functions, including acidification of the lysosomal lumen, protein import from the cytosol, membrane fusion and transport of degradation products to the cytoplasm. The most abundant LMPs are the lysosome-associated membrane protein 1 (LAMP1), LAMP2, lysosomal integral membrane protein 2 (LIMP2) and the tetraspanin CD63 [330]. As demonstrated in Figure 4.7D, a high level of co-localisation was observed with LAMP2 (selected for our co-localisation studies), thus indicating that CNT-complexes end up in the lysosomes after being endocytised.

The recycling endosome not only allows the recycling of plasma membrane components (a branch of the pathway that might need to be avoided in the context of drug delivery) but also enables the cell to traffic molecules back to the trans-golgi network (TGN)/Golgi [331]. Again, Rab proteins were found to regulate this

transport, the Rab 11 GTPase complex. A role for recycling vesicle expressing Rab 11 cannot be completely ruled out from our results because co-localisation was visualised for CNT-complexes and antibodies to Rab11 (Figure 4.7F). The Rab11 GTPase has been localised in recycling endosomes from the trans-golgi network and is required for transport of recycling endosomes back to the plasma membrane. It is feasible that CNT-complexes that reach the vesicles from the secretory pathway are delivered by Rab11-positive vesicles. The trans-golgi trafficking could be validated using antibodies for golgi97. Golgi97 localises the *trans* side of the golgi apparatus and it is believed to participate in the trafficking of vesicles between the golgi stacks and the *trans*-golgi network [338].

4.3.3.2 Co-localisation of CNT-complexes with endosomal/Lysosomal markers

In addition to co-localisation with clathrin antibody (determined by antibody-staining), CNT-complexes also co-localised with transferrin. Transferrin is a monomeric serum glycoprotein that binds iron. After its recognition at the cell surface via transferrin receptors, transferrin is internalised via clathrin dependent endocytosis. Once inside endosomes, the acidic environment favours dissociation of iron from the transferrin. Additionally, after sorting in late endosomes the transferrin reach the golgi apparatus as is subsequently recycled back to the plasma membrane. The co-localisation of CNTs with this protein confirms that they are internalised via clathrin dependent endocytosis and that they undergo sorting in late endosomes. In Figure 4.8A, fluorescently labelled transferrin (Red - Alexa Fluor 546) co-localises with CNT-complexes (green).

Furthermore, fluorescent microscopy can be used as a measure or at least an estimate of the pH in endocytic structures in cell culture models, through a wide range of pH-sensitive molecules as free entities, such as Lysotracker dye. This dye is red-fluorescent that stains acidic compartments in live cells, in particular lysosomes. Thus, Lysotracker can be used together with antibody staining (with LAMP2) to confirm the sequestration of CNT-complexes in lysosomes. As demonstrated in Figure 4.8 B there is an overlap between Lysotracker (red) and CNT-complexes (green), indicating that the CNT-complexes are probably in an acidic compartment.

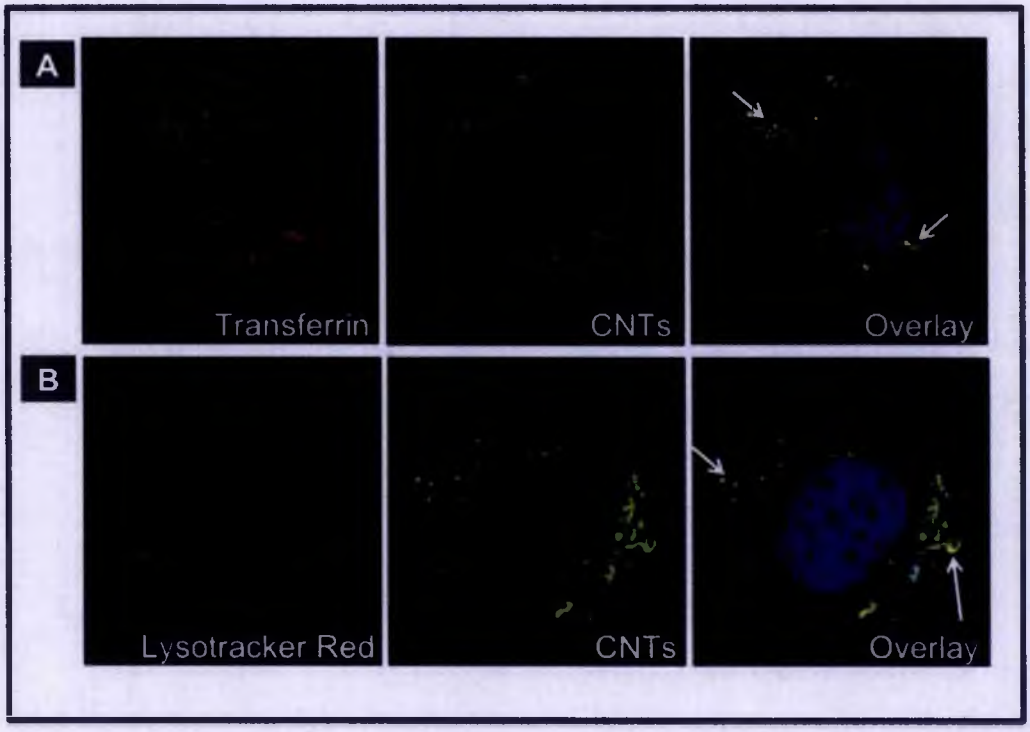

Figure 4.8: Co-localisation of CNT-complexes (green) with endosomal/Lysosomal markers (red) in PC3 cells. Cells exposed to 30 μg/mL of CNT-complexes for 2-hours. (A) co-localisation with transferring-positive endosomes; (B), co-localisation with acidic compartment-lysosomes. In yellow (arrows), cell compartment positive for both CNT-complexes and organelle markers. Nuclei are stained with ToPro3 (blue). Nuclei are stained with ToPro3 (blue).

4.3.3.3 Effect of pathway inhibitory drugs on CNT-complexes localisation

A systematic analysis of intracellular transport pathways is readily achieved by analysing the effects of inhibiting one or more transport processes. A widely used mean for inhibiting transport is to apply a temperature block to cells [332]. Most transport processes, including clathrin-dependent internalisation, will be blocked at 4 °C. Endocytosis is an energy dependent mechanism that is also hindered when incubations are carried out at ATP depleted environments, such as incubation with sodium azide (NaN_3). In our experiments (Figure 4.9 B and C), both incubations at 4 °C and with NaN_3, resulted in inhibition of CNT-complexes uptake in PC3 cells, suggesting an energy dependent mechanism for CNT-complexes internalisation.

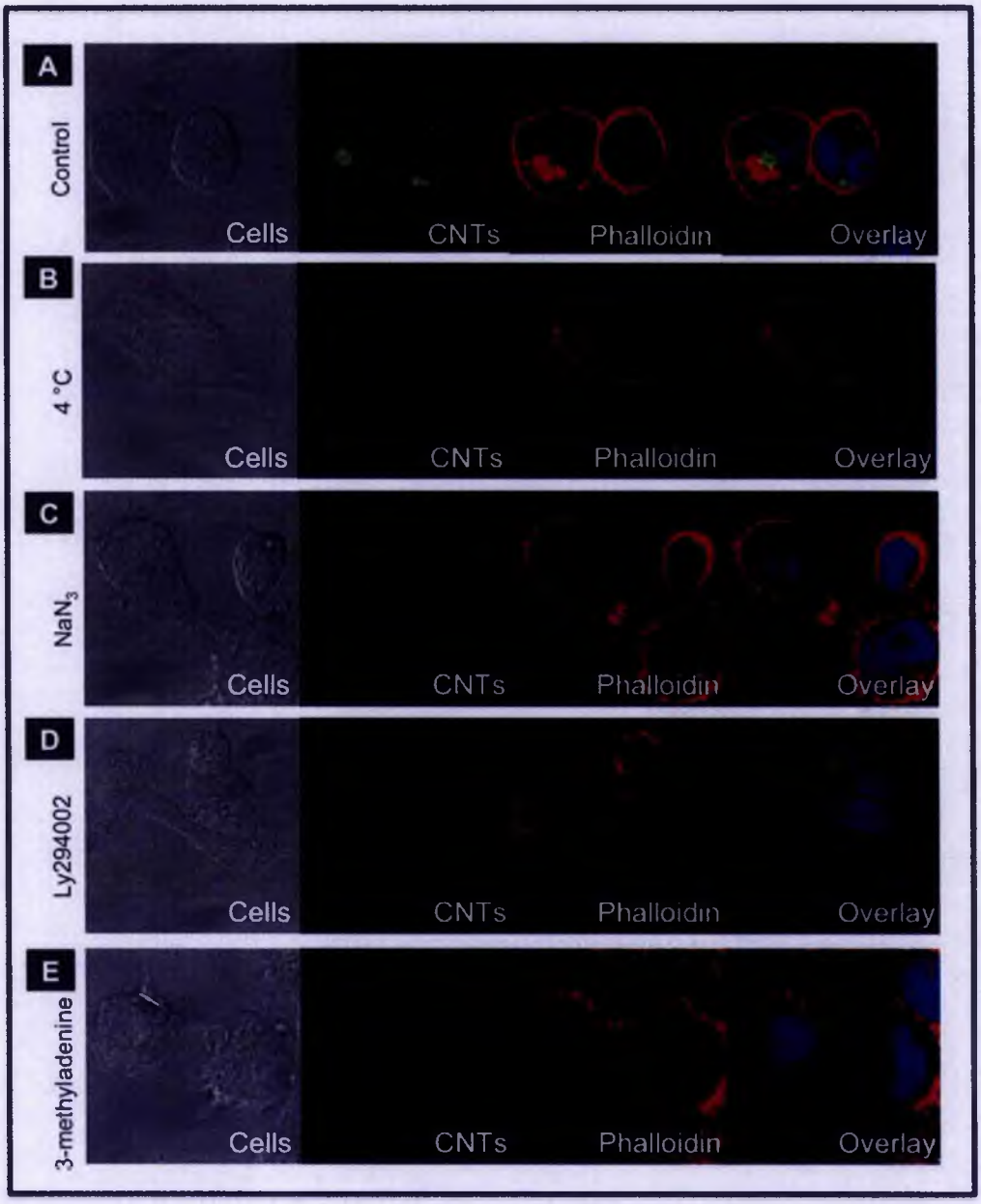

Figure 4.9: Effect of inhibitory conditions for endocytic uptake. Cells exposed to 30 μg/mL of CNT-complexes for 2-hours (A). Effect of incubation at 4 °C on CNT-complexes internalisation (B); effect of pre-incubation with sodium azide (NaN_3) on CNT-complexes internalisation (C); effect of pre-incubation with phosphoinositide 3-kinase inhibitor (Ly214002) on CNT-complexes internalisation (D); effect of pre-incubation with 3 methyadenine on CNT-complexes internalisation (E). Actin filaments (red) stained with Alexa 546 phalloidin and nucleus (blue) stained with ToPro3.

Good examples of pharmacological inhibition of traffic include the use of LY-294002, which is an inhibitor of PI-3 kinase. Phosphoinositide 3-kinases (PI-3 kinase) are a family of enzymes involved in membrane trafficking as well as other molecular processes. Trafficking processes include transiocation to the plasma membrane [340, 341], endocytosis [342, 343], endosome fusion [333], lysosomal protein sorting [345, 346] and transcytosis [334].

Another process involving membrane traffic is autophagy. Autophagy is responsible for accelerated degradation of cell protein during starvation. The process comprises sequestration of cytoplasmic material into large double-membrane vesicles named autophagosomes followed by fusion of these vesicles with lysosomes, and degradation of the sequestered material [335]. It has been shown that LY294002 at concentrations that inhibit PI-3 kinase activity also prevents autophagic sequestration [349]. In addition, 3-methyladenine is a specific inhibitor of autophagic sequestration [336] that also inhibits PI-3 kinase. When LY294002 and 3-methyladenine were employed in our study, we observed a blockage of membrane traffic and endosome fusion preventing CNT-complexes being internalised by PC3 cells (Figure 4.9 D and E). Again, to facilitate the visualisation and confirm lack of CNTs uptake, actin filaments were stained with Alexa 546 phalloidin (red) and the nucleus with ToPro3 (blue), demonstrating that no CNT-complexes were internalised (Figure 4.9).

To summarise the results presented in this chapter Figure 4.10 schematically represents the movement of CNT-complexes during their passage through PC3 cells.

Previous reports, have also found a role for clathrin in CNT endocytosis [132, 140, 144]. Others describe an energy-independent mechanism [126-128, 326] or a combination of the two systems [325]. The results presented here demonstrate an endocytic mechanism for uptake of CNT-complexes. However, the type of mechanism proposed by Mu *et al.* in 2009 [325] cannot be completely ruled out by our study, since confocal microscopy does not have the resolution to observe single nanotubes, instead bundles were visualised. In addition, our study did not consider mitochondrial accumulation, which was observed by Zhou *et al.* 2010 [326]. In their study CNTs were found to cross the cell membranes by direct penetration, therefore it would be interesting to detect if endocytic internalised CNTs would also localise in mitochondria. Nevertheless, our study brings novel findings on the uptake and traffic of CNTs in mammalian cells, allowing identifying cellular organelles in which CNTs localise. Additionally, exocytosis was once again confirmed, with identification of the key organelle responsible for CNTs efflux. For first time recycling endosomes from

the trans-golgi network (Rab11 positive vesicles) were indentified to be responsible for CNTs excretion.

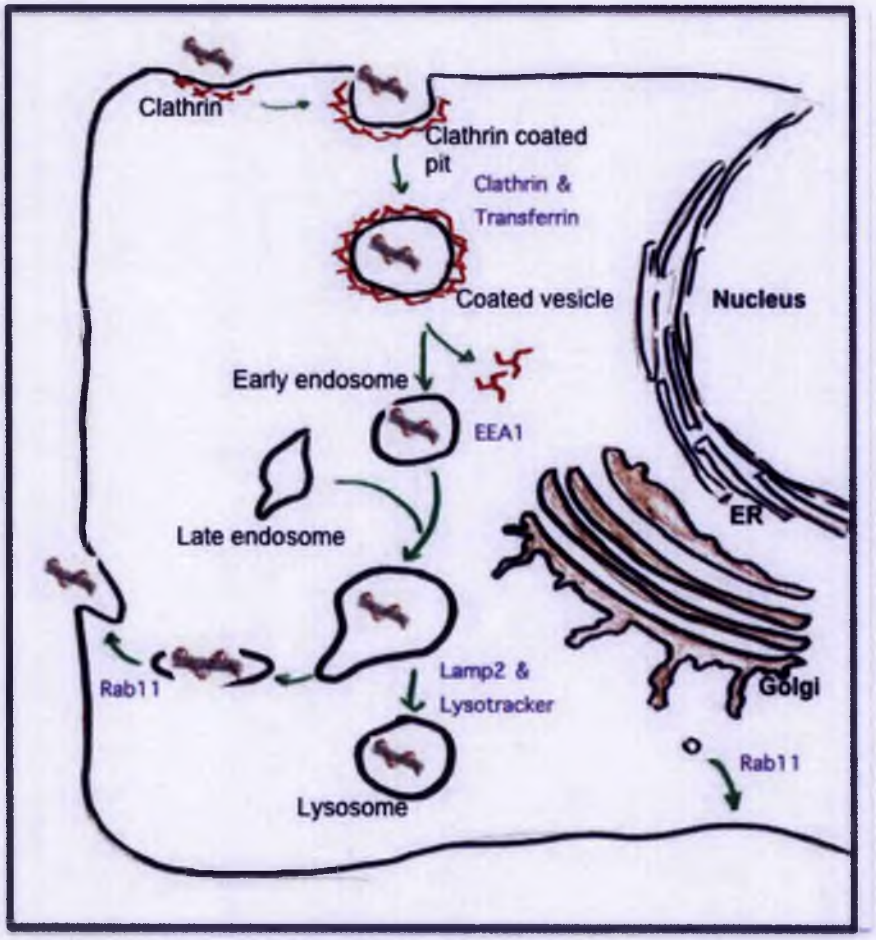

Figure 4.10: Proposed CNT-complexes intracellular trafficking. The internalisation of CNT-complexes was proved to be an energy dependent mechanism, confirmed by incubation at 4 °C and pre-incubation with NaN_3 (Figure 4.9 B and C). Additionally incubation with PI-3 kinase inhibitors, known to interfere with vesicular trafficking, led to reduced internalisation of CNTs (Figure 4.9 D and E). Thus, co-localisation with both Clathrin and transferrin provides evidence for Clathrin mediated endocytosis (Figure 4.7 A and Figure 4.8 A, respectively), after which CNT-complexes undergo sorting in the early endosomes (co-localisation with EEA1 - Figure 4.7 B). CNT-complexes are sequestrated in the lysosomes, which was confirmed by Lamp2 and Lysotracker staining (Figure 4.7 C and Figure 4.8 B, respectively). Finally, it seems that CNT-complexes reach the secretory pathway and are recycled back to the plasma membrane by Rab11-positive vesicles (Figure 4.7 D).

4.4 Conclusions

The objectives of these experiments were to elucidate the mechanism of uptake of CNTs, as well as to determine the intracellular compartments in which they localise. Furthermore, in the previous chapter it was demonstrated that CNTs were lost from cells so investigation the mechanisms of CNTs efflux from cultured cells is further required.

The cytoskeleton is involved in coordinating the organization and dynamics of intracellular architecture, being relevant to understand membrane traffic. Cellular membranes stained with phalloidin (Figures 4.5 and 4.9) showed evidence of regular cell morphology after exposure to CNTs and inhibitory drugs.

From the results presented here we propose an endocytic route for uptake and trafficking of CNT-complexes (functionalised by means of oxidation and wrapping with RNA and polypeptides, Figure 4.2). Evidence of their intracellular localisation was demonstrated by Raman spectroscopy of cells exposed to CNT-complexes (Figure 4.3 and 4.4) and fluorescence (Figure 4.5 and 4.6). The CNT-complexes were endocytosed by capture in clathrin-coated vesicles, revealed by clear co-localisation with both clathrin and transferrin (Figure 4.7 A and Figure 4.8 A, respectively).

Molecules entering cells on endocytic pathways will rapidly experience a drop in pH from neutral to pH 5.9-6.0 in the lumen of early/recycling vesicles, with further reduction from pH 6.0 to 5.0 during progression from late endosomes to lysosomes [337]. In our studies, CNT-complexes were found in early endosomes, which was confirmed by co-localisation with early endosome antigen (EEA) (Figure 4.7 B). CNT-complexes were not sorted for recycling back to the cell membrane (via fast recycling endosomes), as co-localisation with Rab 4 was not observed. Furthermore, the overlapping of CNT-complexes with both LAMP2 antibody and Lysotracker marker (Figure 4.7 C and Figure 4.8 B, respectively) indicates that CNT-complexes becomes sequestrated in lysosomes. In addition, the results indicate that CNT-complexes were also found within vesicles of the secretory pathway, which are delivered by Rab11-positive vesicles (Figure 4.7 D). As a result, it appears that intracellular traffic of CNTs involves both sequestration in lysosomes and recycling back to the plasma membrane via endosomes from the trans-golgi network.

Chapter 5: CNTs for gene delivery and targeting

5.1 Introduction

One of the most important challenges in gene therapy is to correct genetic defects or alter/adjust cellular genetic functions. The main goal is to efficiently, specifically and safely introduce nucleic acid molecules into cells. Since the unravelling and elucidation of the human genome, this provided a major drive to identify human genes implicated in diseases and consequent development of DNA-based drugs for replacement or potential targets for gene silencing. DNA-based drugs present a significant advantage over the currently available low molecular weight drugs; they present selective recognition of molecular targets and pathways, which implies significant efficiency gains and tremendous specificity. These DNA-based therapeutics include plasmids containing transgenes for gene therapy, oligonucleotides for antisense and antigen applications, ribozymes, aptamers, and small interfering RNAs (siRNAs), as described in the general introduction (section 1.1.2).

Plasmids are high molecular weight; double stranded DNA constructs containing transgenes, which encode specific proteins [338]. On a molecular level, plasmid DNA (pDNA) molecules can be considered pro-drugs that, after internalisation, utilise the DNA transcription and translation apparatus in the cell to biosynthesise the therapeutic entity, a protein. Gene therapy involves the use of pDNA to introduce transgenes into cells that inherently lack the ability to produce the protein that the transgene is programmed to generate. The mechanism of action of pDNA requires that plasmid molecules gain access into the nucleus after entering the cytoplasm. The entry of plasmid molecules into the nucleus through the nuclear pores is an extremely challenging and difficult process [338]. The nuclear access or lack of entry eventually controls the efficiency of gene expression [338]. While lack of specific immune response favours the use of pDNA complexes, the limited efficacy and short duration of transgene expression impose major obstacles in the application of non-viral gene delivery techniques. Therefore, a significant advantage of viral DNA vectors is their extremely high transfection efficiency in a variety of human tissues. In viral gene

delivery, the transgene of interest is assembled in the viral genome and the virus uses its innate mechanism of infection to enter the cell and release the expression cassette. The gene then enters the nucleus, integrates into the host gene pool, and is eventually expressed [339].

Despite their high transfection efficiency, there are several concerns over the use of viruses to deliver DNA therapeutics in humans. The major concerns are related to toxicity of the viruses and their potential to generate a strong immune response due to their proteinaceous capsid. In 1999, a death of a patient participating in FDA-approved gene therapy clinical trial from respiratory and multiple organ failure, attributed to lethal immune response to the adenovirus vector used to deliver the gene, led to temporary suspension of all gene therapy trials in the US. Additionally, the integration of therapeutic genes into the host genome by the virus takes place in a random fashion, resulting in no control over the exact location of insertion of the gene. Random gene transfer can generate insertional mutagenesis that may inhibit expression of normal cellular genes or activate oncogenes, with dangerous consequences.

Gene therapy can also be achieved using siRNA technology. As mentioned in the introduction (Section 1.1.1), siRNAs are short double-stranded RNA segments with typical 21- to 23-nucleotide bases that are complementary to the mRNA sequence of the protein whose transcription is to be silenced/blocked [354-356]. Since RNAs do not integrate into the genome, they offer greater safety than plasmid molecules. Furthermore, siRNAs do not have to transfer through the nuclear membrane for their activity and therefore require less sophisticated delivery systems, promising faster development and higher efficiencies compared with plasmid DNA [357].

Successful delivery of siRNA and plasmid DNA into mammalian model organisms has been achieved using a variety of methods, including liposomes, cationic lipids, polymers and nanoparticles. However, despite the appreciable success of, for example, cationic lipids in gene transfer, toxicity is of great concern. Thus, there is an ever-growing need to enhance the available tools that can lead to effective and safe gene delivery and expression. CNTs have recently been developed as gene delivery vectors (more information in section 1.3.4) as a consequence of their ability to efficiently enter mammalian cells, as well as their exceptional electronic and physicochemical properties.

The objective of this chapter is to study the feasibility of applying CNTs to deliver nucleic acids. In order to do so, GFP will be employed as an *in vitro* model. First, the

GFP will be delivered by means of plasmid DNA, using a pAcGFP1-N1 vector that is a mammalian expression vector that encodes GFP from *Aequorea coerulescens.* Additionally, the vector allows further cloning, which could be used in the future, to insert other therapeutic genes, such as p53 (tumour suppressor protein), permitting observation and selection of cells expressing both GFP and p53. Moreover, a cell line that stably expresses GFP was generated using the same GFP expressing vector. Finally, silencing of the GFP gene was evaluated to study CNT-mediated siRNA.

5.2 Experimental section

In this section, an itemized description of the methodology for preparation of CNTs for gene delivery and targeting is described. Details of DNA purification and preparation are presented, as well as CNTs modification and attachment of nucleic acids. Finally, methods for measuring and analysing gene expression and knockdown are described.

5.2.1 Plasmid DNA – pAcGFP-C

pAcGFP1-N1 Vector is a mammalian expression vector that encodes GFP from *Aequorea coerulescens* (Clontech, TaKaRa Bio, USA). The fluorescent protein coding sequence in this construct was human-codon-optimized for efficient expression and enhanced brightness. AcGFP1 protein has an excitation maximum at 475 nm and an emission maximum at 505 nm. The multiple cloning site (MCS) in pAcGFP1-N1 is between the immediate early promoter of CMV(*P* CMV IE) and the AcGFP1 coding sequences. Genes cloned into the MCS will be expressed as fusions to the N-terminus of AcGFP1 if they are in the same reading frame as AcGFP1 and no intervening stop codons. SV40 polyadenylation signals downstream of the AcGFP1 gene direct proper processing of the 3' end of the AcGFP1 mRNA. The vector backbone also contains an SV40 origin for replication in mammalian cells expressing the SV40 T antigen. A neomycin-resistance cassette (Neor), consisting of the SV40 early promoter, the neomycin/kanamycin resistance gene of Tn5, and polyadenylation signals from the Herpes simplex virus thymidine kinase (HSV TK) gene, allows stably

transfected eukaryotic cells to be selected using G418. A bacterial promoter upstream of the gene expresses kanamycin resistance in *E. coli*. The pAcGFP1-N1 backbone also provides a pUC origin of replication for propagation in *E. coli* and an f1 origin for single-stranded DNA production.

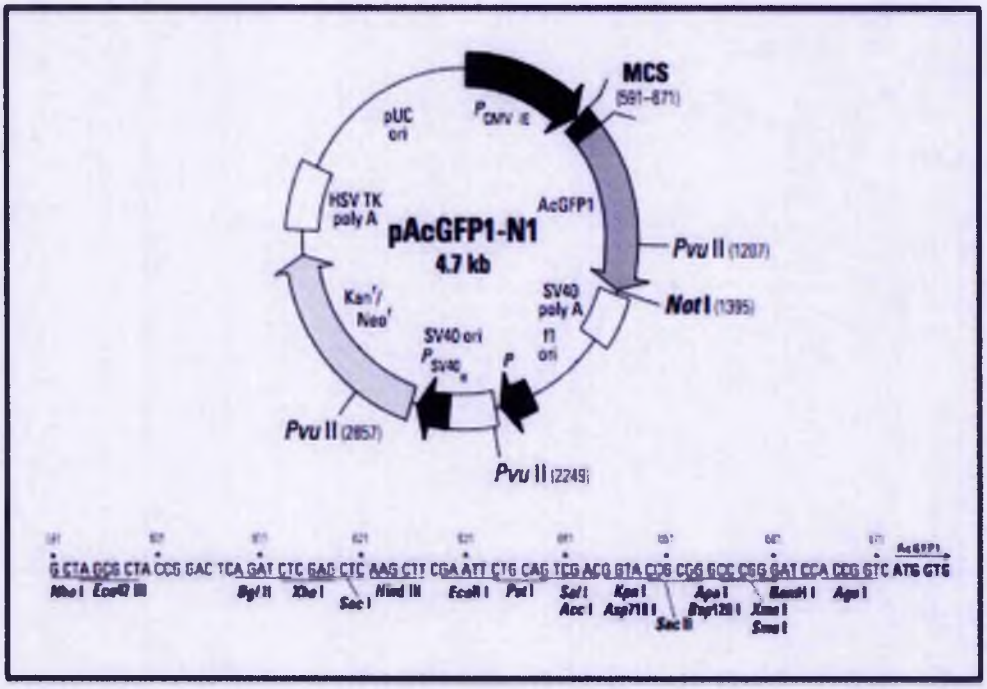

Figure 5.1: Map and multiple cloning site (MCS) of pAcGFP1-N1 Vector. Unique restriction sites and MCS are in bold.

5.2.1.1 Purification of ultrapure supercoild plasmid DNA

Plasmid DNA was purified according to manufacturers instructions (in the manual from Qiagen Tip 100 Sample and Assay Technologies, UK). A modified alkaline lysis procedure followed by binding of plasmid DNA to Qiagen Anion-Exchange Resin under appropriate low-salt and pH conditions. RNA, proteins, dyes, and low-molecular-weight impurities were removed by a medium-salt wash. Plasmid DNA was eluted in a high-salt buffer and then concentrated and desalted by isopropanol precipitation.

5.2.2 Coating of CNTs for binding of nucleic acids

In this chapter different CNT modifications were tested to deliver nucleic acids to mammalian cells. Mainly two wrapping molecules were employed to both modify CNTs, Poly(Lys:Phe) (1:1) (Sigma Aldrich, Poole, UK) and PL-PEG-NH_2 (Avanti Polar Lipids, USA). Both molecules were wrapped around pristine DWNT (DWNT-Poly(Lys:Phe and DWNT-PL-PEG-NH_2, respectively) and oxidised SWNT and DWNT (oxDWNT-Poly(Lys:Phe), oxSWNT-PL-PEG-NH_2, oxDWNT-Poly(Lys:Phe, oxDWNT-PL-PEG-NH_2 respectively) for further binding with negatively charged nucleic acids (pDNA and siRNA). In addition, the binding of polypeptide with nucleic acids prior to CNT binding (Poly(Lys:Phe)-siRNA-oxDWNT and PL-PEG-NH_2-siRNA-oxDWNT, respectively) was tested.

5.2.2.1 Wrapping of pristine DWNT

Solution of PL-PEG-NH_2 and Poly(Lys:Phe) of 2 mg/mL was prepared in sterile sodium bicarbonate buffer (40 mM, pH 9). DWNTs, synthesised by the CCVD technique and with mild acid treatment purification as described by Flahaut *et al.* [247], were then mixed with PL-PEG-NH_2 and Poly(Lys:Phe): 10 mg of DWNT were mixed with 2.5 mL of PL-PEG-NH2 or Poly (Lys:Phe). Tip sonication of the mixture was carried out 6-times at intervals of 10 seconds, followed by extensive sonication in a water bath for 1 to 2-hours. To remove excess PL-PEG-NH2 and Poly (Lys:Phe), the suspension was filtered using a 100 kDa filter device (Amicon Ultra-4 centrifugal filter devices from Millipore) and resuspended in sterile water. Subsequently, the suspension was centrifuged (90-minutes, at 13500 g, room temperature (± 21 °C)) to remove impurities and large nanotube bundles and the supernatant was collected for further attachment of nucleic acids (pDNA and siRNA).

5.2.2.2 Wrapping of oxidised CNT

SWNTs and DWNTs were purified in concentrated nitric acid and oxidised in a mixture of nitric and sulphuric acid [185] (Chapter 2, Section 2.3.1). After oxidation, nanotubes were sterilised by autoclaving at 121 °C for 1 hour and maintained under sterile conditions for the duration of the experiment.

In the same manner as for pristine CNTs, oxidised SWNTs and DWNTs with concentration of 100 µg/mL were mixed with 50 µg/mL of PL-PEG-NH_2 and Poly (Lys:Phe) in sodium bicarbonate buffer, as above), through continuous stirring for 2-hour at room temperature. To remove excess of unbound wrapping molecules, the solution was filtered using a 100 kDa filter device (Amicon Ultra-4 centrifugal filter devices from Millipore). Subsequently, CNT-preparations were resuspended in DNase /RNase free water (Sigma Aldrich, Poole, UK) to a final concentration of 100 µg/mL of CNTs.

In another approach, Poly(Lys:Phe) was conjugated first with nucleic acids (1:1), and prepared in a solution of 0.5 mg/mL in sodium bicarbonate buffer (40 mM, pH 9). While stirring the polypeptide solution, the nucleic acid solution was slowly added according to concentrations described below (Section 5.2.2.3). The reaction was allowed to proceed for 2-hours at room temperature (± 21 °C), with continuous stirring. Finally, oxidised DWNT were added to each vial with a final concentration of 50 µg/mL and the reaction took place via continuous stirring for 2-hours at room temperature (± 21 °C). To remove excess of polypeptide-nucleic acid not bound to CNTs, the suspension of oxidised DWNTs wrapped with Poly(Lys:Phe) (oxDWNT-Poly(Lys:Phe) was filtered using a 100 kDa filter devices[i] (Amicon Ultra-4 centrifugal filter devices from Millipore) and then resuspended in DNase /RNase free water (Sigma Aldrich, Poole, UK).

[i] *CNT-pDNA complexes were not filtered after conjugation due to size of the complex, which exceeded the size of the filter pore in 100 kDa filter devices*

5.2.2.3 Plasmid DNA and siRNA binding to CNTs

pDNA was added to CNT coated with PL-PEG-NH_2 or Poly (Lys:Phe) (50 μg/mL) at final concentration of 5 μg/mL. siRNA was conjugated at a concentration of 0.2 to 1 μM and added to CNTs coated with PL-PEG-NH_2 or Poly (Lys:Phe) (50 μg/mL). The reaction was allowed to proceed for 2-hours at room temperature (± 21 °C), with continuous stirring. The solutions were again filtered using a 100 kDa filter devices (Amicon Ultra-4 centrifugal filter devices from Millipore) to remove the excess of nucleic acids and then resuspended in DNase /RNase free water (Sigma Aldrich, Poole, UK), with a final concentration 100 μg/mL of CNTs.

5.2.3 Analysis of nucleic acid binding to CNT by electrophoresis

Prepared samples (10 μl) of CNT-nucleic acid complexes and controls (oxDWNT-Poly(Lys:Phe)-pDNA, oxDWNT-PL-PEG-NH_2-pDNA, the free DNA and siRNA) were loaded onto an agarose gel (1 %, w/v) for electrophoresis with visualisation by ethidium bromide staining (5 μg/mL).

5.2.4 Creating stable cell lines expressing GFP

PC-3 cells were cultured in RPMI-1640 medium supplemented with 2mM Glutamax™; and HeLa cells were cultured in MEM medium supplemented with 2mM non-essential aminoacids. Additionally, 10 % heat-inactivated FBS, and 1 % penicillin-streptomycin was added to both mediums (Invitrogen, Paisley, UK). Cells were transfected with pAcGFP-N1 plasmid (Clontech, Saint-Germain-en-Laye, France) using Lipofectamine reagent, according to instructions in the manual, and as summarised in section 5.2.5 (Invitrogen, Paisley, UK). GFP expressing cells were selected using 600 μg/mL of geneticin (G418) (Gibco/Invitrogen, Paisley, UK). After 4 weeks of selection cells were sorted for 80-90 % GFP expressing cells, using Fluorescence-activated cell sorting (FACS). Cells were allowed to recover for 8

weeks and re-sorted once more. Excitation was observed using an argon laser at 488 nm at 400 mW with power emission being detected using band pass FITC filter of 535 nm ± 15 nm.

5.2.5 GFP expression and knockdown in mammalian cells

One day before transfection cells were seeded so that they were approximately 50 % confluent, at the time of transfection (either in 24-well plates containing coverslips (13 mm) for fluorescent microscopy or 35 mm sterile petri dishes for flow cytometry).

pDNA transfection in PC3 cells: CNT-pDNA complexes, previously prepared samples (Section 5.2.2), were diluted 1:2 in Opti-MEM media (Invitrogen, Paisley, UK). These complexes were then added to each corresponding well. While, pDNA-Lipofectamine® complexes were prepared according to the instructions in the manual, 1 or 6 µl Lipofectamine®, for 24-well or 35 mm plate, respectively, were combined with 5 µg/mL pDNA and added to each corresponding well. After 4-hours, the media was replaced with fresh completed media containing serum. Then cells were incubated for further 12 to 24-hours at 37 °C in a CO_2 incubator until assaying for gene expression.

siRNA transfection in PC3-GFP and HeLa-GFP cells: For CNT-siRNA transfection previously prepared complexes (Section 5.2.2), were diluted 1:2 in Opti-MEM media (Invitrogen, Paisley, UK). These complexes were then added to each corresponding well. siRNA-Lipofectamine RNAiMAX complexes were prepared according to the instructions in the manual: 1 or 6 µl Lipofectamine RNAiMAX, for 24-well or 35 mm plate, respectively, were combined with 0.2 to 1 µM siRNA and added to each corresponding well. After 4-hours the media was replaced with fresh completed media containing serum. The cells were then incubated for further 24-hours to 1 week at 37 °C in a CO_2 incubator until assaying for gene knockdown.

5.2.6 Sample preparation for fluorescence microscopy

To prevent morphological changes, cells were fixed with 4 % paraformaldehyde (Sigma Aldrich, Poole, UK) solution in PBS, for 1-hour at room temperature, followed by washing cells with sterile PBS and treatment with 0.1% Triton X100 (Sigma Aldrich, Poole, UK) in PBS, for 15 minutes to allow permeabilisation of cell membranes. Cells were then washed 3-times with PBS and finally, To-Pro®-3 (Invitrogen-Molecular Probes, emission 661 nm), monomeric cyanine nucleic acid stain was utilised to visualise the cell nucleus in all samples (concentration of 0.1 μM in PBS). Finally, coverslips were removed from the 24-well plate using fine forceps and were then held vertically against Kleenex tissue to remove excess liquid. A small drop of Vectashield fluid (Vector Laboratories, UK) was placed in a glass slide and the coverslip, cells facing down was positioned on top of the Vectashield drop. After removing the excess of liquid coverslips were sealed using standard commercially available nail lacquer and allowed to air dry.

Images were captured using 63 x lenses of using a Zeiss LSM 510 inverted confocal microscope and analysed using LSM 510 META software (Zeiss). To determine the percentage of GFP expression (after pDNA delivery) and GFP knockdown (after siRNA delivery) cells were counted in 5 different fields. GFP expressing cells will appear green (GFP, emission 505 nm) with nucleus in blue (To-Pro®-3, emission 661 nm), while non-expressing cells will present with only the nucleus stained in blue (To-Pro®-3, emission 661 nm).

5.2.7 Sample preparation for flow cytometry

Suspended cells were obtained by trypsinizing the monolayer of adherent cells and washed twice with ice cold, sterile PBS. Then, cells were washed twice with 0.1% BSA in PBS, and centrifuged (5-minutes, at 300 g, 4 °C). After discarding the supernatant, 500 mL of ice cold PBS were added to cell pellet and mixing gently with 500 mL of cold-buffered 2 % formaldehyde solution, followed by incubation at 4 °C for 1-hour. After fixation, cells were washed once with ice cold PBS, and 1 mL of 70 %

ethanol (previously stored at -20 °C) was added drop-wise to the cell pellet. The suspension was incubated overnight at 4 °C.

Before assaying for gene knockdown, cells were centrifuged and resuspended in the desired volume of PBS.

Dr. Alexandra Bermudez-Fajardo assisted with the flow cytometry measurements, at the flow cytometry and bioimaging facilities at the University of Surrey, using Becton Dickinson FACS Canto flow cytometer analyzer. The measurements permit not only the determination of the percentage of GFP expressing cells in a plot of cell count *vs* FITC intensity but also the mean fluorescence intensity of the population. Data analysis was performed with Flowjo software.

5.3 Results and Discussion

As previously stated, the coating of CNT with polypeptides and polyliposomes allows the further attachment of molecules, such as DNA and siRNA. The polypeptides strongly bind to the DWNTs via van der Waals forces and hydrophobic interactions between aromatic rings of polypeptide and the carbon nanotube sidewalls. Furthermore, the positive charge of the amino group in the polypeptide allows the DWNT-polypeptide complexes to bind the anionic pDNA and siRNA through electrostatic interactions.

5.3.1 DNA purification

pAcGFP1-N1 was transformed into *E. coli* cells and purified using a Qiagen midiQ kit system according to manufacturer instructions. After purification the size of the DNA was examined by digestion with the restriction enzymes Dra III and Pvu II. Figure 5.2 displays the obtained fragments after digestion, demonstrating that the plasmid was successfully purified and suitable for further attachment to CNTs and expression of GFP in mammalian cells.

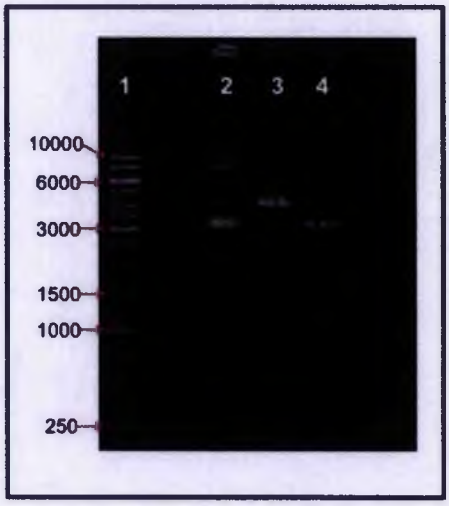

Figure 5.2: Agarose-gel electrophoresis of digested pDNA with restriction enzymes. Lane 1 – Ladder; Lane 2 - undigested DNA; Lane 3 - DNA digested with Dra III (fragments: 3982, 744); and Lane 4 - DNA digested with Pvu II (fragments: 3076, 1042, 608).

5.3.2 Nucleic acid binding to CNTs: gel retardation assay

To test the ability of nucleic acids to bind to CNTs a simple gel retardation method can be used, where the mixtures are analysed by agarose-gel electrophoresis. If a complex of CNT-nucleic acid forms it will be too big to run in the gel and no band will appear. However, if the nucleic acid does not bind to the CNTs to form the complex, the band will appear on the agarose-gel. In our studies different coatings methods were tested, such as pristine DWNTs that were wrapped either with PL-PEG-NH_2 or Poly(Lys:Phe) (DWNT-Poly(Lys:Phe)-pDNA and DWNT-PL-PEG-NH_2-pDNA) oxidised DWNTs and SWNTs wrapped with the same PL-PEG-NH_2 or Poly(Lys:Phe) (oxDWNT-Poly(Lys:Phe)-pDNA, oxDWNT-PL-PEG-NH_2-pDNA; oxSWNT-Poly(Lys:Phe)-pDNA and oxSWNT-PL-PEG-NH_2-pDNA); and PL-PEG-NH_2 or Poly(Lys:Phe) conjugated with pDNA or siRNA and then wrapped around oxidised DWNTs (Poly(Lys:Phe)-pDNA-DWNT and PL-PEG-NH_2-pDNA-DWNT), as described in the methodology.

Figure 5.3 and 5.4 presents the behaviour of different coatings in agarose-gel electrophoresis for pDNA and siRNA, respectively.

Figure 5.3: Agarose-gel electrophoresis of pDNA binding to CNT. Lane 1 – 1 Kb Ladder; Lane 2 and 3 – Poly(Lys:Phe) or PL-PEG-NH_2 respectively, conjugated with DNA wrapped around oxidised DWNTs (Lane 2 – Poly(Lys:Phe)-pDNA-oxDWNT; Lane 3 – PL-PEG-NH_2-pDNA-oxDWNT); Lane 4 - pristine DWNT wrapped with Poly(Lys:Phe) (Lane 4 - DWNT-Poly(Lys:Phe)-pDNA); Lane 5 and 6 - oxidised DWNT wrapped with Poly(Lys:Phe) or PL-PEG-NH_2, respectively and conjugated with pDNA (Lane 5 – oxDWNT-Poly(Lys:Phe)-pDNA; Lane 6 – oxDWNT-PL-PEG-NH_2-pDNA); Lane 7 and 8 – similar to 5 and 6 but using single-walled CNTs (Lane 7 – oxSWNT-Poly(Lys:Phe)-pDNA; Lane 8 – oxSWNT-PL-PEG-NH_2-pDNA); Lane 9 and 10 – controls Poly(Lys:Phe)-pDNA and PL-PEG-NH_2-pDNA, respectively; Lane 10 – pDNA control.

pDNA binding to CNTs was evident for Poly(Lys:Phe) coated, pristine or oxidised CNTs. Complete binding occurred as no band of free DNA could be visualised (Figure 5.3; lane 5 and 7). Coating with PL-PEG-NH_2 resulted in a less intense band when compared with control of pDNA only, indicating that binding had occurred but a significant quantity of unbound free DNA was still present in the solution (Figure 5.3; lane 6 and 8).

Hence, it is pertinent to note that pristine DWNTs wrapped with PL-PEG-NH_2 led to precipitation when conjugated with pDNA and was therefore discarded from the

results presented here. In addition, when PL-PEG-NH_2 or Poly(Lys:Phe) were first bound to pDNA, followed by binding to CNTs, the complexes were found to be unsuitable for gene delivery. This was because these complexes could not be filtered (Section 5.2.2.2), which could lead to free polypeptide-pDNA in solution. Furthermore, as shown in Figure 5.3, lane 9 and 10, control samples of Poly(Lys:Phe)-pDNA and PL-PEG-NH_2-pDNA presented no band for free pDNA. Therefore, it was impossible to assure that delivery of pDNA to cells would be mediated through CNT-delivery and not via polypeptide on its own.

Similar results were obtained for siRNA, in which PL-PEG-NH_2 resulted in a band in the agarose-gel, but the band was less intense than control samples with siRNA only. However, binding was enhanced when Poly(Lys:Phe)-siRNA was employed, as demonstrated in Figure 5.4, lanes 4 and 5.

Figure 5.4: Agarose-gel electrophoresis of siRNA binding to CNT. Lane 1 – 1 Kb Ladder; Lane 2 – PL-PEG-NH_2 conjugated with siRNA wrapped around oxidised DWNTs (Lane 2 – PL-PEG-NH_2-siRNA-oxDWNT); Lane 3 - pristine DWNT wrapped with PL-PEG-NH_2 and conjugated with siRNA (Lane 3 - DWNT-PL-PEG-NH_2-siRNA); Lane 4 – Poly(Lys:Phe) conjugated with siRNA wrapped around oxidised DWNTs (Lane 4 – Poly(Lys:Phe)-siRNA-oxDWNT); Lane 5 - pristine DWNT wrapped with Poly(Lys:Phe) and conjugated with siRNA (Lane 4 - DWNT-Poly(Lys:Phe)-siRNA); Lane 6 – siRNA control; Lane 7 – 100 bp Ladder.

5.3.3 Cellular uptake of CNT-nucleic acid complexes by Raman spectroscopy

In previous chapters, Raman spectroscopy was applied to confirm cellular internalisation of CNT-complexes. In the present chapter this technique was use to demonstrate the ability of CNT-nucleic acids to enter into the cells (Figure 5.5 and 5.6, respectively). Figure 5.5 A, exhibits the G-band peak area for different coatings for delivery of pDNA. As it is clear from the figure oxDWNT-Poly(Lys:Phe)-pDNA had the highest G band intensity suggesting that higher number of CNTs were internalised, in contrast to oxDWNT-PL-PEG-NH_2-pDNA. Pristine DWNTs appeared to have a higher error associated with the measurements (Figure 5.5 A), which could be related to the dispersibility and higher length of the constructs. In contrast to oxidised CNTs, pristine nanotubes have a higher variation in length, which can lead to a lower concentration of CNTs inside some cells in comparison with others. Figure 5.5 B displays the normalised intensity of the G band of oxDWNT-Poly(Lys:Phe)-pDNA obtained for a single cell (inset).

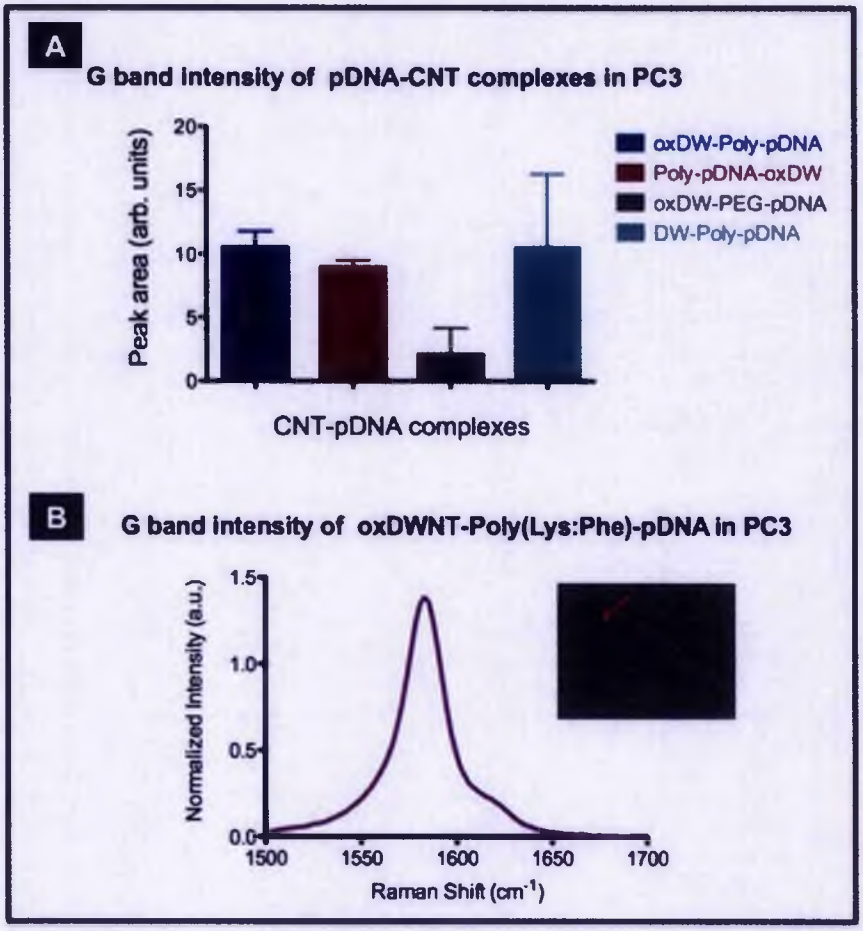

Figure 5.5: Raman spectroscopy of PC3 single cells transfected with pDNA via CNTs. (A) G band peak area for different DWNT-preparations for pDNA delivery into PC3 cells. (B) G band intensity of internalised oxDWNT-Poly(Lys:Phe)-pDNA in PC3 cells. The inset (B) shows cell and region of the measurement. Results presented as Mean±SEM (n=6).

Cellular internalisation of CNT-siRNA complexes was also confirmed by Raman spectroscopy for CNTs, coated with PL-PEG-NH_2, which resulted in a higher intensity of G band (Figure 5.6 A). However, gel retardation assays demonstrated that these complexes bound siRNA less efficiently. It was therefore decided to use Poly(Lys:Phe)-siRNA-oxDWNTs for siRNA delivery. Figure 5.6 B displays the normalised intensity of G band of Poly(Lys:Phe)-siRNA-oxDWNT obtained for a single cell (inset).

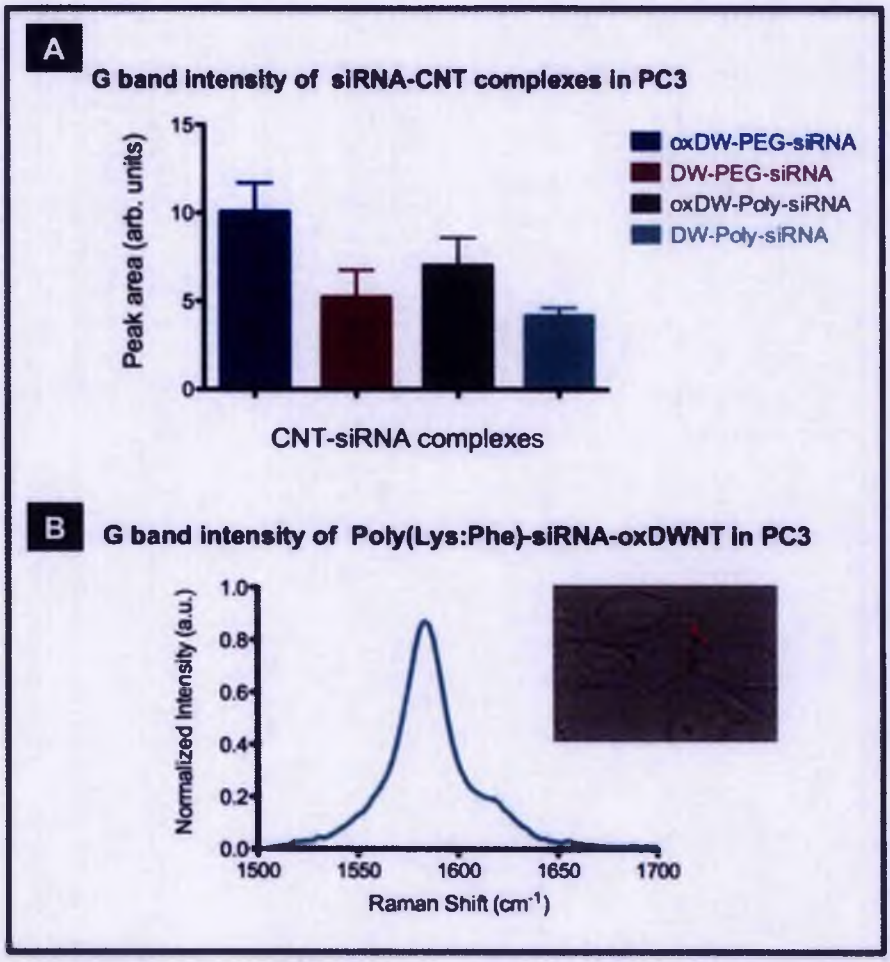

Figure 5.6: Raman spectroscopy of PC3 single cells transfected with siRNA via CNTs. (A) G band peak area for different DWNT-preparations for siRNA delivery into PC3 cells. (B) G band intensity of internalised Poly(Lys:Phe)-siRNA-oxDWNT in PC3 cells. The inset (B) shows cell and region of the measurement. Results presented as Mean±SEM (n=6).

5.3.3.1 Concentration of CNTs-nucleic acid complexes inside cells

CNTs concentration can be determined through G band intensity as demonstrated in Chapter 3. Table 5.1 displays the values of G band obtained for different coatings for pDNA and siRNA delivery. A new calibration curve was determined, with the equation y= 3.096ln(x) – 2.256 (Section 3.3.2.4), since a different wavenumber was selected (785 nm). Comparing concentrations obtained here with the ones obtained for cell lysates (Chapter 3, section 3.3.2.4) there is an evident increase, which can be related to the technique employed. In contrast to cell lysates where only nanotubes in the

cytoplasm were considered, for this study single cells that also detect CNTs at cell surface were analysed by Raman spectroscopy. Nevertheless, the method allows an estimation of CNTs per cell.

Table 5.1: Concentration of CNTs in cells. Correlation between G band intensity and concentration of CNTs was used to determine the concentration of internalised CNTs. (Cell volume = 5.75×10^{-9} µL [299])

Samples	G band area peak (a.u.)	Concentration [i] (µg/mL)	Concentration per cell (pg/cell)
oxDW-Poly-pDNA	10.466	2.027	1.2×10^{-05}
Poly-pDNA-oxDW	8.496	1.864	1.1×10^{-05}
oxDW-PEG-pDNA	6.242	1.657	9.5×10^{-06}
DW-Poly-pDNA	8.59	1.872	1.1×10^{-05}
oxDW-PEG-siRNA	10.122	2.000	1.1×10^{-05}
DW-PEG-siRNA	5.25	1.557	8.9×10^{-06}
oxDW-Poly-siRNA	6.782	1.709	9.8×10^{-06}
DW-Poly-siRNA	4.192	1.443	8.3×10^{-06}

5.3.4 GFP expression in mammalian cells via CNTs

CNT-pDNA complexes were employed for transfection of PC3 cells and GFP gene expression was evaluated by means of confocal microscopy and flow cytometry. Different concentrations of plasmid DNA were tested. Optimal transfection efficiencies were obtained for concentrations of ~5 ng/µL pDNA.

Figure 5.7, illustrates fluorescent microscopy images of PC3 cells expressing GFP (in green), and cells without transfected genes where the nucleus is stained (blue). Different delivery agents were used for transfection of pDNA: Lipofectamine; oxidised

[i] *Concentration of CNTs in the cell was calculated using a logarithmic correlation between G band intensity and CNT concentration (y= 3.096ln(x) – 2.256; where y is the G-band peak area; and x is concentration in µg/mL, $R^2 = 0.945$)*

DWNT wrapped with Poly(Lys:Phe) and PL-PEG-NH_2; and pristine DWNT wrapped with Poly(Lys:Phe). Results revealed that 40 % of cells were expressing GFP when cationic agent, Lipofectamine, was employed. However, CNTs transfection yield dropped significantly. Only a small percentage of GFP expressing cells could be visualised under microscopy for oxDWNT-Poly(Lys:Phe)-pDNA. The remaining CNT-pDNA complexes resulted in inefficient plasmid DNA transfection, in which cells expressing GFP could not be found.

In addition to fluorescence microscopy, samples were also analysed by flow cytometry, Figure 5.8, which exhibits the fluorescence (FITC) *vs* the number of cells for different delivery methods. Furthermore, the inset in each chart represents the results obtained for confocal microscopy, as shown in figure 5.7. Similar to results observed for fluorescent confocal microscopy, Lipofectamine transfection resulted in approximately 40 % GFP expressing cells (Figure 5.8 C). Plasmid transfected via oxDWNT-Poly(Lys:Phe)-pDNA achieved, at best, a maximum of 1 % of GFP expressing cells (Figure 5.8 E). Furthermore, fluorescence was also determined by means of mean fluorescence intensity (MFi) and was found to be 254 for Lipofectamine, 12.8 for oxDWNT-Poly(Lys:Phe)-pDNA, and 5.42 for cells only, revealing that fluorescence increase due to GFP delivery using CNTs is much lower than with Lipofectamine.

The inconsistency between the results of fluorescence microscopy *vs* flow cytometry may be related to the sample size. In confocal microscopy no more than 200 cells were counted, whereas by flow cytometry 10 000 events (i.e., cells) were measured.

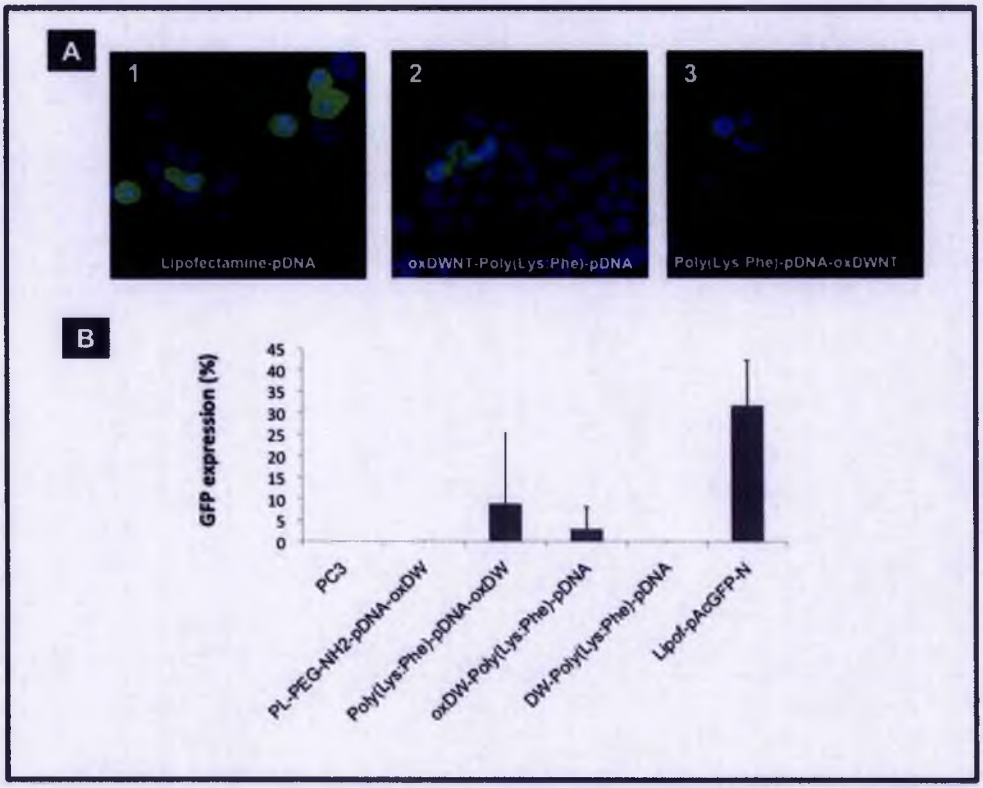

Figure 5.7: Fluorescent microscopy of PC3 cells transfected with pDNA(GFP). GFP expression in PC3 cells transfected with Lipofectamine (A_1) after 24-hours; GFP expression in PC3 cells after incubation with oxDWNT-Poly(Lys:Phe)-pDNA and Poly(Lys:Phe)-pDNA-oxDWNT (A_2 and A_3, respectively). (B) GFP expression by mean of number of expressing cells (%) using different coatings (percentages calculated from number of green cell in 5 different fields).

To obtain efficient gene delivery, not only does the complex has to transverse the plasma membrane, but also must also escape lysosomal degradation, and overcome the nuclear envelope. As a result, the low transfection efficiency of CNT-pDNA might be related to the uptake pathway of the complex, two main critical steps have to be taken into account. Firstly, pDNA could be degraded in the lysosomes after CNT sequestration in these compartments; and secondly CNT-pDNA complexes may be unable to reach the nucleus where replication of plasmid DNA would occur. Thus, the lack of availability at the target site – nucleus, prevents the effective delivery of pDNA by CNTs.

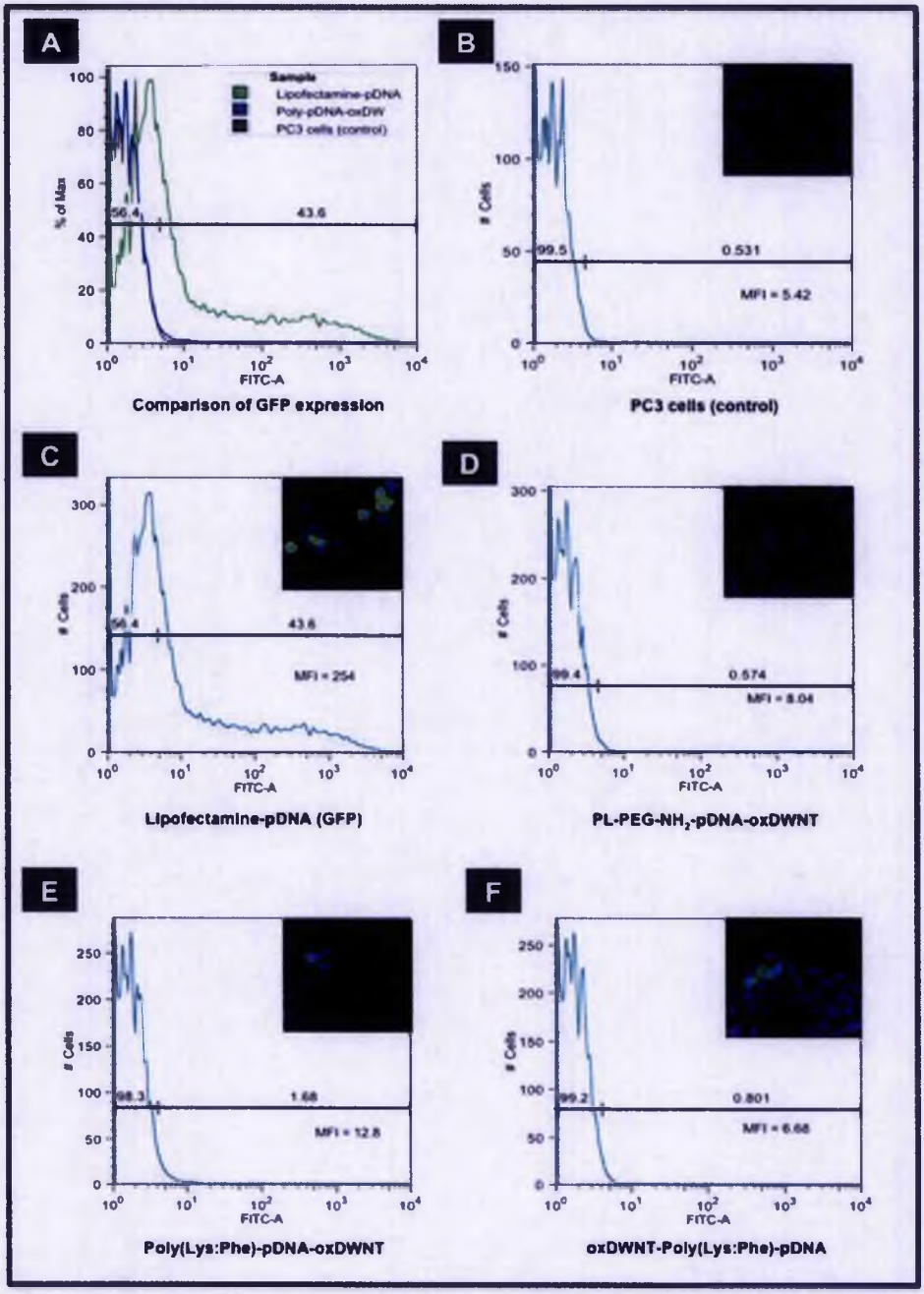

Figure 5.8: Flow cytometry and fluorescent microscopy of PC3 cells transfected with pDNA(GFP). Flow cytometry by measurement of fluorescent cells (%) and mean fluorescence intensity after 24-hours post-transfection. (A) GFP expression, using Lipofectamine and CNTs to deliver pDNA in comparison with PC3 cells only. Control with cells only (B). GFP expression in PC3 cells transfected with Lipofectamine (C); PL-PEG-NH_2-pDNA-oxDWNT(D); Poly(Lys:Phe)-pDNA-oxDWNT(E); oxDWNT-Poly(Lys:Phe)-pDNA (F).

5.3.5 Gene silencing in mammalian cells via CNTs

Small interfering RNAs (siRNAs) are the effector molecules of the RNA interference (RNAi) pathway [358, 359]. They are active in the cytoplasm where the mRNA is translated to a protein and therefore do not have to transfer through the nuclear membrane, which could be advantageous when comparing with pDNA; particularly as the studies above have indicated that transport to the nucleus could be limited for plasmids delivered by CNTs. Herein, investigation of the feasibility of DWNTs to deliver siRNA to mammalian cells was studied. In order to detect gene silencing we developed a HeLa and PC3 cell lines that stably expressed GFP, so that delivery and efficacy of an siRNA silencing the GFP gene could be optimised.

5.3.5.1 Stable cell lines expressing GFP

To ensure rapid reductions in protein levels in response to decreases in mRNA levels, cells were transfected with an enhanced GFP protein, from *Aequorea coerulescens*. Cells were transfected with the GFP-encoding plasmid and the efficiency of transfection was determined by confocal microscopy and flow cytometry (Figure 5.9). Selection of a GFP-expressing clone was achieved by supplementing the media with Geneticin, which killed cells that had not taken up the plasmid. In a final step of selection, GFP-expressing cells were separated from non-expressing ones via FACS (Figure 5.9). As shown in Figure 5.9, cells stably expressing the GFP gene in 80-90 % of cells, after selection via cell sorting by FACS.

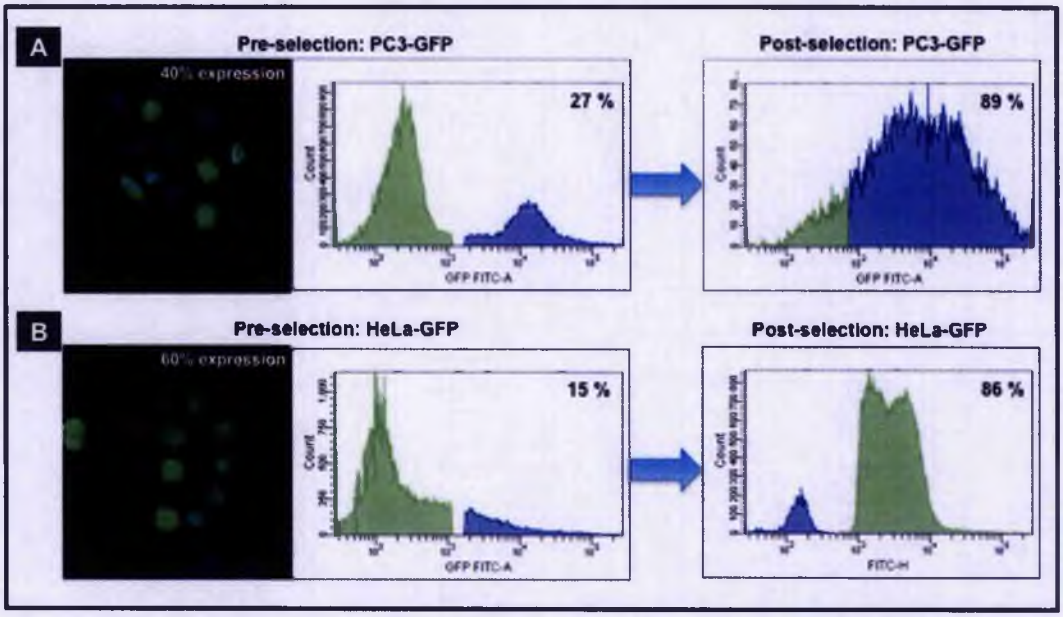

Figure 5.9: Fluorescence microscopy and flow cytometry GFP expressing cells. PC3 (A) and HeLa (B) cells transfected with GFP (pre-selection), and post-sorting of stable cell lines expressing GFP (post-selection).

5.3.5.2 GFP silencing

siRNAs can be introduced directly by transfection or by electroporation, or generated within the cell from a short hairpin RNA expressed from a DNA construct. For our purposes of using CNTs for gene silencing, the expression of siRNA as hairpin structures from plasmid or viral vectors was not considered, as it was revealed in the previous section that CNTs did not efficiently deliver pDNA. Furthermore a study carried out by Gao *et al.* shows that transfection efficiency of CNTs is only 5 %, contrasting with 30 % obtained for Lipofectamine [340]. For this reason, in our studies the synthesised siRNAs were delivered into mammalian cells.

To examine the efficiency of DWNT-delivery of siRNA-based knockdown, HeLa-GFP and PC3-GFP cell lines were transfected with siRNA sequences against GFP and a negative control siRNA sequence. The two functional siRNAs to the same target were used independently to ensure that any biological effect was due to silencing of the target gene and not due to an off-target effect. DWNTs were oxidised and wrapped with PL-PEG-NH_2 or Poly(Lys:Phe) as described in the methodology (Section 5.2.2).

In parallel, a cationic transfection agent, Lipofectamine RNAiMAX, was employed as a control for high transfection efficiencies.

The transfection efficiency and gene knockdown were evaluated by calculating the percentage of cells expressing GFP by fluorescence microscopy and flow cytometry. Cells stably expressing GFP were prepared for both HeLa and PC3, however results obtained were in line with previous results. Thus to simplify the data, only present data relative to PC3 is presented. However, is important to note the significance of using two cell lines to obtain reliable results. Different concentrations of siRNA were tested, from 0.2 to 1 μM, however lower concentrations resulted in 20 % less efficient knockdown; therefore a higher concentration of 1 μM was employed to obtain the data presented here.

Figure 5.10 depicts the silencing effect produced using Lipofectamine. In the first panel (A) the controls can be visualised with above 90 % GFP expressing cells. This is followed by panels B to D showing different time points of incubation post-transfection with Lipofectamine are presented. A maximum silencing effect of 80 % after 72-hours was measured by both confocal microscopy and flow cytometry (Figure 5.10 C). In addition, the mean fluorescence intensity (MFI) for control with Negative-siRNA (NegsiRNA) was 71 units and dropped to 23.3 units when GFP-siRNA was employed.

In contrast, post-transfection with Poly(Lys:Phe)-siRNA-oxDWNT is displayed in Figure 5.11 A to D, and reveals only minor GFP knockdown. Similar to pDNA-delivery, it was apparent that there were certain discrepancies between results obtained for confocal microscopy in comparison with flow cytometry. Higher percentages of knockdown were visualised by confocal microscopy, for example, after one-week of incubation, post-transfection using CNT-complexes, the percentage of knockdown by confocal microscopy was of 17 %, while the knockdown evaluated by flow cytometry was of only 3 %.

Analysing GFP knockdown through flow cytometry – MFI, it was observed that MFI dropped from 121 for Negative-siRNA (control, NegsiRNA) to 115 for GFP-siRNA, after 1-week, demonstrating that CNT complexes did not efficiently deliver siRNA.

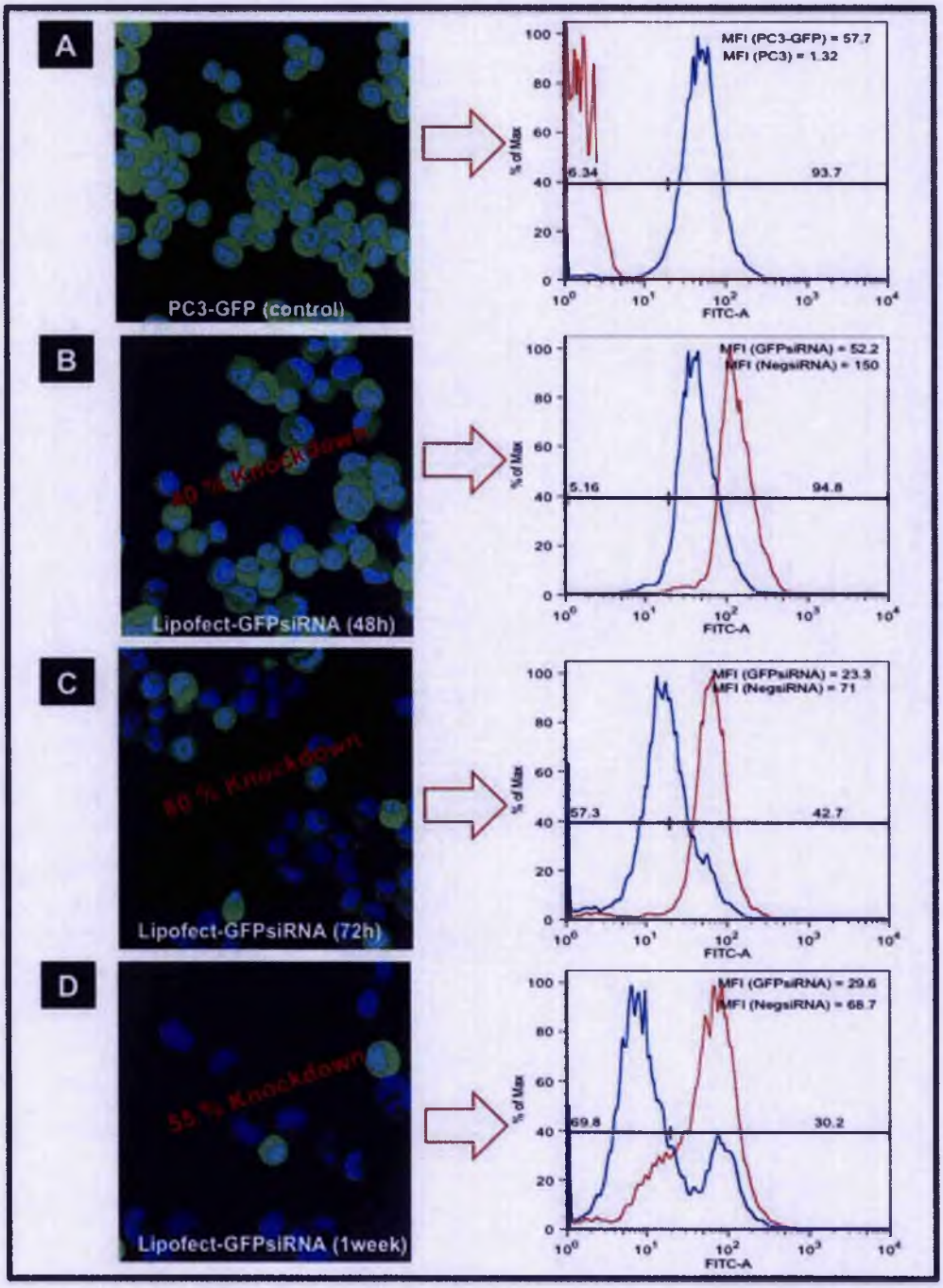

Figure 5.10: Fluorescent microscopy and flow cytometry of PC3-GFP cells transfected with siRNA(GFP) using Lipofectamine. Knockdown of GFP gene evaluated by fluorescent microscopy (left panel) and flow cytometry (right panel) using Lipofectamine at different incubation points: 48 h (B), 72 h (C), and 1 week (D), post-transfection. Control with PC3 stably expressing GFP (A).

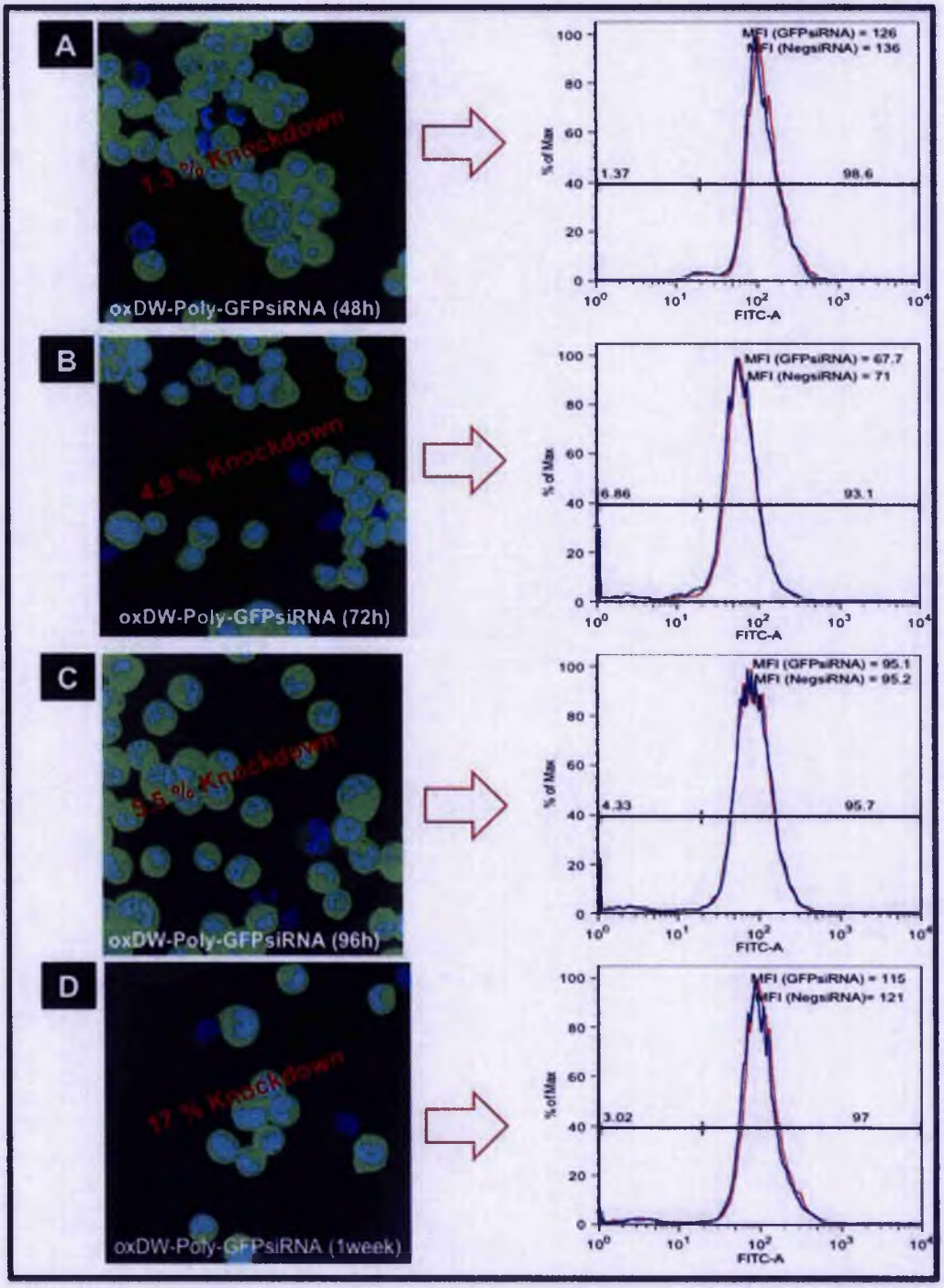

Figure 5.11: Fluorescent microscopy and flow cytometry of PC3-GFP cells transfected with siRNA (GFP) using CNTs. Knockdown of GFP gene evaluated by fluorescent microscopy (left panel) and flow cytometry (right panel) using Poly (Lys: Phe)-siRNA-oxDWNT at different incubation points post-transfection: 48 h (A); 72 h (B); 96 (C); and 1 week (D).

Besides testing different incubation periods, different coatings of DWNT were also examined. Figure 5.12 depicts fluorescent microscopy and flow cytometry data obtained for the different coating methods: Lipofectamine (A: Lipof-GFPsiRNA); pristine DWNT-PL-PEG-NH_2-siRNA (B: DW-PEG-GFPsiRNA); oxidised DWNT wrapped with either PL-PEG-NH_2 or Poly(Lys:Phe) (C and D: oxDW-PEG-GFPsiRNA and oxDW-Poly-GFPsiRNA, respectively).

Flow cytometry of Lipofectamine transfection (Figure 5.12 A) revealed 40 % knockdown of GFP gene, with a drop of MFI from 146 for Neg-siRNA to 73.5 units for GFP-siRNA. A comparable effect was not visualised for any of the CNT preparations (less than 5 %). Pristine DWNT wrapped with PL-PEG-NH_2 (Figure 5.12 B) the MFI dropped from 151 to 136 units, Neg-siRNA and GFP-siRNA respectively. In addition, oxidised DWNT wrapped with Poly(Lys:Phe) or PL-PEG-NH_2 led to insignificant GFP silencing (Figure 5.12 C and D).

Under the experimental conditions employed in these studies, siRNA and pDNA-delivery indicate that CNTs do not efficiently deliver nucleic acids into PC3 and HeLa cell lines. It appears, from Raman spectroscopy of cells exposed to CNT-complexes, that CNTs are being internalised; however the nucleic acids once delivered were not functional, either in the cytoplasm, siRNA; or nucleus demonstrated by pDNA-delivery. This observation might be related with the preparation of the complexes. pDNA and siRNA may be degraded before reaching their target sites; either being degraded before reaching the cells or already inside cells, in endosomes.

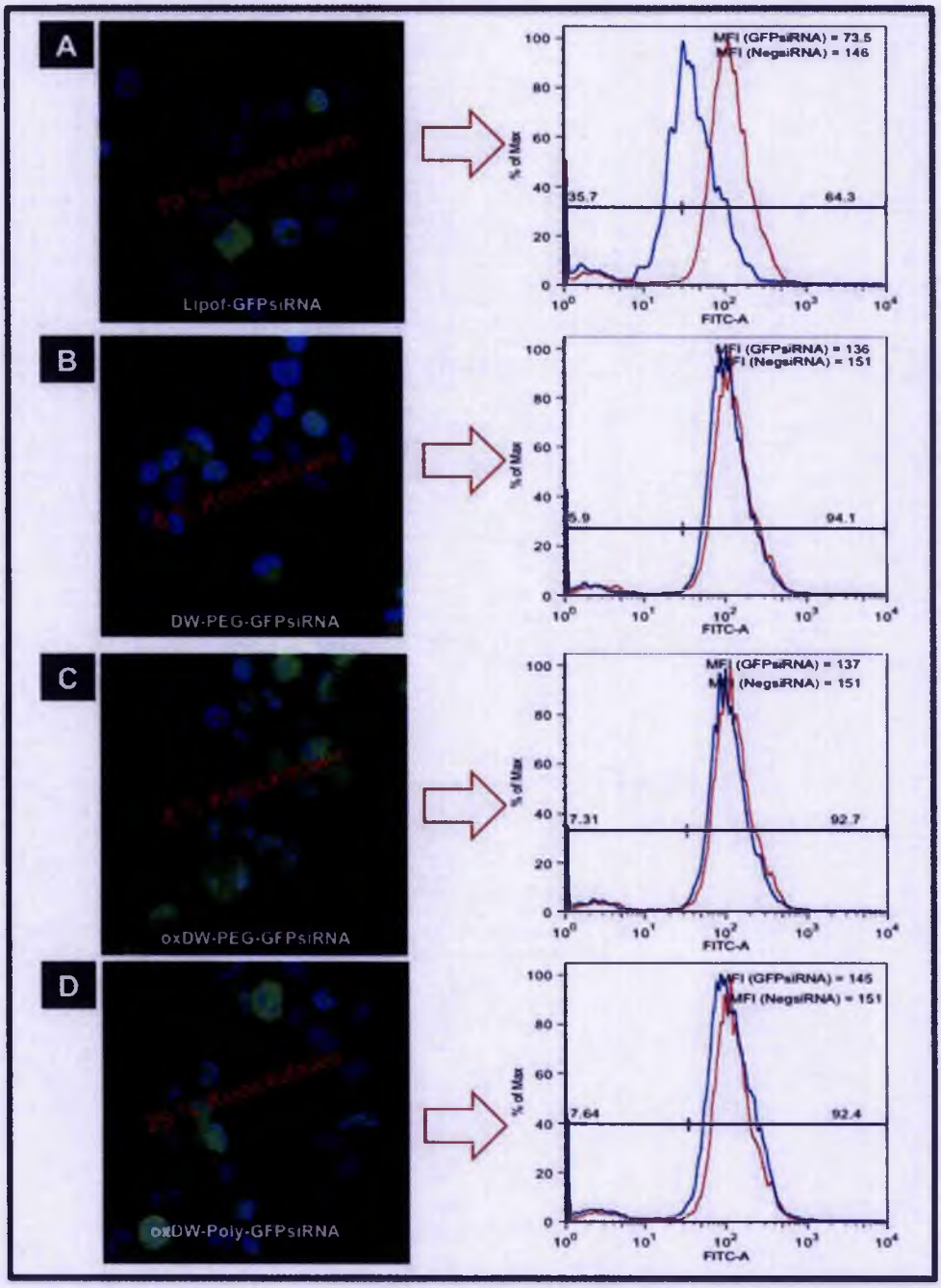

Figure 5.12: Fluorescent microscopy and flow cytometry of PC3-GFP cells transfected with siRNA(GFP) using different CNTs coating. Knockdown of GFP gene evaluated by fluorescent microscopy (left panel) and flow cytometry (right panel), 72-hours post-transfection, using different delivery agents: Lipofectamine (A); DWNT-PL-PEG-NH_2-siRNA (B); PL-PEG-NH_2-siRNA-oxDWNT(C); and Poly(Lys:Phe)-siRNA-oxDWNT(D). siRNA-CNT complexes led to less then 10 % gene knockdown in comparison with 40 % obtained for positive control (Lipofectamine).

5.4 Conclusions

GFP pDNA (pAcGFP1-C from Clontech) was used to study gene delivery and silencing via CNTs. In order to be expressed, it is necessary for the pDNA to enter the cell and to be processed by the cellular machinery. As plasmid DNA alone penetrates into the cells and reaches the nucleus with considerable difficulty, CNTs could be used to enhance gene transfer and expression.

In the literature efficient delivery of nucleic acids has been reported. Pantarotto *et al.* describe efficient delivery of pDNA [127], however in their study different conditions and parameters were applied, such as CNT modification (covalently modification using 1,3-dipolar clycoaddition). In addition, in their study expression of CNTs-pDNA is compared with pDNA alone, a positive control, such as Lipofectamine was not applied. Furthermore different cell lines were employed (CHO cell line).

Similar to what we report in this chapter, Gao *et al.*, uses multi-walled CNTs to deliver plasmid DNA encoding GFP. In their work two cell lines were used (HUVEC and A375) and Lipofectamine was employed as a positive control. They reported 5 % of cells expressing GFP when CNTs are used, compared with 30 % of GFP expressing cells obtained with Lipofectamine [340]. However, evaluation of GFP expression was measured through counting fluorescent cells under the fluorescent microscope. Our experiments revealed that fluorescent microscopy is insufficiently discriminatory to determine GFP expression in a population.

in addition, others groups have studied siRNA delivery in a larger extent. For example, Kam *et al.* reported potent gene silencing by means of siRNA delivery using CNTs. They observed a silencing effect of over 2 fold using SWNTs in comparison with Lipofectamine [174]. Through similar CNT preparation, a later study carried by the same group, Liu *et al.*, showed siRNA delivery into Human T cells and primary cells [175]. *In vitro*, certain T cells and primary cells are still difficult to transfect by non-viral agents, such as liposomes, as in the case of siRNA delivery to T cells [341]. 90 % gene knockdown of CXCR4 and CD4 genes was demonstrated; 3 day post-transfection using SWNTs for siRNA delivery. In contrast, Lipofectamine-delivered siRNA had no silencing effect on these T cells. To demonstrate that this effect was only observed for T cells the authors used Magi cells (which are derived from HeLa cells with high level of expression of CD4 receptors and CXCR4 co-receptors). The results show that both Lipofectamine and SWNT-siRNA caused downregulation of the genes. Conversely, they observed a 90 % knockdown in T cells using SWNT, but this

effect was decreased in Magi cells where the silencing effect was of the order of 40-50 %. Moreover, Lipofectamine presented a knockdown effect of around 60-80% [175]. The study indicates that the choice of the cell type affects the results observed. Additionally, in their studies modification of CNTs consisted of adsorption to SWNT of phospholipid molecules of poly(ethylene glycol) (PL-PEG) chains with a terminal amine or maleinide was employed. Similar to the methodology employed in this chapter. However, in their study, the siRNA was not bound through electrostatic interactions, but through a cleavable scheme, where amine or maleimide terminal on the PL-PEG immobilized on SWNT was conjugated with thiol-modified siRNA. It is possible that this modification provided a more efficient gene delivery system.

Furthermore, a recent study from Al-Jamal *et al.* (2010) reported efficient knockdown of GFP gene through siRNA delivery using a synthesised polycationic Dendron-MWNT [362]. In their study, delivery of siRNA was carried out after transient transfection with GFP-pDNA in A549 cells. GFP knockdown was evaluated by immunoblotting, revealing a decrease of protein levels in comparison with a negative control. Therefore, in their study the siRNA possibly will be protected against degradation by the Dendron-CNT and it is therefore available at the target site, resulting in gene knockdown.

Hence, our results demonstrate nucleic acids become complexed to CNTs, confirmed via gel retardation assays (Figure 5.3 and 5.4). Furthermore, cellular uptake of CNT-complexes was demonstrated by Raman spectroscopy (Figure 5.5 and 5.6). However, nucleic acid molecules did not reach their target sites. Thus, pDNA did not cross the nuclear envelope and thus there was no translation of the GFP protein. In addition, the siRNA was unavailable in the cytoplasm to efficiently block stable transcripted of GFP gene (integrated into the chromosome). The apparent inefficiency of the CNTs for delivery of pDNA and siRNA in our study can mainly be attributed to the methodology by which nucleic acids were bound to CNTs. Leading to a possible degradation of nucleic acids in the media or inside lysosomes.

In the next chapter siRNA will be conjugated onto CNT-complexes using a cleavable disulfide bond, for stronger attachment of the cargo. Followed by the study of the ability to knockdown a gene.

Chapter 6: *Survivin* targeting via CNTs

6.1 Introduction

Evasion of apoptosis, and the ability to proliferate uncontrollably are two molecular traits found in all human cancers [342]. Therefore, anti-apoptotic proteins involved in signalling through specific apoptosis pathways provide targets for possible drug discovery and new anticancer interventions. As described in more detail below, *survivin* is highly expressed in a number of human tumours and it is also involved in tumour cell resistance to anticancer drugs and ionizing radiation. For these reasons it has been proposed as an attractive target for anticancer therapies – particularly gene silencing- based therapies

Two major pathways of apoptosis have been identified in mammalian cells (Figure 6.1). The extrinsic pathway is triggered by the binding of ligands to the cell surface trimeric membrane death receptors and leads to caspase-8 activation [343]. The intrinsic pathway is mediated by mitochondria, which respond to pro-apoptotic signals by releasing cytochrome c, which in turn binds and activates the apoptotic protease-activating factor-1, causing assembly of a multi-protein caspase-activating complex (apoptosome). This leads to activation of caspase-9 and initiation of a protease cascade [344]. The intrinsic and extrinsic pathways converge on downstream effector caspases. Some of these, such as caspase-3 and caspase-7, are targets for suppression by an endogenous family of anti-apoptotic proteins called inhibitor of apoptosis proteins (IAPs), which also interfere with caspase-9 processing, the upstream initiation of mitochondrial pathway of apoptosis [345]. The human genome encodes eight IAP family members (Figure 6.1) including *survivin*. *Survivin* is a 16.5 kDa protein of 142 amino acids and it is composed of a single baculovirus IAP repeat domain (BIR) and an extended C-terminal α-helix coiled domain; it does not contain the RING-finger domain found in other IAPs [367]. The BIR domain is involved in the anti-apoptotic function, in contrast to the coiled domain, which interacts with tubulin structures. *Survivin*, unlike other IAP proteins, is essential for correct completion of mitosis and cell division [346].

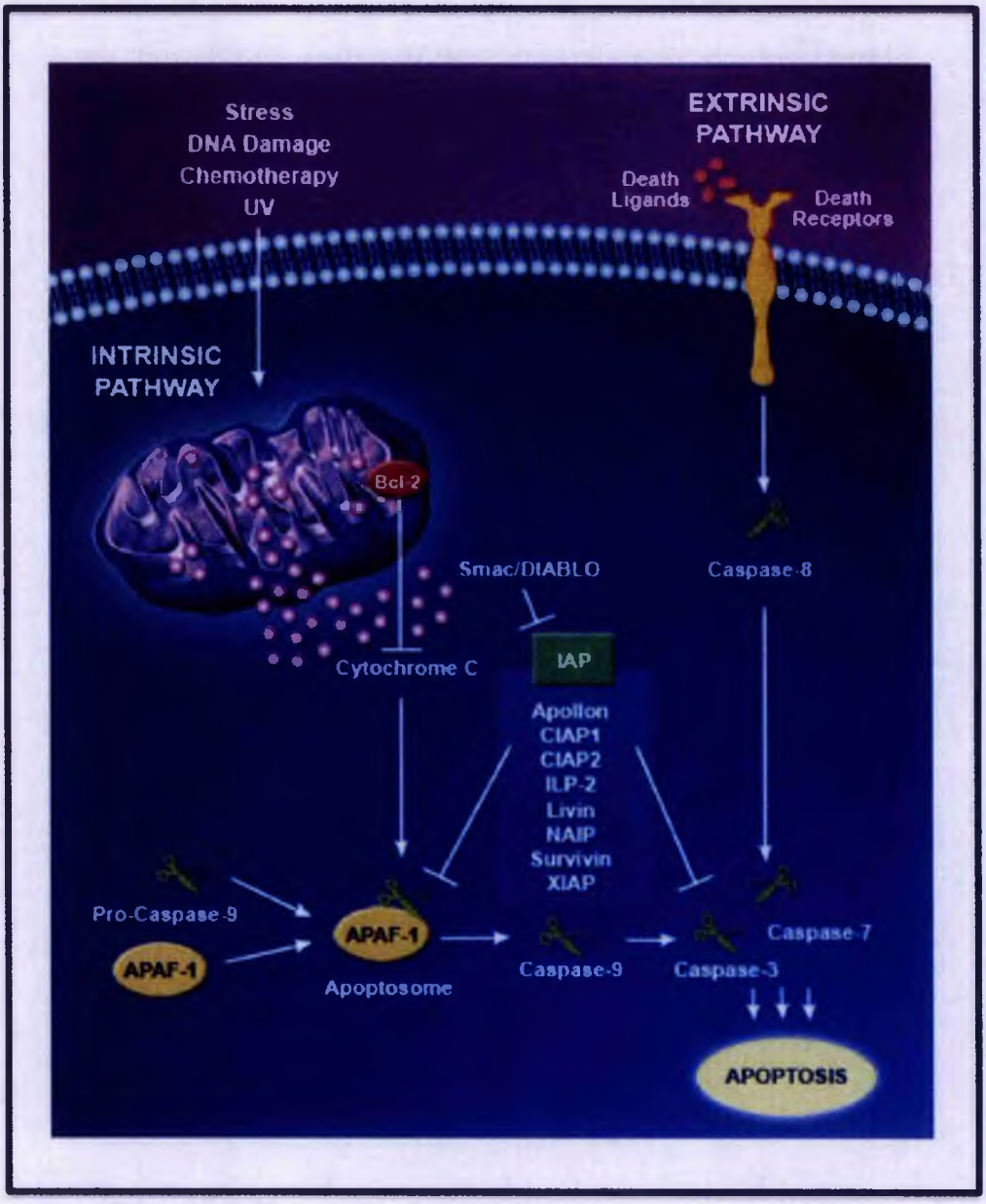

Figure 6.1: IAP proteins inhibit apoptosis by binding to activated caspases. They inhibit signals generated through both the two major pathways of apoptosis: the extrinsic (death receptor mediated) and the intrinsic (mitochondrial mediated) pathways [347].

One of the most significant features of *survivin* it is their differential expression in cancer *versus* normal tissues [348]. In normal tissues, the protein expression is regulated and it is often absent or low in most terminally differentiated tissues [348]. Thus, *survivin* is expressed in normal tissues characterised by self-renewal and proliferation, though in significantly lower levels than in tumour tissue. Importantly, several studies have demonstrated high *survivin* expression in most human solid tumour types and haematologic malignancies, emphasising its status as potential new target for cancer therapies [349]. Expression of *survivin* has also been detected in a variety of benign and preneoplastic lesions including melanocytic nevi, polyps of the colon, breast adenomas, Bowen's disease and hypertrophic actinic keratosis [349], suggesting that re-expression of *survivin* may occur early during malignant transformation or following disturbance in the balance between cell proliferation and cell death [350].

Increasing evidence suggests that *survivin* expression in cancer cells is associated with clinicopathologic variable of aggressive disease and therefore might represent an important prognostic marker for patient outcome. In fact, several studies into different types of solid tumours and haematologic malignancies showed that high levels of *survivin* protein were predictive of tumour progression in terms of either disease free or overall survival [349].

Elimination of the *survivin* pathway should result in the lowering of the anti-apoptotic threshold in cancer cells. Consequently, tumour cells undergo apoptosis directly, or can be used in combination with chemotherapy or radiation therapy. Carvalho *et al.* (2003) were the first to use RNAi approaches to suppress *survivin* in HeLa cells. Following transfection with RNAi for 60-hours they demonstrated depletion of *survivin* in cells with further demonstration of delayed mitosis [351]. A number of other studies using different siRNA have shown that RNAi mediated knockdown of *survivin* was capable of reducing tumour cell proliferation and induced caspase-dependent apoptosis in a variety of human tumour cell line models – in addition to decreasing the growth of established lesions in nude mice [352]. The work described in the following sections has considered the use of siRNA-CNT complexes directed against *survivin*, as an approach to demonstrate *in vitro* cytotoxicity in *survivin* expressing colon and prostate cancer cells.

6.2 Experimental section

In this section, a detailed description of the methodology employed is presented. Firstly, siRNA sequences targeting *survivin* were tested, to select those with highest knockdown effect. Secondly, CNTs were prepared for conjugation with siRNA and thiol-modified siRNA targeting *survivin* gene. Then, the complexes were exposed to cancer cells that overexpress the gene and knockdown was assessed following uptake by western immunoblotting. Finally, the effect of silencing was evaluated by detecting apoptosis using dual staining with annexin for early stage apoptosis (externalisation of phosphatidyl-serine) and propidium iodide for late stage apoptosis (nuclear stain).

6.2.1 Test different *survivin* siRNA sequences using DharmFECT transfection reagent

For the synthetic siRNA employed in the present study it was recommended that DharmaFECT transfection reagent be used (from Dharmacon RNAi technologies, Thermo Fisher Scientific, UK). DharmaFECT-siRNA complexes were prepared according to the manufacture instructions: 3 μL DharmaFECT reagent was combined with 400 μL of serum free culture media and incubated for 5 minutes at room temperature. Next the siRNA was diluted in 400 μL of media to a final concentration of 0.8 μM per 35 mm plate. The solutions were then combined and incubated at room temperature for a further 20 minutes, followed by incubation with cells as described in Section 6.2.3.

siRNA targeting *survivin* gene (BIRC-5 gene, ON-TARGETplus from Dharmacon RNAi technologies, Thermo Fisher Scientific, UK) with following sequences (below) were tested to assess the knockdown efficiency:

Table 6.1: siRNA targeting sequences. *Survivin* target sequences for silencing using siRNA

Molecular weight (g/mol)	Extinction coefficient ($L\ mol^{-1}cm^{-1}$)	nM	µg
Target sequence: GCAAAGGAAACCAACAAUA (J-003459-08)			
13 399.9	376737	5.0	66.9
Target sequence: GGAAAGGAGAUCAACAUUU (J-003459-09)			
13 399.9	379852	5.0	66.9
Target sequence: CACCGCAUCUCUACAUUCA (J-003459-10)			
13 429.9	371130	5.0	67.1
Target sequence: CCACUGAGAACGAGCCAGA (J-003459-11)			
13 459.9	359916	5.0	67.2

6.2.2 CNT-coating for siRNA binding

As stated in the previous chapter siRNA sequences can be bound to CNTs through cleavable disulfide bonds, similar to the approach described by Kam *et al.* [174]. In this chapter the same methodology was apply increase the efficiency of knockdown of the gene *survivin*. Therefore, oxidised DWNT were wrapped with Poly(Lys:Phe) (1:1) (Sigma Aldrich, UK), as this was the methodology that led to higher binding and delivery of siRNA (as shown in Section 5.3.2). Then, both siRNA and thiol modified siRNA (siRNA-SH) were bound, either by electrostatic interactions or through a cross-linker between amine on the Poly(Lys:Phe) and the thiol modified siRNA.

6.2.3 Wrapping of oxidised CNT

DWNTs were purified in concentrated nitric acid and oxidised in a mixture of nitric and sulphuric acid [185] (Chapter 2). After oxidation, nanotubes were sterilised by autoclaving at 121 °C for 1 hour and maintained under sterile conditions for the duration of the experiment.

DWNT at a concentration of 100 µg/mL were mixed with 50 µg/mL of Poly (Lys:Phe) in phosphate buffer (20 mM, pH 7.5), by continuous stirring for 2-hours at room temperature (± 21 °C). To remove excess of unbound molecules, the solution was filtered using a 100 kDa filter devices (Amicon Ultra-4 centrifugal filter devices from Millipore). Next, the CNTs wrapped with Poly (Lys:Phe), (oxDWNT-Poly(Lys:Phe)) were resuspended in DNase /RNase free water (Sigma Aldrich, Poole, UK) to a final concentration of 100 µg/mL of CNTs.

6.2.4 Conjugation with *survivin* siRNA

***Survivin* siRNA:** For siRNA bound through electrostatic interactions, a concentration of 0.8 µM of siRNA was allowed to react with oxDWNT-Poly(Lys:Phe) for 2 hours at room temperature, with continuous stirring. The solutions were again filtered using a 100 kDa filter devices (Amicon Ultra-4 centrifugal filter devices from Millipore) to remove the excess of *survivin* siRNA and then resuspended in DNase /RNase free water (Sigma Aldrich, Poole, UK), with a final concentration 100 µg/mL of CNTs.

Thiol modified *Survivin* siRNA: First a disulfide bond was incorporated; a heterobiofunctional cross-linker (Succinimidyl 6-(3-{2-pyridyldithio}-propionamido) hexanoate) (Sulfo-LC-SPDP, obtained from Pierce/Thermo Fisher Scientific, UK) was employed, for binding to any thiol-containing biomolecule, such as thiol-modified siRNA. 25 µL of Sulfo-LC-SPDP (20 mM) were combined with prepared oxDWNT-Poly(Lys:Phe) diluted 1:1 in PBS (20 mM, pH 7.5) and incubated for 1 hour at room temperature (± 21 °C), with continuous stirring. Excess of cross-linker was removed by filtration using a 100 kDa filter devices (Amicon Ultra-4 centrifugal filter device from Millipore). Next, the thiol modified siRNA (thiol-siRNA) with sequence: 5'-Th CCACUGAGAACGAGCCAGAUU (J-003459-11) was mixed with oxDWNT-

Poly(Lys:Phe)-cross linker and allowed to react for 1 hour at room temperature, with continuous stirring. The solutions were again filtered using a 100 kDa filter device (Amicon Ultra-4 centrifugal filter devices from Millipore) to remove the excess of *survivin* siRNA and then resuspended in DNase /RNase free water (Sigma Aldrich, Poole, UK), with a final concentration 100 µg/mL of CNTs.

6.2.5 *Survivin* knockdown in PC3 cells

To analyse overexpression of *survivin* the following cell lines were employed. As Human prostate cancer models, PC3 (ECACC, Porton Down, Salisbury, UK) and DU145 (ATCC, distributed by LGC Promochem, Teddington, UK) were used. As colon cancer models SW948 and WiDr (ATCC, distributed by LGC Promochem, Teddington, UK) were also used.

24-hours before transfection cells were seeded to allow them to reach 50 % confluency at the time of transfection in 35 mm sterile petri dishes.
CNT-siRNA complexes prepared as previously described (section 6.2.1), were diluted 1:2 in Opti-MEM media (Invitrogen, Paisley, UK). These complexes were then added to each corresponding well, whilst, DharmaFECT-siRNA complexes were prepared according to section 6.2.1 and then pipetted to each well. After 4-hours the media was replaced with fresh completed media (containing serum to give a final concentration of 10 %). The cells were then incubated for a further 72-hours at 37 °C in a CO_2 in order to have a silencing effect. After 72-hours incubation cells were trypsinized and split for either western blotting assay (see section 6.2.4) or for further incubation up to 120-hours. Cells stained with Trypan Blue and counted using an haemocytometer.

6.2.6 Western blotting to confirm *survivin* knockdown

Whole-cell lysates were obtained by trypsinizing the monolayer of adherent cells and washing with PBS at 4°C. Cell pellets were then subjected to osmotic rupture in hypotonic detergent-based buffer (1 mM PMSF, 1 mM $NaVO_4$, 2 µg/mL aprotinin, and 2 µg/mL leupeptin as protease inhibitors, 150 mM NaCl in 50 mM Tris buffer, 0.2 %

SDS, 1% Nonidet P-40, pH 7.5) and 50 µg of protein/sample were then electrophoresed on SDS-polyacrylamide gel electrophoresis gels (Novex system, Invitrogen, UK) with subsequent transfer blotting. Membranes were incubated overnight at 4°C with a primary antibody to *survivin* (Santa Cruz, obtained from Insight Biotechnology, Middlesex, UK). After washing, membranes were incubated with a secondary horseradish peroxidase-linked appropriate species antibody preparation at room temperature (± 21 °C) for 1-hour with chemiluminescence used for visualisation. After the probing of each membrane with the primary antibody of choice, the membrane was stripped and re-probed using a Glyceraldehyde 3-Phosphate Dehydrogenase *GAPDH* antibody (Sigma Aldrich, Poole, UK) to act as a loading control.

6.2.7 Apoptosis detection in PC3 cells treated with siRNA

Cells floating in media and cells in monolayer were recovered and combined for apoptosis assay. Annexin V Biotin Apoptosis Detection Kit (CalBioChem®) was employed according to manufacture. Combined cells were spun down and resuspended in 500 µL of media, then 10 µL media binding reagent was added, followed by 2 µL of Annexin V-FITC and incubated for 30-minutes at room temperature in the dark. Following incubation cells were spun down and resuspended in 500 µL of a cold one time binding buffer. After that, 10 µL propidium iodide was added and samples were placed on ice and away from light, before analysing by flow cytometry. This assay can only be performed on live cells and it is unsuitable for fixed material.

Dr. Helen Coley performed flow cytometry measurements, at the Flow Cytometry and Bioimaging Facilities at University of Surrey, using the Beckman Coulter Epics XL flow cytometer analyser. The measurement permits the determination of the percentage of viable cells, cells in early apoptotic stage, late apoptotic stage and death cells. Data analysis was performed utilizing flowjo software.

6.3 Results and Discussion

In this section the application of CNTs to target tumour cells was studied via delivery of siRNA delivery to target the gene *survivin*. The *survivin* gene was employed owing the differential expression in normal versus tumour cells. In contrast to what was presented in the previous chapter, CNTs-siRNA complexes were prepared via cleavable disulfide bonds, as previously described by Kam *et al.* [174]. This strategy was employed to overcome the possible degradation or loss of siRNA molecules proposed in the previous chapter.

6.3.1 *Survivin* overexpression in different cancer cell lines

Prior to siRNA gene silencing, *survivin* overexpression was examined in different cell lines. Figure 6.2 exhibits western blotting of whole cells lysates from: PC3, WiDr, SW948 and DU145 human cancer cells lines. *Survivin* and *GAPDH* were detected using antibodies specific to the target protein. *GAPDH* is one of the key enzymes involved in glycolysis; it catalyses the reversible oxidative phosphorylation of glyceraldehydes-3-phosphate. The *GAPDH* gene is constitutively and stably expressed at high levels in almost all tissues and cells, and as such is considered to be a "housekeeping" gene. Housekeeping proteins like *GAPDH* are useful as loading controls for western blots. In Figure 6.2, it is demonstrated that both PC3 and SW948 cell lines present higher levels of *survivin* then other two cell lines.

6.3.2 *Survivin* silencing with different siRNA sequences

Various sequences targeting *survivin* gene are available commercially, therefore we decided to examine their silencing effect (Figure 6.3). These siRNA sequences specifically target the baculovirus IAP repeat-containing (BIRC) domain of the *survivin* protein. As presented in Figure 6.3 A, an application of the sequence 8 resulted in poor knockdown effect in PC3 using DarmaFECT as trasfection agent. However, using SW948 cells the silencing effect was efficient with no expression of *survivin* gene protein product evident, after siRNA induced silencing. Silencing effect of sequences 9, 10 and 11 in PC3 are presented in Figure 6.3 B, demonstrating that only sequence 10 and 11 induced knockdown of the *survivin* gene. Thus, sequence 11

(Figure 6.3 C) was selected for further experiments using PC3, with a functional thiol group.

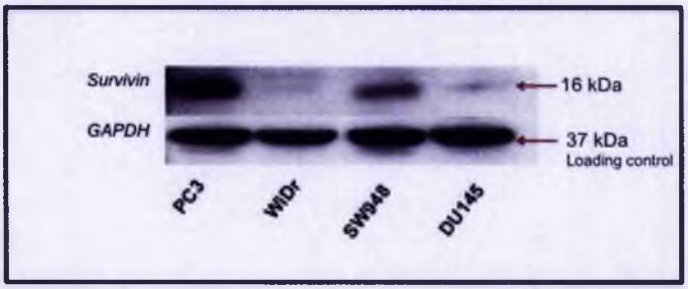

Figure 6.2: Western blotting analysis of *Survivin* overexpression in different cell lines. Expression of *survivin* protein (top) and *GAPDH* (loading control) (bottom) in four different human cancer cells lines: PC3, WiDr, SW948 and DU145. Higher expression of *survivin* protein was obtained for PC3, followed by SW948 cell line with a clear band at 16.5 kDa (*Survivin* molecular weight).

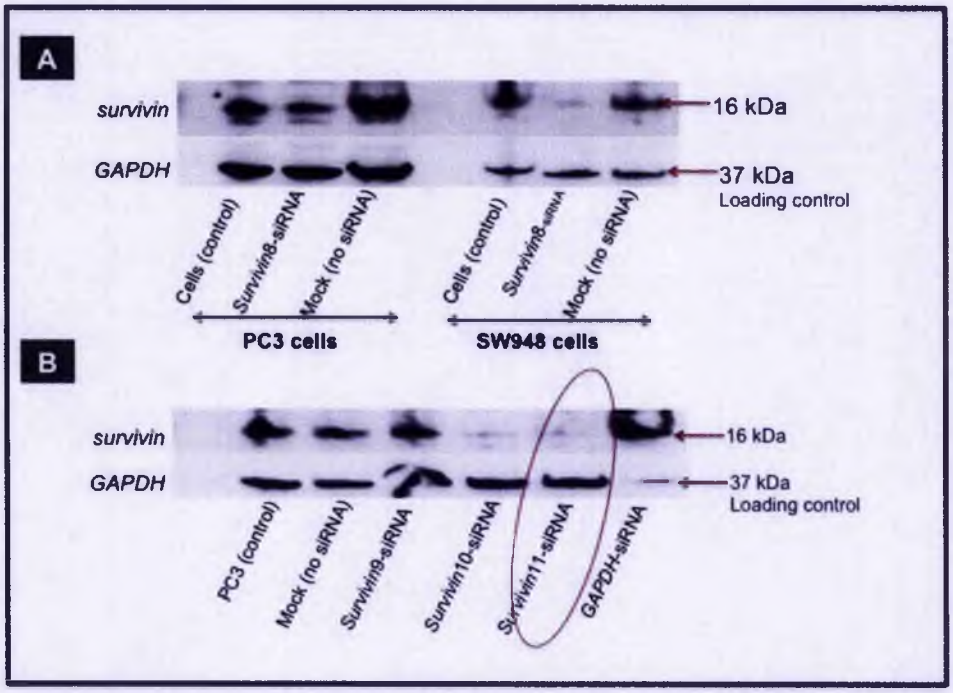

Figure 6.3: *Survivin* siRNAs knockdown effect. Knockdown effect (72-hours after siRNA delivery) of different siRNAs against *survivin*, sequences 8 (A) for PC3 and SW948; and 9, 10 and 11 for PC3 (B) utilising DharmaFECT a transfection reagent. Silencing was evident for sequences 10 and 11. For all samples controls were run in parallel: a control without siRNA; and transfection reagent (DharmaFECT) without siRNA (Mock control). In addition to the primary antibody against *survivin* (16 KDa) but also *GAPDH* (37 KDa) was used as loading control.

6.3.3 *Survivin* silencing using CNTs

An equivalent number of PC3 cells were plated and treated with *survivin* siRNA either delivered through a commercial transfection reagent (DharmaFECT) or CNTs. In the experiments presented, the *survivin* siRNA was attached to CNTs via electrostatic interactions (oxDW-Poly-siRNA) or cleavable disulfide bond (oxDW-Poly-ThiolsiRNA), as described in the methodology.

Table 6.2 presents the number of viable cells after treatment with *survivin* siRNA. It suggests that the transfection reagent was cytotoxic in its own right, since we observed a 4-fold drop in the number of viable cells in the mock control. However when the siRNA was conjugated with the DharmaFECT transfection reagent, there was a decrease of viable cells of 2.3-fold relative to the mock control, suggesting that cells might be dying due to silencing of *survivin* gene, which is entirely plausible given its biological function. siRNA delivered using CNT either via electrostatic interactions or disulfide bond revealed no significant decrease in cell viability (same order of magnitude).

Table 6.2: Viable cells after treatment with *survivin* siRNA. Dead cells were differentiated by staining with trypan blue.

Samples	Viable cells
PC3 control	3.50×10^5
Mock control	0.90×10^5
*Survivin*siRNA (DharmaFECT)	0.40×10^5
oxDW-Poly-siRNA	3.30×10^5
oxDW-Poly-ThiolsiRNA	2.80×10^5

Western blotting of whole cell lysates presented in Figure 6.4 reveals the silencing effect when CNTs were employed. The knockdown effect was very noticeable when DharmaFECT was used to transfect *survivin* siRNA, which lead to complete knockdown of *survivin* gene after only 72 hours. However, for siRNA-CNT complexes little or no silencing effect was apparent. Yet, the *GAPDH* loading controls reveals

that for CNT samples more protein was loaded into the gel in comparison with PC3 control. In addition the band for oxDW-Poly-ThiolsiRNA is weaker than the one observed for oxDW-Poly-siRNA, which suggests that the approach of cleavable disulfide bond increases the efficiency of knockdown. Overall, a low efficiency of silencing was observed when cells were transfected with siRNA-CNT complexes.

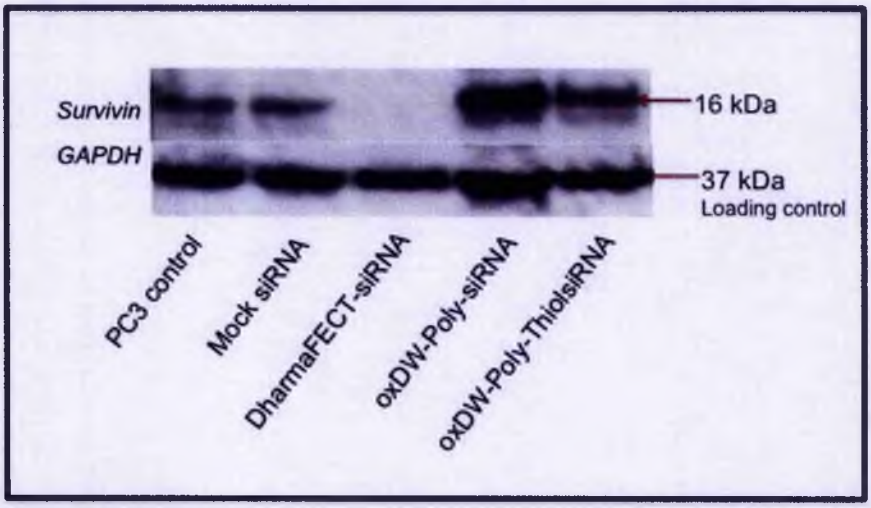

Figure 6.4: *Survivin* knockdown using CNTs. oxDWNT wrapped with Poly(Lys:Phe), and siRNA bound through electrostatic interaction (oxDW-Poly-siRNA) or via disulfide bond (oxDW-Poly-ThiolsiRNA) were employed to evaluate silencing effect of these complexes (72-hours after siRNA delivery). Controls without siRNA, mock control and positive control (DharmaFECT) were also employed. Membranes were re-probed with *GAPDH* (37 KDa) serving as loading control.

6.3.4 Apoptosis detection in PC3 cells treated with *Survivin* siRNA

Apoptosis is a fundamental mode of cell death in health and pathological states and has a regulatory function during normal development, in tissue homeostasis, and in some disease processes. Certain morphologic features are part of the apoptotic pathway, including loss of plasma membrane asymmetry and attachment, condensation of the cytoplasm and nucleus, and internucleosomal cleavage of DNA. Loss of plasma membrane is one of the earliest features. In apoptotic cells, the membrane phospholipid phosphatidylserine (PS) translocates from the inner to the

outer leaflet of the plasma membrane, thereby exposing PS to the external cellular environment. Annexin V is a 35-36 kDa Ca_2^+ dependent phospholipid-binding protein that has a high affinity for PS, and binds to cells with exposed PS. Annexin V may be conjugated to fluorochromes including FITC. This format retains its high affinity for PS and thus serves as a sensitive probe for flow cytometric analysis of cells that are undergoing apoptosis. FITC Annexin V staining precedes the loss of membrane integrity that accompanies the latest stages of cell death resulting from either apoptotic or necrotic processes. Thus, staining with FITC Annexin V is typically used in conjunction with a vital dye such as propidium iodide (PI) allowing identification of early apoptotic cells (PI negative, FITC Annexin V positive). Viable cells with intact membranes exclude PI. In contrast the membranes of dead and damaged cells are permeable to PI. As a result, cells that are considered viable are FITC Annexin V and PI negative; cells that are in early apoptosis are FITC Annexin V positive and PI negative; and cells that are in late apoptosis or already dead are both FITC Annexin V and PI positive. This assay does not distinguish between cells that have undergone late stage apoptotic death *versus* those that have died as a result of a necrotic pathway because in either case, the dead cells will stain with PI. Figure 6.5 presents different distribution of cell populations in the flow cytometry chart, which differs for each sample.

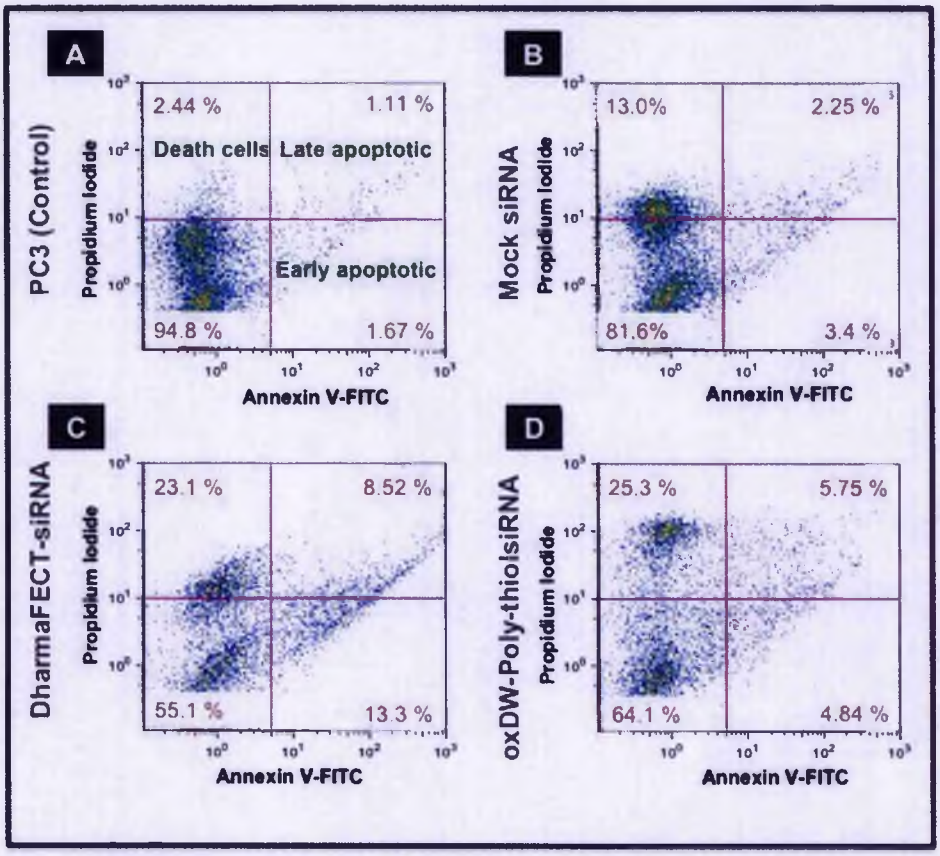

Figure 6.5: Therapeutics of *Survivin* knockdown. Apoptosis measured using an annexin V-FITC apoptosis detection kit, which allows detection of apoptosis by flow cytometry. As displayed in (A) viable cells are FITC negative (bottom left corner), while early apoptotic are FITC positive (bottom right corner). Propidium iodide (PI) was used to distinguish between: death cells, PI positive (top left corner); and late apoptotic or necrotic cells, PI and FITC positive (top right corner). PC3 control (A), transfection reagent without siRNA (Mock siRNA) (B), *survivin* siRNA transfected using Dharmafect (DharmaFECTsiRNA) (C), *survivin* thiol-modified siRNA transfected using oxDWNT-Poly(Lys:Phe) (oxDW-Poly-thiolsiRNA) (D).

To summarise, Figure 6.6 represents a graph showing the percentage of cells *vs* cell samples, at different apoptotic stages. The results obtained demonstrated that control with cells alone (not transfected) presents a high level of viable cells, above 90 %. It could also be seen that oxDW-Poly-siRNA behave very similar to the Mock control suggesting, that the siRNA did not reach their target site and therefore does not cause cells to undergo apoptosis. Similar results were found in the previous chapter (Chapter 5) in which siRNA-CNT complexes were unable to knock down the GFP gene. However, delivery of siRNA attached to CNTs via cleavable disulfide

bond, oxDW-Poly-thiolsiRNA, revealed a decrease in viable cells (64.1% compared to 94.8 in controls) suggesting that siRNA-CNT complexes are capable of silencing the *survivin* gene and thus can cause inhibition of caspases and promote apoptosis in cells.

As illustrated in Figure 6.6 there was an increase in the percentage of cells that were dead or at apoptotic stage: with PC3 control, 5.22 % < oxDW-Poly-siRNA 18.24 % < Mock control 18.64 % < oxDW-Poly-thiolsiRNA 35.89 % < DharmaFECTsiRNA 44.92 %. Therefore, it appears that siRNA-CNT complexes are capable of delivering siRNA to cells and thereby inducing apoptosis. The apparent increase in *survivin* silencing and consequent apoptosis or death, compared to western blot analysis, may be associated with an increase in incubation time. Cells were incubated for 72-hour prior to knockdown evaluation by western blotting, whereas for the apoptosis assay, the incubation lasted 120-hours. Therefore, in order to produce a silencing effect, cells may require longer incubation periods with siRNA-CNTs complexes.

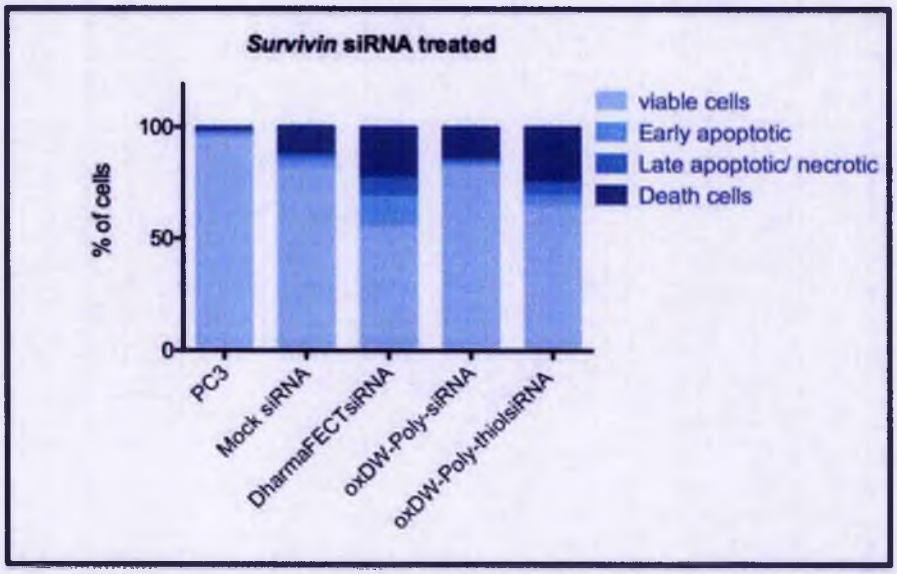

Figure 6.6: Flow cytometry analysis of apoptosis in cells treated with *survivin* siRNA. Percentage of cells *vs* cell samples: PC3 cells; transfection reagent without siRNA (Mock siRNA); *survivin* siRNA transfected using Dharmafect (DharmaFECTsiRNA); *survivin* siRNA transfected using oxDWNT-Poly(Lys:Phe) (oxDW-Poly-siRNA); *survivin* thiol-modified siRNA transfected using oxDWNT-Poly(Lys:Phe) (oxDW-Poly-thiolsiRNA), at different apoptotic stages. Similar apoptotic effect was obtained for thiol modified siRNA-CNT complexes in comparison to positive control (DharmaFECT).

6.4 Conclusions

Survivin function is at the interface between the regulation of apoptosis and the control of cell proliferation. Moreover *survivin* has been described as a molecule that is overexpressed in most human cancers but not in normal tissues. In Figure 6.2 it is evident of the high level of *survivin* expression in prostate and colon cancer cell lines (PC3 and SW948, respectively). Thus, by restoring apoptosis via siRNA targeting with this key anti-apoptotic protein (*survivin*) could have important therapeutic implications. siRNAs are effector molecules that block the synthesis of a protein. These molecules are complementary to sequence on the target mRNA, which drives the assembly of an RNA-protein complex on the target mRNA, preventing it from being translated into a protein. The outcome of silencing by a siRNA targeting *survivin* was illustrated in Figure 6.3, in which a DharmaFECT was employed to deliver different sequences of siRNA. Complete knockdown was obtained for sequence 5'-CCACUGAGAACGAGCCAGAUU -3', which was selected for modification (thiol-group) and attachment to CNTs in the work described.

Recently, CNTs have been tested for siRNA delivery as an alternative to common cationic lipids, known to cause a certain degree of toxicity. Here, we report a CNT-preparation method to improve the efficiency of delivery of siRNA that in comparison with the method employed in the previous chapter differs in the strategy of attachment of siRNA molecule. Therefore, a cleavable disulfide bond approach was adopted to study the ability of CNTs to target cancer. The methodology includes the application of oxidised DWNT wrapped Poly(Lys:phe), followed by siRNA conjugation via a crosslinker to bind thiol-contalning siRNA.

The number of viable cells (Table 6.2) indicated that incubation with CNT induced no significant cell death (PC3 control was $3.5x10^5$ cell/mL whereas, CNTs had 2.8 to $3.3x10^5$ cell/mL viable cells).

Survivin knockdown using siRNA-CNT complexes was evaluated using an immunobloting assay; Figure 6.4 showing western immunoblotting data indicates a poor silencing effect of these complexes post 72-hours incubation. This time frame was considered sufficient to stop the synthesis of *survivin* gene when siRNA transfection was prepared using DharmaFECT transfection reagent. In addition, following this 72-hours period cells were subcultured and incubated for a further 48-

hours. Subsequently, cells were subjected to assessment of apoptosis using an Annexin V-FITC kit and analysed by flow cytometry. The results revealed that in fact, thiol modified siRNA-CNT complexes cause cells to die, possibly through apoptosis. As illustrated oxDW-Poly-thiolsiRNA complexes Figure 6.5 and 6.6 led to 4.84 % of cells at an early apoptotic stage, 5.75 % of cells at late apoptosis and 25.3 % of cells were assessed as in late stage of cell death. However since the percentage of death cells in PC3 control is 3.54 % it may be assume that cells are dying due to an external event, in particular the delivery of siRNA and targeting of *survivin*.

As described in the previous chapter as well as introductory part (section 1.3.3 and 5.4) the delivery of siRNA using carbon nanotubes has been extensively study in the recent years. Apart from the siRNA target, such as the employed in this study the gene *survivin*, another important factor is the CNT preparation. A variety of methods have been employed consisting of non-covalent and covalent modifications of CNT, such as wrapping with phospholipid PEG[174] or amino functionalisation via dipolar cycloaddition [171]. In addition the binding of siRNA can also be perform through electrostatic interactions[171, 353] or via disulfide bonds[174, 175]. The results presented here, revealed an improvement when siRNA was bound through disulfide bonds to oxidised CNT wrapped with a polypeptide. The polypeptide applied (Poly(Lys:Phe)) contains several amino groups and therefore it is able to condensate high number of siRNA molecules. As a result, this new methodology may improve the blood circulation time when used in an *in vivo* system and it would be important to evaluate the efficacy in, i.e., animal model. *Survivin* is a protein that inhibits apoptosis, resulting in uncontrollable proliferation. *Survivin* is highly expressed in many tumours but in normal tissues the protein expression is regulated being often absent or low[348]. Thus, the silencing of *survivin* using CNTs could be used to equilibrate and balance, cell proliferation and apoptosis. By these means cancer cells were able to recognise and undergo programmed cell death.

Chapter 7: Final conclusions and future work

This thesis provides valuable contribution towards the elucidation of the use CNTs (DWNT) as nano-vehicles to treat cancer. The primary aim of this research was to investigate the feasibility of the use of these nanocarries (DWNT) to deliver different nucleic acids inside specific cellular compartments. Thus, the following is a summary of the major findings that were relevant to fulfil this aim.

For the design of a nanotube to treat cancer, it is important to control the size range of the biomolecular entity – CNTs. In the present study, pristine DWNTs were prepared and oxidised in order to obtain an uniform size range, length 200 – 2000 nm and diameter of 0.7 - 2.13 nm. Furthermore, dispersibility and biocompatibility of this nanomaterial is also of particular importance. Herein, CNTs prepared by oxidation were sterilised and wrapped with biomolecules, such as RNA, polyliposome (PL-PEG-NH_2), and polypeptide (Poly(Lys:Phe)), which led to stable solutions (CNTs disperse in aqueous solution for several months).

Findings obtained in the work performed in Chapter 3 revealed that CNTs are taken up and eventually loss by the cells. An earlier report by Jin *et al.* had described exocytosis of CNTs; however, this study established a more innovative description of *in vitro* uptake and release of the CNTs. The results show that CNTs are inside the cells and not at the cell surface, once only cytoplasm was considered in the cell lysate analysis. Furthermore, non-toxicity was observed at a cellular level from both Raman analyses and western blot techniques. The evaluation of DNA/RNA; proteins; and lipids by Raman spectroscopy studies, revealed no differences in these cell components. Moreover, results obtained by western blotting indicated that CNTs do not induce cellular stress (via activation of phosphorylated MAPK). Evidences from these studies highlighted that the CNTs outer walls are being modified during their passage through the cells and that nearly all CNTs are eventually released. Although, degradation of CNTs has already been reported by others [307, 308], additional investigation on the mechanism by which CNTs are being degraded and the process involved would be relevant.

The intracellular localisation of the CNTs after uptake and their trafficking inside the cell was elucidated in Chapter 4. Mechanistically CNT-complexes understudied were

internalised via an energy dependent mechanism. CNTs were sorted in early endosomes (EE), followed by sequestration into lysosomes. Ultimately, CNT-complexes reached the secretory pathway and are recycled back to the plasma membrane.

Results obtained in Chapter 5, demonstrated the ability of CNTs to deliver a cargo inside the cells. Results have shown that binding the cargo (pDNA or siRNA) through electrostatic interactions resulted in inefficient GFP expression as well as knockdown. However, if a disulfide cleavable bond was employed to attach siRNA (Chapter 6), it was possible to perceive an effect, caused by the delivery of siRNA through CNT-complexes.

Chapter 6 further describes the effects of silencing of the *survivin* gene. Current cancer therapy involves high-level toxicity and is relatively poorly targeted. Yet, much has been done to identify new tumour-specific targets, as well as innovative drug delivery systems. An example of a tumour-specific target is the interference with cancer (causing) genes; such as *survivin* gene. The overall the results obtain in our studies show an increase in apoptotic cells. Even though, these results were unable to confirm a decrease in protein levels by immunoblotting. We found subsequently that siRNA-CNT complexes required longer incubation periods in order to be efficient, compared with conventional transfection agents. These promising results reveal that CNTs are indeed able to deliver cargoes into cancer cells. Thus, these findings suggested the potential capabilities of these nanomaterials to various biomedical applications.

It has been particular evident that additional studies may be required in order to further identify the therapeutic efficiency of these nanomaterials. The following paragraphs elaborate on some of the main suggestions that can be considered.

Future work, would involve the translation from the *in vitro* model to an *in vivo* system. It would be certainly imperative to understand how the same system, i.e. degradation of CNT, has the same behave *in vivo*, alongside with their biodistribution.

In our studies we employed DWNT, this nanomaterial owns advantages in comparison to SWNT and MWNT. Specifically, DWNT have smaller diameters than MWNT, and in contrast to SWNT their outer wall can be modified without loosing the physical and mechanical properties of CNTs that are maintained by the inner wall. In addition, DWNT benefits from their Raman spectroscopic features, by which it is

possible to determine changes in the outer wall by analysis of diameters via RBM modes.

Besides due to CNT preparations (that contain free carboxylic acid groups) further modification is possible through covalent attachment of cargoes. For example anti-cancer agents, targeting moieties and imaging molecules could be inserted. Therefore, the synergistic effect of combining siRNA silencing with an anti-cancer drug could be examined, in addition to specific targeting of cell receptors via application of antibodies/peptides onto the surface of CNTs.

Finally, for an intensive analysis of the uptake mechanism of CNTs, the study should be carried out in live cells. By GFP-tagging resident components of a compartment would allow imaging of the morphology and dynamics of these compartments in real-time. Additionally complementary studies using TEM would be relevant to identify other pathways of internalisation, as described by Mu *et al.* [325], in which not only it was observed that an endocytic pathway but also that CNTs can pierce cell membranes to gain direct access to the cytoplasm.

References

1. Ferrari, M., *Cancer nanotechnology: opportunities and challenges.* Nat Rev Cancer, 2005. **5**: p. 161-71.
2. Farokhzad, O.C. and R. Langer, *Nanomedicine: developing smarter therapeutic and diagnostic modalities.* Adv Drug Deliv Rev, 2006. **58**(14): p. 1456-9.
3. Liu, Y., H. Miyoshi, and M. Nakamura, *Nanomedicine for drug delivery and imaging: a promising avenue for cancer therapy and diagnosis using targeted functional nanoparticles.* Int J Cancer, 2007. **120**(12): p. 2527-37.
4. Brannon-Peppas, L. and J.O. Blanchette, *Nanoparticle and targeted systems for cancer therapy.* Adv Drug Deliv Rev, 2004. **56**(11): p. 1649-59.
5. Kawasaki, E.S. and A. Player, *Nanotechnology, nanomedicine, and the development of new, effective therapies for cancer.* Nanomedicine, 2005. **1**(2): p. 101-9.
6. McNeil, S.E., *Nanotechnology for the biologist.* J Leukoc Biol, 2005. **78**(3): p. 585-94.
7. Zhang, L., et al., *Nanoparticles in medicine: therapeutic applications and developments.* Clin Pharmacol Ther, 2008. **83**(5): p. 761-9.
8. James, N.D., et al., *Liposomal doxorubicin (Doxil): an effective new treatment for Kaposi's sarcoma in AIDS.* Clin Oncol, 1994. **6**(5): p. 294-6.
9. Muggia, F.M., *Doxil in breast cancer.* J Clin Oncol, 1998. **16**(2): p. 811-2.
10. Schluep, T., et al., *Preclinical efficacy of the camptothecin-polymer conjugate IT-101 in multiple cancer models.* Clin Cancer Res, 2006. **12**(5): p. 1606-14.
11. Kircher, M.F., et al., *A multimodal nanoparticle for preoperative magnetic resonance imaging and intraoperative optical brain tumor delineation.* Cancer Res, 2003. **63**(23): p. 8122-5.
12. Neuwelt, E.A., et al., *Imaging of iron oxide nanoparticles by MR and light microscopy in patients with malignant brain tumours.* Neuropathol Appl Neurobiol, 2004. **30**(5): p. 456-71.
13. Oyewumi, M.O., et al., *Comparison of cell uptake, biodistribution and tumor retention of folate-coated and PEG-coated gadolinium nanoparticles in tumor-bearing mice.* J Control Release, 2004. **95**(3): p. 613-26.
14. Schellenberger, E.A., et al., *Annexin V-CLIO: a nanoparticle for detecting apoptosis by MRI.* Mol Imaging, 2002. **1**(2): p. 102-7.
15. Harisinghani, M.G., et al., *Noninvasive detection of clinically occult lymph-node metastases in prostate cancer.* The New England Journal of Medicine, 2003. **348**(25): p. 2491-9.
16. Winter, P.M., et al., *Molecular imaging of angiogenesis in early-stage atherosclerosis with alpha(v)beta3-integrin-targeted nanoparticles.* Circulation, 2003. **108**(18): p. 2270-4.
17. Perez, J.M., et al., *Viral-induced self-assembly of magnetic nanoparticles allows the detection of viral particles in biological media.* J Am Chem Soc, 2003. **125**(34): p. 10192-3.
18. Zhang, Y., et al., *Self-assembled coatings on individual monodisperse magnetite nanoparticles for efficient intracellular uptake.* Biomed Microdevices, 2004. **6**(1): p. 33-40.

19. Yan, F., et al., *Synthesis and characterization of silica-embedded iron oxide nanoparticles for magnetic resonance imaging.* J Nanosci Nanotechnol, 2004. **4**(1-2): p. 72-6.
20. Levy, L., et al., *Nanochemistry: Synthesis and Characterization of Multifunctional Nanoclinics for Biological Applications.* Chem. Mater., 2002. **14** (9): p. 3715–21.
21. May, D.J., J.S. Allen, and K.W. Ferrara, *Dynamics and fragmentation of thick-shelled microbubbles.* IEEE Trans Ultrason Ferroelectr Freq Control, 2002. **49**(10): p. 1400-10.
22. Bloch, S.H., P.A. Dayton, and K.W. Ferrara, *Targeted imaging using ultrasound contrast agents. Progess and opportunities for clinical and research applications.* IEEE Eng Med Biol Mag, 2004. **23**(5): p. 18-29.
23. Duncan, R., *The dawning era of polymer therapeutics.* Nat Rev Drug Discov, 2003. **2**(5): p. 347-60.
24. Gillies, E.R. and J.M. Frechet, *Designing macromolecules for therapeutic applications: polyester dendrimer-poly(ethylene oxide) "bow-tie" hybrids with tunable molecular weight and architecture.* J Am Chem Soc, 2002. **124**(47): p. 14137-46.
25. Cohen, M.H., et al., *Microfabrication of silicon-based nanoporous particulates for medical applications.* Biomed Microdevices, 2004. **5**(3): p. 253-9.
26. He, X.X., et al., *Bioconjugated nanoparticles for DNA protection from cleavage.* J Am Chem Soc, 2003. **125**(24): p. 7168-9.
27. Li, X., et al., *Porosified silicon wafer structures impregnated with platinum anti-tumor compounds: fabrication, characterization, and diffusion studies.* Biomed Microdevices, 2000. **2**(4): p. 265-72.
28. Hirsch, L.R., et al., *Nanoshell-mediated near-infrared thermal therapy of tumors under magnetic resonance guidance.* Proc Natl Acad Sci U S A, 2003. **100**(23): p. 13549-54.
29. Iijima, S., *Carbon nanotubes: past, present, and future.* Physica B: Condensed Matter, 2002. **323**(1-4): p. 1-5.
30. Peer, D., et al., *Nanocarriers as an emerging platform for cancer therapy.* Nat Nano, 2007. **2**(12): p. 751-60.
31. Lodish, H.B., A.; Zipursky, S. L.; Matsudaira, P.; Balimore, D.; Darnell, J. , *Molecular Cell Biology*. 2000, New York: W. H. Freeman and Company.
32. Atkins, J.H. and L.J. Gershell, *Selective anticancer drugs.* Nat Rev Drug Discov, 2002. **1**(7): p. 491-2.
33. Huang, P.S. and A. Oliff, *Drug-targeting strategies in cancer therapy.* Curr Opin Genet Dev, 2001. **11**(1): p. 104-10.
34. Moses, M.A., H. Brem, and R. Langer, *Advancing the field of drug delivery: taking aim at cancer.* Cancer Cell, 2003. **4**(5): p. 337-41.
35. Jain, R.K., *Delivery of molecular and cellular medicine to solid tumors.* Adv Drug Deliv Rev 2001. **46**(1-3): p. 149-68.
36. Yuan, F., M. Dellian, and D. Fukumura, *Vascular permeability in human tumor xenograft: Molecular size dependence and cutoff size.* Cancer Res, 1995. **55**(17): p. 3752-6.
37. Couvreur, P. and C. Vauthier, *Nanotechnology: intelligent design to treat complex disease.* Pharm Res, 2006. **23**(7): p. 1417-50.
38. Torchilin, V.P., *Recent advances with liposomes as pharmaceutical carriers.* Nat Rev Drug Discov, 2005. **4**(2): p. 145-60.
39. Hobbs, S.K., et al., *Regulation of transport pathways in tumor vessels: role of tumor type and microenvironment.* Proc Natl Acad Sci U S A, 1998. **95**(8): p. 4607-12.

40. Jain, R.K., *Transport of molecules in the tumor interstitium: a review.* Cancer Res, 1987. **47**(12): p. 3039-51.
41. Maeda, H., et al., *Tumor vascular permeability and the EPR effect in macromolecular therapeutics: a review.* J Control Release, 2000. **65**(1-2): p. 271-84.
42. Kirpotin, D.B., et al., *Antibody targeting of long-circulating lipidic nanoparticles does not increase tumor localization but does increase internalization in animal models.* Cancer Res, 2006. **66**(13): p. 6732-40.
43. Farokhzad, O.C., et al., *Nanoparticle-aptamer bioconjugates: a new approach for targeting prostate cancer cells.* Cancer Res, 2004. **64**(21): p. 7668-72.
44. Farokhzad, O.C., et al., *Targeted nanoparticle-aptamer bioconjugates for cancer chemotherapy in vivo.* Proc Natl Acad Sci U S A, 2006. **103**(16): p. 6315-20.
45. Chiu, S.J., N.T. Ueno, and R.J. Lee, *Tumor-targeted gene delivery via anti-HER2 antibody (trastuzumab, Herceptin) conjugated polyethylenimine.* J Control Release, 2004. **97**(2): p. 357-69.
46. Cheng, J., et al., *Formulation of functionalized PLGA-PEG nanoparticles for in vivo targeted drug delivery.* Biomaterials, 2007. **28**(5): p. 869-76.
47. Bagalkot, V., et al., *An aptamer-doxorubicin physical conjugate as a novel targeted drug-delivery platform.* Angew Chem Int Ed Engl, 2006. **45**(48): p. 8149-52.
48. Arencibia, J.M., et al., *Targeting of doxorubicin to ES-2 human ovarian cancers in nude mice by linking to an analog of luteinizing hormone-releasing hormone improves its effectiveness.* Int J Oncol, 2001. **19**(3): p. 571-7.
49. Kurreck, J., *Antisense technologies. Improvement through novel chemical modifications.* Eur J Biochem, 2003. **270**(8): p. 1628-44.
50. Doudna, J.A. and T.R. Cech, *The chemical repertoire of natural ribozymes.* Nature, 2002. **418**(6894): p. 222-8.
51. Miyagishi, M., M. Hayashi, and K. Taira, *Comparison of the suppressive effects of antisense oligonucleotides and siRNAs directed against the same targets in mammalian cells.* Antisense Nucleic Acid Drug Dev, 2003. **13**(1): p. 1-7.
52. Kretschmer-Kazemi Far, R. and G. Sczakiel, *The activity of siRNA in mammalian cells is related to structural target accessibility: a comparison with antisense oligonucleotides.* Nucleic Acids Res, 2003. **31**(15): p. 4417-24.
53. Grunweller, A., et al., *Comparison of different antisense strategies in mammalian cells using locked nucleic acids, 2'-O-methyl RNA, phosphorothioates and small interfering RNA.* Nucleic Acids Res, 2003. **31**(12): p. 3185-93.
54. Juliano, R., et al., *Mechanisms and strategies for effective delivery of antisense and siRNA oligonucleotides.* Nucleic Acids Res, 2008. **36**(12): p. 4158-71.
55. Cheunga, W., Pontorieroa, F., Taratulaa, O., Chena, A. M., He, H., *DNA and carbon nanotubes as medicine.* Adv Drug Deliv Rev, 2010. **62**(6): p. 633-49.
56. Dykxhoorn, D.M. and J. Lieberman, *The silent revolution: RNA interference as basic biology, research tool, and therapeutic.* Annu Rev Med, 2005. **56**(1): p. 401-23.
57. de Fougerolles, A., et al., *Interfering with disease: a progress report on siRNA-based therapeutics.* Nat Rev Drug Discov, 2007. **6**(6): p. 443-53.
58. Fire, A., et al., *Potent and specific genetic interference by double-stranded RNA in Caenorhabditis elegans.* Nature, 1998. **391**(6669): p. 806-11.
59. Elbashir, S.M., et al., *Duplexes of 21-nucleotide RNAs mediate RNA interference in cultured mammalian cells.* Nature, 2001. **411**(6836): p. 494-8.
60. Hutvagner, G. and P.D. Zamore, *A microRNA in a multiple-turnover RNAi enzyme complex.* Science, 2002. **297**(5589): p. 2056-60.
61. Grimm, D., et al., *Fatality in mice due to oversaturation of cellular microRNA/short hairpin RNA pathways.* Nature, 2006. **441**(7092): p. 537-41.

62. Stark, G.R., et al., *How cells respond to interferons.* Annu Rev Biochem, 1998. **67**: p. 227-64.
63. Pei, Y. and T. Tuschl, *On the art of identifying effective and specific siRNAs.* Nat Methods, 2006. **3**(9): p. 670-6.
64. Reynolds, A., et al., *Rational siRNA design for RNA interference.* Nat Biotechnol, 2004. **22**(3): p. 326-30.
65. Kim, D.H., et al., *Synthetic dsRNA Dicer substrates enhance RNAi potency and efficacy.* Nat Biotechnol, 2005. **23**(2): p. 222-6.
66. Reynolds, A., et al., *Induction of the interferon response by siRNA is cell type- and duplex length-dependent.* RNA, 2006. **12**(6): p. 988-93.
67. Schwarz, D.S., et al., *Asymmetry in the assembly of the RNAi enzyme complex.* Cell, 2003. **115**(2): p. 199-208.
68. Khvorova, A., A. Reynolds, and S.D. Jayasena, *Functional siRNAs and miRNAs exhibit strand bias.* Cell, 2003. **115**(2): p. 209-16.
69. Whitehead, K.A., R. Langer, and D.G. Anderson, *Knocking down barriers: advances in siRNA delivery.* Nat Rev Drug Discov, 2009. **8**(2): p. 129-38.
70. Gartel, A.L. and E.S. Kandel, *RNA interference in cancer.* Biomol Eng., 2006. **23**(1): p. 17-34.
71. Fu, G.F., et al., *RNA interference remarkably suppresses bcl-2 gene expression in cancer cells in vitro and in vivo.* Cancer Biol Ther, 2005. **4**(8): p. 822-9.
72. Kim, P.J., et al., *Survivin and molecular pathogenesis of colorectal cancer.* The Lancet, 2003. **362**(9379): p. 205-209.
73. Ling, X. and F. Li, *Silencing of antiapoptotic survivin gene by multiple approaches of RNA interference technology.* Biotechniques, 2004. **36**(3): p. 450-4, 456-60.
74. Wang, Y., et al., *Downregulation of survivin by RNAi inhibits the growth of esophageal carcinoma cells.* Cancer Biol Ther, 2005. **4**(9): p. 974-8.
75. Kappler, M., et al., *Knockdown of survivin expression by small interfering RNA reduces the clonogenic survival of human sarcoma cell lines independently of p53.* Cancer Gene Ther, 2004. **11**(3): p. 186-93.
76. Krysan, K., et al., *Cyclooxygenase 2-dependent expression of survivin is critical for apoptosis resistance in non-small cell lung cancer.* Cancer Res, 2004. **64**(18): p. 6359-62.
77. Inoue, T., et al., *Modulation of scratching behavior by silencing an endogenous cyclooxygenase-1 gene in the skin through the administration of siRNA.* J Gene Med, 2007. **9**(11): p. 994-1001.
78. Fattal, E. and A. Bochot, *Ocular delivery of nucleic acids: antisense oligonucleotides, aptamers and siRNA.* Adv Drug Deliv Rev, 2006. **58**(11): p. 1203-23.
79. Palliser, D., et al., *An siRNA-based microbicide protects mice from lethal herpes simplex virus 2 infection.* Nature, 2006. **439**(7072): p. 89-94.
80. Grzelinski, M., et al., *RNA interference-mediated gene silencing of pleiotrophin through polyethylenimine-complexed small interfering RNAs in vivo exerts antitumoral effects in glioblastoma xenografts.* Hum Gene Ther, 2006. **17**(7): p. 751-66.
81. Kim, D.H. and J.J. Rossi, *Strategies for silencing human disease using RNA interference.* Nat Rev Genet, 2007. **8**(3): p. 173-84.
82. Sanhai, W.R., et al., *Seven challenges for nanomedicine.* Nat Nanotechnol, 2008. **3**(5): p. 242-44.
83. Tasciotti, E., et al., *Mesoporous silicon particles as a multistage delivery system for imaging and therapeutic applications.* Nat Nanotechnol, 2008. **3**(3): p. 151-7.
84. Ferrari, M., *The mathematical engines of nanomedicine.* Small, 2008. **4**(1): p. 20-5.

85. Vinogradov, S.V., E.V. Batrakova, and A.V. Kabanov, *Nanogels for oligonucleotide delivery to the brain.* Bioconjug Chem, 2004. **15**(1): p. 50-60.
86. Lockman, P.R., et al., *Brain uptake of thiamine-coated nanoparticles.* J Control Release, 2003. **93**(3): p. 271-82.
87. Steiniger, S.C., et al., *Chemotherapy of glioblastoma in rats using doxorubicin-loaded nanoparticles.* Int J Cancer, 2004. **109**(5): p. 759-67.
88. Kreuter, J., *Influence of the surface properties on nanoparticle-mediated transport of drugs to the brain.* J Nanosci Nanotechnol, 2004. **4**(5): p. 484-8.
89. Russell-Jones, G.J., L. Arthur, and H. Walker, *Vitamin B12-mediated transport of nanoparticles across Caco-2 cells.* Int J Pharm, 1999. **179**(2): p. 247-55.
90. Chen, L.T. and L. Weiss, *The role of the sinus wall in the passage of erythrocytes through the spleen.* Blood, 1973. **41**(4): p. 529-37.
91. Braet, F., et al., *Structure and dynamics of the fenestrea-associated cytoskeleton of rat liver sinusoidal endothelial cells.* Hepatology, 1995. **21**(1): p. 180-9.
92. Bogunia-Kubik, K. and M. Sugisaka, *From molecular biology to nanotechnology and nanomedicine.* Biosystems, 2002. **65**(2-3): p. 123-38.
93. Harris, J.M. and R.B. Chess, *Effect of pegylation on pharmaceuticals.* Nat Rev Drug Discov, 2003. **2**(3): p. 214-21.
94. Gao, X., et al., *In vivo cancer targeting and imaging with semiconductor quantum dots.* Nat Biotechnol, 2004. **22**(8): p. 969-76.
95. Campbell, R.B., S.V. Balasubramanian, and R.M. Straubinger, *Influence of cationic lipids on the stability and membrane properties of paclitaxel-containing liposomes.* J Pharm Sci, 2001. **90**(8): p. 1091-105.
96. Brigger, I., C. Dubernet, and P. Couvreur, *Nanoparticles in cancer therapy and diagnosis.* Adv Drug Deliv Rev, 2002. **54**(5): p. 631-51.
97. Moghimi, S.M. and J. Szebeni, *Stealth liposomes and long circulating nanoparticles: critical issues in pharmacokinetics, opsonization and protein-binding properties.* Prog Lipid Res, 2003. **42**(6): p. 463-78.
98. Pridgen, E.M., R. Langer, and O.C. Farokhzad, *Biodegradable, polymeric nanoparticle delivery systems for cancer therapy.* Nanomed, 2007. **2**(5): p. 669-80.
99. Romberg, B., W.E. Hennink, and G. Storm, *Sheddable coatings for long-circulating nanoparticles.* Pharm Res, 2008. **25**(1): p. 55-71.
100. Moghimi, S.M., A.C. Hunter, and J.C. Murray, *Long-circulating and target-specific nanoparticles: theory to practice.* Pharmacol Rev, 2001. **53**(2): p. 283-318.
101. Owens, D.E., 3rd and N.A. Peppas, *Opsonization, biodistribution, and pharmacokinetics of polymeric nanoparticles.* International Journal of Pharmaceutics, 2006. **307**(1): p. 93-102.
102. Simionescu, M., N. Simionescu, and G.E. Palade, *Morphometric data on the endothelium of blood capillaries.* J Cell Biol, 1974. **60**(1): p. 128-52.
103. Brigham, K.L., *Estimations of permeability properties of pulmonary capillaries (continuous endothelium).* Physiologist, 1980. **23**(1): p. 44-6.
104. Ryan, U.S., et al., *Fenestrated endothelium of the adrenal gland: freeze-fracture studies.* Tissue Cell, 1975. **7**(1): p. 181-90.
105. Braet, F., et al., *Contribution of high-resolution correlative imaging techniques in the study of the liver sieve in three-dimensions.* Microsc Res Tech, 2007. **70**(3): p. 230-42.
106. Maeda, H., *The enhanced permeability and retention (EPR) effect in tumor vasculature: the key role of tumor-selective macromolecular drug targeting.* Adv Enzyme Regul, 2001. **41**: p. 189-207.

107. Greish, K., *Enhanced permeability and retention of macromolecular drugs in solid tumors: a royal gate for targeted anticancer nanomedicines.* J Drug Target, 2007. **15**(7-8): p. 457-64.
108. O'Connell, M., *Carbon nanotubes: properties and applications*. 2006, Eikos, Franklin, MA CRC
109. Kroto, H.W., et al., *C60 Buckminsterfullerene.* Nature, 1985. **318**: p. 162-3.
110. Yakobson, B.I., Avouris, P., *Mechnical properties of carbon nanotubes.* Topics in Applied physics 2001: Springer 40.
111. Odom, T.W., et al., *Structure and electronic properties of carbon nanotubes.* J. Phys. Chem. B, 2000. **104**(13): p. 2794-809.
112. Dresselhaus, M.S.D., G.; Eklund, P. C. , *Science of Fullerenes and Carbon Nanotubes.* 1996, New York, NY, San Diego, CA Academic Press.
113. Liu, J., et al., *Fullerene pipes.* Science, 1998. **280**(5367): p. 1253-56.
114. Chen, R.J., et al., *Noncovalent functionalization of carbon nanotubes for highly specific electronic biosensors.* Proc Natl Acad Sci U S A, 2003. **100**(9): p. 4984-89.
115. Kam, N.W.S., et al., *Nanotube molecular transporters: Internalization of carbon nanotube-protein conjugates into mammalian cells.* J Am Chem Soc, 2004. **126**(22): p. 6850-51.
116. Bianco, A., et al., *Biomedical applications of functionalised carbon nanotubes.* Chem Commun (Camb), 2005(5): p. 571-7.
117. Cherukuri, P., et al., *Near-infrared fluorescence microscopy of single-walled carbon nanotubes in phagocytic cells.* J Am Chem Soc, 2004. **126**(48): p. 15638-39.
118. Liu, Z., et al., *Carbon nanotubes in biology and medicine: in vitro and in vivo detection, imaging and drug delivery.* Nano Res, 2009. **2**(2): p. 85-120.
119. Liu, Z., et al., *Supramolecular chemistry on water-soluble carbon nanotubes for drug loading and delivery.* Acs Nano, 2007. **1**(1): p. 50-6.
120. Tans, S.J., Devoret, M. H., Dai, H. J., Thess, A., Smalley, R. E., Geerligs, L. J., Dekker, C., *Individual single-walled carbon nanotubes as quantum wires.* Nature, 1997. **386**: p. 474-7.
121. Kam, N.W.S., et al., *Carbon nanotubes as multifunctional biological transporters and near-infrared agents for selective cancer cell destruction.* Proc Natl Acad Sci U S A, 2005. **102**(33): p. 11600-5.
122. O'Connell, M.J., et al., *Band gap fluorescence from individual single-walled carbon nanotubes.* Science, 2002. **297**(5581): p. 593-6.
123. Welsher, K., et al., *Selective probing and imaging of cells with single walled carbon nanotubes as near-infrared fluorescent molecules.* Nano Lett, 2008. **8**(2): p. 586-90.
124. Heller, D.A., et al., *Single-walled carbon nanotube spectroscopy in live cells: Towards long-term labels and optical sensors.* Advance Materials, 2005. **17**(23): p. 2793 - 9.
125. Rao, A.M., et al., *Diameter-Selective Raman Scattering from Vibrational Modes in Carbon Nanotubes.* Science, 1997. **275**(5297): p. 187-91.
126. Pantarotto, D., et al., *Translocation of bioactive peptides across cell membranes by carbon nanotubes.* Chem Commun (Camb), 2004(1): p. 16-17.
127. Pantarotto, D., et al., *Functionalized carbon nanotubes for plasmid DNA gene delivery.* Angew Chem Int Ed Engl., 2004. **43**(39): p. 5242 - 6.
128. Kostarelos, K., et al., *Cellular uptake of functionalized carbon nanotubes is independent of functional group and cell type.* Nat Nanotechnol, 2007. **2**(2): p. 108-13.
129. Lopez, C.F., et al., *Understanding nature's design for a nanosyringe.* Proc Natl Acad Sci U S A, 2004. **101**(13): p. 4431-4.

130. Lacerda, L.R., S.; Prato, M.; Bianco, A.; Kostarelos, K., *Cell-penetrating CNTs for delivery of therapeutics.* NanoToday, 2007. **2**(6): p. 38-43.
131. Kam, N.W.S. and H.J. Dai, *Carbon nanotubes as intracellular protein transporters: Generality and biological functionality.* J Am Chem Soc, 2005. **127**(16): p. 6021-26.
132. Kam, N.W.S., Z.A. Liu, and H.J. Dai, *Carbon nanotubes as intracellular transporters for proteins and DNA: An investigation of the uptake mechanism and pathway.* Angew Chem Int Ed Engl., 2006. **45**(4): p. 577-81.
133. Meinke, M., et al., *Chemometric determination of blood parameters using visible-near-infrared spectra.* Applied Spectroscopy, 2005. **59**(6): p. 826-35.
134. Becker, M.L., et al., *Length-dependent uptake of DNA-wrapped single-walled carbon nanotubes.* Adv Materials, 2007. **19**(7): p. 939-45.
135. Jorio, A., et al., *Structural (n, m) determination of isolated single-wall carbon nanotubes by resonant Raman scattering.* Phys Rev Lett, 2001. **86**(6): p. 1118-21.
136. Saito, R.D., G.; Dresselhaus, M. S., *Physical Properties of Carbon Nanotubes* 1998, London: Imperial College Press
137. Strano, M.S., et al., *Assignment of (n, m) Raman and optical features of metallic single-walled carbon nanotubes.* Nano Lett., 2003. **3**(8): p. 1091-6.
138. Doorn, S.K., et al., *Resonant Raman excitation profiles of individually dispersed single walled carbon nanotubes in solution.* Appl. Phys. A, 2004. **78**(8): p. 1147-55.
139. Chin, S.F., et al., *Amphiphilic helical peptide enhances the uptake of single-walled carbon nanotubes by living cells.* Exp Biol Med, 2007. **232**(9): p. 1236-44.
140. Yehia, H., et al., *Single-walled carbon nanotube interactions with HeLa cells.* J Nanobiotechnology, 2007. **5**(8): p. 3155-63.
141. Lamprecht, C., et al., *AFM imaging of functionalized carbon nanotubes on biological membranes.* Nanotechnology, 2009. **20**(43): p. 434001-7.
142. Jin, H., D.A. Heller, and M.S. Strano, *Single-particle tracking of endocytosis and exocytosis of single-walled carbon nanotubes in NIH-3T3 cells.* Nano Lett., 2008. **8**(6): p. 1577-85.
143. Chithrani, B.D. and W.C.W. Chan, *Elucidating the mechanism of cellular uptake and removal of protein-coated gold nanoparticles of different sizes and shapes.* Nano Letters, 2007. **7**(6): p. 1542-50.
144. Jin, H., et al., *Size-dependent cellular uptake and expulsion of single-walled carbon nanotubes: single particle tracking and a generic uptake model for nanoparticles.* Acs Nano, 2009. **3**(1): p. 149-58.
145. Lacerda, L., et al., *Intracellular trafficking of carbon nanotubes by confocal laser scanning microscopy.* Adv Materials, 2007. **19**(11): p. 1780-84.
146. Singh, R., et al., *Tissue biodistribution and blood clearance rates of intravenously administered carbon nanotube radiotracers.* Proc Natl Acad Sci U S A, 2006. **103**(9): p. 3357 - 62.
147. Maynard, A.D., et al., *Exposure to carbon nanotube material: aerosol release during the handling of unrefined single-walled carbon nanotube material.* J Toxicol Environ Health A, 2004. **67**(1): p. 87-107.
148. Huczko, A., et al., *Combustion synthesis as a novel method for production of 1-D SiC nanostructures.* J Phys Chem B, 2005. **109**(34): p. 16244-51.
149. Lam, C.W., et al., *Pulmonary toxicity of single-wall carbon nanotubes in mice 7 and 90 days after Intratracheal instillation.* Toxicol Sci. , 2004. **77**(1): p. 126-34.
150. Warheit, D.B., et al., *Comparative pulmonary toxicity assessment of single-wall carbon nanotubes in rats.* Toxicol Sci. , 2004. **77**(1): p. 117 - 25.
151. Shvedova, A.A., et al., *Unusual inflammatory and fibrogenic pulmonary responses to single-walled carbon nanotubes in mice.* Am J Physiol Lung Cell Mol Physiol, 2005. **289**(5): p. L698-708.

152. Yokoyama, A., et al., *Biological behavior of hat-stacked carbon nanofibers in the subcutaneous tissue in rats.* Nano Lett, 2005. **5**(1): p. 157-61.
153. Sato, Y., et al., *Influence of length on cytotoxicity of multi-walled carbon nanotubes against human acute monocytic leukemia cell line THP-1 in vitro and subcutaneous tissue of rats in vivo.* Mol Biosyst, 2005. **1**(2): p. 176-82.
154. Christie M. Sayes, John D. Fortner,, Wenh Guo,, Delina Lyon,, Adina M. Boyd,, Kevin D. Ausman,, Yizhi J. Tao,,, Balaji Sitharaman,, Lon J. Wilson,,, Joseph B. Hughes,, Jennifer L. West,, and, Vicki L. Colvin, , *The Differential Cytotoxicity of Water-Soluble Fullerenes.* Nano Letters 2004 **4** ((10)): p. 1881-1887.
155. Sayes, C.M., et al., *Functionalization density dependence of single-walled carbon nanotubes cytotoxicity in vitro.* Toxicol Lett, 2006. **161**(2): p. 135-42.
156. Wang, H., et al., *Biodistribution of carbon single-wall carbon nanotubes in mice.* J Nanosci Nanotechnol, 2004. **4**(8): p. 1019-24.
157. Lacerda, L., et al., *Dynamic Imaging of functionalized multi-walled carbon nanotube systemic circulation and urinary excretion.* Adv Materials, 2008. **20**(2): p. 225-30.
158. Lacerda, L., et al., *Carbon-nanotube shape and individualization critical for renal excretion.* Small, 2008. **4**(8): p. 1130-2.
159. Lacerda, L., et al., *Tissue histology and physiology following intravenous administration of different types of functionalized multiwalled carbon nanotubes.* Nanomed, 2008. **3**(2): p. 149-61.
160. Cherukuri, P., et al., *Mammalian pharmacokinetics of carbon nanotubes using intrinsic near-infrared fluorescence.* Proc Natl Acad Sci U S A, 2006. **103**(50): p. 18882-6.
161. Liu, Z., et al., *In vivo biodistribution and highly efficient tumour targeting of carbon nanotubes in mice.* Nat Nanotechnol, 2007. **2**(1): p. 47-52.
162. Zavaleta, C., et al., *Noninvasive Raman spectroscopy in living mice for evaluation of tumor targeting with carbon nanotubes.* Nano Lett, 2008. **8**(9): p. 2800-5.
163. Liu, Z., et al., *Circulation and long-term fate of functionalized, biocompatible single-walled carbon nanotubes in mice probed by Raman spectroscopy.* Proc Natl Acad Sci U S A, 2008. **105**(5): p. 1410-5.
164. Georgakilas, V., et al., *Purification of HiPCO carbon nanotubes via organic functionalization.* J Am Chem Soc, 2002. **124**(48): p. 14318-9.
165. Singh, R., et al., *Binding and condensation of plasmid DNA onto functionalized carbon nanotubes: Toward the construction of nanotube-based gene delivery vectors.* J Am Chem Soc, 2005. **127**(12): p. 4388-96.
166. Ye Liu, D.-C.W.W.-D.Z.X.J.C.-B.H.T.S.C.S.H.G.K.W.L., *Polyethylenimine-Grafted Multiwalled Carbon Nanotubes for Secure Noncovalent Immobilization and Efficient Delivery of DNA.* Angewandte Chemie International Edition, 2005. **44**(30): p. 4782-4785.
167. Boussif, O., et al., *A versatile vector for gene and oligonucleotide transfer into cells in culture and in vivo: polyethylenimine.* Proc Natl Acad Sci U S A, 1995. **92**(16): p. 7297-301.
168. Ogris, M., et al., *The size of DNA/transferrin-PEI complexes is an important factor for gene expression in cultured cells.* Gene Ther, 1998. **5**(10): p. 1425-33.
169. Wang, x., Ren, J., Qu, X., *Targeted RNA interference of cyclin A2 mediated by functionalized single-walled carbon nanotubes induces proliferation arrest and apoptosis in chronic myelogenous leukemia K562 cells.* ChemMedChem, 2008. **3**(6): p. 940-5.
170. Zhang, Z., et al., *Delivery of telomerase reverse transcriptase small interfering RNA in complex with positively charged single-walled carbon nanotubes suppresses tumor growth.* Clin Cancer Res, 2006. **12**(16): p. 4933-9.

171. Podesta, J.E., et al., *Antitumor activity and prolonged survival by carbon-nanotube-mediated therapeutic siRNA silencing in a human lung xenograft model.* Small, 2009. **5**(10): p. 1176-85.
172. Yang, R., et al., *Single-walled carbon nanotubes-mediated in vivo and in vitro delivery of siRNA into antigen-presenting cells.* Gene Ther, 2006. **13**(24): p. 1714-23.
173. Yang, X., et al., *Multi-functionalized single-walled carbon nanotubes as tumor cell targeting biological transporters.* J Nanopart Res, 2008. **10**(5): p. 815-22.
174. Kam, N.W.S., Z. Liu, and H.J. Dai, *Functionalization of carbon nanotubes via cleavable disulfide bonds for efficient intracellular delivery of siRNA and potent gene silencing.* J Am Chem Soc, 2005. **127**(36): p. 12492-3.
175. Liu, Z., et al., *siRNA delivery into human T cells and primary cells with carbon-nanotube transporters.* Angew Chem Int Ed Engl. , 2007. **46**(12): p. 2023-7.
176. Rojas-Chapana, J., et al., *Multi-walled carbon nanotubes for plasmid delivery into Escherichia coli cells.* Lab Chip, 2005. **5**(5): p. 536-9.
177. Cai, D., et al., *Highly efficient molecular delivery into mammalian cells using carbon nanotube spearing.* Nat Methods, 2005. **2**(6): p. 449-54.
178. Wu, W., et al., *Targeted delivery of amphotericin B to cells by using functionalized carbon nanotubes.* Angewandte Chemie-International Edition, 2005. **44**(39): p. 6358-6362.
179. Chen, J., et al., *Functionalized single-walled carbon nanotubes as rationally designed vehicles for tumor-targeted drug delivery.* J. Am. Chem. Soc., 2008. **130** (49): p. 16778-85.
180. Pastorin, G., et al., *Double functionalisation of carbon nanotubes for multimodal drug delivery.* Chem Commun (Camb). 2006. **21**(11): p. 1182-4.
181. Ali-Boucetta, H., et al., *Multiwalled carbon nanotube-doxorubicin supramolecular complexes for cancer therapeutics.* Chem Commun (Camb). 2008(4): p. 459-61.
182. Feazell, R.P., et al., *Soluble single-walled carbon nanotubes as longboat delivery systems for Platinum(IV) anticancer drug design.* J Am Chem Soc, 2007. **129**(27): p. 8438-9.
183. Hampel, S., et al., *Carbon nanotubes filled with a chemotherapeutic agent: a nanocarrier mediates inhibition of tumor cell growth.* Nanomedicine (Lond), 2008. **3**(2): p. 175-82.
184. Dhar, S., et al., *Targeted single-wall carbon nanotube-mediated Pt(IV) prodrug delivery using folate as a homing device.* J Am Chem Soc, 2008. **130**(34): p. 11467-76.
185. Heister, E., et al., *Triple functionalisation of single-walled carbon nanotubes with doxorubicin, a monoclonal antibody, and a fluorescent marker for targeted cancer therapy.* Carbon, 2009. **47**(9): p. 2152-60.
186. McDevitt, M.R., et al., *Tumor targeting with antibody-functionalized, radiolabeled carbon nanotubes.* J Nucl Med, 2007. **48**(7): p. 1180-9.
187. Liu, Z., et al., *Drug delivery with carbon nanotubes for in vivo cancer treatment.* Cancer Res, 2008. **68**(16): p. 6652-60.
188. Villa, C.H., et al., *Synthesis and biodistribution of oligonucleotide-functionalized, tumor-targetable carbon nanotubes.* Nano Lett, 2008. **8**(12): p. 4221-8.
189. Bhirde, A.A., et al., *Targeted killing of cancer cells in vivo and in vitro with EGF-directed carbon nanotube-based drug delivery.* Acs Nano, 2009. **3**(2): p. 307-16.
190. Dhar, S., et al., *Targeted delivery of cisplatin to prostate cancer cells by aptamer functionalized Pt(IV) prodrug-PLGA-PEG nanoparticles.* Proc Natl Acad Sci U S A, 2008. **105**(45): p. 17356-61.
191. Liu, Z., et al., *Supramolecular chemistry on water-soluble carbon nanotubes for drug loading and delivery.* Acs Nano, 2007. **1**(1): p. 50-56.

192. Shao, N., et al., *Integrated molecular targeting of IGF1R and HER2 surface receptors and destruction of breast cancer cells using single wall carbon nanotubes.* Nanotechnology, 2007. **18**(31): p. 315101.
193. Chakravarty, P., et al., *Thermal ablation of tumor cells with antibody-functionalized single-walled carbon nanotubes.* Proc Natl Acad Sci U S A, 2008. **105**(25): p. 8697-702.
194. Gannon, C.J., et al., *Carbon nanotube-enhanced thermal destruction of cancer cells in a noninvasive radiofrequency field.* Cancer, 2007. **110**(12): p. 2654-65.
195. Kang, B., et al., *Cancer-cell targeting and photoacoustic therapy using carbon nanotubes as "bomb" agents.* Small, 2009. **5**(11): p. 1292-301.
196. Klingeler, R., S. Hampel, and B. Buchner, *Carbon nanotube based biomedical agents for heating, temperature sensoring and drug delivery.* Int J Hyperthermia, 2008. **24**(6): p. 496-505.
197. Wust, P., et al., *Magnetic nanoparticles for interstitial thermotherapy - feasibility, tolerance and achieved temperatures.* Int J Hyperthermia, 2006. **22**(8): p. 673-85.
198. Poland, C.A., et al., *Carbon nanotubes introduced into the abdominal cavity of mice show asbestos-like pathogenicity in a pilot study.* Nat Nanotechnol, 2008. **3**(7): p. 423-8.
199. Zhu, L., et al., *DNA damage induced by multiwalled carbon nanotubes in mouse embryonic stem cells.* Nano Lett, 2007. **7**(12): p. 3592-7.
200. Kagan, V.E., et al., *Direct and indirect effects of single walled carbon nanotubes on RAW 264.7 macrophages: Role of iron.* Toxicology Letters, 2006. **165**: p. 88 - 100.
201. Lin, Y., et al., *Visible luminescence of carbon nanotubes and dependence on functionalization.* J Phys Chem B, 2005. **109**: p. 14779-82.
202. Lu, Q., et al., *RNA polymer translocation with single-walled carbon nanotubes.* Nano Lett, 2004. **4**(12): p. 2473-7.
203. Worle-Knirsch, J.M., K. Pulskamp, and H.F. Krug, *Oops they did it again! Carbon nanotubes hoax scientists in viability assays.* Nano Lett, 2006. **6**(6): p. 1261-8.
204. Garibaldi, S., et al., *Carbon nanotube biocompatibility with cardiac muscle cells.* Nanotechnology, 2006. **17**(2): p. 391-7.
205. Flahaut, E., et al., *Investigation of the cytotoxicity of CCVD carbon nanotubes towards human umbilical vein endothelial cells.* Carbon, 2006. **44**: p. 1093-9.
206. Chen, X., et al., *Interfacing Carbon Nanotubes with Living Cells.* J Am Chem Soc, 2006. **128**(19): p. 6292-3.
207. Koyama, S., et al., *Role of systemic T-cells and histopathological aspects after subcutaneous implantation of various carbon nanotubes in mice.* Carbon, 2006. **44**(6): p. 1079-92.
208. Zhu, Y., et al., *Dependence of the cytotoxicity of MWCNTs on the culture medium.* Nanotechnology, 2006. **17**: p. 4668-74.
209. Dumortier, H., et al., *Functionalized carbon nanotubes are non-cytotoxic and preserve the functionality of primary immune cells.* Nano Lett, 2006. **6**(7): p. 1522-8.
210. Hu, H., et al., *Chemically functionalized carbon nanotubes as substrates for neuronal growth.* Nano Lett, 2004. **4**(3): p. 507-11.
211. Ji, S.R., et al., *Carbon nanotubes in cancer diagnosis and therapy.* Biochim Biophys Acta, 2010. **1806**(1): p. 29-35.
212. Bottini, M., et al., *Multi-walled carbon nanotubes induce T lymphocyte apoptosis.* Toxicol Lett, 2006. **160**(2): p. 121-6.
213. Sayes, C.M., et al., *Functionalization density dependence of single-walled carbon nanotubes cytotoxicity in vitro.* Toxicol Lett., 2006. **161**(2): p. 135-42.
214. Wick, P., et al., *The degree and kind of agglomeration affect carbon nanotube cytotoxicity.* Toxicol Lett, 2007. **168**(2): p. 121-31.

215. Prylutskaa, S.V., I.I. Grynyuka, and O.P. Matyshevska, *Estimation of multi-walled carbon nanotubes toxicity in vitro.* Physica E, 2008. **40** (7): p. 2565-9.
216. Cheng, C., et al., *Toxicity and imaging of multi-walled carbon nanotubes in human macrophage cells.* Biomaterials, 2009. **30**(25): p. 4152-60.
217. Simon-Deckers, A., et al., *In vitro investigation of oxide nanoparticle and carbon nanotube toxicity and intracellular accumulation in A549 human pneumocytes.* Toxicology, 2008. **253**(1-3): p. 137-46.
218. Muller, J., et al., *Respiratory toxicity of multi-wall carbon nanotubes.* Toxicol Appl Pharmacol, 2005. **207**(3): p. 221-31.
219. Yang, S.T., et al., *Long-term accumulation and low toxicity of single-walled carbon nanotubes in intravenously exposed mice.* Toxicol Lett, 2008. **181**(3): p. 182-9.
220. Miyawaki, J., et al., *Toxicity of single-walled carbon nanohorns.* Acs Nano, 2008. **2**(2): p. 213-26.
221. Schipper, M.L., et al., *A pilot toxicology study of single-walled carbon nanotubes in a small sample of mice.* Nat Nanotechnol, 2008. **3**(4): p. 216-21.
222. Yang, F., et al., *Pilot study of targeting magnetic carbon nanotubes to lymph nodes.* Nanomedicine (Lond), 2009. **4**(3): p. 317-30.
223. Strano, M.S., et al., *Understanding the nature of the DNA-assisted separation of single-walled carbon nanotubes using fluorescence and Raman spectroscopy.* Nano Lett, 2004. **4**(4): p. 543-50.
224. Moore, V.C., et al., *Individually suspended single-walled carbon nanotubes in various surfactants.* Nano Lett, 2003. **3**(10): p. 1379-82.
225. Zheng, M., et al., *Structure-based carbon nanotube sorting by sequence-dependent DNA assembly.* Science, 2003. **302**(5650): p. 1545-8.
226. Donnelly, J., K. Berry, and J.B. Ulmer, *Technical and regulatory hurdles for DNA vaccines.* Int J Parasitol., 2003. **33**(5-6): p. 457-67.
227. Kariko, K., et al., *Suppression of RNA recognition by Toll-like receptors: The impact of nucleoside modification and the evolutionary origin of RNA.* Immunity, 2005. **23**(2): p. 165-75.
228. Yu, M.F., et al., *Tensile loading of ropes of single wall carbon nanotubes and their mechanical properties.* Phys Rev Lett, 2000. **84**(24): p. 5552-5.
229. Saito, R., et al., *Electronic structure of chiral graphene tubules.* Appl. Phys. Lett, 1992. **60**(18): p. 2204-6.
230. Saito, R., et al., *Electronic structure of graphene tubules based on C60.* Phys Rev B Condens Matter., 1992. **46**(3): p. 1804-11.
231. Hamada, N., S.-i. Sawada, and A. Oshiyama, *New one-dimensional conductors: Graphitic microtubules.* Phys. Rev. Lett., 1992. **68**(10): p. 1579-81.
232. Kaiser, A.B., G. Düsberg, and S. Roth, *Heterogeneous model for conduction in carbon nanotubes.* Phys. Rev. B 1998. **57**(3): p. 1418-21.
233. Reilly, R.M., *Carbon nanotubes: Potential benefits and risks of nanotechnology in nuclear medicine.* J Nucl Med, 2007. **48**(7): p. 1039-42.
234. Poole, C.P.O., Frank J., *Introduction to nanotechnology* 2003, Hoboken, New Jersey: Wiley.
235. Mintmire, J.W., B.I. Dunlap, and C.T. White, *Are fullerene tubules metallic?* Phys Rev Lett, 1992. **68**(5): p. 631-4.
236. Xie, S.S., et al., *Synthesis and characterization of aligned carbon nanotube arrays.* Adv Materials, 1999. **11**(13): p. 1135-8.
237. Ajayan, P.M., *Nanotubes from carbon.* Chem. Rev, 1999. **99**(7): p. 1787-800.
238. Dai, L.M., et al., *Conjugated polymers for light-emitting applications.* Adv Materials, 2001. **13**(12-13): p. 915-25.
239. Rao, C.N.R., et al., *Nanotubes.* Chemphyschem, 2001. **2**(2): p. 78-105.

240. Bahr, J.L., et al., *Dissolution of small diameter single-wall carbon nanotubes in organic solvents?* Chem Commun 2001(2): p. 193-4.
241. Nikolaev, P., et al., *Gas-phase catalytic growth of single-walled carbon nanotubes from carbon monoxide.* Chem Phys Lett, 1999. **313**(1-2): p. 91-97.
242. Bandow, S., et al., *Purification of single-wall carbon nanotubes by microfiltration.* J Phys Chem B, 1997. **101**(44): p. 8839-42.
243. Duesberg, G.S., et al., *Separation of carbon nanotubes by size exclusion chromatography.* Chem Commun, 1998(3): p. 435-6.
244. Holzinger, M., et al., *A new purification method for single-wall carbon nanotubes (SWNTs).* Appl Phys A, 2000. **70**(5): p. 599-602.
245. Flahaut, E., Peigney, A., Laurent, Ch., Rousset, A. , *Synthesis of single-walled carbon nanotube-Co-MgO composite powders and extraction of the nanotubes.* J. Mater. Chem., 2000(10): p. 249-52.
246. Costa, S., *Purification and iron filling of carbon nanotubes*. 2009, West pomeranian University Technology: Szczecin. p. 168.
247. Flahaut, E., et al., *Gram-scale CCVD synthesis of double-walled carbon nanotubes.* Chem Commun (Camb), 2003(12): p. 1442-3.
248. R. R. Bacsa, C.L., A. Peigney, P. Puech and W. S. Bacsa, *Chirality of internal metallic and semiconducting carbon nanotube.* Phys Rev., 2002. **65**.
249. Bacsa, R., et al., *Chirality of internal metallic and semiconducting carbon nanotube.* Phys Rev B, 2002. **65**(16): p. 161404-8.
250. Rosca, I.D., et al., *Oxidation of multiwalled carbon nanotubes by nitric acid.* Carbon, 2005. **43**(15): p. 3124-31.
251. Hirsch, A., *Functionalization of single-walled carbon nanotubes.* Angew Chem Int Ed Engl, 2002. **41**(11): p. 1853-9.
252. Bahr, J.L. and J.M. Tour, *Covalent chemistry of single-wall carbon nanotubes.* J Mater Chem 2002. **12**(7): p. 1952-8.
253. Sun, Y.P., et al., *Functionalized carbon nanotubes: properties and applications.* Acc. Chem. Res., 2002. **35**(12): p. 1096-104.
254. Niyogi, S., et al., *Chemistry of single-walled carbon nanotubes.* Acc. Chem. Res., 2002. **35**(12): p. 1105-13.
255. Banerjee, S., T. Hemraj-Benny, and S.S. Wong, *Covalent surface chemistry of single-walled carbon nanotubes.* Adv Materials 2005. **17**(1): p. 17-29.
256. Tasis, D., et al., *Soluble carbon nanotubes.* Chem Eur J, 2003. **9**(17): p. 4000-8.
257. Katz, E. and I. Willner, *Biomolecule-functionalized carbon nanotubes: Applications in nanobioelectronics.* Chemphyschem, 2004. **5**(8): p. 1085-104.
258. Tasis, D., et al., *Chemistry of carbon nanotubes.* Chem. Rev., 2006. **106**(3): p. 1105-36.
259. Staros, J.V., R.W. Wright, and D.M. Swingle, *Enhancement by N-Hydroxysulfosuccinimide of water-soluble carbodiimide-mediated coupling reactions.* Anal Biochem. , 1986. **156**(1): p. 220-2.
260. Haggenmueller, R., et al., *Comparison of the quality of aqueous dispersions of single wall carbon nanotubes using surfactants and biomolecules.* Langmuir, 2008. **24**(9): p. 5070-8.
261. Jeynes, J.C.G., et al., *Generation of chemically unmodified pure single-walled carbon nanotubes by solubilizing with RNA and treatment with ribonuclease A.* Adv Materials, 2006. **18**(12): p. 1598-602.
262. Bustamante, C., C. Rivetti, and D.J. Keller, *Scanning force microscopy under aqueous solutions.* Curr Opin Struct Biol, 1997. **7**(5): p. 709-16.
263. Hansma, H.G., et al., *Properties of biomolecules measured from atomic force microscope images: A review.* J Struct Biol, 1997. **119**(2): p. 99-108.

264. Muller, D.J., et al., *Electrostatically balanced subnanometer imaging of biological specimens by atomic force microscope.* Biophys J, 1999. **76**(2): p. 1101-11.
265. Shao, Z.F., et al., *Biological atomic force microscopy: What is achieved and what is needed.* Adv Phys, 1996. **45**(1): p. 1-86.
266. O'Connell, M.J., et al., *Reversible water-solubilization of single-walled carbon nanotubes by polymer wrapping.* Chem Phys Lett, 2001. **342**(3-4): p. 265-71.
267. Kataura, H., et al., *Optical properties of single-wall carbon nanotubes.* Synt Met, 1999. **103**(1-3): p. 2555-8.
268. Itkis, M.E., et al., *Purity evaluation of as-prepared single-walled carbon nanotube soot by use of solution-phase near-IR spectroscopy.* Nano Lett, 2003. **3**(3): p. 309-14.
269. Monthioux, M., et al., *Sensitivity of single-wall carbon nanotubes to chemical processing: an electron microscopy investigation.* Carbon, 2001. **39**(8): p. 1251-72.
270. Kim, P., et al., *Electronic density of states of atomically resolved single-walled carbon nanotubes: Van Hove singularities and end states.* Phys Rev Lett, 1999. **82**(6): p. 1225-8.
271. Kukovecz, A., et al., *On the stacking behavior of functionalized single-wall carbon nanotubes.* J. Phys. Chem. B, 2002. **106**(25): p. 6374-80.
272. Kukovecz, A., Kramberger, Ch., Georgakilas, V., Prato, M., Kuzmany, H. , *A detailed Raman study on thin single-wall carbon nanotubes prepared by the HiPCO process.* Eur. Phys. J. B, 2002. **28**(2): p. 223-30.
273. Bandow, S. and S. Asaka, *Effect of the growth temperature on the diameter distribution and chirality of single-wall carbon nanotubes.* Phys. Rev. Lett., 1998. **80**(17): p. 3779-81.
274. Dresselhaus, M.S. and P.C. Eklund, *Phonons in carbon nanotubes.* Adv Phys, 2000. **49**(6): p. 705-814.
275. Jishi, R.A., et al., *Phonon modes in carbon nanotubules.* Chem Phys Lett, 1993. **209**(1-2): p. 77-82.
276. Jorio, A., et al., *Characterizing carbon nanotube samples with resonance Raman scattering.* New Journal of Physics, 2003. **5**: p. -.
277. Jorio, A., et al., *Resonance Raman spectra of carbon nanotubes by cross-polarized light.* Phys. Rev. Lett., 2003. **90**(10): p. 107403.
278. Brar, V.W., Samsonidze, Ge. G., Dresselhaus, M. S., Dresselhaus, G., Saito, R., Swan, A. K., Ünlü, M. S., Goldberg, B. B., Souza Filho, A. G., Jorio, A., *Second-order harmonic and combination modes in graphite single-wall carbon nanotube bundles and isolated single-wall carbon nanotubes.* Phys. Rev. B, 2002. **66**(1): p. 1554181-10.
279. Souza, M., et al., *Single and double resonance Raman G-band processes in carbon nanotubes.* Phys. Rev. B, 2004. **69**(24): p. 241403-6
280. Brown, S.D.M., et al., *Second-order resonant Raman spectra of single-walled carbon nanotubes.* Phys. Rev. B, 2000. **61**(11): p. 7734-42.
281. Almofti, M.R., et al., *Cationic liposome-mediated gene delivery: biophysical study and mechanism of internalization.* Arch Biochem Biophys, 2003. **410**(2): p. 246-53.
282. Raffa, V., et al., *Can the properties of carbon nanotubes influence their internalization by living cells?* Carbon, 2008. **46**(12): p. 1600-10.
283. Oberdorster, G., et al., *Principles for characterizing the potential human health effects from exposure to nanomaterials: elements of a screening strategy.* Part Fibre Toxicol, 2005. **2**(8): p. 1-35.
284. Nel, A., et al., *Toxic potential of materials at the nanolevel.* Science, 2006. **311**(5761): p. 622-7.

285. Lam, C.W., et al., *A review of carbon nanotube toxicity and assessment of potential occupational and environmental health risks.* Crit Rev Toxicol, 2006. **36**(3): p. 189-217.
286. Panessa-Warren, B.J., et al., *Biological cellular response to carbon nanoparticle toxicity.* J. Phys.: Condens. Matter, 2006. **18**(33): p. S2185-201.
287. Smart, S.K., et al., *The biocompatibility of carbon nanotubes.* Carbon, 2006. **44**(6): p. 1034-47.
288. Oberdorster, G., E. Oberdorster, and J. Oberdorster, *Nanotoxicology: an emerging discipline evolving from studies of ultrafine particles.* Environ Health Perspect., 2005. **113**(7): p. 823-39.
289. Monteiro-Riviere, N.A., et al., *Multi-walled carbon nanotube interactions with human epidermal keratinocytes.* Toxicol Lett, 2005. **155**(3): p. 377-84.
290. Jia, G., et al., *Cytotoxicity of carbon nanomaterials: single-wall nanotube, multi-wall nanotube, and fullerene.* Environ Sci Technol, 2005. **39**(5): p. 1378-83.
291. Shvedova, A., et al., *Exposure to carbon nanotube material: assessment of nanotube cytotoxicity using human keratinocyte cells.* J Toxicol Environ Health A, 2003. **66**(20): p. 1909-26.
292. Magrez, A., et al., *Cellular toxicity of carbon-based nanomaterials.* Nano Lett, 2006. **6**(6): p. 1121-5.
293. Cui, D., et al., *Effect of single wall carbon nanotubes on human HEK293 cells.* Toxicol Lett, 2005. **155**(1): p. 73-85.
294. Manna, S.K., et al., *Single-walled carbon nanotube induces oxidative stress and activates nuclear transcription factor-kB in human keratinocytes.* Nano Letters, 2005. **5**(9): p. 1676-84.
295. Ding, L., et al., *Molecular characterization of the cytotoxic mechanism of multiwall carbon nanotubes and nano-onions on human skin fibroblast.* Nano Lett, 2005. **5**(12): p. 2448-64.
296. Chlopek, J., et al., *In vitro studies of carbon nanotubes biocompatibility.* Carbon, 2006. **44**(6): p. 1106-11.
297. Templeton, R.C., et al., *Life-cycle effects of single-walled carbon nanotubes (SWNTs) on an estuarine meiobenthic copepod.* Environ Sci Technol, 2006. **40**(23): p. 7387-93.
298. Warheit, D.B., *What is currently known about the health risks related to carbon nanotube exposures?* Carbon, 2006. **44**(6): p. 1064-9.
299. Cooper, S., *Control and maintenance of mammalian cell size.* Bmc Cell Biology, 2004. **5**(35): p. 1-21.
300. Jeynes, C., *Possible biomedical applications of carbon nanotubes functionalised with RNA or DNA,* in *School of Biomedical and Molecular Sciences.* 2007, University of Surrey.
301. Heller, D.A., et al., *Optical detection of DNA conformational polymorphism on single-walled carbon nanotubes.* Science, 2006. **311**(5760): p. 508-11.
302. Krafft, C., et al., *Mapping of single cells by near infrared Raman microspectroscopy.* Vib Spec, 2003. **32**(1): p. 75-83.
303. Notingher, I., et al., *Spectroscopic study of human lung epithelial cells (A549) in culture: Living cells versus dead cells.* Biopolymers, 2003. **72**(4): p. 230-40.
304. Krafft, C., et al., *Identification of organelles and vesicles in single cells by Raman microspectroscopic mapping.* Vib Spec, 2005. **38**(1-2): p. 85-93.
305. Dresselhaus, M.S., et al., *Raman spectroscopy on isolated single wall carbon nanotubes.* Carbon, 2002. **40**(12): p. 2043-61.
306. Saito, Y., et al., *Interlayer spacings in carbon nanotubes.* Phys Rev B, 1993. **48**(3): p. 1907-9.

307. Allen, B.L., et al., *Biodegradation of single-walled carbon nanotubes through enzymatic catalysis.* Nano Lett, 2008. 8(11): p. 3899-903.
308. Liu, X., R.H. Hurt, and A.B. Kane, *Biodurability of Single-Walled Carbon Nanotubes Depends on Surface Functionalization.* Carbon, 2010. **48**(7): p. 1961-9.
309. Puppels, G.J., et al., *Raman microspectroscopic approach to the study of human granulocytes.* Biophys J, 1991. **60**(5): p. 1046-56.
310. Verrier, S., et al., *In situ monitoring of cell death using Raman microspectroscopy.* Biopolymers, 2004. **74**(1-2): p. 157-62.
311. Benchimol, S., D. Pim, and L. Crawford, *Radioimmunoassay of the cellular protein p53 in mouse and human cell lines.* EMBO J, 1982. **1**(9): p. 1055-62.
312. Kastan, M.B., et al., *Participation of p53 protein in the cellular response to DNA damage.* Cancer Res, 1991. **51**(23 Pt 1): p. 6304-11.
313. Yonish-Rouach, E., et al., *Wild-type p53 induces apoptosis of myeloid leukaemic cells that is inhibited by interleukin-6.* Nature, 1991. **352**(6333): p. 345-7.
314. Levine, A.J., *p53, the cellular gatekeeper for growth and division.* Cell, 1997. **88**(3): p. 323-31.
315. Oren, M. and V. Rotter, *Introduction: p53--the first twenty years.* Cell Mol Life Sci, 1999. **55**(1): p. 9-11.
316. Giaccia, A.J. and M.B. Kastan, *The complexity of p53 modulation: emerging patterns from divergent signals.* Genes Dev, 1998. **12**(19): p. 2973-83.
317. Prives, C., *Signaling to p53: breaking the MDM2-p53 circuit.* Cell, 1998. **95**(1): p. 5-8.
318. Carroll, A.G., et al., *p53 oncogene mutations in three human prostate cancer cell lines.* Prostate, 1993. **23**(2): p. 123-34.
319. Ikeda, M., et al., *Extracellular signal-regulated kinases 1 and 2 activation in endothelial cells exposed to cyclic strain.* Am J Physiol, 1999. **276**(2 Pt 2): p. H614-22.
320. Wei, M.L., et al., *GLUT4 and transferrin receptor are differentially sorted along the endocytic pathway in CHO cells.* J Cell Biol, 1998. **140**(3): p. 565-75.
321. Yamashiro, D.J., et al., *Segregation of transferrin to a mildly acidic (pH 6.5) para-Golgi compartment in the recycling pathway.* Cell, 1984. **37**(3): p. 789-800.
322. Bucci, C., et al., *The small GTPase rab5 functions as a regulatory factor in the early endocytic pathway.* Cell, 1992. **70**(5): p. 715-28.
323. Ren, M., et al., *Hydrolysis of GTP on rab11 is required for the direct delivery of transferrin from the pericentriolar recycling compartment to the cell surface but not from sorting endosomes.* Proc Natl Acad Sci U S A, 1998. **95**(11): p. 6187-92.
324. Stenmark, H. and V.M. Olkkonen, *The Rab GTPase family.* Genome Biol, 2001. **2**(5): p. 1-7.
325. Mu, Q., D.L. Broughton, and B. Yan, *Endosomal leakage and nuclear translocation of multiwalled carbon nanotubes: developing a model for cell uptake.* Nano Lett, 2009. **9**(12): p. 4370-5.
326. Zhou, F., et al., *New insights of transmembranal mechanism and subcellular localization of noncovalently modified single-walled carbon nanotubes.* Nano Lett, 2010. **10**(5): p. 1677-81.
327. Parton, R.G. and K. Simons, *The multiple faces of caveolae.* Nat Rev Mol Cell Biol, 2007. **8**(3): p. 185-94.
328. Aniento, F., et al., *Cytoplasmic dynein-dependent vesicular transport from early to late endosomes.* J Cell Biol, 1993. **123**(6 Pt 1): p. 1373-87.
329. Luzio, J.P., et al., *Relationship between endosomes and lysosomes.* Biochem Soc Trans, 2001. **29**(Pt 4): p. 476-80.
330. Saftig, P. and J. Klumperman, *Lysosome biogenesis and lysosomal membrane proteins: trafficking meets function.* Nat Rev Mol Cell Biol, 2009. **10**(9): p. 623-35.

331. Ghosh, R.N., et al., *An endocytosed TGN38 chimeric protein is delivered to the TGN after trafficking through the endocytic recycling compartment in CHO cells.* J Cell Biol, 1998. **142**(4): p. 923-36.
332. Saraste, J., G.E. Palade, and M.G. Farquhar, *Temperature-sensitive steps in the transport of secretory proteins through the Golgi complex in exocrine pancreatic cells.* Proc Natl Acad Sci U S A, 1986. **83**(17): p. 6425-9.
333. Jones, A.T. and M.J. Clague, *Phosphatidylinositol 3-kinase activity is required for early endosome fusion.* Biochem J, 1995. **311 (Pt 1)**: p. 31-4.
334. Cardone, M. and K. Mostov, *Wortmannin inhibits transcytosis of dimeric IgA by the polymeric immunoglobulin receptor.* FEBS Lett, 1995. **376**(1-2): p. 74-6.
335. Seglen, P.O. and P.B. Gordon, *Amino acid control of autophagic sequestration and protein degradation in isolated rat hepatocytes.* J Cell Biol, 1984. **99**(2): p. 435-44.
336. Seglen, P.O. and P.B. Gordon, *3-Methyladenine: specific inhibitor of autophagic/lysosomal protein degradation in isolated rat hepatocytes.* Proc Natl Acad Sci U S A, 1982. **79**(6): p. 1889-92.
337. Maxfield, F.R. and T.E. McGraw, *Endocytic recycling.* Nat Rev Mol Cell Biol, 2004. **5**(2): p. 121-32.
338. Uherek, C. and W. Wels, *DNA-carrier proteins for targeted gene delivery.* Adv Drug Deliv Rev, 2000. **44**(2-3): p. 153-66.
339. Kamiya, H., et al., *Intracellular trafficking and transgene expression of viral and non-viral gene vectors.* Adv Drug Deliv Rev, 2001. **52**(3): p. 153-64.
340. Gao, L.Z., et al., *Carbon nanotube delivery of the GFP gene into mammalian cells.* Chembiochem, 2006. **7**(2): p. 239-42.
341. Novina, C.D., et al., *siRNA-directed inhibition of HIV-1 infection.* Nat Med, 2002. **8**(7): p. 681-6.
342. Hanahan, D. and R.A. Weinberg, *The hallmarks of cancer.* Cell, 2000. **100**(1): p. 57-70.
343. Yuan, J., *Transducing signals of life and death.* Curr Opin Cell Biol, 1997. **9**(2): p. 247-51.
344. Cryns, V. and J. Yuan, *Proteases to die for.* Genes Dev, 1998. **12**(11): p. 1551-70.
345. Deveraux, Q.L. and J.C. Reed, *IAP family proteins--suppressors of apoptosis.* Genes Dev, 1999. **13**(3): p. 239-52.
346. Crook, N.E., R.J. Clem, and L.K. Miller, *An apoptosis-inhibiting baculovirus gene with a zinc finger-like motif.* J Virol, 1993. **67**(4): p. 2168-74.
347. http://www.imgenex.com/emarketing/081606_LivinorSurvivin/LivinorSurvivin_forweb.htm.
348. Ambrosini, G., C. Adida, and D.C. Altieri, *A novel anti-apoptosis gene, survivin, expressed in cancer and lymphoma.* Nat Med, 1997. **3**(8): p. 917-21.
349. Altieri, D.C., *Survivin, versatile modulation of cell division and apoptosis in cancer.* Oncogene, 2003. **22**(53): p. 8581-9.
350. Pennati, M., M. Folini, and N. Zaffaroni, *Targeting survivin in cancer therapy: fulfilled promises and open questions.* Carcinogenesis, 2007. **28**(6): p. 1133-9.
351. Carvalho, A., et al., *Survivin is required for stable checkpoint activation in taxol-treated HeLa cells.* J Cell Sci, 2003. **116**(Pt 14): p. 2987-98.
352. Li, Q.X., et al., *Survivin stable knockdown by siRNA inhibits tumor cell growth and angiogenesis in breast and cervical cancers.* Cancer Biol Ther, 2006. **5**(7): p. 860-6.
353. Al-Jamal, K.T., et al., *Enhanced cellular internalization and gene silencing with a series of cationic dendron-multiwalled carbon nanotube:siRNA complexes.* FASEB J. , 2010. **(in press).**

Appendix 1: CNT preparations for gene delivery[3]

In order to use carbon nanotubes as delivery agent it is necessary to render them dispersible in water. This can be achieved by the non-specific absorption of polypeptides, such as poly(lys:Phe), polylyposomes as PL-PEG-NH_3 and RNA onto the CNT sidewalls. These molecules were also used to wrap around soluble CNT produced by oxidation processes. Poly(lys:Phe) and PL-PEG-NH_3 were selected for CNT wrapping because they permit the linkage of other molecules, such as DNA, since they carry cationic groups that can bind to negatively charged DNA.

Initially SWNTs, DWNTs and MWNTs were employed for extensive analyses of CNT dispersions after coating with several surfactants (Figure A-1.1): benzalkonium chloride, polyethyleneimine (PEI), 1-pyrenemethylamide hydrochloride (PMA), 1,2-distearoyl-sn-glycero-3-phosphoethanolamine-N-[amino(polyethylene glycol)2000 (PL-PEG-NH_2), 1-stearoyl-2-hydroxy-sn-glycero-3-phosphocholine (Lyso-PC), 1,2,dipalmitoyl-sn-glycero-3-phosphoethanolamine (DPPE), Poly(Lys:Phe, 1:1) hydrobromide and Poly(Lys:Tyr, 1:9) hydrobromide. With the final aim of using CNT for gene delivery surfactants were selected for their ability bind negatively charged plasmid DNA since these compounds carry cationic groups such as amine and choline. The methods to obtain stable dispersion consisted of mixing pristine CNTs with surfactants solution. The adsorption of the surfactants onto CNT sidewalls was then promoted by sonication (Methodology: CNT (0.15 mg to 2 mg) was mixed with 1 mL of surfactant (0.3 $mg.mL^{-1}$). The mixture was ultrasonicated in a Soniprep for 40 s, followed by sonication for 2 h in water bath (3 W) at room temperature. Centrifugation at 13200 rpm for 10 minutes was performed to sediment large bundles and uncoated CNT, obtaining in the supernatant a stable dispersion of CNTs). The dispersion yields were measured by VIS-NIR spectroscopy. Absorption at 730 nm was selected as the working wavelength to estimate the amount of dispersed CNTs. CNTs present strong absorbance at this region of the spectra, while surfactants do not absorb, therefore the signal for CNTs is free of background absorption and can be used as an estimate of CNT concentration.

[3] Work was performed in collaboration with Dr. Vanesa Sanz-Beltran at university of surrey

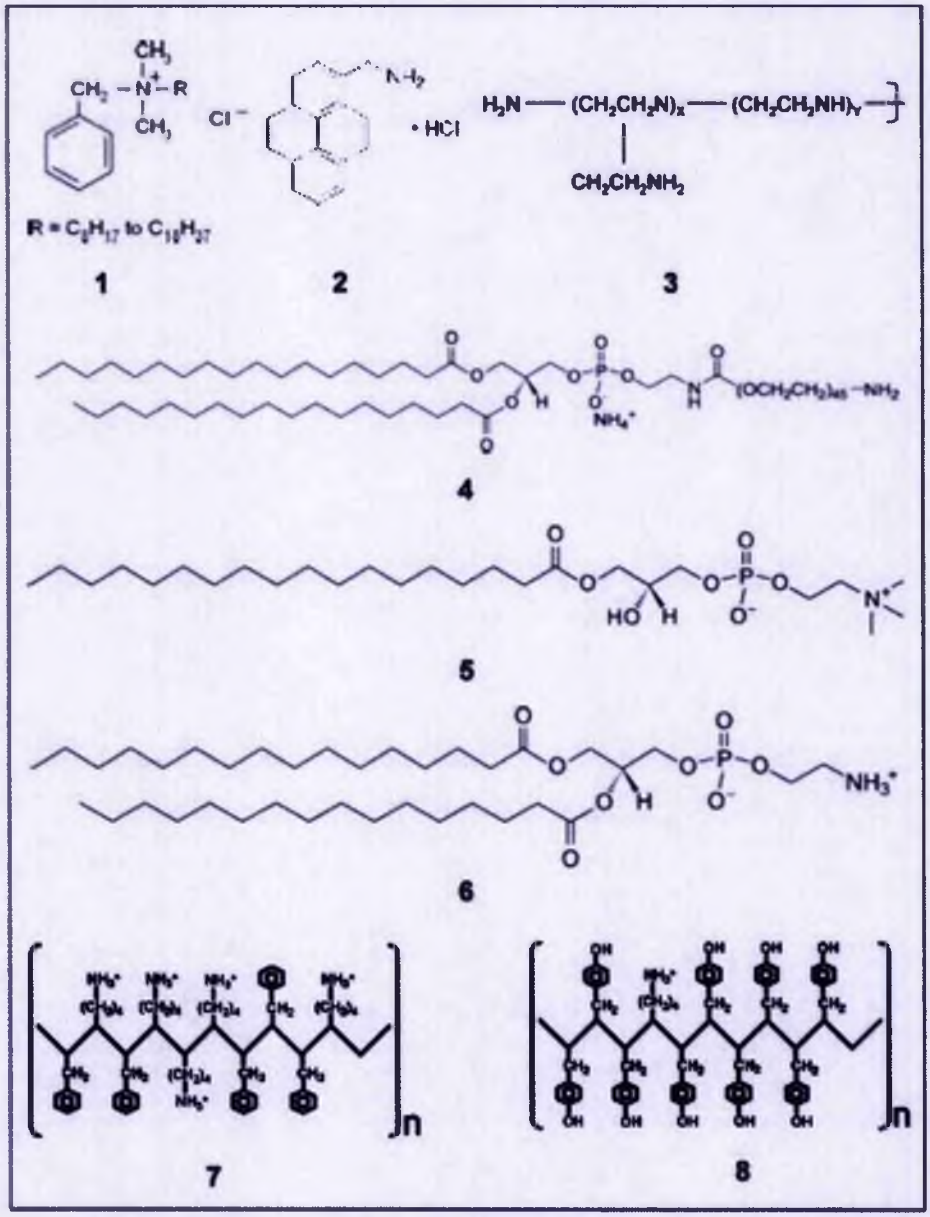

Figure A-1.1: Surfactant chemical structures. Surfactant structures: (1) benzalkonium chloride, (2) pyrenemethylamine (PMA), (3) polyethylenimine (PEI), (4) 1,2-distearoyl-*sn*-glycero-3-phosphoethanolamine-N-[amino(polyethylene glycosl)2000] (PL-PEG-NH_2), (5) 1-stearoyl-2-hydroxy-*sn*-glycero-3-phosphocholine (Lyso PC), (6) 1,2-dipalmitoyl-sn-glycero-3-phosphoethanolamine (DPPE), (7) Poly(Lys:Phe, 1:1), 8) Poly(Lys:Tyr, 1:9).

Figure A-1.2 exhibits dispersion yields for SWNTs, DWNTs and MWNTs coated with different surfactants (non-covalent adsorption of Benzalkonium, PEI, PMA, PL-PEG-NH_2, Lyso-PC, DPPE, Poly(Lys:Phe) and Poly(Lys:Tyr). Higher dispersion was obtained with PL-PEG-NH_2 for SWNTs, Poly(Lys:Phe) for DWNT and LysoPC for MWNTs. Furthermore; the dispersion yields are higher for MWNTs and SWNTs than for DWNTs.

The ability of CNTs to complex DNA was also studied by gel retardation assay (Figure A-1.3). As presented PEI was more efficient (Figure A-1.3 A), followed by Poly(Lys:Phe) (Figure A-1.3 C) and then PL-PEG-NH_2 (Figure A-1.3 B). Besides better efficiency for DNA complexation, PEI is cytotoxic and therefore Poly(Lys:Phe) appears to be a better candidate for DNA delivery. In addition concentrations of surfactants can be reduced if the CNTs were first modified by oxidation.

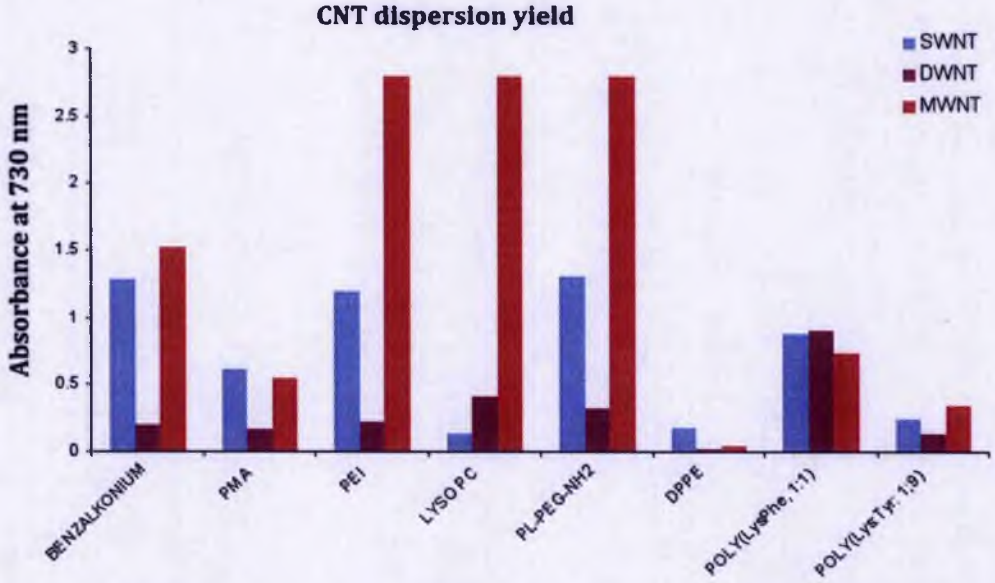

Figure A-1.2: CNT dispersion yield. Absorbance of CNT suspension at 730 nm plotted for each surfactant and type of CNT (SWNTs, DWNTs and MWNTs). Different degree dispersion was achieved depending on the surfactant was well as nanotube type. SWNT and DWNT appear to be more difficult to disperse than MWNT. SWNT present higher dispersion when coated with PL-PEG-NH_2, while DWNT are better dispersed with Poly(Lys:Phe).

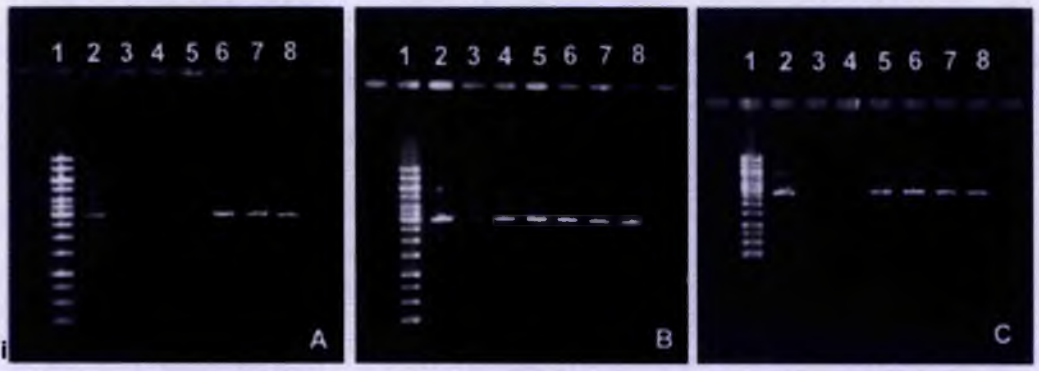

Fi

NH_2 and (C) poly(Lys:Phe, 1:1). Lane 1: ladder, lane 2: pGL3 plasmid alone 6.8 $ng.mL^{-1}$, lanes 3-8: CNT:plasmid DNA complexes with plasmid 6.8 $ng.mL^{-1}$ and different dilutions of CNTs from 1/1 to $1/10^5$ (1/1 refers to the best conditions found for solubilisation of CNTs: 51 $mg.mL^{-1}$ for PEI, 56 $mg.mL^{-1}$ for PL-PEG-NH_2 and 37 $mg.mL^{-1}$ for poly(Lys:Phe, 1:1).

Appendix 2: CNT uptake by fluorescence

Time dependent uptake of CNTs was studied by confocal microscopy, between 5 minutes and 4 hours as shown in Figure A.1. In these experiments HeLa cells were cultured in 24 well plates containing poly-$_L$-lysine-coated coverslips, using MEM medium. When the cells reached 80 % confluence, they were incubated with oxidized DWNT wrapped with Poly(Lys:Phe) and Fluorescein (oxDW-Poly-FS) at a concentration of ~30 µg/ml (CNT preparation: Poly(Lys:Phe) for final concentration 0.5 mg/ml was added to oxidised DWNT, 0.5 mg/ml. Bath sonication of the mixture was carried out for 1-2 h. The suspension was then centrifuged at 4000 g for 30 min to remove impurities and large nanotubes bundles that aggregate as the sediment, and the supernatant was subsequently collected. Fluorescein was attached to amino groups of the polypeptide by incubation for 2 h at room temperature under stirring. To remove excess of phospholipids/fluorescein the suspension was filtered and then resuspended in water). The cells were subsequently trypsonised and cytospun, following fixation in with 4% paraformaldehyde. Finally, fixed cells where incubated with nuclear staining (TO-PRO®-3) for 10 min, washed several times with PBS and slide was mounted for further analysis on confocal microscope Zeiss LSM 510.

Figure A.1 exhibits carbon nanotube uptake by ceils, where in the first plan it is shown the internalised oxidised DWNT wrapped with Poly(Lys:Phe) and Fluorescein in green, second plan show the nuclei stained in blue and finally in the third plan both internalised carbon nanotubes and nuclear staining. Similar to the results obtained to Raman, there is a confirmation of internalisation of carbon nanotubes after 30 min incubation by confocal microscopy. Additionally to those results there is evidence that, after 5 min incubation with the complexes, these complexes are attaching to the cell membrane (Figure A.1). Cells were also incubated with carbon nanotubes at 4 C, which resulted in no internalisation, suggesting that endocytosis is the mechanism of cell entry.

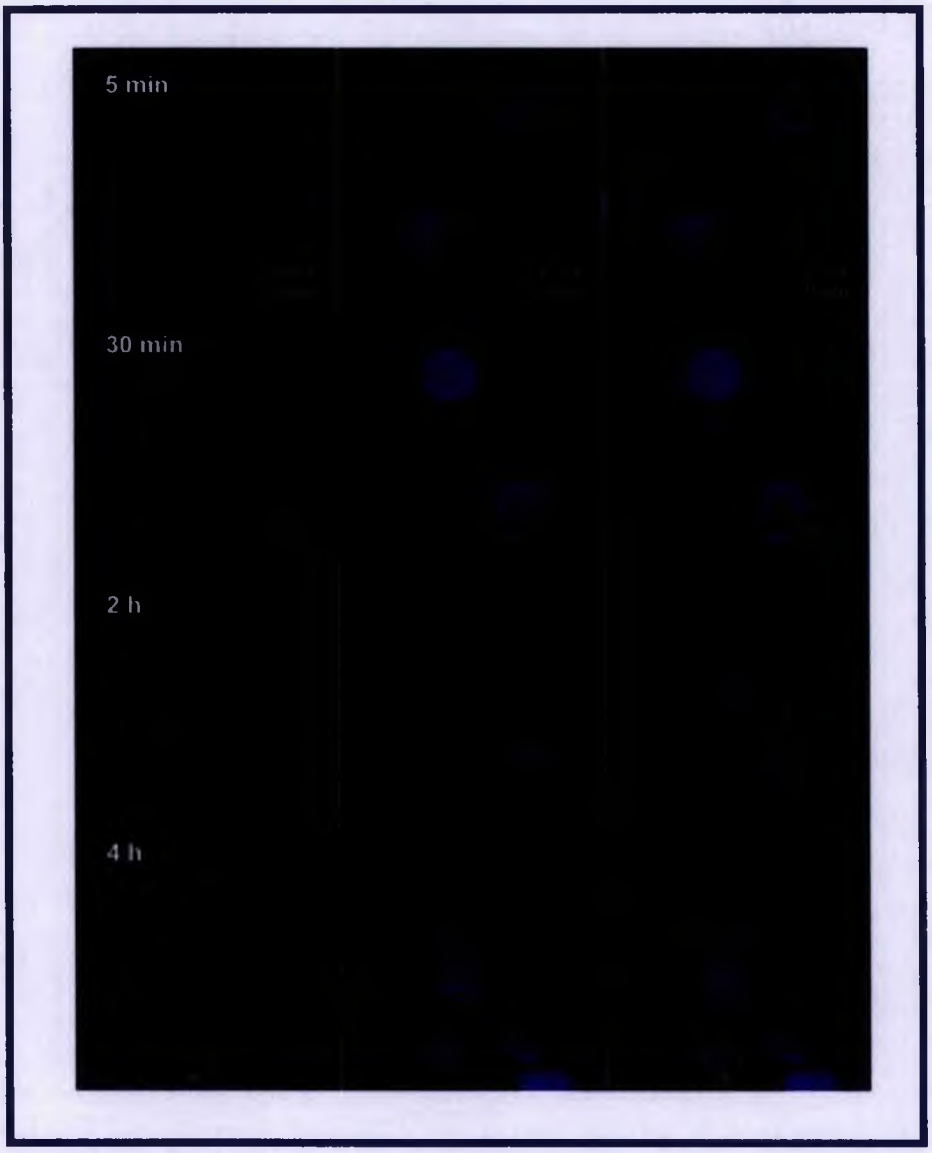

Figure A-2.1: Time dependent uptake of fluorescent CNTs. Fluorescent microscopy of HeLa cells transfected with Fluorescein labelled CNTs and nuclei were stained with blue fluorescent TO-PRO®-3.

Appendix 3: Study and optimisation of endocytosis of CNTs

The study of the mechanism of entry presented in chapter 4 was carried out in both HeLa and PC3 cells. HeLa cells were used at an initial stage and as shown in Figure A-3.1 co-localisation with transferrin and Lysotracker was evident. However, it was observed a certain degree of accumulation of CNTs in cell membranes. In order to optimise the methodology and assure co-localisation is occurring within the specific cellular compartments (avoid binding of stainings to CNTs), different conditions to minimise CNT accumulation in cell membranes were tested (Figure A-3.2).

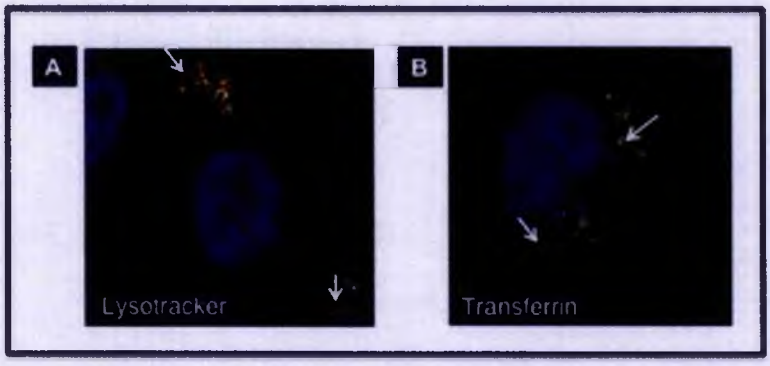

Figure A-3.1: Co-localisation of CNTs with specific cellular compartments. HeLa cells incubated with oxDWNT-Poly-FS for 30-minutes, were stained with Lysotracker red (A) and Transferrin (B), nuclei were stained with blue fluorescent TO-PRO®-3. In yellow (arrows), cell compartment positive for both CNTs and organelle markers.

In Figure A-3.2 A and B cells were incubated with CNT for 5 to 30-minutes, it is shown the CNT accumulate in the membranes. Moreover it was possible to visualize CNTs outside cells (Figure A-3.2 B), in the slide, to which Lysotracker dye was then able to bind, resulting in a false positive. In a first attempt cells were washed with a mixture of acids (0.1 M glycine with 0.1 M NaCl, pH = 3). However, this treatment was not sufficient to remove all accumulated CNT and as shown in Figure A-3.2 C it was possible to see dark spots in and out of the cells. Another treatment employed was a quick wash with trypsin (by adding trypsin and removing (1-5-seconds) followed by wash with PBS, Figure A-3.2 E), which resulted in loss of number of cells, shrinking and cell aggregation. Consequently, cells exposed to CNTs were also trypsonised and cell suspension was centrifuged onto a glass slide by cytospin (Figure A-3.2 E). This treatment allowed to remove CNT accumulated at cell membranes, but the morphology of the adherent cells was greatly altered and their round shape was not

ideal for our co-localisation studies. Finally, cellscrub buffer was employed (as described in section 4.2.2.2) revealing characteristic cell morphology of adherent cells, with nanotubes within the cell membranes and in plan with the nucleus (Figure A-3.2 F).

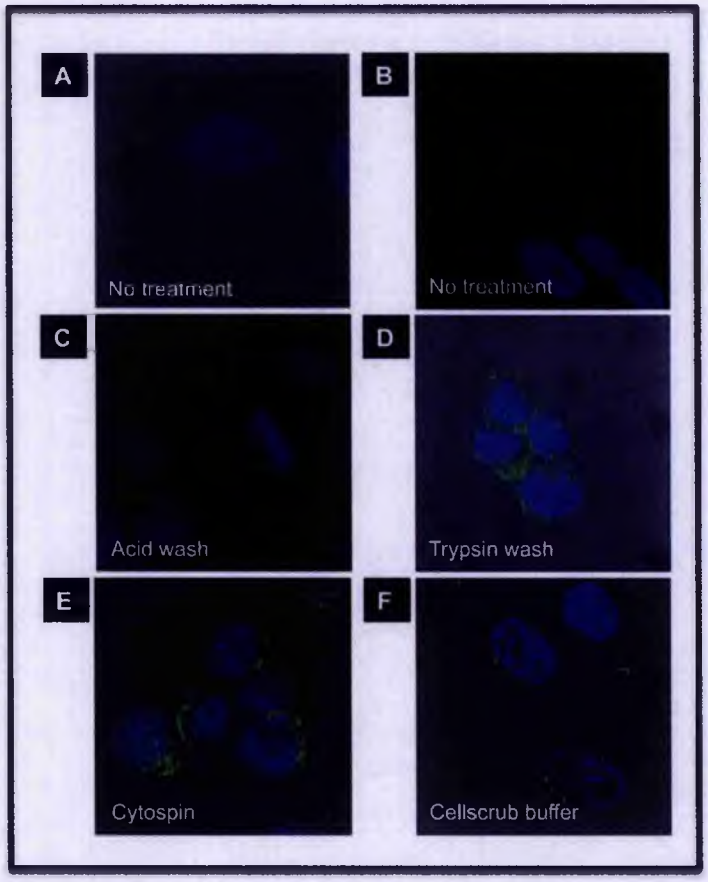

Figure A-3.2: Different treatment conditions to remove non-internalised CNTs. In, A and B is shown controls of cells without any treatment. A, CNT were found in cell membrane and dark spots can be visualised due to CNT accumulation. In B is shown that CNTs on the slide (out of cell) co-localise with Lysotracker. In C, cells were washed with a mixture of glycine with NaCl, which was not enough to remove CNTs accumulation. In D cells were quickly washed with trypsin (D). In addition, suspension cells (trypsonised cells) were centrifuged onto glass slides by cytospin (E). Finally, washing of cells with cellscrub buffer (F). Nucleus were stained with blue fluorescent TO-PRO®-3.